Investigating the Influence of Inflammatory Mediators on Non-inflammatory Features of Sporadic Inclusion Body Myositis *In Vitro*

A thesis submitted for the degree of Doctor of Philosophy

University College London (UCL)

Bryony McCord

2023

Declaration

I, Bryony McCord confirm that the work presented in my thesis is my own. Where information has been derived from other sources, I confirm that this has been indicated in the thesis.

Signed:

Abstract

Sporadic inclusion body myositis (sIBM) is a progressive muscle disease causing weakness and ambulation difficulty. Muscle of sIBM patients presents with inflammation and degeneration. CD8+ T cells infiltrate affected muscles and inflammatory cytokines are upregulated. Degenerative/non-inflammatory features are observed including sarcoplasmic accumulation of proteins such as TDP-43 and p62, and TDP-43 sarcoplasmic mislocalisation. The cause of sIBM symptoms is poorly understood and there are no effective treatments. Further understanding of the interaction between inflammatory and non-inflammatory features of sIBM may elucidate potential treatment targets.

This thesis aimed to explore the effect of inflammation on non-inflammatory features of sIBM in healthy human myotubes. The effects of IL-1β and IFNγ, conditioned medium or coculture with a cytotoxic immune cell line TALL-104 on p62 and TDP-43 sarcoplasmic aggregation, protein expression, and TDP-43 subcellular localisation was investigated. Using 3D myotube cultures termed myobundles, the effect of inflammatory conditions on force generation was examined.

No treatment caused aggregation of TDP-43, suggesting these inflammatory factors do not trigger TDP-43 sarcoplasmic aggregation in these cells. IL-1β+IFNγ combined but not these cytokines separately caused increased size of p62 puncta, but this may represent increased autophagic flux instead of dysfunctional p62 aggregation. Active force from myobundles representing muscle strength was not affected by IL-1β+IFNγ or TALL-104 coculture after 48 hours incubation. IL-1β+IFNγ increased half relaxation time and time to peak force, suggesting fatigue induction. This indicates acute exposure to inflammatory cytokines or cytotoxic immune cells may not trigger muscle weakness.

Overall, these results highlight TDP-43 aggregation may not be influenced by inflammatory factors, but alterations in p62 can occur with simultaneous multiple inflammatory insults in cultured muscle cells. This work suggests further investigations of myobundle cultures with sIBM-like inflammatory mediators may be warranted to investigate muscle weakness.

Impact statement

Sporadic inclusion body myositis (sIBM) leads to progressive muscle weakness, especially affecting ambulation and fine motor skills in the hands which can lead to a dependency on walking aids and decreased quality of life. Despite reasonable understanding of the pathological features of sIBM, both clinically and physiologically, the underlying mechanisms that lead to muscle weakness are still not clearly understood. Furthermore, there are no effective treatments for sIBM patients that either halt or ameliorate progressive loss of muscle strength. There is a clear need for a better understanding of the interaction of different pathological mechanisms of sIBM, and how these can influence muscle weakness. This could help pave the way for investigations of potential treatment targets.

This project aimed to elucidate whether specific inflammatory mediators contribute to non-inflammatory features that are similar to those observed in sIBM, namely protein aggregation and mislocalisation, to answer the question of whether inflammation can act as a trigger for protein aggregation. The results suggested that there was no clear effect of inflammation on protein aggregation or mislocalisation.

Furthermore, the project utilised a previously developed 3D method of growing muscle cells called myobundles that can respond to electrical stimulation and generate force, thus mimicking native muscle function better than traditional cell culture techniques. By utilising myobundles it was possible to examine how different sIBM-like conditions influence muscle strength in a quantifiable manner, without requiring animal models. Myobundles could be further utilised to investigate pathological features relevant to sIBM to see whether they cause weakness to improve our understanding of this disease. Potentially, myobundles could be used for pre-clinical testing of potential treatment options.

Overall, this study helped our understanding of the influence of inflammatory factors on skeletal muscle cells, by showing that inflammation may not cause specific features of protein aggregation, and by showing that myobundles are a useful tool for

investigating causes of muscle weakness and as a platform for testing potential treatments.

Acknowledgements

I would like to acknowledge those who have helped me throughout my time at UCL, without which this project would not have been possible. Thank you to my supervisors Professor Richard Day and Dr Massimiliano Cerletti for their advice, guidance, help, and time over the years. A massive thank you to Dr Tim West, Royal Veterinary College (Hawkshead Campus) for all his patience and help. For demonstrating his force transducer set up, for answering my never-ending basic questions, and for designing and co-creating the electrodes used in this project. Without his help I would have been unlikely to ever figure out how to navigate the myobundle force measurements. Thank you also to Steve Amos, RVC who helped design and fabricated the electrodes that were used in this project.

Thank you to all the members of the applied biomedical engineering group (ABEG) during my time there. Dr. Alex Popov helped me get established during my first rotation, and to Dr Chara Simitzi, Dr Katya Paliashvili and Dr Francesco di Maggio I am thankful for their company and guidance. Dr Annalisa Bettini helped feed my cells on many occasions, let me pinch her reagents when needed, and was always a listening ear. Mar Casajuana Ester, Julia Linke, and Haowei Wang were also great companions during my time at ABEG and occasionally helped me out with reagent changes or checking equipment for which I am grateful.

I would also like to thank those who have given me guidance through the PhD process, including Dr Paul Frankel who gave good advice during my upgrade, and Dr Venkat Reddy who also advised me during my upgrade and beyond. Thank you to the members of the Rockefeller Building confocal unit for their training and technical help, members of the B-made hub in the Bartlett including Martyn Carter who 3D printed the negative moulds for fabrication of the myobundles, Dr Gareth Thompson at Digitimer for advising on the electrode stimulation hardware, and Robert Jones at Linton Instrumentation for his extensive help with understanding the acquisition software and hardware for measuring myobundle force.

A big thank you (and apologies) to all friends and family who have helped support me along the way, and who have listened to me complain copiously when things did not

go to plan. A special thank you to Jack Wickett for sticking by me through the highs and lows of navigating through this work and supporting me from both near and afar.

This project was funded by the Medical Research Council through the UCL-Birkbeck MRC Doctoral Training Partnership.

Table of contents

Declaration **2**

Abstract **3**

Impact statement **4**

Acknowledgements **6**

Table of contents **8**

Table of figures and tables **15**

List of abbreviations **19**

Chapter 1. Introduction **23**

1.1 Skeletal muscle function 23
1.2 Sporadic inclusion body myositis clinical features and diagnosis 25
1.3 Muscle force in sIBM 26
1.4 Comorbidities in sIBM 28
1.5 Non-inflammatory features of sIBM 29
1.6 TDP-43 32
1.7 p62 35
1.8 Inflammatory features of sIBM 38
1.9 Interleukin 1β 40
1.10 Interferon γ 42
1.11 CD8+ T cells 46
1.12 Clinical trials in sIBM 52
1.13 Other idiopathic inflammatory myopathies 55
1.14 Autoantibody anti-NT5c1A 57
1.15 *In vivo* investigations of sIBM 58
1.16 Primary human cell culture 60
1.17 *In vitro* investigations of sIBM 61
1.18 Sestrins 62
1.19 Hypotheses and aims 64

Chapter 2. General methods **67**

2.1 Skeletal muscle-derived cell culture 67

2.2 Treatment of myotubes with IL-1β and IFNγ 68
2.3 Cytotoxicity assay 68
2.4 Immunofluorescent microscopy 69
2.5 TDP-43 localisation 70
2.6 p62 particle analysis 70
2.7 TDP-43 sarcoplasmic aggregate analysis 71
2.8 SDS PAGE and Western blotting 72
2.9 ELISA 76
2.10 Statistics and figure preparation 77
Chapter 3. Basal characterisation of myogenic cells 79
3.1 Introduction 79
3.1.1 Myogenesis 79
3.1.2 TDP-43, p62 and sestrins in myogenesis 81
3.1.3 Aims and hypotheses 81
3.2 Methods 83
3.2.1 Cell culture 83
3.2.2 Acetylcholinesterase assay 83
3.2.3 Myofusion index and nuclei per myotube 83
3.2.4 SDS PAGE and Western blotting 84
3.3 Results 85
3.3.1 Basic donor characterisation and myofusion index of myogenic donors 85
3.3.2 Acetylcholinesterase expression was not different between undifferentiated and differentiated myogenic cells 85
3.3.3 Myotubes were capable of spontaneously contracting 85
3.3.4 Myosin heavy chain expression, number of nuclei per myotube, and myofusion index was higher during differentiation than proliferation 86
3.3.5 TDP-43 localisation was consistent and protein levels remained constant during myogenesis 90
3.3.6 p62 levels did not change during differentiation 90
3.3.7 Sestrin-2 was highest on day 7 of differentiation 90
3.3.8 Sestrin-1 protein levels were highest on day 4 of myogenesis 91
3.4 Discussion 95
3.4.1 Myogenic differentiation 96
3.4.2 TDP-43, p62, and sestrins during myogenesis 98
3.4.3 Summary 99

Chapter 4. Effect of IL-1β and IFNγ on myotubes 101

4.1 Introduction 101

4.1 Aims and hypotheses 101

4.2 Methods 103

4.2.1 Treatment of myotubes with IL-1β and IFNγ 103

4.2.2 Cytotoxicity assay 103

4.2.3 Immunofluorescent microscopy 103

4.2.4 TDP-43 localisation with IL-1β + IFNγ treatment 103

4.2.5 p62 puncta and TDP-43 sarcoplasmic aggregate analysis 103

4.2.6 Nuclear p62 puncta analysis 103

4.2.7 SDS PAGE and Western blotting 104

4.3 Results 105

4.3.1 IL-1β and IFNγ alone or in combination are not cytotoxic to cultured myotubes 105

4.3.2 IL-1β and IFNγ combined caused increased p62 puncta size 105

4.3.3 TDP-43 sarcoplasmic aggregation was not affected by IL-1β and IFNγ combined 106

4.3.4 TDP-43 subcellular localisation was not altered by treatment with IL-1β and IFNγ combined 109

4.3.5 p62 puncta size or frequency were not affected by IL-1β or IFNγ treatment individually 110

4.3.6 TDP-43 sarcoplasmic aggregation was not affected by IL-1β or IFNγ 111

4.3.7 TDP-43 subcellular localisation was not affected by IL-1β or IFNγ 113

4.3.8 p62 expression was increased with IL-1β and LC3II/LC3I ratio was increased with IL-1β+IFNγ 115

4.3.9 p62 nuclear puncta size or frequency was not affected by IL-1β or IFNγ 118

4.3.10 Sestrin-2 protein levels were increased with IFNγ, but not IL-1β or combined IL-1β and IFNγ treatment 119

4.3.11 Control conditions with IL-1β+IFNγ or IL-1β/IFNγ experiments were comparable 119

4.4 Discussion 121

4.4.1 TDP-43 122

4.4.2 LC3 125

4.4.3 IL-1β and p62 126

4.4.4 IFNγ or IL-1β+IFNγ and p62 128

4.4.5 Sestrins 129

4.4.6 Summary 130
Chapter 5. Effect of macrophage conditioned medium on myotubes 133
5.1 Introduction 133
5.1.1 Aims and hypothesis 135
5.2 Methods 136
5.2.1 THP-1 cell culture 136
5.2.2 Treatment of myogenic cells with macrophage conditioned medium 136
5.2.3 Cytotoxicity assay 136
5.2.4 Treatment of THP-1 cells with myotube conditioned medium 137
5.2.5 p62 particle analysis, TDP-43 sarcoplasmic aggregate analysis, and TDP-43 localisation 138
5.2.6 ELISA for IL-6, IL-12 p70, IL-1β, and TNFα 138
5.2.7 SDS PAGE and Western blotting 138
5.3 Results 139
5.3.1 Morphology, IL-6 and TNFα levels were different between M(PMA) and M(IFNγLPS) macrophages 139
5.3.2 Macrophage conditioned media was not cytotoxic to myotubes 139
5.3.3 Macrophage conditioned medium did not cause p62 aggregation 139
5.3.4 Macrophage conditioned medium did not cause TDP-43 aggregation 141
5.3.5 TDP-43 subcellular localisation was not affected by macrophage conditioned medium 142
5.3.6 Macrophage conditioned medium did not affect sestrin-1 or sestrin-2 expression 145
5.3.7 Treating macrophages with myotube differentiation medium abrogated cytokine release 146
5.4 Discussion 149
5.4.1 p62, TDP-43, and sestrins 150
5.4.2 Myotube secretory factors 150
5.4.3 THP-1 cells as model macrophages 152
5.4.4 Summary 153
Chapter 6. Effect of TALL-104 conditioned medium and co-culture on myotubes ... 155
6.1 Introduction 155
6.1.1 CD8+ T cells in sIBM 155
6.1.2 Natural killer cells 155
6.1.3 TALL-104 cell line 156

6.1.4 Aims and hypothesis 158
6.2 Methods 159
6.2.1 TALL-104 cell culture 159
6.2.2 Collection of TALL-104 conditioned medium 159
6.2.3 Treatment of myotubes with TALL-104 conditioned medium and cytotoxicity assay 159
6.2.4 TALL-104 myotube coculture and cytotoxicity assay 160
6.2.5 IFNγ and TNFα ELISA of cocultured TALL-104 160
6.2.6 TDP-43 localisation with TALL-104 conditioned medium and coculture 160
6.2.7 TDP-43 aggregate and p62 puncta analysis with TALL-104 conditioned medium and coculture 160
6.2.8 Treatment of TALL-104 with myotube conditioned medium 161
6.3 Results 162
6.3.1 TALL-104 conditioned medium was not cytotoxic to myotubes 162
6.3.2 Inflammatory primed myotubes may affect activation of TALL-104 cells 162
6.3.3 p62 puncta frequency or size was not affected by TALL-104 secreted factors 164
6.3.4 TDP-43 aggregates were more likely in myotubes treated with TALL-104 CM, but aggregate size or frequency was not affected 164
6.3.5 TDP-43 subcellular localisation was not affected by TALL-104 secreted factors 166
6.3.6 TALL-104 coculture was cytotoxic to myotubes 168
6.3.7 Coculturing TALL-104 with myotubes lead to increased IFNγ and TNFα secretion from TALL-104 at higher E:T ratio 168
6.3.8 TALL-104 cells attached to and invaded myotubes 171
6.3.9 TALL-104 coculture did not affect p62 puncta size or frequency 171
6.3.10 TDP-43 aggregates were less likely in TALL-104 cocultured myotubes, but TDP-43 aggregate size or frequency was not affected 171
6.3.11 TDP-43 subcellular localisation was affected by TALL-104 coculture 174
6.4 Discussion 177
6.4.1 TALL-104 cytotoxicity and activity with myotubes 177
6.4.2 Secreted factors from TALL-104 179
6.4.3 p62 180
6.4.4 A role for cytotoxic immune cells in TDP-43 localisation? 181
6.4.5 Summary 183
Chapter 7. Myobundle culture with cytokine treatment or TALL-104 coculture 185

7.1 Introduction 185
7.1.1 3D models of skeletal muscle 185
7.1.2 Aims and hypotheses 188
7.2 Methods 190
7.2.1 CAD positive moulds 190
7.2.2 Generation of silicone moulds for myobundle culture 190
7.2.3 Preparation of Velcro® anchors and Cerex® frames 191
7.2.4 Processing of silicone moulds and anchors/frames for cell culture 192
7.2.5 Myobundle preparation and culture 192
7.2.6 Myobundle treatment 193
7.2.7 Set up of organ bath hardware and software 194
7.2.8 Measurement of contractile myobundle force 195
7.2.9 Analysis of active force 195
7.2.10 Analysis of force kinetics 196
7.2.11 Embedding and sectioning myobundles 198
7.2.12 Preparation of myobundle sections for immunofluorescent staining 198
7.2.13 Immunofluorescent labelling of myobundle sections 199
7.2.14 Analysis of myobundle sections 199
7.3 Results 201
7.3.1 Discontinuation of Velcro mould design 201
7.3.2 Myobundles exhibited standard responses to voltage and frequency changes 201
7.3.3 Active force was not affected by IL-1β or IFNγ treatment 203
7.3.4 Tetanus kinetics were affected by IL-1β and IFNγ combined treatment 203
7.3.5 Cross sectional area or myotube area was not affected by cytokine treatment 205
7.3.6 IFNγ treatment decreased actinin striation frequency of myotubes in myobundles 205
7.3.7 Active twitch or tetanic force was not altered by TALL-104 coculture 208
7.3.8 TALL-104 coculture did not affect tetanus kinetics 209
7.3.9 TALL-104 coculture did not affect fatigue responses 210
7.3.10 Cross sectional area was not affected by TALL-104 coculture but myotube area may decrease 211
7.3.11 Few TALL-104 cells infiltrated into myobundles 212
7.3.12 Actinin striation frequency was not affected by TALL-104 coculture 214
7.4 Discussion 215

7.4.1 Myobundles responded in a physiological manner with similar parameters to previous results 215
7.4.2 IL-1β and IFNγ treatment of myobundles 217
7.4.3 TALL-104 coculture with myobundles 220
7.4.4 Fatigue in sIBM 223
7.4.5 Previous models of muscle weakness in sIBM 224
7.4.6 Summary 226
Chapter 8. General discussion and future work 229
8.1 Discussion 229
8.1 Experimental considerations 229
8.2 Sestrins 232
8.3 Inflammatory cytokines 233
8.4 Inflammatory cells 233
8.5 A role for TDP-43 “pathology” in healthy muscle? 235
8.6 Considerations for future preclinical sIBM research 237
8.7 Summary 239
8.2 Future work 240
8.2.1 IL-1β and IFNγ signalling 240
8.2.2 Analysis of autophagy with IL-1β+IFNγ 240
8.2.3 TDP-43 protein detection in the insoluble fraction and subcellular fractionation 240
8.2.4 Testing mitochondrial structure and function 241
8.2.5 Macrophage coculture 241
8.2.6 Combined treatment of conditioned media 242
8.2.7 Expanding coculture of myobundles with cytotoxic cells 242
8.2.8 Analysis of calcium handling in myobundles 243
8.2.9 TDP-43 and p62 analysis in myobundles 243
8.2.10 TDP-43/p62 overexpression 244
8.2.11 Manipulation of sestrins in cytotoxic T cells 244
References 245
Appendix 275

Table of figures and tables

Declaration 2

Abstract 3

Impact statement 4

Acknowledgements 6

Table of contents 8

Table of figures and tables 15

List of abbreviations 19

Chapter 1. Introduction 23

Figure 1.1 Structure of the sarcomere during relaxation and contraction. 24

Figure 1.2 Structure of skeletal muscle fibre. 27

Figure 1.3 Pathological features of sIBM. 30

Figure 1.4 Functions of TDP-43. 34

Figure 1.5 Role of p62 in autophagy. 37

Figure 1.6 p62 in the ubiquitin proteasome system. 39

Figure 1.7 Mechanisms of IFNγ action in skeletal muscle. 45

Figure 1.8 Activation of CD8 T cells. 48

Figure 1.9 Mechanisms of cytotoxic T cell mediated cell death. 49

Chapter 2. General methods 67

Figure 2.1 Diagram of TDP-43 and p62 analysis. 72

Table 2.1 Antibodies for Western blotting. 75

Chapter 3. Basal characterisation of myogenic cells 79

Figure 3.1 Process of myogenic differentiation. 80

Figure 3.2 Muscle cell donor characteristics. 87

Figure 3.3 Acetylcholinesterase expression was not different between myoblasts and myotubes. 88

Figure 3.4 Spontaneous contraction of myotubes in culture. 88

Figure 3.5 Differentiation over time in myogenesis. 89

Figure 3.6 Myosin heavy chain during myogenesis. 89

Figure 3.7 Examples of TDP-43 localisation classification. 91
Figure 3.8 TDP-43 localisation and expression during myogenesis. 92
Figure 3.9 p62 during myogenesis. 93
Figure 3.10 Sestrin-2 and sestrin-1 follow different expression patterns during myogenesis. 94
Chapter 4. Effect of IL-1β and IFNγ on myotubes 101
Figure 4.1 Cytotoxicity of IL-1β and IFNγ alone or in combination on myotubes. 106
Figure 4.2 TDP-43 and p62 staining with IL-1β and IFNγ. 107
Figure 4.3 p62 puncta size was increased with IL-1β+IFNγ. 108
Figure 4.4 Examples of TDP-43 and p62 aggregates in myotubes. 108
Figure 4.5 TDP-43 aggregate size or frequency was not affected by IL-1β+IFNγ... 109
Figure 4.6 IL-1β+IFNγ does not affect TDP-43 localisation. 111
Figure 4.7 TDP-43 and p62 in IL-1β or IFNγ treated myotubes. 112
Figure 4.8 p62 puncta frequency or size was not affected by IL-1β or IFNγ treatment. 113
Figure 4.9 TDP-43 aggregate size or frequency was not affected by IL-1β or IFNγ. 114
Figure 4.10 IL-1β or IFNγ does not affect TDP-43 localisation. 116
Figure 4.11 p62 expression was increased with IL-1β and LC3II/LC3I ratio increased with IL-1β+IFNγ. 117
Figure 4.12 p62 nuclear puncta were not affected by IL-1β or IFNγ treatment. ... 118
Figure 4.13 Sestrin-2 and sestrin-1 expression with IL-1β and IFNγ treatment. ... 120
Chapter 5. Effect of macrophage conditioned medium on myotubes 133
Figure 5.1 Schematic of method for secreted factors from macrophages treated with myotube conditioned medium. 137
Figure 5.2 Characterisation of macrophage inflammatory priming. 140
Figure 5.3 Cytotoxicity of macrophage conditioned medium to myotubes. 141
Figure 5.4 Images of p62 and TDP-43 in macrophage conditioned medium-treated myotubes. 142
Figure 5.5 p62 puncta analysis and protein expression was not affected by macrophage conditioned medium. 143
Figure 5.6 TDP-43 aggregation or protein expression was not affected by macrophage secreted factors. 144

Figure 5.7 TDP-43 localisation with macrophage conditioned medium. 145

Figure 5.8 Sestrin-2 or sestrin-1 protein expression was not altered by conditioned medium from M(PMA) or M(IFNγLPS) macrophages. 147

Figure 5.9 Inflammatory primed myotubes caused macrophages to secrete more IL-6 than unprimed myotubes. 148

Chapter 6. Effect of TALL-104 conditioned medium and co-culture on myotubes ... 155

Figure 6.1 Cytotoxicity of TALL-104 conditioned medium on myotubes. 163

Figure 6.2 Effect of inflammatory conditioned myotube medium on TALL-104 IFNγ secretion. 163

Figure 6.3 p62 and TDP-43 with TALL-104 conditioned medium. 165

Figure 6.4 TALL-104 conditioned medium did not affect p62 puncta size or frequency. 165

Figure 6.5 TALL-104 conditioned medium did not affect TDP-43 aggregate frequency, size, or colocalisation with p62. 166

Figure 6.6 TDP-43 subcellular localisation was not affected by TALL-104 conditioned medium. 167

Figure 6.7 TALL-104 coculture was cytotoxic to myotubes. 169

Figure 6.8 IFNγ and TNFα secretion from TALL-104 cells co-cultured with myotubes. 170

Figure 6.9 Attachment and invasion of myotubes by TALL-104 cells. 172

Figure 6.10 p62 and TDP-43 in myotubes treated with IL-2 control or TALL-104 coculture. 173

Figure 6.11 Coculture of TALL-104 cells with myotubes did not affect p62 particle size or frequency. 173

Figure 6.12 TDP-43 aggregate frequency or size was not affected by TALL-104 coculture. 174

Figure 6.13 TDP-43 subcellular localisation was affected by TALL-104 coculture. 176

Chapter 7. Myobundle culture with cytokine treatment or TALL-104 coculture 185

Figure 7.1 Design and fabrication of negative and positive Velcro and Cerex myobundle moulds. 191

Figure 7.2 Myobundle attached to Cerex frame. 194

Figure 7.3 Schematic of myobundle preparation and stimulation. 196

Figure 7.4 Examples of force characteristics. 197

Figure 7.5 Force characteristics of myobundles. 202
Figure 7.6 Myobundles respond to acetylcholine stimulation. 202
Figure 7.7 Active twitch and tetanus force with IL-1β, IFNγ or combined. 203
Figure 7.8 Tetanus kinetics with IL-1β, IFNγ or combined. 204
Figure 7.9 Cross sectional area and myotube area of myobundles was not affected by cytokine treatment. 206
Figure 7.10 Striated sarcomeric alpha actinin was lower with IFNγ and IL-1β+IFNγ treatment. 207
Figure 7.11 Active tetanus force with TALL-104 coculture with shaking. 208
Figure 7.12 Active twitch or tetanus force was not affected by TALL-104 coculture. 209
Figure 7.13 Force kinetics were not affected by TALL-104 coculture. 210
Figure 7.14 Fatigue with continuous tetanic stimulation was not affected by TALL-104 coculture. 212
Figure 7.15 TALL-104 coculture does not affect cross sectional area but may affect myotube area. 213
Figure 7.16 Sarcomeric alpha actinin striations in myotubes were not affected by TALL-104 coculture. 214
Table 7.1 Models for sIBM strength testing. 226
Chapter 8. General discussion and future work 229
References 245
Appendix 275
Appendix Table 0.1. Myogenic donors used by figure. 278
Appendix Figure 0.1 Uncropped blot images. 293
Appendix Figure 0.2 Lack of nuclear TDP-43 in early passage myotubes. 294

List of abbreviations

AB	Amyloid beta
AChE	Acetylcholinesterase
ALS	Amyotrophic lateral sclerosis
ANOVA	Analysis of variance
APC	Antigen presenting cell
APP	Amyloid precursor protein
ATP	Adenosine triphosphate
bFGF	basic Fibroblast growth factor
CAD	Computer-aided design
CaMKIV	Calcium/calmodulin-dependent kinase 4
CC	Co-culture
CCL	Chemokine C-C ligand
CCR	C-C chemokine receptor
CD	Cluster of differentiation
CM	Cell mask OR conditioned media
COX	Cytochrome C oxidase
CSA	Cross sectional area
CTD	C terminal domain
CTL	Cytotoxic T lymphocyte
DAPI	4',6-diamidino-2-phenylindole
DMEM	Dulbecco's modified eagle's medium
DMSO	Dimethyl Sulfoxide
DNA	Deoxy-ribonucleic acid
DTNB	5,5'-dithiobis(2-nitrobenzoic acid)
E:T	Effector to target ratio
ER	Endoplasmic reticulum
FACS	Fluorescently activated cell sorting
FBS	Foetal bovine serum
FTLD	Frontotemporal lobar disease
GAPDH	Glyceraldehydte-3-phosphate
GAS	Gamma interferon activated sites
HCS	High content screening
HLA	Human leukocyte antigen
HSKMDC	Human skeletal muscle derived cells
HSMM	Human skeletal muscle myoblasts
(s)IBM	(sporadic) inclusion body myositis
IFNGR	Interferon gamma receptor
IFNγ	Interferon gamma
IIM	Idiopathic immune myopathy
IL-1β	Interleukin 1 beta
IL-1R1	Interleukin 1 receptor type 1
IL-1Ra	Interleukin 1 receptor antagonist

IL-6	Interleukin 6
IMNM	Immune-mediated necrotising myositis
iPSC	Induced pluripotent stem cell
IQR	Interquartile range
JAK	Janus kinase
KLRG1	Killer cell lectin like receptor G1
LC3	Microtubule-associated protein 1A/1B-light chain 3
LDH	Lactate dehydrogenase
LGL	Large granular lymphocyte
LPS	Lipopolysaccharide
MACS	Magnetically-activated cell sorting
MAPK	Mitogen-activated protein kinase
MFI	myofusion index
MHC	Major histocompatibility complex, or myosin heavy chain
mTOR	Mammalian target of rapamycin
NF-κB	Nuclear factor kappa B
NK	Natural killer (cell)
NKT	Natural killer T (cell)
NT5c1A	cytosolic 5'-nucleotidase 1A antibody
NTD	N-terminal domain
PAGE	polyacrylamide gel electrophoresis
(D)PBS	(Dulbecco's) phosphate buffered saline
PDMS	Polydimethyl siloxane
PFA	Paraformaldehyde
PVDF	Polyvinylidene difluoride
RIPA	radio immunoprecipitation assay
RNA	Ribonucleic acid
ROS	Reactive oxygen species
RPMI	Roswell park memorial institute
SAA	Sarcomeric alpha actinin
SDS	Sodium dodecyl sulphate
SEM	Standard error of the mean
shRNA	Short hairpin ribonucleic acid
STAT	Signal transducers and activators of transcription
T-ALL	T cell acute lymphoblastic leukaemia
TBS-T	Tris buffered saline-tween 20
TDP-43	TAR (transactive response) DNA binding protein 43
Tem	T effector memory
Temra	T effector memory re-expressing CD45RA
TIR	Toll-interleukin receptor
TNF	Tumour necrosis factor
TRAIL	Tumour necrosis factor related apoptosis-inducing ligand
UPS	Ubiquitin proteasome system
VCP	Valosin-containing protein

xg	Times gravity

Chapter 1: Introduction

Chapter 1. Introduction

1.1 Skeletal muscle function

One of the main functions of skeletal muscle is facilitating movement of the body. Within skeletal muscle, regularly repeating structures called sarcomeres are the functional unit. Sarcomeres are composed of actin and myosin, as well as sarcomeric accessory proteins including troponin and tropomyosin. Skeletal muscle contraction operates via the sliding filament theory. During rest, the troponin-tropomyosin complex blocks the myosin binding sites on actin. During excitation-contraction coupling, calcium ions enter the sarcoplasm which bind to troponin, revealing myosin binding sites. The myosin heads then bind actin in cross-bridges and undergo a conformational change that requires release of inorganic phosphate formed by hydrolysis of ATP, pulling themselves along the actin filaments in a power stroke. Detachment of myosin head from actin requires ATP to initiate a new powers stroke (1, 2). Figure 1.1 highlights the structure of a sarcomere during relaxation and contraction, obtained from (2).

Excitation contraction coupling is the process by which the motor neurone transmits a signal for skeletal muscle contraction. At the motor end plate, the action potential in the motor neurone causes release of acetylcholine into the neuromuscular junction. Acetylcholine binds nicotinic acetylcholine receptors on the motor end plate on the sarcolemma of skeletal muscle. Activation of the acetylcholine receptors by its ligand causes the receptor's associated cation channel to open, allowing passage of Na^+ ions into the sarcoplasm which depolarises the motor end plate in an end plate potential. This potential flows from the end plate to the adjacent resting muscle causing activation of voltage gated Na^+ channels for further propagation of the signal (3). The action potential propagates down T tubules, specialised invagination of the sarcolemma that continue towards the centre of the muscle fibre and align closely with the sarcoplasmic reticulum, which itself is aligned closely to the I and A bands of sarcomeres (4) (Figure 1.2). Action potentials travelling through the T-tubule activate

voltage-gated dihydropyridine receptors on the T-tubule, which causes opening of ryanodine receptors on the terminal cisternae of the sarcoplasmic reticulum which triggers efflux of calcium that is stored in the terminal cisternae into the sarcoplasm (3, 5). This calcium release then initiates the power stroke as described above. The action of the neuromuscular junction can be recapitulated by stimulating isolated skeletal muscle with electrodes in organ bath set ups (6).

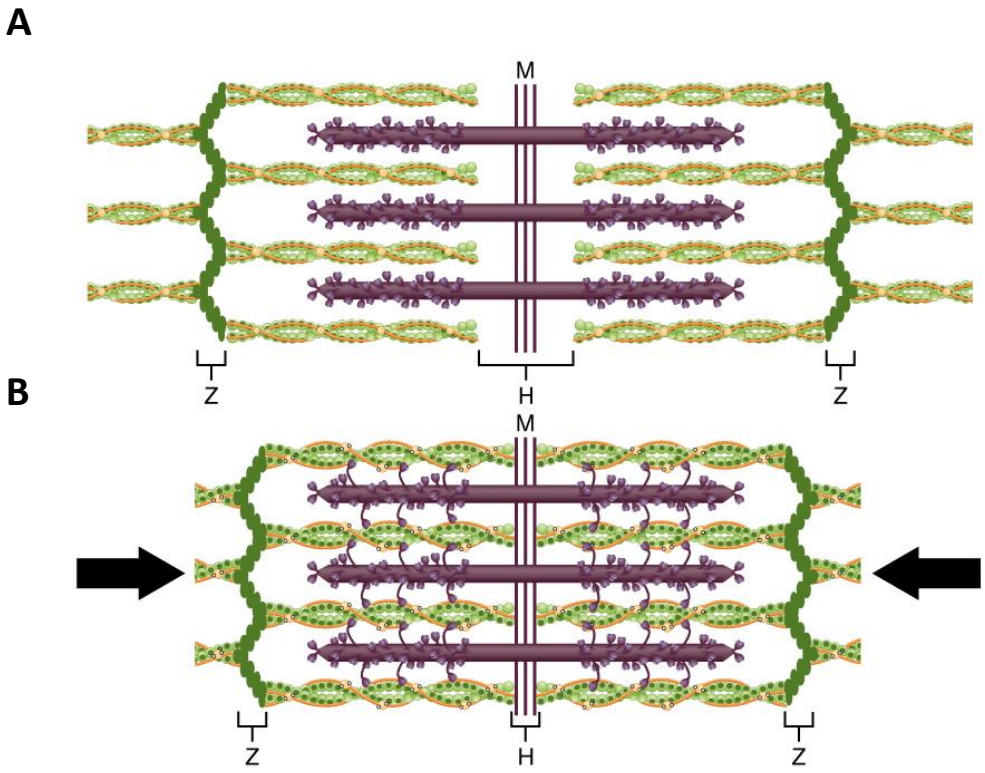

Figure 1.1 Structure of the sarcomere during relaxation and contraction.

The sarcomere is the functional unit of skeletal muscle contained within the Z-bands. The image shows sarcomeric structure during (A) relaxation and (B) contraction. The sarcomere is composed of thick myosin filaments (purple) and thin actin filaments (light green). The sarcomere is composed of zones. The H-zone contains thick myosin filaments only. The M-line contains cytoskeletal elements including myomesin and obscurin. During relaxation, troponin and tropomyosin (yellow, attached to actin) block the myosin binding sites. During contraction, the Z bands move closer and the H zone becomes smaller. Available under a creative commons licence, adapted from: (2).

1.2 Sporadic inclusion body myositis clinical features and diagnosis

Sporadic inclusion body myositis (sIBM) is the most common form of myositis in people over the age of 50 (7, 8). sIBM belongs to a group of conditions called inflammatory myopathies which also includes dermatomyositis, polymyositis, and necrotising autoimmune myopathy. The prevalence of sIBM is difficult to estimate because of its rarity. In those over the age of 50 prevalence is 3.5-18.2 per 100,000 (9-11). However, the prevalence may be higher due to under-diagnosis and misdiagnosis as related conditions, especially polymyositis. The combination of the rarity of the disease and the difficulty of accurate diagnosis causes a delay between disease onset and diagnosis on average of 5 years (12).

Symptoms of sIBM include muscle weakness often beginning in the finger flexors and quadriceps, with presentation usually asymmetrical affecting the non-dominant limb more. Patients have difficulty standing and walking, are more prone to falls, and have reduced grip strength. The disease is slowly progressive with symptoms worsening over time, and patients may require mobility aids such as wheelchairs. Muscle strength declines at a rate of between 3.5-28 % per year depending on the assessment method used. The average time to requiring mobility aids is 10 years for a walking stick (13) and 10-15 years for a wheelchair (10, 13). A common progressive symptom is dysphagia, which occurs in up to 40-86 % of cases and can be a cause for mortality (13-15). At present, there is no effective treatment for sIBM patients.

Diagnosis of sIBM is currently based on a combination of clinical presentations and abnormalities in muscle biopsies. Three major sets of diagnostic criteria for sIBM have been used. One of the most widely used diagnostic methods relies on histological biopsy observations as part of the Griggs criteria, where a definite diagnosis is defined as having mononuclear cell invasion into non-necrotic fibres, vacuolated fibres and intracellular amyloid deposits/15-18nm tubofilaments. A possible diagnosis in the Griggs criteria includes mononuclear infiltration without other histological findings, but with clinical features such as muscle weakness in finger flexors and quadriceps with age at diagnosis over 30 (16). However these histological features present differently depending on time of diagnosis and area of biopsy, which could potentially lead to

underdiagnosis (14). Furthermore, the sensitivity of using these features of sIBM for diagnosis has been called into question (17), as some histological findings are found with very low frequency in affected fibres. The Neuromuscular Disease Centre at the MRC criteria developed in 2008/2009 (18) included the Griggs criteria as pathologically defined IBM. It also included a diagnostic classification that necessitates clinical findings, termed clinically defined IBM. This includes pathological features of mononuclear invasion or increased MHC I or rimmed vacuoles, dropping the need for amyloid deposits or tubofilaments and not requiring all pathological findings at once. Clinically defined IBM also includes duration of weakness over 12 months, age at diagnosis over 35, and relative weakness higher in finger flexors and knee extensors. This set or criteria also includes a possible IBM diagnosis based on presentation of some but not all features of pathologically and clinically defined IBM. The most recent diagnostic criteria for sIBM is the ENMC criteria which classifies sIBM as either clinico-pathologically defined, clinically defined, or probable (19), following a similar methodology to the MRC criteria. The ENMC includes a higher age at onset of over 45 years, the need for either as opposed to both knee extensor and finger flexor weakness, and a serum creatine kinase cut off in the clinically defined group. All three groups in the ENMC criteria also include assessment of protein accumulation, either of amyloid or other proteins including p62 and TDP-43.

1.3 Muscle force in sIBM

The main symptom of sIBM is progressive muscle weakness that usually begins in the quadriceps and finger flexors. It is not known what causes the weakness in sIBM. One way in which muscle strength is assessed is manual muscle testing (MMT). The function of different muscles is graded by the observer on a scale based on how the muscle performs against gravity or against force applied by the examiner (20). In a 12-year follow-up investigation of sIBM patients, MMT scores decreased from initial observation, with a mean decline of 3.5 % per year (21). Another method of measuring muscle strength is dynamometry that quantitatively measures muscle strength (22). The average knee extension strength in 22 sIBM patients was found to be approximately 45 Newton metres (Nm), which the investigators noted is much less

than the approximate 130 Nm observed for healthy older adults. However, no direct comparisons with control cases was undertaken (23). A retrospective review of 53 sIBM patients found a decrease in knee extensor strength was indicative of the need for mobility devices such as canes (24). Handheld dynamometry revealed the mean rate of strength decline per year was 5.4 % with an initial reading of 2996 ± 913 N vs 1473 ± 753 N after 12 years (21).

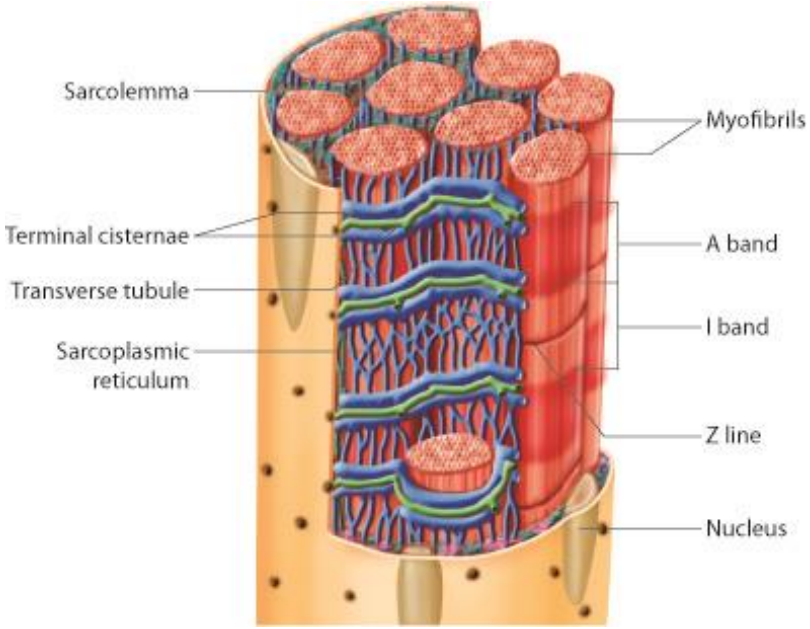

Figure 1.2 Structure of skeletal muscle fibre. Transverse tubules (T-tubules) extend from the sarcolemma into the centre of the fibre and are closely aligned to the sarcoplasmic reticulum. Source: (25).

Muscle strength can be influenced by muscle-extrinsic considerations such as neuronal and tendonous factors as well as intrinsic muscle parameters such as muscle size and fibre-type composition (26, 27). Electromyography is a technique used to record electrical activity in muscle, and can be used to distinguish if muscle weakness is caused by neurogenic or myopathic factors (28). Electromyography of sIBM patients shows high amplitude and long duration of motor unit potentials (29-31) which can

indicate reinnervation after denervation (29), or may be due to remodelling of motor units after muscle degeneration and regeneration (32). Despite these findings that may highlight a neurogenic component of weakness, sIBM is considered a myopathic disease (31, 33) with denervation not being a main contributor to skeletal muscle weakness.

1.4 Comorbidities in sIBM

sIBM is associated with a modest decrease in survival, with the most common cause of mortality being respiratory failure and pneumonia (10, 34-36), mostly caused by dysphagia. Dysphagia is one of the most common comorbidities in sIBM, especially later in the disease progression. In a case series of 18 sIBM patients, dysphagia was present in 67 % (37). Peripheral neuropathy is also a common comorbidity in sIBM with 36 % of 50 sIBM patients experiencing this condition (34). sIBM patients have been found to have an increase in cross sectional area of their sciatic nerve compared to healthy controls (38).

Other common comorbidities include hypertension, hyperlipidemia, and diabetes mellitus (37, 39). However, a separate study found no difference in the occurrence of diabetes mellitus in sIBM compared to age matched non-sIBM controls, therefore the association between sIBM and diabetes is currently unclear (34). It is suggested care needs to be taken with prescriptions in sIBM as corticosteroids (prescribed in other inflammatory myopathies including polymyositis) can exacerbate hypertensive problems (37). Case reports have described the coexistence of sIBM with some rare conditions. For example, some sIBM patients have been identified with concomitant Sjögren's syndrome (34, 40, 41) or systemic sclerosis (42-44). Other organ systems may also be involved. For example, 59 % of sIBM patients in a small cohort study had weakness within the muscles controlling ventilation based on forced vital capacity results (45).

sIBM has been associated with T cell large granular lymphocytic (LGL) leukaemia, a rare disease involving indolent clonal expansion of cytotoxic T cells that are large in size with abundant cytoplasm (46). In a study of 38 patients with sIBM, it was found that 58

% met the diagnostic criteria for T cell large granular lymphocytic leukaemia with clonal expansion of large granular T cells (47), suggesting some CD8 cells in sIBM may be neoplastic in nature.

1.5 Non-inflammatory features of sIBM

The pathological features of sIBM are illustrated in Figure 1.3. These features can broadly be classified as non-inflammatory/degenerative or inflammatory. Non-inflammatory features of sIBM include rimmed vacuoles, which are areas of localised degeneration in muscle fibres (48). Inclusion bodies are also observed, which are protein aggregates within the sarcoplasm and rimmed vacuoles. Many different proteins have been identified as aggregated within inclusion bodies (49), and 213 proteins were found upregulated within rimmed vacuoles compared to non-vacuolated sIBM muscle regions (50). This includes proteins previously described in sIBM such as TDP-43 and p62. The presence of TDP-43 and p62 as non-inflammatory features of sIBM is described in Section 1.6 and Section 1.7 respectively. Rimmed vacuoles contained proteins involved in the extracellular matrix, sarcolemma, and actin dynamics, with the most represented pathway being proteins involved in autophagy and protein folding (50). Ubiquitin is found aggregated in sIBM muscle fibres (51) suggesting disruption of protein degradation mechanisms such as the ubiquitin proteosome system (UPS) and autophagy. Despite the presence of rimmed vacuoles being a diagnostic factor of the Griggs criteria, and the high specificity this feature has for sIBM, the sensitivity of rimmed vacuoles in sIBM fibres can be low. In haematoxylin and eosin stained sections, the percentage of vacuolated fibres was 0.2 – 8.7 % with a mean of 3.3 % (52). In 20 % of sIBM cases, rimmed vacuoles may not be observed (53), and are sometimes only detectable after multiple muscle biopsies, making diagnosis of sIBM when analysing for rimmed vacuoles difficult (54).

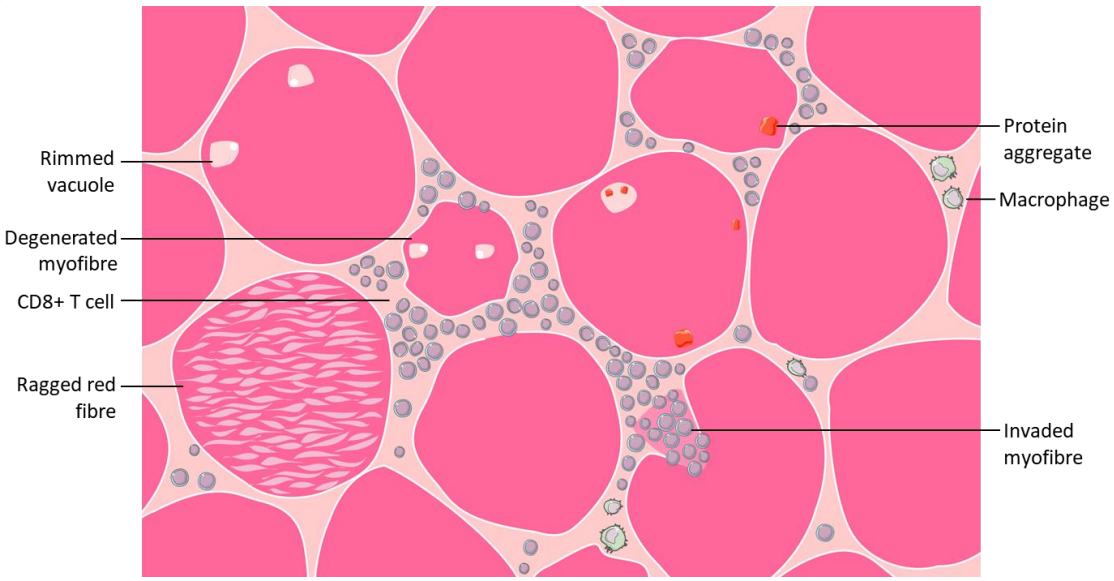

Figure 1.3 Pathological features of sIBM. Some myofibres show degeneration and are smaller in size. Rimmed vacuoles of localised areas of myofibre degeneration are observed, which can contain protein aggregates. Mitochondrial network abnormalities show as ragged red fibres under Gömöri trichrome histological staining. There is a strong presence of infiltrating immune cells that are largely composed of cytotoxic T cells, and to a lesser extent other immune cells such as macrophages. Immune cells infiltrate into the endomysium surrounding muscle fibres and invade into the muscle fibres themselves.

Another protein reported to be aggregated in inclusion bodies is amyloid-β (55-57). However, the importance of amyloid-β in sIBM pathology has been called into question, with its role in sIBM suggested to be overstated (58). The presence of amyloid β aggregates in sIBM myofibres may be low, with some studies showing as low as between 0 (59) and 0.4 % (60) of myofibres containing amyloid deposits using different methods. On the other hand, amyloid β was found over-represented in rimmed vacuoles compared to other areas of the sarcoplasm (50). Some investigations of amyloid β in sIBM have relied on detection methods that do not differentiate amyloid β from its precursor protein (amyloid precursor protein, APP), which may be an important distinction as APP may be detected in regenerating myofibres in many muscle diseases (61, 62).

Dysfunctional mitochondria are also observed in sIBM as ragged red fibres (63) showing increase in mitochondrial volume and number (64), and cytochrome c oxidase (COX)-negative but succinate dehydrogenase (SDH) positive fibres fibres (65). COX is also known as complex IV and is part of the electron transport chain in mitochondria (66) whilst SDH, also known as complex II, is part of both the Krebs cycle and the respiratory chain and functions to feed electrons to the electron transport chain (67). COX genes are encoded by the mitochondrial genome whilst SDH is encoded by the nuclear genome, and thus COX- SDH+ fibres may show defects in mitochondrial DNA (68). Indeed, deletions in mitochondrial DNA are found in affected COX deficient fibres (69, 70). The deletion load of *MT-ND4*, a gene encoding the NADH-ubiquinone oxidoreductase chain 4 protein of complex I (71) was higher in COX deficient compared to COX normal fibres in sIBM (70). The number of T lymphocytes in muscle tissue correlated with the amount of respiratory deficient fibres identified, however T lymphocytes were not always directly associated with respiratory deficient fibres (70).

Muscle-intrinsic pathology can be observed including variable diameter of muscle fibres with observable atrophy and some necrosis (45). The mean fibre diameter has been reported to be lower in sIBM fibres compared to healthy control (72). Further, sIBM muscle contains increased connective and adipose tissue (45), which may occur due to prolonged muscle damage. There is also an upregulation of MHC I (major histocompatibility complex I) on muscle fibres (73-75), suggesting antigen presentation of skeletal muscles which may contribute to the immune involvement.

sIBM is not a genetic disease with Mendelian inheritance, but certain polymorphisms are associated with sIBM susceptibility. The International Myositis Genetics Consortium (MYOGEN) has performed large scale genetic studies of inflammatory myopathy patients using Illumina Immunochip genotyping arrays. Genetic studies of sIBM have been reviewed by Nagy *et al* (76). MYOGEN data has revealed that in sIBM patients compared to controls, the HLA region was most strongly associated with sIBM, but HLA genotypes were not associated with age of disease onset (77). Targeted whole exome sequencing of *VCP* (valosin containing protein) and *SQSTM1* (p62) found 7/181 sIBM patients had missense variants in these genes. Two of the variants, one

each for *SQSTM1* and *VCP*, were overexpressed in sIBM compared to control (78). VCP missense mutations have also been found in other studies (79). Deep sequencing of mitochondrial DNA (mtDNA) revealed sIBM patients had increased levels of large duplications and deletions in the mitochondrial genome, which was associated with higher levels of heteroplasmy (more than one mtDNA type) (80). Recently, the presence of sex chromosome aneuploidy in myositis patients compared to healthy controls was investigated. It was found that more males with sIBM had XXY (Klinefelter syndrome) than healthy controls and the known occurrence rate of Klinefelter syndrome in the general population (81).

1.6 TDP-43

Trans-activation response (TAR) DNA binding protein 43 (TDP-43) is a DNA/RNA binding protein that belongs to the heterogenous nuclear ribonucleoprotein family. The protein structure is composed of an N-terminal domain containing a nuclear export signal, two RNA binding domains one containing a nuclear localisation signal, and a glycine-rich C terminal domain (82, 83). The nuclear export signal is redundant in TDP-43, as it is not required for export out of the nucleus (84, 85). As different sized fluorescent tags affect TDP-43 nuclear export, it is suggested that TDP-43 efflux may be due to passive diffusion (85), and that the presence of RNA in the nucleus may retain TDP-43, preventing its movement to the cytoplasm (84). On the other side, TDP-43 import from the cytoplasm is regulated by karyopherin α in an energy-dependent manner (86) and requires a functional nuclear localisation signal (87).

TDP-43 has a plethora of roles surrounding DNA and RNA processing, such as mRNA transport and stability and splicing regulation. In axonal cells, TDP-43 forms ribonucleoprotein granules for transport of mRNA with assistance of microtubules (88). TDP-43 also has roles in stress sensing and cell survival, by forming stress granules with halted mRNA transcripts (89). These stress granules aim to promote cell survival by sequestering mRNAs and RNA-binding proteins during the exposure to cellular stresses such as oxidative or osmotic stress (90). The regulation of TDP-43 is under its own control via a negative feedback loop where TDP-43 binds to its own mRNA, causing mRNA instability, preventing overexpression (91, 92).

TDP-43 is found in insoluble inclusions in patients with amyotrophic lateral sclerosis (ALS) and frontotemporal lobar degeneration (FTLD). In ALS, 25-35 kDa fragments of the C-terminus of TDP-43 are formed through caspase activity. These fragments are the predominant form of TDP-43 in ALS inclusions (88). The majority (up to 97%) of patients with ALS have inclusions of TDP-43 in neurones (82). TDP-43 mutations are found in 3 % of familial ALS cases and 2 % of sporadic cases (93, 94).

TDP-43 is found aggregated within the sarcoplasm in sIBM (95, 96). The protein levels of the full length 43 kDa TDP-43 protein were increased in sIBM patient muscle compared to healthy controls (97). A separate study found no increase in 43 kDa full length TDP-43 but an increase in 35 kDa, 25 kDa and phosphorylated TDP-43 compared to controls in the soluble fraction of protein lysates. However, further solubilisation of proteins with SDS (sodium dodecyl sulphate) buffer showed increased full length TDP-43 in sIBM compared to control muscle (98). There was no difference between healthy controls or polymyositis and sIBM for the levels of *TARDBP* mRNA (99). sIBM myofibres with high intra-sarcoplasmic TDP-43 also have intense mitochondrial staining (98). Whilst there is broad dysregulation of TDP-43 in sIBM, so far no mutations have been found. In 6 patients with sIBM, no exonic mutations in TDP-43 were observed (100). Larger scale analyses of TDP-43 mutations could be conducted as in other diseases like ALS TDP-43 mutations have been, albeit rarely, identified (101).

The nuclear localisation of TDP-43 was observed to be decreased in sIBM compared to healthy controls (96). The presence of TDP-43 within the sarcoplasm with a lack of nuclear TDP-43 has been suggested as a marker of sIBM, with its presence detected in 25 % of myofibres compared to 2.8 % positivity for the traditional sIBM marker of rimmed vacuoles (100). TDP-43 was found accumulated in all biopsies of those classified as having definite sIBM, and 31 % of possible sIBM cases (95), although a separate study found only 67 % of sIBM cases were positive for TDP-43 aggregates (102). TDP-43 inclusions are also found in other muscle diseases including oculopharyngeal muscular dystrophy, desminopathy, myotilinopathy, and hereditary IBM (none of which are inflammatory myopathies) (103), showing sIBM is not the only muscle disease displaying with TDP-43 aggregates.

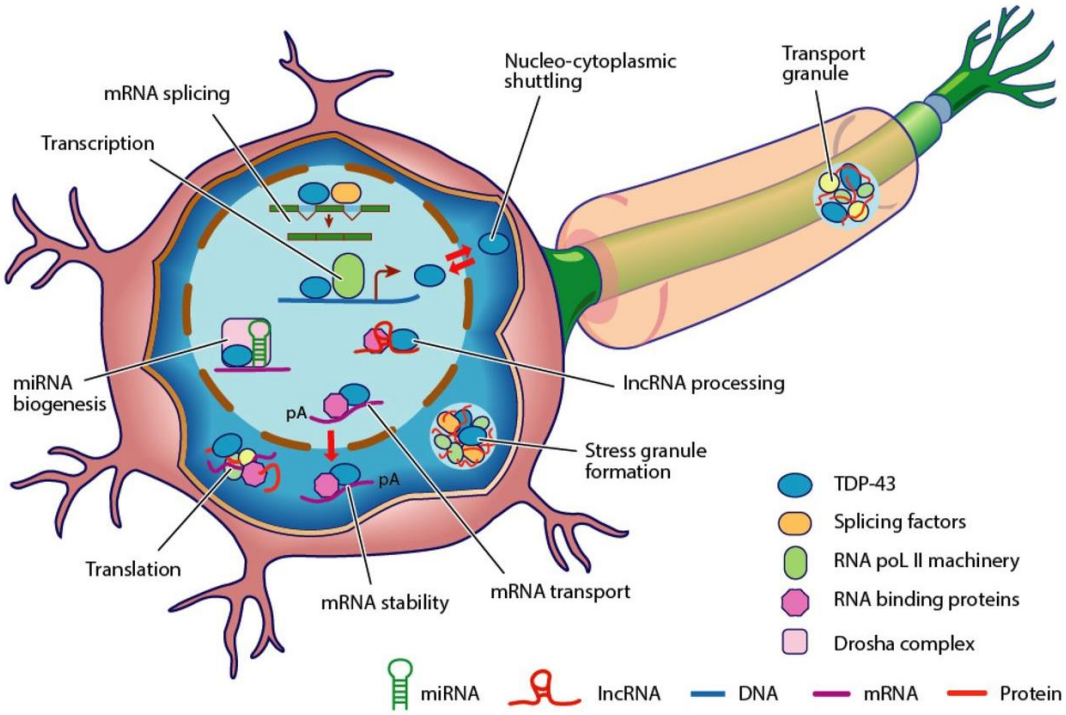

Figure 1.4 Functions of TDP-43. Diagram showing TDP-43 functions related to RNA in neurones including mRNA splicing and transcription. The main functions of TDP-43 are within the nucleus, however it is also involved in stress granule formation, translation, and stability of cytoplasmic mRNA molecules. Available under a creative commons licence. pA-mRNA stability. Reproduced with modification from de Boer *et al* (82).

It is not clear how the pathological alterations of TDP-43 aggregation and cytoplasmic mislocalisation may cause detrimental effects in sIBM. A possible explanation is that when TDP-43 is sequestered in cytosolic inclusions, it loses its ability to perform its homeostatic functions, including roles in the nucleus related to RNA processing. This is evidenced by decreased RNA stability, reduced splicing, and presence of cryptic exons with TDP-43 pathology. In mice overexpressing mutant TDP-43 lacking a nuclear localisation signal, cytoplasmic expression of TDP-43 without nuclear TDP-43 caused neuronal toxicity, with only occasional TDP-43 inclusion bodies observed. This suggests loss of nuclear TDP-43 expression is sufficient to cause pathological effects (104)

without TDP-43 aggregates in neurological diseases. Furthermore, sIBM patient muscle has widespread alterations in RNA metabolism pathways compared to controls (99).

Cryptic exons are located in introns and are usually excluded from mature mRNAs molecules (105). Their inclusion in mature mRNAs can lead to splice variants causing premature stop codons or frameshift mutations. TDP-43 is involved in the removal of cryptic exons from some mRNAs (106). In ALS-FTLD cases which present with TDP-43 cytoplasmic mislocalisation and inclusions, cryptic exon repression was impaired (107). A study compared the effects of conditional TDP-43 deletion in either muscle, neurones, or stem cells. TDP-43 deletion caused cryptic exon inclusion and disrupted mRNA processing. Some cryptic exons shared similarity amongst the three targeted tissues, whereas the majority were specific to certain cell types (108). This is corroborated by a study comparing cryptic exons in the mouse myoblast cell line C2C12 compared to the motor neurone-like cell line NSC-34. This study also showed that sIBM patient muscle had altered TDP-43-controlled cryptic exon inclusion compared to control patients in the ASAP2 (ArfGAP with SH3 domain, ANK repeat and PH domain 2-containing protein 2) protein (109). Furthermore, detection of cryptic exons in sIBM muscle samples was shown to be 84 % sensitive and 99 % specific in the detection of sIBM compared to healthy control and other muscle disease patients (110). The cell-type specific effect of TDP-43 deletion on cryptic exon inclusion is an important consideration showing results from ALS/neuronal may not translate into the same effects in muscle.

1.7 p62

p62 is also known as sequestosome 1. Its main role is in involvement of degradation of ubiquitinated protein aggregates through selective autophagy, as p62 functions as a ubiquitinated cargo receptor (Figure 1.5). In autophagy p62 delivers cargo via its LIR domain (111). p62 is transcriptionally regulated by oxidative stress and starvation, therefore p62 has a role in stress responses (111). As well as its role in autophagy, p62 can also act as an adaptor protein for shuttling of polyubiquitinated proteins to the proteasome, which forms part of the ubiquitin proteasome system (UPS) (Figure 1.6). Like autophagy, the UPS is involved in degradation of proteins. The active or 26S

proteasome is a complex of a catalytic core particle (20S) and regulatory particles (19S) that functions to hydrolyse and degrade target proteins (112). In the cytoplasm, p62 bound to polyubiquitinated targets is able to recruit the proteasome through its PB1 domain. p62 is also able to shuttle to the nucleus, where it recruits the proteasome to polyubiquitinated targets (111, 113). p62 is regulated by both the UPS and autophagy. When the UPS is downregulated or pharmacologically inhibited with epoxomicin, protein levels of p62 increase. On the other hand, p62 is itself degraded during autophagy, therefore its protein levels decrease with increasing autophagic activity (114). These opposing effects of the UPS and autophagy mean p62 operates as a bridge between the two pathways. Increased expression of p62 negatively regulates the UPS, whereas autophagic activity is increased (111, 115).

As with TDP-43, p62 is aggregated within the sarcoplasm of sIBM patients (61, 95), and its protein levels are increased in sIBM compared to that of healthy controls (116). p62 aggregates are often associated with vacuolated areas in affected sIBM fibres (75, 117). Myofibres with high p62 levels also show high levels of TDP-43 and mitochondrial staining (98). There was also increased protein expression of p62 (as well as TDP-43) in sIBM muscles compared to healthy controls but decreased levels of proteins associated with mitochondrial complexes I and III, suggesting a link between p62 and TDP-43 abnormalities and mitochondrial pathologies in sIBM (98). In a mouse-xenograft model where sIBM muscle was engrafted into immunodeficient mice, p62 aggregation could be observed in the xenografts. Depletion of human T cells did not affect the presence of p62 aggregates or other non-inflammatory features including TDP-43 pathology or rimmed vacuoles in xenograft fibres (110), suggesting either that non-inflammatory features including p62 aggregation occurs independently of T cell infiltration, or that p62 aggregation due to T cell infiltration is not reversible after T cell depletion.

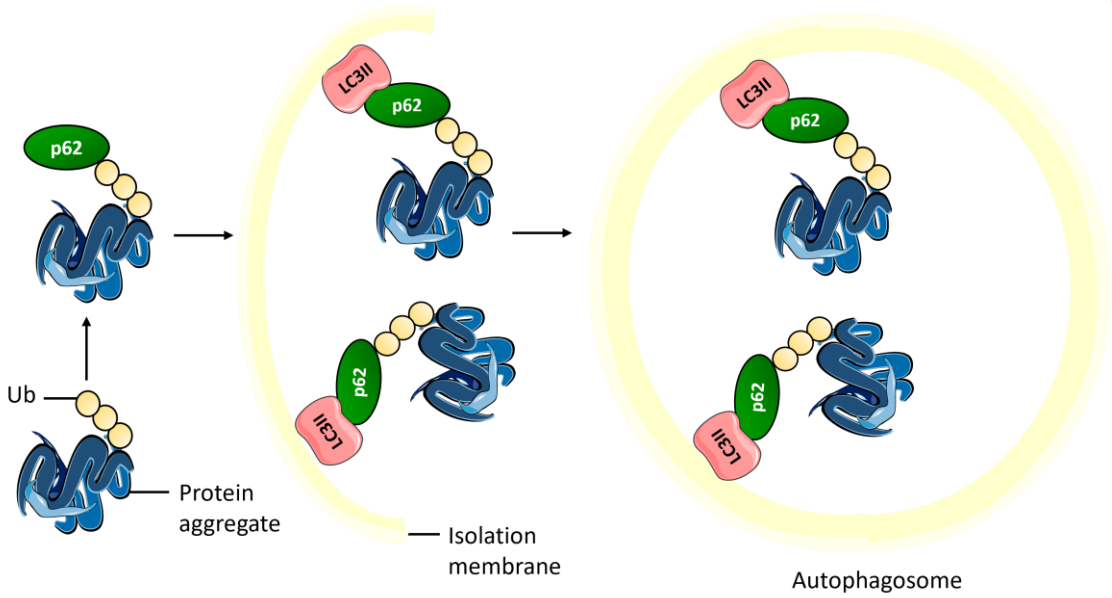

Figure 1.5 Role of p62 in autophagy. p62 binds to polyubiquitinated chains on protein aggregates in the cytoplasm for selective delivery to autophagosomes. LC3II binds p62 during formation of the isolation membrane, which encloses around the cargo forming the autophagosome. Autophagosome cargo is then delivered to lysosomes for degradation (not shown). Ub – ubiquitin.

p62 has been suggested as an sIBM marker as it can be found in 100 % of definite sIBM cases and 37 % of possible cases (95). In differentiating between sIBM and polymyositis, a combination of p62 with TDP-43 was found to be a sensitive method for identifying sIBM, whilst TDP-43 and LC3 offered the highest sensitivity and specificity (102). However, p62 can be found in small puncta in other myositis conditions like polymyositis, dermatomyositis, and IMNM, but large p62 aggregates were found mostly in sIBM muscle samples. The p62 aggregates in sIBM muscle were up to approximately 10 µm long. Approximately half of the p62 aggregates colocalised with LC3, suggesting a potential role of defective selective autophagy in sIBM (118). As described in Section 1.13, IMNM also shows p62 in skeletal muscle with a more diffuse staining pattern. LC3 was also accumulated in IMNM muscle fibres (117), suggesting

sIBM may not be the only inflammatory myopathy with potentially defective autophagic pathways. In a separate study, p62 immunostaining was absent in healthy muscle biopsies but present in patients with inflammatory myopathies including sIBM, dermatomyositis, polymyositis, and IMNM, as well as in non-inflammatory myopathic conditions. The accumulation of p62 was associated with severity of muscle damage. p62 mRNA expression was decreased in sIBM compared to healthy controls and other inflammatory myopathies. The authors concluded that accumulation of p62 in muscle is a response to muscle injury and not a specific biomarker for sIBM. Despite this, p62 was present in a higher percentage of sIBM cases (92 %) than other inflammatory myopathies (polymyositis 29 %, dermatomyositis 57 %, IMNM 87 %). Furthermore, p62 was the only examined inflammatory myopathy that displayed perivacuolar p62 immunostaining pattern (in 19 % biopsies) (119), which may represent a more specific but not sensitive p62 marker in sIBM.

1.8 Inflammatory features of sIBM

Within skeletal muscle fibres of sIBM patients, infiltrates of mononucleated immune cells can be seen in the endomysium as well as in the muscle fibres. Interestingly, the invaded fibres appear non-necrotic, suggesting an autoimmune reaction or antigen presentation from skeletal muscle (120). There is a strong presence of CD8+ T cells as well as to a lesser extent other immune cells including macrophages and dendritic cells (8, 61, 121). CD68+ macrophages can be found infiltrating into the endomysium of sIBM patients (45). Proteomic profiling of skeletal muscle of 13 sIBM patients compared to non-sIBM controls with myalgia symptoms showed has been conducted to investigate macrophages found in sIBM muscle. This showed upregulation of CD74, signal transducer and activator of transcription 1 (STAT1), and CD163. CD74 was found in endomysial macrophages, whereas STAT1 was expressed in macrophages that were actively involved in myophagocytosis (122). Both pro- and anti-inflammatory macrophages are found within sIBM muscle (123). However, compared to other inflammatory myopathies there was no difference in infiltrating macrophage levels (124).

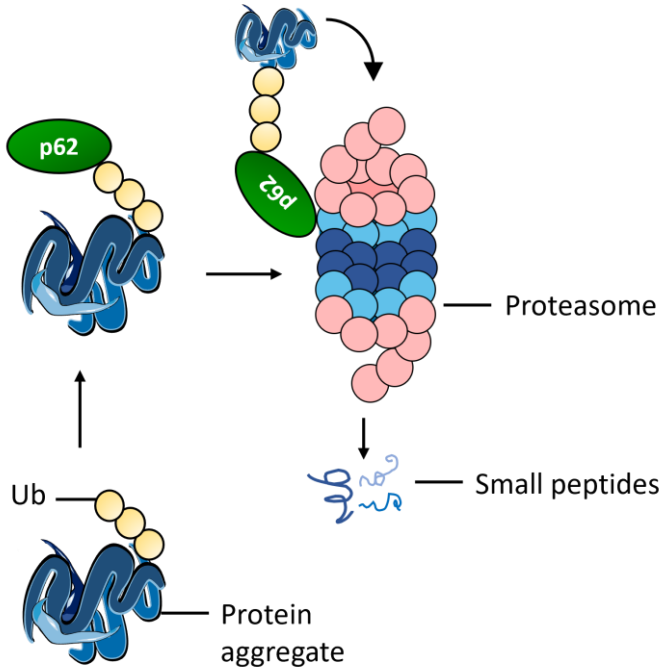

Figure 1.6 p62 in the ubiquitin proteasome system. p62 binds to polyubiquitinated chains on protein aggregates in the cytoplasm or nucleus. Binding of p62 to the proteasome delivers the polyubiquitinated cargo for degradation into smaller peptides. The ubiquitin is recycled for further use. Ub- ubiquitin

A range of genes for cytokines and chemokines are found upregulated in sIBM compared to other inflammatory myopathies including interferon γ (IFNγ), tumour necrosis factor α (TNFα), interleukin (IL)-7, and IL-32, as well as chemokines such as C-X-C motif ligand (CXCL)-9, CXCL-10, and chemokine C-C ligand (CCL) 13 (124). The secretion levels of CXCL-9, CXCL-10, CCL-2, IL-12, and IL-1 receptor antagonist (IL-1RA) were increased in sIBM patient sera compared to healthy controls, and sIBM patients had a higher frequency of CD8+IFNγ+ cells than controls (125). IFNγ and TNFα are both produced by CD8+ T cells and cause cytotoxic or cytostatic responses (126). CXCL9 and CXCL10 are secreted by cells including monocytes and fibroblasts and are involved in recruitment of T cells and natural killer cells. Both CXCL9 and CXCL10 are induced via IFNγ (127). CCL13 and CCL2 are involved in chemotaxis of a wide range of immune cells (128, 129). These cytokines and chemokines are pro-inflammatory, showing

inflammatory engagement of the immune system in sIBM. However IL-1RA is an antagonist of the pro-inflammatory IL-1 receptor and has anti-inflammatory effects (130).

It is possible there is no singular cause of sIBM. A wide plethora of mechanisms are implicated in its pathogenesis, making it difficult to study causal relationships within the disease, as well as developing targeted therapies. Due to its association with older age, the disease could be linked to environmental factors that precipitate over time, or be due to age-related defects in homeostatic mechanisms. The lack of efficacy of immunosuppressant medication has been highlighted as evidence that the non-inflammatory phenotypes of sIBM may be more important in its pathogenesis (61). However, to date, no treatment targeting degenerative pathways has shown clinical efficacy either (reviewed in Section 1.12). It is possible that neither one of these factors is the sole cause, but an interplay between the two could influence sIBM pathology and progression. There are many unanswered questions relating to the clinical and histological findings of sIBM. It is not known why sIBM affects males more frequently than females, why the presentation is asymmetrical with non-dominant limbs more affected with initial involvement of finger flexors and knee extensors, or what mechanisms are contributing to muscle weakness.

1.9 Interleukin 1β

IL-1β is a pro-inflammatory cytokine produced by inflammatory cells including macrophages (131). IL-1β signals through the IL-1 receptor type 1 (IL-1R1) which also binds IL-1α and IL-1Ra (interleukin 1 receptor antagonist). When IL-1α or IL-1β binds to IL-1R1, it undergoes a conformational change allowing binding of IL-1R3, and IL-1R1 co-receptor. The intracellular TIR (toll-interleukin receptor) domains of IL-1R1 and IL-1R3 are brought into proximity for binding of MyD88 (132), which leads to a cascade of signalling proteins culminating in NF-κB (nuclear factor κB) signalling (133). NF-κB is a transcription factor involved in many immune and inflammatory responses including the expression of pro-inflammatory cytokines, chemokines, adhesion molecules, and anti-apoptotic factors to promote cell survival in immune cells (134).

Skeletal muscle sparsely expresses IL-1R1 on the sarcolemma (135), and cultured human myogenic cells express IL-1R1 with the highest expression at the start of differentiation. Furthermore, human myogenic cells constitutively express IL-1β, with increased expression in myotubes compared to proliferating progenitors. Adding exogenous IL-1β one day after seeding cells lead to an increase in DNA breaks in myogenic cells, suggesting excess IL-1β in the muscle may cause cell death (136). After exercise, IL-1β production is increased in muscle for a short duration (137). Further, treatment of C2C12 cells with IL-1β causes production of IL-6 via MAP kinase (mitogen activated protein kinase) and NF-κB signalling (138). When differentiated C2C12 cells were treated with IL-1β, myotube diameter was decreased compared to control, and atrophic genes including *Trim63* and *Fbxo32* were upregulated, showing IL-1β can promote muscle atrophy (139).

When differentiating mouse C2C12 cell line are treated with IL-1β, there is an increase in protein synthesis at the initial phases of differentiation compared to untreated cells, but this difference is resolved at later differentiation stages. Further, IL-1β treatment during differentiation increased production of myogenic proteins myosin heavy chain, myogenin, and myoD (140). IL-1β also affects skeletal muscle cell proliferation. Addition of IL-1β to C2C12 or primary rat cells caused increased proliferation of myogenic precursors (141). Overall, IL-β appears to play a pleiotropic role in skeletal muscle by causing atrophy, but also promoting myokine secretion and benefiting myogenic differentiation.

It is not clear if IL-1β is upregulated in sIBM compared to other inflammatory myopathies. A study based on compiled microarray data showed no difference in IL-1β mRNA expression between sIBM and grouped other inflammatory myopathies polymyositis, dermatomyositis, non-specific myositis, and normal muscle (124). A separate study found no difference in the amount of IL-1β in serum from patients with sIBM compared to those with dermatomyositis, polymyositis, or IMNM (124, 125). However IL-1β was detected in muscle of three sIBM patients, whilst being undetectable in polymyositis and dermatomyositis (142). IL-1β mRNA expression was also detected in one case of sIBM but not in healthy controls (143). Infiltrating immune

cells in sIBM were found to be positive for IL-1β but not the muscle fibres themselves, whereas in dermatomyositis the fibres show sarcoplasmic IL-1β (144). However, this is contradicted by another study showing strong IL-1β immunoreactivity in sIBM muscle fibres as well as upregulation of its mRNA compared to healthy controls (145). Therefore the expression of IL-1β in sIBM patient muscle may be highly variable, and its presence may not be specific compared to other inflammatory myopathies. As described in Section 1.12, sIBM patients have been treated with therapies targeting IL-1β including canakinumab and anakinra. As with all clinical trials so far, this did not show clinical benefit.

1.10 Interferon γ

IFNγ is a potent antiviral inflammatory cytokine, that is also involved in activating neutrophils and macrophages in the defence against bacteria and fungi (146). It is produced by CD4+ T helper cells, CD8+ T cells, natural killer cells, B cells, natural killer T cells, and antigen presenting cells (APCs) including dendritic cells and macrophages (147, 148). IFNγ is the only member of the type II family of interferons and it signals through the type II interferon receptor composed of two subunits: IFNGR1 and IFNGR2 (IFNGR – interferon gamma receptor). Binding of IFNγ to its receptor causes dimerization of the receptor subunits which triggers autophosphorylation and activation of associated janus activated kinases (JAKs, JAK1 and JAK2) (149). Activated JAKs then phosphorylate STAT1, which causes its homodimerisation and activation, translocation to the nucleus, and promotion of gene expression by binding γ interferon activation sites (GAS) on genes (150). This describes the canonical pathway of IFNγ receptor signalling. IFNγ can also signal through non-canonical pathways. For example, when STAT1 is not present, IFNGR signalling can instead activate STAT3 for activation of genes under the regulation of GAS. In some cell types, IFNγ signalling can also lead to activation of other pathways including MAPK (mitogen-activated protein kinase) pathway, showing a diverse mode of action of IFNγ signalling (151).

As well as having effects on immune cells, IFNγ can exert effects on skeletal muscle. Figure 1.7 shows mechanisms of IFNγ signalling in muscle. Myofibres express both IFNγ and its receptor during muscle injury in mice, as well as in C2C12 cells (152). Major

histocompatibility complex (MHC) class II is usually only expressed on APCs such as monocytes/macrophages and dendritic cells for presentation of antigens to CD4+ T helper cells (153). However, the expression of MHC II can be induced in other non-antigen presenting cells through exposure to IFNγ. MHC II expression is under regulation of CIITA (class II transactivator) which is induced by exposure to IFNγ (154). CIITA is a transcriptional co-activator that does not directly bind DNA but co-ordinates transcription activation through recruitment of other proteins involved in transcription and phosphorylation of RNA polymerase II (155). In non-APCs, IFNγ signalling through CIITA results in expression of MHC II mRNA (156) and protein in human skeletal muscle cells (157).

IFNγ can inhibit the differentiation of mouse C2C12 myoblasts into myotubes, through myogenin repression via CIITA. This effect is reversible with removal of IFNγ (156). Conversely, addition of IFNγ receptor blocking antibodies in wild type mice caused reduced myogenic cell proliferation and decreased fibre regeneration, which was also accompanied by reduced macrophage infiltration with muscle injury. Furthermore, cultured mouse C2C12 cells treated with IFNγ blocking antibody showed reduced cell counts, proliferation, and fusion to myotubes (152) showing endogenous IFNγ production is important for muscle cell homeostasis, proliferation and differentiation. Exogenous IFNγ aided muscle repair after laceration in a mouse model by inhibiting pro-fibrotic transforming growth factor β signalling, preventing fibrosis (158). When cultured human 3D functional skeletal muscle constructs were treated with IFNγ, their force production was decreased and signs of atrophy were observed, which was mediated through JAK-STAT signalling (159). Together, this suggesting a complex and contradictory role of IFNγ signalling in muscle repair, homeostasis, and injury.

Exposure to IFNγ, as well as other inflammatory cytokines and oxidative stress, can cause formation of the immunoproteasome. This resembles the standard proteasome, except with different catalytic core proteins. The transcription of the genes comprising the immunoproteasome catalytic subunits (proteasome subunit beta type (PSMB)8, PSMB9, and PSMB10) is induced by IFNγ (160). The immunoproteasome also associates with a different regulatory complex called PA28, whilst the standard

proteasome associates with PA700 (161). One of the main functions of both the proteasome and immunoproteasome is targeted breakdown of polyubiquitinated proteins for later display by MHC I (160). In mouse C2C12 cells undergoing differentiation, there was an upregulation of immunoproteasome mRNA and increased proteasomal activity. Furthermore, knockdown of the immunoproteasome subunit PSMB9 prevented differentiation (162), suggesting the immunoproteasome is essential for mouse muscle differentiation. The expression of the immunoproteasome under skeletal muscle disease conditions including aging, denervation, and Duchenne muscular dystrophy is increased (161, 163, 164), showing that the immunoproteasome may also have deleterious effects in skeletal muscle, or may be activated in disease conditions to compensate for muscle damage.

Calcium/calmodulin dependent protein kinase IV (CaMKIV) is a multifunctional serine/threonine kinase involved in transduction of calcium signalling for a range of biological functions including cell cycle regulation, apoptosis, and T cell maturation (165, 166). A study by Gu *et al* found that CaMKIV is inducible with IFNγ exposure in both myoblasts and myotubes of C2C12 cells and primary murine myogenic progenitors. The addition of IFNγ was associated with increased expression of IL-1β and IL-6 mRNA in myoblasts and myotubes, as well as increased TNFα in myotubes only. Silencing of CaMKIV with shRNA (short hairpin RNA) prevented the upregulation of IL-1β and TNFα, whilst IL-6 upregulation was prevented in myoblasts with a dampening effect in myotubes (167). A separate study found that IFNγ also stimulated secretion of IL-1β from C2C12 myotubes (168). This shows CaMKIV is involved in proinflammatory cytokine production in myogenic cells, and that IFNγ exposure in myogenic cells stimulates further inflammation. IL-6 modulation has also been found to be under control of CIITA with a complex relationship. Overexpression of CIITA in C2C12 cells caused increased IL-6 expression, whereas knockdown of CIITA had the same result, showing a CIITA-independent mechanism of IL-6 also exists in muscle cells (169). The study by Gu *et al* also found that exposure to IFNγ increased the number of myoblasts and myotubes expressing costimulatory proteins CD40, CD86, ICAM-1, as well as the co-inhibitory factor PD-1. Silencing of CaMKIV prevented the upregulation

of the costimulatory proteins whilst PD-1 was still increased, showing IFNγ signalling through CaMKIV is involved in the upregulation of the costimulatory proteins (167).

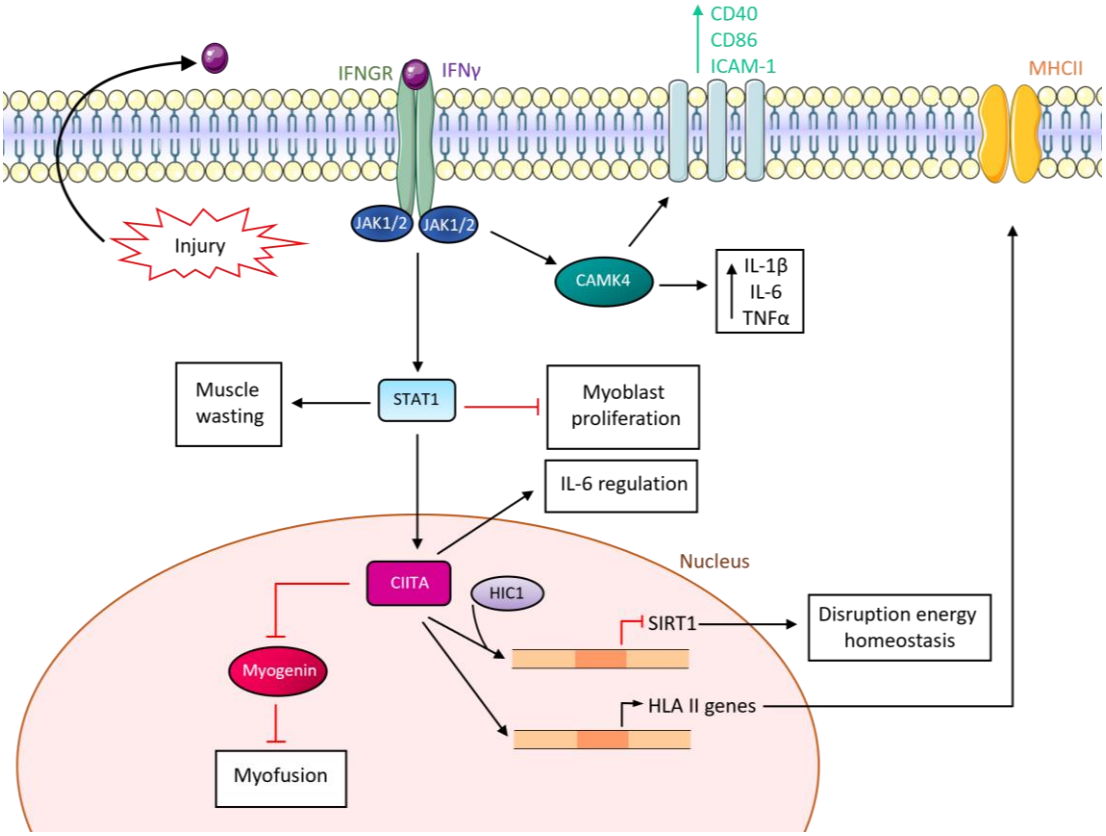

Figure 1.7 Mechanisms of IFNγ action in skeletal muscle. Binding of IFNγ to the interferon gamma receptor (IFNGR) canonically signals through the JAK-STAT signal transduction pathway. Activation of STAT has pleiotropic roles within skeletal muscle, including inhibition of myoblast proliferation and induction of muscle wasting. CIITA can be activated by JAK-STAT signalling. In muscle CIITA activates transcription of HLA II genes, which leads to expression of MHC II in muscle cells. Further, CIITA with the help of HIC1 transportation is involved in the prevention of SIRT1 transcription, which leads to decrease in genes responsible for energy homeostasis. CIITA also inhibits the activity of myogenin in myoblasts but not myotubes, causing inhibition of myogenesis/myofusion. IFNγ can also cause increased transcription of inflammatory cytokines via a CaMK4 axis. Furthermore, activation of CAMK4 in response to IFNγ can increase expression of CD40, CD86, and ICAM-1 on skeletal muscle cells, which are lymphocyte costimulatory receptors. Finally, in response to skeletal muscle injury, muscle cells can themselves secrete IFNγ for activation of immune cells. STAT – signal transducer and activator of transcription, CIITA – class II major histocompatibility complex transactivator, HIC1 – hypermethylated in cancer protein 1, SIRT1 – sirtuin 1, HLA – human leukocyte antigen, MHC II, major histocompatibility complex II, CAMK4 – calcium/calmodulin-dependent protein kinase type IV, ICAM-1 – intracellular adhesion molecule 1.

IFNγ is also involved in dysregulated energy homeostasis in skeletal muscle and is linked to type 2 diabetes (170). SIRT1 (sirtuin 1) is a protein that functions as a histone deacetylase and transcription factor (171). It is involved in energy homeostasis, nutrient responses, longevity, and response to chronic inflammation (172). Exposure of mouse C2C12 cells to IFNγ caused downregulation of SIRT1 transcription and protein expression. This was controlled through IFNγ-induced CIITA upregulation, with CIITA being recruited to the SIRT1 promoter via HIC1 (hypermethylated in cancer 1). CIITA and HIC1 recruit HDAC4 (histone deacetylase 4) to the SIRT1 promoter where HDAC4 represses SIRT1 transcription by deacetylation of core histones (173). The IFNγ-induced SIRT1 downregulation was accompanied by reduced expression of genes involved in energy metabolism (170).

IFNγ transcripts are elevated in sIBM compared to control and other inflammatory myopathies (124, 174). In sIBM myofibres attacked by CD8+ T cells, upregulation of IFNγ receptor 2 (IFNGR2) was observed compared to healthy or non-attacked myofibres. The amount of IFNGR2 upregulation partially correlated with the number of attacking CD8+ cells (73). Transcription of the guanylate-binding protein 6 (GBP6) gene, which is induced by IFNγ signalling (175), was 7 times higher in sIBM compared to controls or other inflammatory myopathies (176). Proteins and transcripts of the immunoproteasome are elevated in sIBM (and other inflammatory myopathies) compared to healthy controls and immunoproteasome staining in sIBM muscle colocalised with MHC I expression (124, 177).

1.11 CD8+ T cells

CD8+ T cells are part of the adaptive immune response where they specifically target virally or bacterially infected or neoplastic cells. CD8+ cytotoxic T lymphocytes (CTL) are MHC class I restricted, where they require antigen presentation via MHC class I for full activation. Figure 1.8 shows the process of CD8 T cell activation and differentiation to either effector or memory subsets (original source (2)). Activation of naïve CTLs usually requires antigen presentation via antigen presenting cells (APC) such as dendritic cells, and co-stimulation from CD4 cells that recognise the same antigen being presented. The CD4 cells themselves release IL-2 for CTL activation, and also

stimulate the APC to upregulate costimulatory molecules such as 4-1BBL for further T cell activation (178). For full activation of the CTL, the T cell receptor (TCR)-MHC activation signal must be accompanied by a co-stimulatory signal through CD28 on CTLs interacting with CD80 or CD86 on antigen presenting cells, macrophages, or B cells. This costimulatory signal enhances the stimulation and proliferation of CTLs (179).

The main function of cytotoxic T cells is killing of target cells. Once naïve CD8+ T cells differentiate into effector cells with the priming from APCs, they are capable of killing cells displaying the antigen to which they have been primed. CTLs induce apoptosis of target cells via two mechanisms. In the first, cytotoxic effector molecules granzymes and perforin that are stored in cytotoxic granules are released. The release of cytotoxic granule contents occurs through an immunological synapse, where adhesion molecules attach the CTL to the surface of the target cell (180). Release of cytotoxic granules is directed towards the point of contact with the target cell through reorganisation of the T cell's microtubule cytoskeleton and cytotoxic granule stores. The process of directed release of cytotoxic granules is dependent on calcium influx into CTLs (181).

Perforin perforates the target cell membrane for entry of granzymes. Multiple granzymes exist; most notable are granzyme A, B and K that are all serine proteases. Granzyme A triggers caspase-independent apoptosis by causing mitochondrial damage by cleaving the mitochondrial protein NDUSF3 (NADH:ubiquinone oxidoreductase core subunit S3) and releasing reactive oxygen species (ROS). The ROS cause an endoplasmic reticulum associated complex called SET to translocate to the nucleus where it causes DNA damage. Granzyme A also directly degrades nuclear proteins such as histones and DNA repair proteins (182, 183). Granzyme K functions in a similar way to granzyme A through caspase-independent disruption of the mitochondria (184). Granzyme B activates caspase 3 and the pro-apoptotic Bcl-2 protein BID (BH3 interacting domain death agonist). Cleavage of BID into its truncated form t-BID allows it to damage mitochondria, releasing cytochrome c (185). This leads to apoptosome

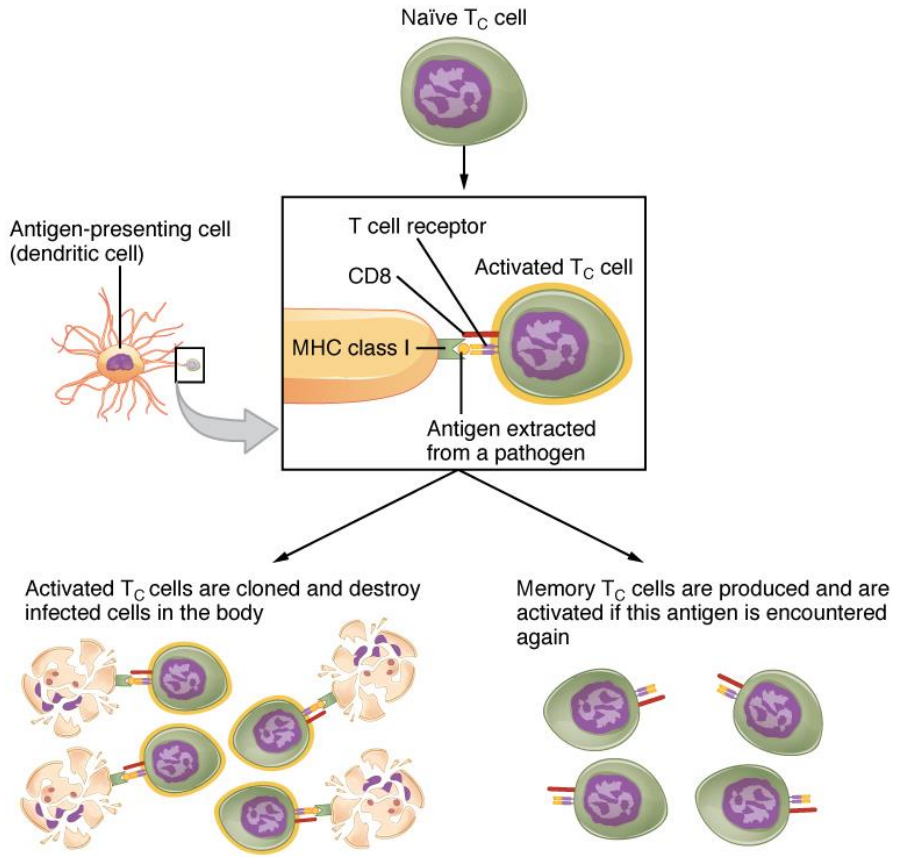

Figure 1.8 Activation of CD8 T cells. Naïve cytotoxic CD8+ T cells (T_c cells) are activated upon presentation of an antigen via MHC I, to which the T cell receptor binds. CD8+ T cells differentiation into either effector cells via clonal expansion which destroy infected/transformed cells displaying the original antigen. Alternatively, CD8+ cells differentiate to memory cells in case the same antigen is encountered later. Available under a creative commons licence (2).

formation from oligomerised Apaf-1 protein. Apoptosome causes pro-caspase 9 to self-cleave, and activated caspase 9 then activates downstream effector caspases including caspase 3 which cleave a wide variety of proteins leading to cell death (178, 183). Caspase 3 cleaves ICAD (inhibitor of caspase-activated DNase) for activation of CAD (caspase-activated Dnase) which causes DNA fragmentation (186, 187).

CTLs are also capable of triggering target cell apoptosis through Fas signalling. Cytotoxic T cells express Fas ligand (FasL) on their surface. This binds to Fas on the surface of target cells, causing recruitment of Fas-associated death domain (FADD) to the Fas receptor in target cells. FADD then causes the autolysis of inactive pro-

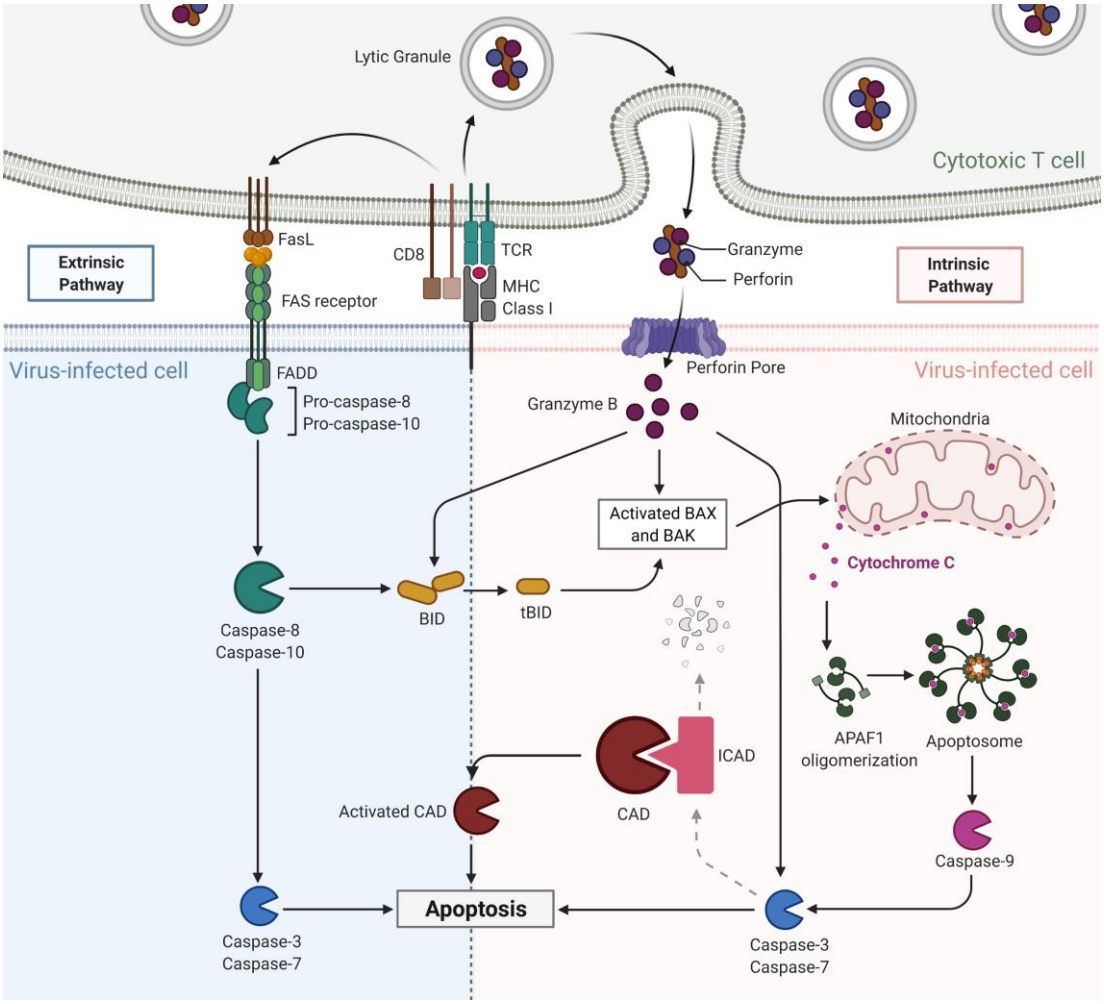

Figure 1.9 Mechanisms of cytotoxic T cell mediated cell death. Mechanisms of cell death induced by cytotoxic T cells in virally infected cells. Cytotoxic T cells release the contents of cytotoxic granules including perforin and granzymes. Perforin forms pores in the target cell membrane for entrance of granzymes. Granzymes B activates intrinsic apoptosis through cleavage of BID, activation of BAX and BAK, and downstream caspase activation. Cytotoxic T cells also cause extrinsic apoptosis through binding of Fas ligand (FasL) to Fas receptor on target cell membranes. This causes activation of caspase 8 or caspase 10 which cleave bid and lead to activation of downstream effector caspases. Image available under a creative commons licence: (188).

caspases 8 or 10, converting them into their active caspase forms. Active caspase 8 or caspase 10 can then go on to cause cell death through activation of downstream caspases 3, 6, and 7, or through cleavage of BID. Fas-mediated cell death is slower than granzyme-mediated apoptosis, but the two pathways are interconnected to ensure

efficient killing of target cell populations (189). CTLs can also use a similar mechanism to trigger extrinsic apoptosis via the death ligand TRAIL (tumour necrosis factor related apoptosis-inducing ligand) that interacts with DR4 and DR5 on target cells, leading to caspase 8 activation (190). Figure 1.9 shows the mechanisms of both granzyme-mediated and Fas-mediated cell death.

CD8+ T cells can be categorised based on their effector and memory capabilities through their expression of different markers. T central memory (Tcm) cells are located largely in lymph nodes and express high levels of CD62L and CCR7. CCR7 and CD62L are involved in homing to secondary lymphoid organs. T effector memory (Tem) cells express low levels of CD62L and CCR7. Tem cells express molecules (chemokine receptors and integrins) for homing to sites of inflammation in the tissue. Tem are highly cytotoxic whereas Tcm have higher capacity to proliferate with lower cytotoxicity (191). CD45RA is usually expressed in naïve T cells that have not previously been exposed to antigenic stimulation. However, effector memory T cells are capable of re-expressing CD45RA (Temra). Temra cells are highly differentiated and show low proliferation whilst maintaining cytotoxic functionality (192). Temra cells can be negative for the coreceptors CD27 and CD28 (193), as well as CCR7, and have low expression of CD127 (191).

Cytotoxic T cells also secrete cytokines, most notably IFNγ and TNFα. IFNγ upregulates the expression of MHC I on cells for further presentation of antigens and recognition by CTLs. IFNγ also activates macrophages, and it can trigger death of intracellular parasites (194). TNFα exists either as a secreted form or a membrane bound form. TNFα can act with IFNγ to increase the activation of macrophages. Furthermore, TNFα itself is capable of causing cell death when it binds to TNF receptor I (TNFR1) (178). TNFR1 is a death receptor and signals in a similar way to the Fas receptor, as they both belong to the TNF receptor superfamily. As well as activating apoptosis, signalling through TNFR1 can also activate NF-κB signalling which conversely can lead to anti-apoptotic effects (195).

CD8+ T cells are the largest immune cell subgroup infiltrating in sIBM muscle, and have been observed to be minimally proliferative and differentiated towards an effector cell

phenotype with high cytotoxicity. Different markers have been identified on CD8 T cells in sIBM. Killer cell lectin like receptor G1 (KLRG1) has been found on CD8 T cells invading the muscle as well as those in the blood in sIBM patients (124). KLRG1 is an inhibitory receptor that binds N-, E- and R-cadherins (196). Its expression is induced in subsets of effector CD8 T cells that are highly cytotoxic and that have received strong activation signals (197). In sIBM, KLRG1 was found co-expressed with cytotoxic genes including granzymes and perforin (124). In 10 sIBM patient samples, 79 % of CD8 cells surrounding muscle fibres were positive for KLRG1 (198).

CD57 is a cell surface-bound sulphated carbohydrate that is a marker of terminally differentiated senescent T cells and natural killer cells that have been repeatedly exposed to antigen (47, 199). The percentage of CD8+ T cells in sIBM muscle that are also positive for CD57 was found to be 48 % (198). Unlike KLRG1 which is thought to be expressed during earlier phases of T effector memory polarisation, CD57 is expressed during the terminal differentiated effector phase, although the two markers are often co-expressed (124, 200). CD8 cells that invade into the myofibres are CD57+, and the number of CD8+CD57+ cells correlated with the size of large granular lymphocytes in sIBM (47).

When comparing peripheral blood cells from healthy and sIBM patients using unsupervised analysis, an increased frequency of CD8+ T cells expressing T-bet, a transcription factor involved in differentiation of naïve CD8+ T cells, was found. Further, increased frequency of terminally differentiated T effector memory re-expressing CD45RA (Temra) cells was observed in sIBM patients. These T-bet+CD8+ T cells also expressed CD57. There was also a decrease in the co-stimulatory receptors CD27 and CD28 in non-senescent CD8+ T cells in sIBM compared to healthy controls (7). In comparison to amputee controls, transcriptomics of sIBM patients showed dysregulation of calcium-based apoptotic T cell signalling (201), suggesting T cells are not responding to homeostatic apoptotic signals. A recent study characterised peripheral blood mononuclear cells (PBMCs) isolated from sIBM and other idiopathic inflammatory myopathies and compared them to healthy controls (202). There was no difference in the total amount of CD8+ cells, however sIBM patients had a higher

percentage of Temra CD8 cells compared to healthy controls, and fewer of these Temra cells were CD28+. Unlike the findings from Dzangué-Tchoupou *et al* (7), and Greenberg *et al* (124) these peripheral Temra cells did not overexpress CD57. More Terma cells were however positive for CD18, a marker of T cell activation and adhesion. Finally, more CD8 Temra cells in sIBM were also positive for IFNγ or TNFα than Temra from healthy counterparts (202). Overall, these results suggest a role for CD8+ effector memory cells that are senescent, highly cytotoxic, and resistant to normal homeostatic apoptotic queues in sIBM.

1.12 Clinical trials in sIBM

Unfortunately, there are currently no treatments for sIBM that show clinical benefit. Other inflammatory myopathies such as dermatomyositis and polymyositis respond to immunosuppressants such as corticosteroids, however these have no long-term benefit when given to sIBM patients (61). In fact, immunosuppressive treatment in sIBM patients may be associated with lower survival outcomes (8) and more severe disability (203). Intravenous immunoglobulin (IVIG) was previously thought to be a treatment option for sIBM. Patients treated with IVIG showed improvements in manual muscle testing scores, however these effects were not sustained long term (204). Blinded randomised clinical trials have shown no clinical benefit of IVIG treatment in sIBM (205, 206). Numerous recent clinical trials have focussed on targets other than the involvement of the immune system in sIBM (8, 120). Here, the largest recent clinical trials will be reviewed. This information is available from the US National Library of Medicine clinical trials.gov (available at: https://clinicaltrials.gov/). Many of these trials have been extensively reviewed by Naddaf *et al* (8), and more recently (120).

Bimagrumab BYM338 is a human monoclonal antibody raised against activin type II receptor (207), developed to prevent muscle loss. Binding of endogenous ligands including myostatin to activin type II receptors on muscle results in negative regulation in muscle growth (208, 209). Bimagrumab was tested in sIBM (RESILIENT); randomised, multi-centre double-blind, and placebo controlled trial using intravenous administration every 4 weeks for a minimum of 48 weeks. Three concentrations of

bimagrumab were trialled at 1, 3, or 10 mg/kg. Bimagrumab showed a good safety profile. However, the phase IIb clinical trial failed to meet its primary endpoint of improvement in 6 minute walk distance compared to placebo (210). An extension of the RESILENT trial examined the long-term efficacy and safety after two years' treatment. Two-year treatment also showed a good safety profile, however there was still no improvement in 6 minute walk distance (211). Previous studies have shown conflicting results of myostatin levels in sIBM, with one study showing a transcriptional decrease in myostatin in sIBM compared to healthy controls (212), with another showing an increase in myostatin associated with amyloid aggregates (213). A large retrospective study has recently shown serum myostatin levels are lower in sIBM compared to healthy control patients, and myostatin levels correlated positively with manual muscle testing (MMT8) (214). Therefore further reducing the efficacy of endogenous myostatin may not provide clinical benefit in sIBM patients.

Sirolimus is a form of rapamycin that acts by inhibiting mammalian target of rapamycin (mTOR). The aim of utilising sirolimus in sIBM is to ameliorate dysfunctional autophagic pathways, as well as utilising its immunosuppressive effects via inhibition of IL-2 signalling (215) and blocking proliferation of T cells (216). Sirolimus has been used in a randomised, double blind, placebo controlled, single centre phase IIb clinical trial with oral administration. The primary endpoint was a change from baseline to 12 months for maximal voluntary knee extension strength. The study failed to meet its primary endpoint and other muscle strength tests. However, sirolimus showed improvement in assessment of disability index, 6 minute walk distance, and thigh fat fraction. For safety, treatment with oral sirolimus resulted in 4/22 patients experiencing serious adverse events that improved after discontinuation of sirolimus treatment (216). Regardless of these concerns, the improvement in some secondary outcome measures means sirolimus is currently being investigated in a multicentre phase III (120) trial. In a case report of a single sIBM patient who relied on mobility aids, oral sirolimus showed clinical benefit with patient able to walk unaided, with improvements in manual muscle testing scores, and lack of progression of dysphagia (217).

Arimoclomol is a small molecule that upregulates the heat shock response by inducing heat shock proteins to prevent protein misfolding (218). Arimoclomol was found to be safe and well tolerated with four months treatment in a randomised, double blinded placebo-controlled trial of safety. There was also weak evidence that arimoclomol positively impacted functional and muscle contraction testing (219). A phase II/III clinical trial of arimoclomol for sIBM was conducted. A press release from Orphazyme, the company responsible for the clinical trial, showed that arimoclomol failed to meet its primary endpoint of halting disease progression assessed by the IBM Functional Rating Scale (220).

Non-pharmacological interventions in sIBM have also been investigated, for example using exercise regimens. A small randomised controlled trial was conducted with 12 weeks blood flow restricted exercise training versus a no exercise control group. There was no effect on the primary outcome of self-reported physical function. However, knee extensor muscle strength was unaltered in the treatment group compared to baseline but decreased in the control group, suggesting a preventative effect of blood flow restricted exercise on sIBM progression (221). The same group characterised the presence of immune cells before and after blood flow restricted exercise in a separate group of patients. This showed there was increased infiltration of natural killer cells expressing CD8 (CD3-CD8+) with the exercise regimen and no change in the no exercise control group. There was no change after exercise in the CD8+ T cell or macrophage fractions (123). Finally, it was found that there were no markers of hypertrophy or satellite cell proliferation or activation after blood flow restricted exercise, despite the protective effects of this treatment (222).

Other smaller clinical trials have also been conducted. For example phenylbutyrate (clinical trial identifier NCT04421677), pioglitazone (NCT03440034), lithium (NCT00917956), and etanercept (223). Anakinra is an antagonist for IL-1 receptor, and its use in sIBM was explored. In a small pilot study of four patients there was no improvement in muscle strength (224). Canakinumab is a monoclonal antibody against IL-1β that is currently approved for the treatment of rheumatic disorders including Still's disease and systemic juvenile idiopathic arthritis (225). In five sIBM patients

treated with canakinumab, there was no consistent stabilisation or improvement in grip force or total muscle strength (226), and no patient showed improvement in these measures. ABC008 is a monoclonal antibody against KLRG1, examined in sIBM for its ability to deplete differentiated cytotoxic T cells. Results from an ongoing trial of ABC008 in sIBM show 6 patients treated with single dose of ABC008 had depletion of KLRG1+ CD8+ T cells (227).

There is a variety of primary endpoints used in sIBM clinical trials. A consensus on which primary endpoints to use that accurately reflects clinical benefit to sIBM patients would help standardise trials and make comparisons between different trials easier (228). Interest in using imaging methods such as magnetic resonance imaging (MRI) in sIBM is growing. It has been proposed that quantitative MRI could be utilised in clinical trial outcomes to study treatment efficacy and effects of treatments on pathological processes. MRI may also be a useful method for monitoring disease progression that has the benefit over muscle biopsies of being non-invasive (229-231).

1.13 Other idiopathic inflammatory myopathies

sIBM belongs to a group of conditions called idiopathic inflammatory myopathies (IIM) which share the features of muscle weakness and inflammation of skeletal muscle (232). The original cause for all IIMs is unknown. The IIMs are comprised of: sIBM, polymyositis, dermatomyositis, antisynthetase syndrome, immune-mediated necrotising myositis (IMNM), and overlap myositis (233). sIBM shares some similarities with other IIMs, but is separated by its refractoriness to treatment. Corticosteroids, which reduce inflammation and immune activation (234), are commonly used in the treatment of polymyositis, dermatomyositis, antisynthetase syndrome, and IMNM (235, 236).

sIBM is most similar to polymyositis and many sIBM patients are originally misdiagnosed with this condition (237). In polymyositis, cytotoxic T cells and macrophages surround and infiltrate non-necrotic myofibres. Sarcolemmal expression of MHC I is also observed (233, 238). Patients display with symmetrical muscle weakness which may be accompanied by elevated creatine kinase levels (238). Many

patients originally diagnosed as having polymyositis have later gone one to develop features of other inflammatory myopathies (239). Therefore the prevalence of polymyositis is likely lower than originally thought, with some calling into question its existence entirely, suggesting it as a non-specific description of other inflammatory myopathies (240). Polymyositis likely does exist as a distinct pathological entity, but was historically used as a less specific term which included conditions that now have their own names (241).

Polymyositis with mitochondrial pathology (PM-mito) is a rare subset of polymyositis. As the name suggests, there is mitochondrial involvement with COX-deficient fibres. PM-mito shares many similarities with sIBM including involvement of knee extensors, slow progression of weakness, lack of response to corticosteroid treatment, and endomysial inflammation. However, muscle weakness progresses more slowly in PM-mito than sIBM (242). It has been suggested that PM-mito may actually reflect an early stage of sIBM. Indeed, patients with PM-mito can go on to be diagnosed with sIBM. In 13 of 14 PM-mito cases, patients were later diagnosed with clinically defined sIBM (243). There are differences in the pathogenic features between the conditions, for example KLRG1 lymphocytes are upregulated in sIBM compared to PM-mito (243). If PM-mito is an early stage of sIBM, this represents a clinical phenotype in which treatments for the prevention of further sIBM features could be tested.

Dermatomyositis can affect children where it is termed juvenile dermatomyositis, as well as adults. In adults dermatomyositis affects females more frequently than males with an average age of 57 (244, 245). It presents with a skin rash in the large majority of cases as well as muscle weakness (232). A heliotrope rash showing purple discolouration around the eyes is characteristic of dermatomyositis, and Gottron's sign, a rash that can progress to scales on the fingers, can also be observed (238). Dermatomyositis presents with symmetrical weakness in the proximal muscles with subacute onset (246). Other organ systems can also be affected in dermatomyositis including blood vessels, joints, oesophagus and lungs (247). Dermatomyositis is characterised by perifascular myofibre apoptosis and necrosis with blood vessel damage (233). The pattern of muscle atrophy in dermatomyositis may be due to

capillary destruction which leads to localised hypoxia. Perivascular immune infiltrates predominantly composed of B cells can also be observed (238). INFα and IFNβ inducible genes are highly expressed in dermatomyositis muscle (248). Autoantibodies can be detected in this condition including anti-mi-2 (249, 250), anti NXP-2, and anti-MDA-5 (251).

IMNM usually presents with rapidly progressive muscle weakness and is the most severe and disabling of the IIMs. Many patients also report experiencing myalgia. Muscle weakness mostly affects proximal muscles of the lower limbs (252). Myofibre necrosis and presence of macrophages and CD8 cells are observed in IMNM. Furthermore, sarcoplasmic p62 is observed. However, contrary to the aggregates seen in sIBM, IMNM shows diffuse sarcoplasmic expression (75, 117). There are three categories of IMNM based on the presence of autoantibodies; IMNM with signal recognition particle (SRP) antibodies, with HMGGCR (3-hydroxy-3-methylglutaryl-coenzyme A reductase) antibodies, and seronegative IMNM (253).

Antisynthetase syndrome is characterised by antibodies against aminoacyl transferase RNA synthetases such as anti-Jo1 antibodies. Muscle damage can be described as perifascular necrotic, with presence of clonally expanded T cells (233). The symptoms of antisynthetase syndrome can include interstitial lung disease, Raynaud's phenomenon, arthritis, myositis, muscle weakness (236) and myalgia (254). Phagocytosis of perifascular necrotic muscle via macrophages is observed, but no inflammatory endomysial infiltrates are found in antisynthetase syndrome (254).

Overlap syndrome is a term used to describe the co-occurrence of idiopathic inflammatory myopathies with a separate autoimmune disease or connective tissue disease. For example, polymyositis and dermatomyositis sometimes occur with systemic sclerosis (255).

1.14 Autoantibody anti-NT5c1A

Currently there is no singular biomarker for sIBM, although an autoantibody has been identified called anti-NT5c1A (cytosolic 5'-nucleotidase 1A). The epitope recognised by this antibody (NT5c1A also known as cN1A or Mupp44) was found in perinuclear

regions and colocalised with vacuole rims in skeletal muscle of sIBM patients (256). This was originally thought to be specific for sIBM, however these antibodies have now been identified in autoimmune diseases including systemic erythematous lupus (SLE) and Sjögren's syndrome, and it does not appear specific to diseases involving the muscular system (257). The sensitivity of anti-NT5c1A in sIBM is 33-72 % with most studies reporting sensitivity of below 50 % (256, 258-263). Patients with anti-NT5c1A antibodies were more likely to take longer to stand compared to those without the antibody, but there was no difference in the 6 minute walk test, a measure of functional exercise capacity (263). A retrospective analysis found correlations between presence of anti-NT5c1A antibodies and disease severity, with positive patients having a higher mortality risk due to respiratory disease, more likely to have excess cytochrome oxidase deficient fibres, and higher rate of facial muscle weakness. Anti-NT5c1A antibody was not associated with time to use of a mobility aid but was weakly associated with overall need for mobility aids (260). Overall, the sensitivity of anti-NT5c1A antibody appears variable and its function in sIBM are not clear. Further work is needed to elucidate the mechanism of action of anti-NT5c1A in sIBM.

1.15 *In vivo* investigations of sIBM

A large amount of what we currently know about sIBM has been obtained through patient muscle samples. Investigating pathological features in patient biopsies is highly valuable, however it does not offer a dynamic platform to investigate interactions between features or causation. *In vivo* models of sIBM are useful for examining pathological mechanisms relevant to sIBM, for testing potential treatments, and examining cause and effect. Animal models for sIBM have previously been reviewed in 2008 by Katsumata and Ascherman (264), and more recently by Afzali *et al* (265).

One model used to investigate sIBM is transgenic valosin-containing protein (VCP) mouse models. This protein belongs to the ATPases associated with diverse cellular activities (AAA+) family that has a wide variety of cellular functions including protein degradation, autophagy, and apoptosis (266). In humans, mutations in VCP cause inclusion body myositis associated with Paget's disease of the bone with frontotemporal dementia (IBMPFD). This is an autosomal dominant disease that

affects multiple organ systems, and patients experience similar muscle symptoms and pathology to sIBM. This can include muscle weakness, fibre atrophy, and TDP-43 sarcoplasmic inclusions. However, there is no evidence of endomysial inflammation in IBMPFD (267). There is evidence of VCP variants being over-represented in sIBM patients (78). VCP mutations can be used to model some of the degenerative features of sIBM. A transgenic mouse model exists where mutant VCP is expressed; the mice develop similar pathologies to IBMPFD including progressive muscle weakness, rimmed vacuoles, disorganised mitochondria, and TDP-43 inclusions. Furthermore, muscle of transgenic VCP mice showed inflammatory infiltrations (268). VCP mice also have decreased muscle strength compared to wild type controls. Mouse models carrying VCP mutations have been utilised to assess the effect of potential treatments such as arimoclomol (219).

The muscle-specific overexpression of APP under the control of the muscle creatine kinase promoter (MCK-betaAPP model) has also been used to model degenerative features of sIBM. Overexpression of APP in transgenic mice lead to formation of centralised nuclei, infiltration of neutrophils but not macrophages or T cells, and decreased motor performance (269). Later studies of the same MCK-betaAPP model showed that higher expression of the APP transgene was found in type II fast twitch compared to type I slow twitch fibres, which was also found in sIBM muscle samples (270). This model was also modified to have knock-in gene expression of the presenilin-1 gene, part of the γ secretase complex involved in cleavage of APP (271). Additional expression of presenilin-1 resulted in higher intracellular β amyloid$_{42}$ (a toxic isoform (272)) expression, and infiltration of CD8+ cells (273). However, attempts to reproduce the original MCK-betaAPP model results were unsuccessful with no detection of amyloid β or fibrillar amyloid deposits in muscle, potentially due to problems expressing or incorporating the transgene in later mouse lineages (274).

Another method for recreating the degenerative features of sIBM in animal models is treating Wistar rats with chloroquine to inhibit autophagy. This shows increased presence of rimmed vacuoles, β amyloid deposition, and increased protein expression of atrophic genes (275). In this model, rats undergoing resistance exercise treatment

reduced the accumulation of β amyloid and rimmed vacuoles, decreased atrophy, and increased mitochondrial biogenesis (276). Other animal models or *in vivo* investigations of sIBM include but are not limited to immunisation of mice with sIBM patient-derived anti-cN1A antibodies (261) and feeding rabbits with cholesterol-enriched diets (277).

Recently, a xenograft model of sIBM has been created in which sIBM patient muscle tissue is engrafted into the hindlimb of immunodeficient mice (110). The grafts maintained sIBM characteristics including infiltration by human CD8+ T cells, rimmed vacuoles, and protein inclusions. Most importantly, this model recapitulates the two major components of sIBM pathology; degenerative features and immune involvement. Arguably, due to its semi-humanised nature using patient samples, this animal model has the greatest ability to recapitulate real-world sIBM pathology. And therefore offers potential for use in pre-clinical screening of therapeutics.

1.16 Primary human cell culture

C2C12 cells are a mouse cell line generated from a subclone of a normal adult mouse cell line (278)**.** These cells are a useful model to study myogenic processes, however their clonality and murine origin mean the applicability of C2C12 cell findings to human processes are limited. Whilst humans and mice share similarities in their muscle cell characteristics, there are also differences. For example, both humans and mice have the muscle stem cell of satellite cells, but murine quiescent satellite cells express CD34 whilst human cells do not (279).

Using primary human cells alleviates problems associated with using a clonal lineage whilst ensuring relevance to human-specific physiology. Using primary myogenic cells from multiple human donors means results are not specific for one individual. However, using primary human myogenic cultures also has caveats. For example, most primary cells experience replicative senescence where cells withdraw from the cell cycle, limiting the amount of time these cells can be used in culture. Contaminating cells may also be present in primary muscle cell preparations. In some preparations, serial passaging results in cultures being over-run with fibroblasts (280, 281).

Furthermore, whilst using multiple primary human cell lines has broader applicability than mouse cells or a single human donor, this also introduces inter-donor variability and heterogeneity between samples which can cause wide variation in results.

1.17 *In vitro* investigations of sIBM

In vitro models offer a system in which cause and effect can be investigated. One of the predominant ways in which sIBM characteristics have been modelled *in vitro* is using transgenic expression of amyloid precursor protein (APP) (219, 282, 283). Ahmed *et al* (219) found that transfecting primary rat muscle cells with human β APP caused inclusion body formation containing protein aggregates of β-APP, ubiquitin, and TDP-43 in myotubes. Furthermore, β-APP overexpression caused TDP-43 to mislocalise to the cytoplasm and not be expressed in the nucleus. MHC I protein expression was also increased by β-APP overexpression. Therefore, overexpression of APP recapitulated some of the key non-inflammatory features of sIBM. Other models have relied on addition of pharmacological agents to cause dysregulation of cellular pathways. The addition of tunicamycin or thapsigargin to cause endoplasmic reticulum stress (284, 285), or epoxomysin to inhibit the 26S proteosome system (116, 286) has been investigated. For example, treating normal human primary myotubes with epoxomicin caused increased expression of p62 protein (116), and αB crystallin (286). These culture systems rely principally on modelling the degenerative feature of protein aggegation and dysfunctional protein degradation pathways.

Addition of inflammatory cytokines to myotube cultures has also been used to model sIBM. Treatment with IL-1β and IFNγ can recapitulate both inflammatory and degenerative features of sIBM. Combination treatment of human primary myotubes with IL-1β and IFN-γ caused upregulation of pro-inflammatory chemokines and cytokines CXCL-9, CCL-3, CCL-4, IL-6, and IL-1β. Furthermore, IL-1β either alone or combined with IFNγ increased APP expression when visualised with immunofluorescent microscopy, and combined IL-1β and IFNγ increased APP protein expression (145). In a similar set of experiments, primary human myotubes treated with IL-1β and IFNγ showed increased αB-crystallin expression as well as increased APP (287). αB crystallin is a heat shock protein that is found to be upregulated in sIBM

fibres with a mean positivity of 9.8 % of sIBM fibres. Polymyositis fibres can also be positive for αB crystallin (288). The protein expression of αB crystallin was also upregulated in sIBM compared to neurogenic muscular atrophy control muscle samples (289).

It was found that the release of HMGB1 (high mobility group box 1) from primary human myotubes treated with IL-1β and IFNγ was elevated compared to untreated myotubes after 24 and 48 hours (290). HMGB1 is a nuclear protein involved in chromatin architecture (291) that can also be secreted as an inflammatory cytokine or alarmin when it binds to RAGE (receptor for advanced glycosylation end products). HMGB1 may be associated with amyloid β pathology in Alzheimer's Disease (292). Due to this and the fact RAGE and HMGB1 were found upregulated in dermatomyositis and polymyositis (293, 294), the authors (290) anticipated HMGB1 and RAGE would also be upregulated in sIBM. Indeed, as well as IL-1β and IFNγ inducing HMGB1 in myotubes, sIBM muscle samples had increased protein (but not mRNA) expression of HMGB1 (290). IL-1β and IFNγ treatment but not these cytokines individually have also been shown to upregulate the mRNA expression of iNOS (inducible nitric oxide synthase) and nitrotyrosine in primary human myotubes (295). Nitrotyrosine is a marker of oxidative stress (296), and together with iNOS has been found in sIBM muscle (297). Another cytokine used in modelling inflammatory stress in sIBM is TNFα (219, 295), which has been investigated alone or in combination with IL-1β and/or IFNγ. For example, rat myotubes exposed to IL-1β or TNFα had increased expression of APP and amyloid-β, but an absence of inclusion bodies was observed (219).

1.18 Sestrins

Sestrins are evolutionarily conserved proteins located predominantly in the cytoplasm. They function as detectors of leucine and cellular stress, and can exert their functionality through inhibition of mTORC (mammalian/mechanistic target of rapamycin complex) signalling (298). In humans there are three forms of sestrin proteins (numbered 1 to 3), with sestrin-2 being the best characterised of the three. Sestrin-2 contains three major protein domains; an N terminal structuring domain (NTD), a loop linker domain, and a C-terminal domain (CTD). The NTD has antioxidant

activity whereas the CTD and the linker domain are responsible for leucine binding. The CTD is also responsible for GATOR 2 binding for mTORC1 inhibition (299).

Sestrin-2 is important in the regulation of mitophagy by aiding translocation of parkin to defective mitochondria, an initiating step in mitophagy (300). In *Drosophila melanogaster*, where there is only one sestrin orthologue (termed dSesn), loss of sestrin causes mitochondrial dysfunction including disorganised crystae, muscle degeneration and thoracic muscle sarcomeric structure loss, and cardiac malfunction. An increase in reactive oxygen species was also observed as well as accumulation of polyubiquitinated proteins (301).

SESN1 (Sestrin-1) belongs to a group of genes called growth arrest and DNA damage-inducible (GADD) genes, and is highly expressed in skeletal muscle. It shares some of the same functions of sestrin-2 including nutrient sensing, inhibition of mTORC1, and induction of autophagy. Its expression is regulated by p53 and FoXO (302). In muscle, sestrin-1 is regulated by exercise. 48 hours after resistance exercise, the expression of sestrin-1 protein was increased, which was also observed under chronic exercise conditions (303). However, in a separate study exposing mice to chronic aerobic exercise, the levels of sestrin-1 were decreased, whereas acute aerobic exercise increased sestrin-1 expression (304). This suggests different forms of exercise may lead to differential activation of sestrin-1. Sestrin-2 also plays a role in skeletal muscle homeostasis as well as response to exercise, with sestrin phosphorylation increased by exercise training in healthy active men, whilst protein expression was not affected by acute or chronic resistance exercise (303). On the other hand, chronic aerobic exercise reduced sestrin-2 levels in mice, similar to sestrin-1 (304). Further, over-expression of dSesn increased exercise endurance even without training, and sestrin-null *Drosophila* had no increased endurance with exercise training (305) suggesting an important role for sestrins in mediating exercise endurance.

Sestrin-2 can also prevent atrophy in aged skeletal muscle through inhibition of mTORC1 signalling (306). Furthermore, aged mice that were double-knockout for sestrin-1 and 2 had a reduction in muscle stem cells and a decreased ability to regenerated injured muscle (307). In men aged 65-80 compared to those aged 18-30,

sestrin-1 mRNA was upregulated but sestrin-1 protein expression was decreased. Further, sestrin-2 protein quantity was not affected by age, but older men had lower expression of the delta isoform of sestrin-2, representing a highly phosphorylated state (308).

Due to their stress sensing abilities and inhibition of mTORC1, sestrins have been touted as protective against ageing (309). However, in the immune system sestrins have been associated with detrimental ageing. In T cells of older humans and mice, there was a higher presence of a complex termed sestrin-dependent MAPK activation complex (sMAC) that inhibited T cell functionality through simultaneous activation of ERK (extracellular signal-regulated kinase), JNK, and p38 (310). In differentiated senescent-like CD8+ T cells there was an association of sestrin-2 with a protein complex of NKG2D and DAP12 that promoted cytotoxicity. Decreasing sestrin-2 levels decreased this protein complex, and also restored T cell receptor signalling (311).

It appears that sestrins have beneficial stress sensing and muscle regenerating effects, but negative age-associated mechanisms within the immune system. Sestrins have not previously been implicated in sIBM. However, due to their functions in muscle homeostasis, mitochondrial regulation, stress sensing, and potential pathophysiology in ageing immune cells, sestrins may play a role in this disease. Sestrins are regulated by cell stress responses that are implicated in sIBM, namely the unfolded protein response activated with ER stress (312). Furthermore, when ER stress was induced in hepatocytes, overexpression of sestrin-2 prevented ER-stress induced cell death (312, 313).

1.19 Hypotheses and aims

The over-arching hypotheses of the thesis are two-fold. First, that the inflammatory features of sIBM cause the non-inflammatory phenotypes within skeletal muscle. Second, that inflammation is the causative factor for muscle weakness in sIBM.

The major aim of this project is to investigate whether inflammatory mediators can cause non-inflammatory features in human skeletal muscle cells that are observed in sIBM. This will be achieved by examining cultures of healthy primary human myotubes

exposed to different inflammatory conditions, building on previous work with inflammatory cytokine treatment, as well as investigating novel inflammatory insults for myotube responses. The non-inflammatory features relevant to sIBM that will be focussed on are TDP-43 and p62 sarcoplasmic protein aggregation as well as TDP-43 mislocalisation. The second aim of this thesis is to investigate whether certain inflammatory insults can cause muscle weakness, by utilising a previously published functional 3D muscle construct called myobundles to test active force generation.

This thesis is structured so that Chapters 4, 5, and 6 investigate the effects on TDP-43 and p62 of different inflammatory mediators. Chapter 3 characterises TDP-43 and p62 through myogenesis. The focus of Chapter 7 is investigating force generation from myobundles under two inflammatory conditions examined in Chapter 4 and Chapter 6.

Chapter 2:
General Methods

Chapter 2. General methods

All reagents were purchased from ThermoFisher Scientific, UK unless otherwise stated.

2.1 Skeletal muscle-derived cell culture

Skeletal muscle-derived cells from Lonza Clonetics™ (UK, CC-2580) or Cook MyoSite® (USA, SK-1111) were grown in either Skeletal Muscle Growth Media (ready-to-use) (Promocell®, Germany, C23060) supplemented with 1 % penicillin-streptomycin and 10 % foetal bovine serum (FBS), or Ham's F10 nutrient mix supplemented with 20 % FBS, 1 µM dexamethasone (Sigma, UK), 10 ng/mL basic fibroblast growth factor (bFGF, Peprotech, UK), and 1 % penicillin-streptomycin. Appendix Table 0.1 shows a breakdown of which donors were used for which experiments. Cells were differentiated in N2 differentiation medium: DMEM/F12 1:1, 1 % N2 supplement, 1 % L-glutamine, 1 % insulin-transferrin-selenium, and 0.2 % penicillin-streptomycin. Cells were maintained at 37 °C with 5 % CO_2 in a humidified incubator. Cells were routinely passaged by washing once with phosphate buffered saline (PBS) and incubating in 4 mL 1 % trypsin-EDTA (Sigma, UK T3924) per T75 flask for approximately 5 minutes at 37 °C. Trypsin was neutralised with an equal volume of F10 medium containing 20 % FBS and cells were counted using a NucleoCounter NC-200 with Via1-Cassettes™ (both ChemoMetec, Denmark). Cell solution was centrifuged at 220 xg for 5 minutes, supernatant discarded and pellet resuspended in 10 mL fresh growth media for addition to a new T75 flask. Skeletal muscle derived cells were split at approximately 70 % confluency.

Skeletal muscle-derived cells were used between passages 4 and 7 with most experiments conducted at passage 7. For seeding cells for fluorescent microscopy, 13 mm round coverslips (VWR, UK) were sterilised in 70 % ethanol for approximately 30 minutes before coating with ready-to-use Geltrex (A1569601) for 1 hour at room temperature. Light microscopy images of cells in culture were taken with a Zeiss Primovert inverted microscope with Zeiss Axiocam 105 color camera.

Skeletal muscle-derived cells were cryopreserved in freezing solution: 40 % FBS, 10 % dimethyl sulfoxide (DMSO) and 50 % growth medium, after trypsinising as described above. Two to three cryovials were prepared per T75 flask. The cell pellet was resuspended in freezing solution, aliquoted into cryovials, and frozen in a Mr. Frosty™ freezing container containing 2-isopropanol at -80 °C. Cryovials were transferred to liquid nitrogen vapour phase for long-term storage. To defrost cells, cryovials were removed from liquid nitrogen storage and quickly warmed until the cryovial contents were liquid. The contents of the cryovial was transferred into approximately 5 mL prewarmed growth medium and centrifuged at 220 xg to remove DMSO. Cell pellet was resuspended in fresh growth medium and added to a T75 flask.

2.2 Treatment of myotubes with IL-1β and IFNγ

Cytokines were prepared in 0.1 % w/v bovine serum albumin (BSA) in PBS, 0.2µm filtered. Recombinant human IL-1β and IFNγ (both Peprotech, UK 300-02 and 200-01B respectively) were used at the following concentrations: IL-1β 20 ng/mL IFNγ 750 ng/mL, either as a combined treatment or as individual cytokines. Proliferating skeletal muscle cells were seeded in 24 well plates at a density of $4x10^4$ cells/well and grown for 48 hours in Skeletal Muscle Cell Growth Medium or Ham's F10 medium. Only one proliferation medium was used per set of experiments. After which, cells were differentiated to myotubes with N2 differentiation medium. After 7 days differentiation, inflammatory cytokines IL-1β+IFNγ, cytokines individually, or control (vehicle control equal volume of 0.1 % w/v BSA or no treatment control) was added in N2 medium for 48 hours without additional medium change.

2.3 Cytotoxicity assay

Cytotoxicity upon addition of inflammatory mediators was measured using CytoTox 96® non-radioactive cytotoxicity assay (Promega, UK G1780) following manufacturer's instructions. The assay is based on the measurement of lactate dehydrogenase (LDH) release from cells that have lost plasma membrane integrity, indicating cell death. Cytotoxicity was measured in 50 µL samples of medium from the cultured cells after treatment with relevant inflammatory mediators or controls as described in

subsequent chapters. Substrate solution was prepared by adding 12 mL of assay buffer to the powdered substrate mix. 50 µL of substrate solution was added to samples for 30 minutes at room temperature in the dark, before addition of 50 µL of stop solution, and optical density read at 492 nm using a Multiskan™ FC plate reader. Results were normalised to a medium-only control and a positive cytotoxicity control, where cells were incubated in lysis solution for 45 minutes before commencing the assay. Cytotoxicity was expressed as a percentage of the positive lysis control.

2.4 Immunofluorescent microscopy

Skeletal muscle-derived cells were seeded on Gibco Geltrex-coated 13 mm round coverslips in 24 well plates. The cells were allowed to proliferate for 48 hours before differentiation for 5 or 7 days before treatment (listed in subsequent chapters). All volumes for immunofluorescence reagents were 300 µL per well unless otherwise stated. At the appropriate time point, medium was removed, cells were washed with PBS, and fixed with 4 % paraformaldehyde solution (Fisher Scientific, UK 12777847) for 10 minutes at room temperature. Paraformaldehyde solution was removed, washed once and fresh PBS was added. Cells were stored at 4 °C for up to two weeks at this point. Cells were permeabilised with 0.1 % v/v triton X 100 in PBS for 15 minutes before being blocked with 5 % goat serum in PBS for 30 minutes to 1 hour. Primary antibodies sestrin-2 1:150 TDP-43 1:150 and p62 1:100 (all from Proteintech, UK, see Table 2.1 for product codes) diluted in blocking buffer were added by inverting the coverslip onto a 30 µL drop of antibody solution on Parafilm®, and incubating in a humidified chamber overnight at 4 °C. After washing 3 times in PBS for 5 minutes each, coverslips were incubated in Alexa Fluor™-conjugated (Alexa Fluor™ 488 anti-rabbit (A-11008) or Alexa Fluor™ 546 anti-mouse(A-11030)) secondary antibodies at 1:350 (Invitrogen, UK) for 1 hour at room temperature. Cells were washed and HCS CellMask™ red or deep red was added at 1:5000 in PBS for 30 minutes to visualise all cell contents. HCS CellMask™ red was only used with Alexa Fluor™ 488 secondary, HCS CellMask™ deep red was used with Alexa Fluor™ 546. Afterwards, DAPI (4',6-diamidino-2-phenylindole) at 5 µg/mL in PBS was added for 5 minutes. After washing, cells were mounted onto glass slides with DAKO fluorescence mounting medium

(Agilent, USA), left for up to two hours for mounting media to dry, and sealed with clear nail polish.

To analyse TDP-43, p62 and sestrin-2 distribution, images were captured using an Olympus IX81-ZDC inverted widefield fluorescent microscope with Micro-manager open source software. For p62 and TDP-43 aggregation analysis, cells were imaged using a Zeiss LSM 980 Airyscan 2 inverted confocal microscope with Zen Blue software. For each secondary antibody used, a control was imaged on each microscope where cells were incubated with secondary antibody only to check for non-specific staining, with no non-specific staining visualised at the laser/emitter intensities used.

2.5 TDP-43 localisation

TDP-43 localisation in skeletal muscle-derived cells was assessed using widefield fluorescent microscopy at 10 X magnification. DAPI and HCS CellMask™ staining was used to observe subcellular compartments of the nucleus and sarcoplasm respectively. Based on the observed staining TDP-43 was classified as being within the nucleus, sarcoplasm, nucleus and sarcoplasm, or neither (not expressed). Localisation was quantified for both single nucleated and multinucleated cells. Localisation was expressed as a percentage of total number of cells observed with HCS CellMask™ for each localisation compartment. For Chapters 4, 5, and conditioned medium experiments of Chapter 6, TDP-43 localisation analysis was conducted blinded.

2.6 p62 particle analysis

Four z-stacks composed of six images each with voxel depth 0.3 µm were obtained using confocal microscopy at 63 X magnification for Chapter 4 and Chapter 5 using a Zeiss LSM980 Airyscan 2. For Chapter 6, eight z-stacks each composed of two images approximately 0.9 µm apart were captured with a Zeiss LSM 800 upright confocal microscope. Images were analysed using NIH Image J (USA). Obtained images were split into individual colour channels and converted to 8-bit. p62 and HCS CellMask™ channels were manually thresholded. p62 particle frequency and size was determined in the p62 channel using NIH Image J using the “analyse particles” function with pixel size over 2 for 512x512 sized images or pixel size over 3 for 1024x1024 sized images.

p62 frequency was the total number of particles obtained per image with the “analyse particles” function and p62 size was the average particle size per image. p62 particle frequencies were normalised to percentage area coverage per image using HCS CellMask™ staining, to account for differences in myotube size. In the thresholded cell mask channel, percentage area of image coverage was obtained with the following macro:

```
setOption("BlackBackground", false);
run("Convert to Mask", "method=Default background=Dark");
run("Despeckle", "stack");
run("Fill Holes", "stack");
macro "Measure Stack" {
     saveSettings;
     setOption("Stack position", true);
     for (n=1; n<=nSlices; n++) {
       setSlice(n);
       run("Measure");
    }
    restoreSettings;
 }
```

From line 5, the measure stack macro was obtained from https://imagej.nih.gov/ij/macros/Measure_Stack.txt. Depending on the cell layout within the image, the “Fill Holes” function was omitted to prevent background areas being filled in and counted as myotube. p62 particle analysis was conducted blinded.

2.7 TDP-43 sarcoplasmic aggregate analysis

The same images for p62 analysis were used for TDP-43 sarcoplasmic aggregate analysis as myotubes were stained for both p62 and TDP-43. Sarcoplasmic aggregates were identified manually in 3 of 6 slices (first, middle, last) of z-stacks as punctate areas of staining. Using Image J, freehand regions were drawn around aggregates to

measure their area in μm^2. TDP-43 aggregate frequencies were normalised to percentage area coverage per image of cell mask staining using the cell mask coverage results obtained in Section 2.6. TDP-43 colocalisation with p62 was assessed for each identified TDP-43 aggregate using thresholded p62 and TDP-43 channels. Any area of overlap between TDP-43 and p62 objects over two pixels was considered colocalised. Percentage colocalisation is the percentage of TDP-43 aggregates that colocalised with p62 puncta for all aggregates observe for one donor under one condition. TDP-43 aggregate analysis was conducted blinded.

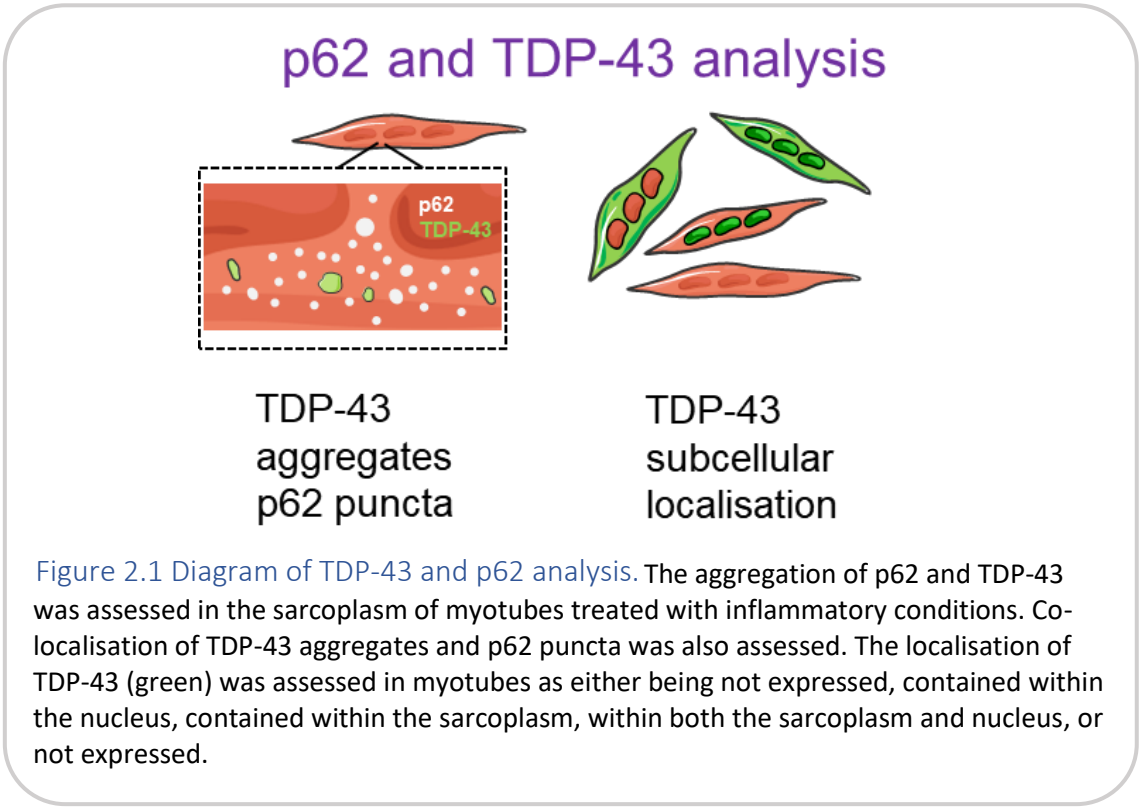

Figure 2.1 Diagram of TDP-43 and p62 analysis. The aggregation of p62 and TDP-43 was assessed in the sarcoplasm of myotubes treated with inflammatory conditions. Co-localisation of TDP-43 aggregates and p62 puncta was also assessed. The localisation of TDP-43 (green) was assessed in myotubes as either being not expressed, contained within the nucleus, contained within the sarcoplasm, within both the sarcoplasm and nucleus, or not expressed.

2.8 SDS PAGE and Western blotting

SDS PAGE (sodium dodecyl sulphate polyacrylamide gel electrophoresis) and Western blotting was performed to analyse relative protein expression between conditions. Myotubes were seeded directly onto 6 wells of tissue culture treated 24 well plates. After differentiation for 7 days and inflammatory treatment for 2 days, cells were lysed in RIPA (radio immunoprecipitation assay) buffer (Sigma-Aldrich, UK) with Pierce

protease and phosphatase inhibitors. Cells were washed with ice cold PBS twice before 45 µL RIPA buffer was added per well and left for 5 minutes. After which, 1000 µL pipette tips were used to scrape cells into solution. Cells in RIPA buffer were transferred to microcentrifuge tubes and incubated at 4 °C with either shaking or rotation for 30 minutes. Lysates were centrifuged at 4 °C at 16000 xg for 20 minutes and the aqueous phase was transferred to new microcentrifuge tubes for storage at -80 °C until later use.

Protein concentration of lysates was determined using a Micro Lowry kit with Peterson's modification (Sigma, UK) or Pierce bicinchoninic acid (BCA) assay kit. Only one type of protein assay kit was used per chapter. For Micro Lowry, fresh BSA (Sigma, UK) standards were prepared in distilled water from 400 µg/mL to 50 µg/mL, with water blank. 20 or 30 µL of sample was prepared to a volume of 500 µL in distilled water. To each sample and standard, 500 µL of Lowry reagent was added and incubated for 20 minutes at room temperature, after which 250 µL Folin and Ciocalteu's phenol working solution was added and left for 30 minutes at room temperature. 100 µL of each sample and standard mix was transferred to a 96 well plate and absorbance was read at 620 nm using a Multiskan™ FC plate reader. The blank reading was subtracted from the samples and standards. A standard curve was plotted from the prepared standards and used to calculate sample total protein amount based on original volume of sample. For the BCA assay, fresh BSA standards were prepared in distilled water from 25 to 2000 µg/mL. 25 µL of sample, standard or water blank were added to a 96 well plate. Standards were added in duplicate. BCA working reagent was prepared by mixing 50 parts BCA reagent A with 1 part BCA reagent B. 200 µL of working reagent was added to samples and standards and incubated at 37 °C for 30 minutes. The plate was cooled at room temperature for 5 minutes before reading absorbance at 562 nm using a Tecan plate reader. The blank reading was subtracted from standards and samples. Standard curves were generated from the standards and used to calculate protein amount in samples.

Approximately 10 µg of protein was denatured by heating at 95 °C for 5 minutes in Bolt™ SDS sample buffer and Bolt™ reducing agent with a combined volume of 60 µL.

PAGE separation is a method for separating proteins based predominantly on their size. Samples and prestained protein ladder (Proteintech, UK PL0001) were loaded into the wells of a Bolt™ 4-12 % Bis-Tris 1 mm mini protein gels. PAGE separation was conducted in Bolt™ MOPS running buffer at 200 V for approximately 35 minutes or until sample loading band ran near to the end of the gel. Novex XCell SureLock™ electrophoresis tanks were used. After electrophoresis, gels were liberated from their cases and gel foot was cut off. Polyvinylidene difluoride (PVDF) membranes were activated for 2 minutes in methanol, washed once in water and twice in Bolt™ MOPS transfer buffer, and added to a transfer sandwich as follows: 3X blotting sponges, filter paper, gel, activated membrane, filter paper, 3X blotting sponges. After adding filter paper on top of the membrane, bubbles were pressed out using a stripette gently rolled over the filter paper. The sandwich was pressed tightly between the blot module, added to the transfer tank, and the blot module was filled with Bolt™ MOPS transfer buffer. Western blotting was performed for 70 minutes at 30 V. After which, membranes were blocked with 5 % w/v skimmed milk powder in TBS-T (1% v/v Tris buffered saline (Cell Signalling Technology, UK) in distilled water with 0.1 % v/v Tween 20 for 1 hour. Primary antibodies (see Table 1) were added in milk overnight at 4 °C with gentle rocking. Membranes were washed in TBS-T three times with rocking for 5-10 minutes each. Secondary antibodies goat anti-mouse HRP (horseradish peroxidase) and donkey anti-rabbit HRP (Proteintech, UK) were added at 1:2000 for 1 hour at room temperature, after which membranes were re-washed in TBS-T.

For detection of protein bands, Pierce™ ECL (enhanced chemiluminescence) Western Blotting Substrate was made fresh and added to the membrane for 1 minute before pouring off. Membranes were developed using either X-ray exposure film or direct imaging. For film-based detection, CL-XPosure™ films were placed on top of ECL stained membranes wrapped in plastic in the dark. Exposure time was optimised for each antibody. Films were developed in the dark with an SRX-101A processor (Konica Minolta, UK). For Chapter 5 and LC3 in Chapter 4, a SynGene G:Box gel documentation and analysis system was used to directly image membranes. Representative cropped Western blots are displayed with approximate location of nearest ladder marker.

The same membrane was used to detect multiple target proteins. Between staining for some proteins, membranes were stripped using Restore™ Western blot Stripping Buffer for up to 1 hour at room temperature with shaking followed by up to 40 minutes at 37 °C. Membranes were washed and re-blocked with 5 % milk-TBS-T, re-probed with secondary antibody and re-exposed to check primary antibody removal. Densitometry was performed on scanned film or saved direct images using Image J, and protein of interest normalised to glyceraldehyde 3-phosphate dehydrogenase (GAPDH) loading control. Developed films were scanned using an Epson scanner with a calibration step ladder with known values using the y = a+b*ln(x-c) function in Image J. Direct images of membranes from SynGene G:box gel documentation were calibrated using image J using the "uncalibrated OD" function.

Membranes were probed for combinations of sestrin-2, sestrin-1, p62, TDP-43, myosin heavy chain, LC3 and GAPDH (see Table 2.1 for antibodies and concentrations). For long term storage, all membranes except those used in Chapter 5 were stripped as described above before drying completely at room temperature and freezing at -80 °C with membrane sandwiched between filter paper and cardboard. For Chapter 5 membranes, long term storage was carried out in the same way without stripping. For analysis of sestrin-1 and LC3, membranes were defrosted at room temperature, reactivated with methanol for 1 minute, and re-blocked with 5 % milk

Primary antibody	**Primary dilution**
Sestrin-2, mouse (Proteintech 66297-1-Ig)	1:1000 (2 µg/mL)
Sestrin-1, rabbit (Proteintech 21668-1-AP)	1:400 (1.75 µg/mL)
GAPDH, mouse (Proteintech, 6004-1-Ig)	1:5000 (0.2 µg/mL)
TDP-43, rabbit (Proteintech, 10782-2-AP)	1:2000 (0.2 µg/mL)
p62/SQSTM1, mouse (Proteintech, 66184-1-Ig)	1:2500 (0.53 µg/mL)
Myosin heavy chain, mouse (DSHB, MF20)	1:48 (0.5 µg/mL)
LC3, rabbit (Proteintech 14600-1-AP)	1:1:250 (0.4 µg/mL)

Table 2.1 Antibodies for Western blotting.

(sestrin-1) or 3 % w/v 0.2 µm filtered BSA (LC3) for 1 hour before re-probing. After probing following the above steps, membranes were re-frozen at -80 °C without stripping. Uncropped blot scans or images are available in Appendix Figure 0.1.

2.9 ELISA

DuoSet® Enzyme-linked immunosorbent assays (ELISA) were purchased from R&D systems, UK. Human IFN gamma (DY285B) human IL-12 p70 (DY1270) human IL-6 (DY206), and human TNF alpha (DY210) were used. ELISA is a technique for measuring and quantifying secreted factors such as cytokines, growth factors or chemokines in media collected from cells or biological samples. ELISA were performed following manufacturer's instructions. Between each step (except after addition of substrate solution) plates were washed three times with wash buffer (PBS with 0.05 % v/v tween 20) and blotted to remove all liquid. All incubation steps were conducted at room temperature.

Nunc MaxiSorp™ immunoplates were coated with 100 µL recommended dilutions of capture antibody in PBS, sealed with plate sealers, and incubated overnight. Plates were blocked with 0.2 µm filtered 1 % w/v BSA (reagent diluent) for 1 hour, before incubation of samples and standards diluted in reagent diluent for 2 hours in sealed plates. Reagent diluent was used as a blank. Recommended concentrations of detection antibody diluted in reagent diluent were added for 2 hours in sealed plates. Streptavidin horse radish peroxidase (HRP) diluted in reagent diluent was incubated for 20 minutes before washing and addition of substrate solution (1:1 mix hydrogen peroxide and tetramethylbenzidine, R&D Systems, UK) for 20 minutes. Colour development was halted with 2N sulphuric acid. Optical density was determined using a Multiskan™ FC plate reader by subtracting readings at 540 nm from 450 nm to account for any imperfections in the plate. Blank optical density results were subtracted from sample and standard results. Standard curve was generated using $\log_{10}$ optical density of the standard concentrations, which was used to calculate sample concentrations.

2.10 Statistics and figure preparation

Graph plotting and statistics were performed using Graphpad Prism 7. Normality of data was tested using Shapiro-Wilk normality test and appropriate analyses listed in each results chapter used. For data not showing a normal distribution, non-parametric tests were used, except for two-way ANOVA where normality was not tested. Results are displayed and listed as mean ± standard error of mean (SEM) for normally distributed data or median ± interquartile range for non-normally distributed data. TDP-43 localisation was displayed as mean ± SEM. Statistical significance was set at $p < 0.05$, with $0.075 > p > 0.05$ results described as "weak evidence". For $0.075 > p > 0.05$ significance was not indicated on graphs. When more than one treatment was tested at a time, post-hoc testing was conducted for differences between the control condition and each treatment condition. Illustrated diagrams were prepared with Servier Medical Art (https://smart.servier.com/). Images available under a creating commons licence were also used.

Chapter 3: Basal characteristics of myogenic cells

Chapter 3. Basal characterisation of myogenic cells

3.1 Introduction

3.1.1 Myogenesis

In vitro studies of muscle are often conducted using either proliferating myogenic cells called myoblasts or differentiated myotubes. Myoblasts differentiate into myotubes in a process called myogenesis or myofusion. In this process, proliferating myoblasts are removed from the cell cycle forming myocytes. Myocytes merge their sarcolemmas together creating multi-nucleated myotubes. In embryonic development or during *in vivo* skeletal muscle repair, these myotubes would go on to fuse together to form myofibrils, and eventually myofibres. In adult regenerating skeletal muscle, myoblasts can fuse either with each other generating new myotubes, or with existing myofibres (314, 315).

Muscle-specific stem cells exist, called satellite cells which are marked by their Pax7 expression (316). *In vivo,* satellite cells are positioned between muscle fibres and the basal lamina. They form a quiescent stem cell pool that are activated to build new skeletal muscle, for example after injury or during exercise (314, 317) (Figure 3.1). Four myogenic regulatory factors (MRFs) MyoD, Myf5, myogenin, and MRF4 are involved in proliferation and differentiation of myogenic lineage cells both during development and postnatally. Pax7 binds to enhancers of MyoD and promoters of Myf5, triggering their expression. When satellite cells are activated, most co-express MyoD, Myf5 and Pax7, with MyoD and Myf5 expression continuing in proliferating myoblasts. MyoD activates myogenin leading to initiation of differentiation, which is accompanied by downregulation of MyoD. Both MyoD and myogenin have auto-regulatory functions, controlling their own expression. Differentiated myotubes are marked by joint expression of MyoD, myogenin, and MRF4, with myogenin and MRF4 regulating expression of myotube genes such as myosin heavy chain (318-320). Other pathways are also involved in myogenesis. Wnt signalling through T cell factor (TCF) is essential for differentiation of primary human myotubes, with a specific level of pathway

activity required for successful myofusion (321). Two muscle-specific fusion proteins are responsible for driving myoblast to myotube fusion; myomaker and myomerger-minion-myomixer. These two proteins together are capable of causing multinucleated fusion between fibroblasts expressing these factors (322), showing these proteins are the driving force for myofusion.

In vitro, myogenesis can be quantified by the ratio of nuclei present in a myotube compared to those in single nucleated cells. This is termed the myofusion index (MFI) (323). Other measures of myofusion include the number of nuclei within a myotube, with higher nuclei count representing a more differentiated culture. Furthermore, the expression of proteins regulated in myogenesis can be examined. Myosin heavy chain (MHC), which forms part of the contractile apparatus of skeletal muscle, increases with increasing time of differentiation (324, 325). Alternative methods of assessing

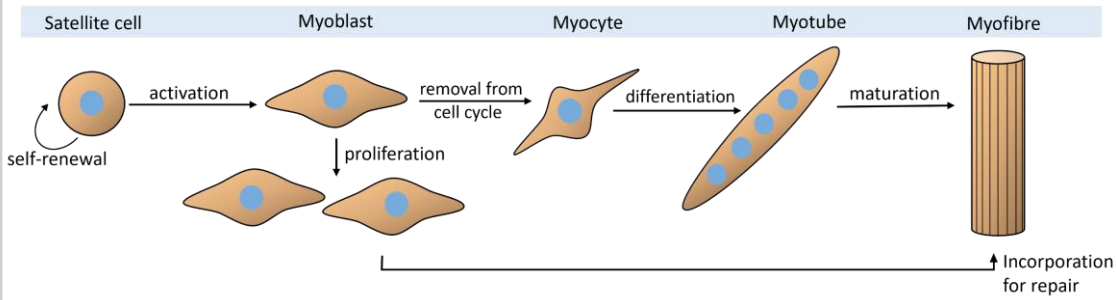

Figure 3.1 Process of myogenic differentiation. Satellite cells are the stem cells of muscle and maintain a quiescent pool which become activated upon muscle injury or hypertrophy. Myoblasts are capable of proliferation and can integrate into existing myofibres for repair. Myocytes are incapable of proliferation and differentiate to form multi-nucleated myotubes. *In vivo* but not *in vitro*, myotubes assemble into myofibres.

myogenesis have also been proposed, for example using the activity of acetylcholinesterase (AChE) in cultured muscle cells (326). Using CD56+ sorted myogenic cells, this study found acetylcholinesterase activity reflected the ability of cells to fuse into myotubes. The amount of AChE activity was positively correlated with the myofusion index.

3.1.2 TDP-43, p62 and sestrins in myogenesis

TDP-43 is involved in the regulation of myogenesis. Whilst it is usually found located in the nucleus, it can be observed in small granules termed myo-granules in the sarcoplasm of healthy cells. These myo-granules are found located at sites of newly forming sarcomeres and bind mRNA molecules important in myogenesis, namely sarcomeric proteins including titin and myosin. Furthermore, depletion of *TARDBP* in C2C12 cells caused growth arrest and cell death, showing TDP-43 is essential in skeletal muscle (327). A role for TDP-43 in forming neuromuscular synapses has also been demonstrated using *Drosophila* models and RNA interference experiments (328).

There are limited investigations into changes in p62 during myogenesis. *In vitro*, increased time of differentiation of myotubes lead to a decrease in total p62 protein expression. This was due to increased autophagic flux during differentiation of myotubes, as p62 is degraded with autophagy, and accompanied by increased LC3II expression (329). Sestrin-2 mRNA levels are highly elevated on day two of C2C12 cell differentiation, whereas there is no difference in *SESN2* mRNA expression at later differentiation time points (330). Sestrin-1/2 knockout mice have altered metabolism and mTORC1 signalling in satellite cells as well as increased satellite cell proliferation. Furthermore, aged sestrin-1/2 knockout mice have an increased loss of satellite cells and reduced skeletal muscle repair (307). This shows that sestrins are important for maintaining the quiescent pool of satellite cells. Overall, TDP-43, p62, and sestrins are regulated or involved in myogenesis.

3.1.3 Aims and hypotheses

The aim of this chapter is to characterise basal myogenesis in cultured skeletal muscle-derived cells and to examine whether the proteins of interest p62, TDP-43, and sestrins are altered during myogenesis. This is to examine if differences in myogenic differentiation between donors may influence analyses of these proteins under other experimental conditions.

It is hypothesised that markers of myoblast fusion including nuclei per myotube, myofusion index, myosin heavy chain (MHC) expression, and AChE expression will

increase with increased time of differentiation. As TDP-43 has previously been shown to be involved in myogenesis through formation of myo-granules, it is hypothesised that TDP-43 subcellular localisation and protein expression will change through myogenesis. It is hypothesised that p62 protein expression will decrease with increased time of differentiation. Sestrin-1 and sestrin-2 protein expression during myogenesis have not been extensively examined previously, therefore the hypothesis for their expression during myogenesis is two-tailed.

3.2 Methods

3.2.1 Cell culture

Skeletal muscle-derived cells were cultured as described in Section 2.1. 8 x10^4 cells/mL (4x10^4 cells per 24-well) was used as a concentration for cell seeding. For myofusion index, cells were seeded on Geltrex-covered slides, proliferated for 2 days, before differentiation for 9 days. For acetylcholinesterase assay, the same concentration of cells was used but seeded directly into 24 well plates.

3.2.2 Acetylcholinesterase assay

Acetylcholinesterase assay based on the Ellman's assay (331) was used to measure AChE expression in undifferentiated myogenic progenitors and myotubes differentiated for 7 days (DMEM/F12, 2 % horse serum, 1 % L-glutamine, 1 % penicillin-streptomycin), following the protocol described in Thurner *et al* with modifications (326). Cells were grown in 24 well plates, media was removed at the appropriate time point and 300 µL 3 mM 5,5'-dithiobis(2-nitrobenzoic acid) (DTNB,Sigma Aldrich, UK) in American Public Health Association Phosphate (APHA) buffer (13.11 g potassium phosphate monobasic, 3.89 g sodium carbonate, and 0.5 mL Triton X 100 in 500 mL distilled water) was added to cells for 2 minutes at room temperature. At the same time DTNB was also added to a standard curve (250 to 1.95 mU/mL) of acetylcholinesterase from electric eel (in APHA buffer, Sigma Aldrich, UK). After two minutes, 50 µL 15 mM acetylthiocholine iodide (Sigma Aldrich, UK) in distilled water was added to samples and standards and incubated for 20 minutes at room temperature in the dark, after which the absorbance was read at 405 nm with a Tecan plate reader. Sample activity of AChE was determined from the standard curve of absorbances and known concentrations of AChE from electric eel.

3.2.3 Myofusion index and nuclei per myotube

Cells were seeded on Geltrex coated 13 mm coverslips and proliferated for two days in either F10 growth media or SMG growth media. Only one growth medium was used per experiment. For experiments examining differentiation over time, day 0

differentiation was collected after two days proliferation. Media was then switched to N2 differentiation media, with slides collected and fixed with 4 % paraformaldehyde solution on days 4 and 7 of differentiation, or day 9 for myofusion index (MFI) per donor.

MFI was defined as the ratio of nuclei contained within a myotube with three or more nuclei relative to the total number of nuclei, expressed as a percentage. Myofusion index was calculated from widefield fluorescent images stained for DAPI and HCS CellMask™ following the staining protocol as defined in Section 2.4. For individual donors, MFI was calculated based on averages from four images at 10 X and two biological repeats. For MFI during myogenesis, a widefield stitched image with 10 % overlap of 16 individual 10 X images was taken and a region of interest was selected encompassing 35 % of the stitched image using NIH Image J. This region of interest was used to calculate MFI and nuclei per myotube of myotubes containing over 3 nuclei.

3.2.4 SDS PAGE and Western blotting

SDS PAGE and Western blotting was conducted as previously described in Section 2.8. Cell lysates were collected at day 0, 4, and 7 of differentiation. Blots were stained for p62, TDP-43, sestrin-1 and sestrin-2, and myosin heavy chain at the dilutions defined in Table 2.1.

3.3 Results

3.3.1 Basic donor characterisation and myofusion index of myogenic donors

Figure 3.2 A shows a table containing characteristics of the most commonly used myogenic donors as listed by the suppliers. Appendix Table 1 contains a list of which donors were used to generate each figure in this thesis. Myofusion index (MFI) was measured for each donor (Figure 3.2 B), except HSKMDC 12 which was only used in Chapter 7. The range of MFI between donors was between 19 % and 76 % with a mean across all tested donors of 39 %. There was no association of MFI with BMI (r^2 = 0.093 p = 0.515) or age (r^2 = 0.386 p =0.100) of donors.

3.3.2 Acetylcholinesterase expression was not different between undifferentiated and differentiated myogenic cells

To examine whether the expression levels of acetylcholinesterase in skeletal muscle-derived cells could be used as a measure of myotube differentiation, a modified Ellman's assay (331) was used. For 14 myogenic donors including 7 donors that were only used for this experiment, there was no significant difference in AChE activity between proliferating myogenic precursors and myotubes differentiated for 7 days (Figure 3.3). The mean acetylcholinesterase activity in the undifferentiated group was 12.5 ± 1.9 mU.

3.3.3 Myotubes were capable of spontaneously contracting

Spontaneous contraction of myotubes was occasionally observed after 5-9 days differentiation. Myotubes that contracted appeared elevated above the plane of the tissue culture surface (Figure 3.4), potentially due to increased width of myotubes or partial detachment. Myotube spontaneous contraction was observed in both untreated tissue culture wells and on coverslips coated with Geltrex. Contraction was only observed for a brief period of less than five minutes after removing cells from culture incubators, before myotube contraction slowed, then stopped. Spontaneous contraction was not observed in all cultured donors, the donors in which spontaneous contraction was most frequently observed were HSMM 1, HSKMDC 2, and HSKMDC 9.

3.3.4 Myosin heavy chain expression, number of nuclei per myotube, and myofusion index was higher during differentiation than proliferation

To further characterise myogenesis, protein levels of myosin heavy chain (MHC) were assessed using Western blotting on days 0, 4, and 7 of differentiation (Figure 3.6). Compared to proliferating myoblasts on day 0, there was a significant upregulation of myosin heavy chain on day 4 and day 7 of differentiation with approximately 15-fold and 24-fold increase respectively. However, there was not a significant difference in MHC expression between day 4 and day 7.

The number of nuclei per myotube and the MFI were also examined during differentiation as markers of myogenesis (Figure 3.5). There was a significantly higher number of nuclei per myotube on the differentiation timepoints day 4 and 7 compared to proliferation on day 0 (Figure 3.5 A). The median number of nuclei was 3 ± 4, 6 ± 7, and 6 ± 9.0 for day 0, 4, and 7 respectively. However, there was no difference in the number of nuclei per myotube between day 4 and day 7. As the median nuclei per myogenic precursor (myoblast) was above 1, proliferating cultures contain some cells that have already begun differentiated into myotubes. There was a higher myofusion index on both day 4 and day 7 compared to day 0 (Figure 3.5 B). The median myofusion index was 0 ± 3 %, 47 ± 27 %, and 53 ± 50 % for day 0, 4, and 7 respectively. However, there was no difference between nuclei per myotube or MFI on day 4 to day 7.

A

Donor	Company source	Age	Sex	BMI	Ethnicity	Smokes?	Drinks alcohol?
HSMM 1	Lonza	17	F	19	Caucasian	Y	Y
HSMM 2	Lonza	25	M	33	Black	N	Y
HSMM 3	Lonza	20	F	unknown	Caucasian	N	Y
HSKMDC 2	Cook MyoSite	18	M	21	Caucasian	N	N
HSKMDC 3	Cook MyoSite	41	M	25	Caucasian	Y	Y
HSKMDC 4	Cook MyoSite	32	F	42	Caucasian	Y	N
HSKMDC 6	Cook MyoSite	36	F	26	Caucasian	Y	Y
HSKMDC 9	Cook MyoSite	51	M	26	Caucasian	N	N
HSKMDC 12	Cook MyoSite	18	F	25	Caucasian	N	N

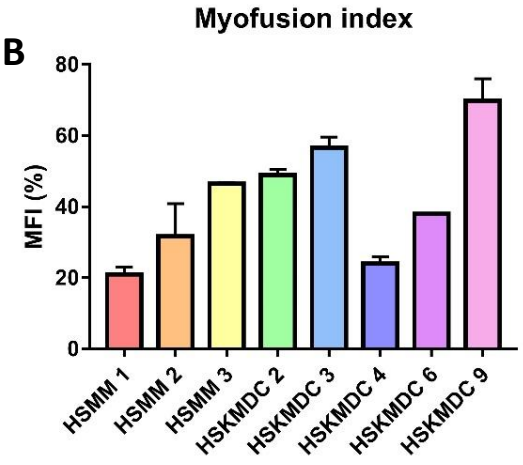

Figure 3.2 Muscle cell donor characteristics.

(A) Table showing the characteristics of commercially sourced muscle cells. (B) Myofusion index (MFI) of the most commonly used donors after 9 days of differentiation. MFI is the percentage of nuclei within a myotube compared to the total number of nuclei. n = 2 biological repeats. HSMM – human skeletal muscle myoblasts, HSKMDC – human skeletal muscle-derived cells. BMI – body mass index.

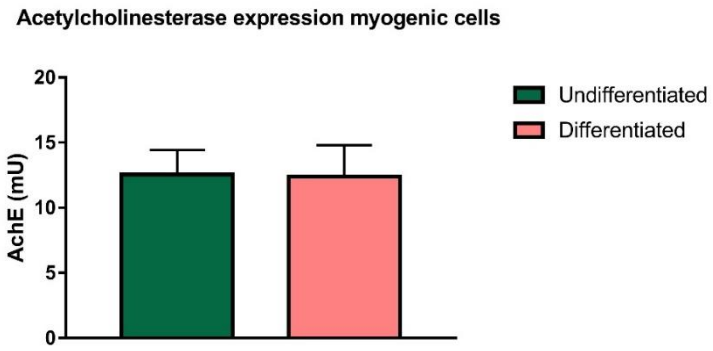

Figure 3.3 Acetylcholinesterase expression was not different between myoblasts and myotubes. The expression of acetylcholinesterase was not different between undifferentiated myogenic cells and differentiated myotubes (Student's T test, p = 0.956). n = 14 myogenic donors.

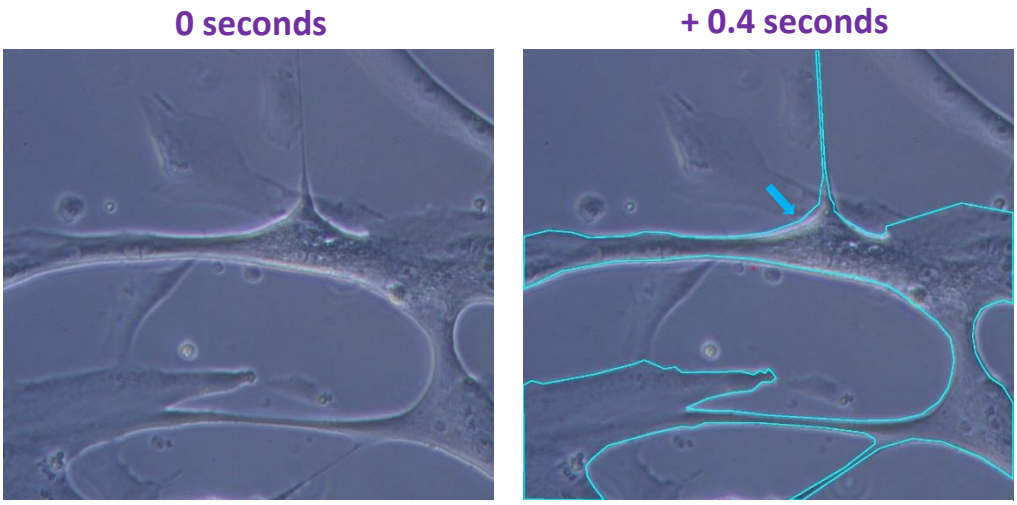

Figure 3.4 Spontaneous contraction of myotubes in culture. Outline from timepoint 0 seconds overlayed at + 0.4 seconds (blue line), showing contractile movement (blue arrow).

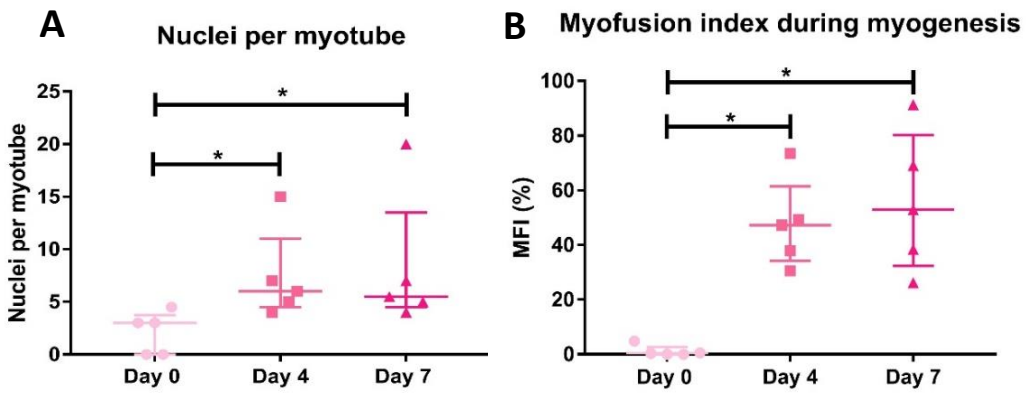

Figure 3.5 Differentiation over time in myogenesis. (A) Number of nuclei per myotube, with a minimum of 3 nuclei. There was a significant increase in nuclei from day 0 to day 4, and day 0 to day 7, but not between day 4 and 7 (Kruskal-Wallis test with Dunn's multiple comparisons p = 0.0428, p = 0.0428, p = 0.999 respectively). (B) Myofusion index (MFI) calculating the percentage of nuclei inside a myotube (minimum 3 nuclei) compared to total nuclei count. There was a significant difference in MFI between day 0 and day 4, and day 0 and day 7, but not day 4 and day 7 (Kruskal-Wallis test with Dunn's multiple comparisons p = 0.0397, p = 0.0139, and p = 0.999 respectively. n = 5 myogenic donors.

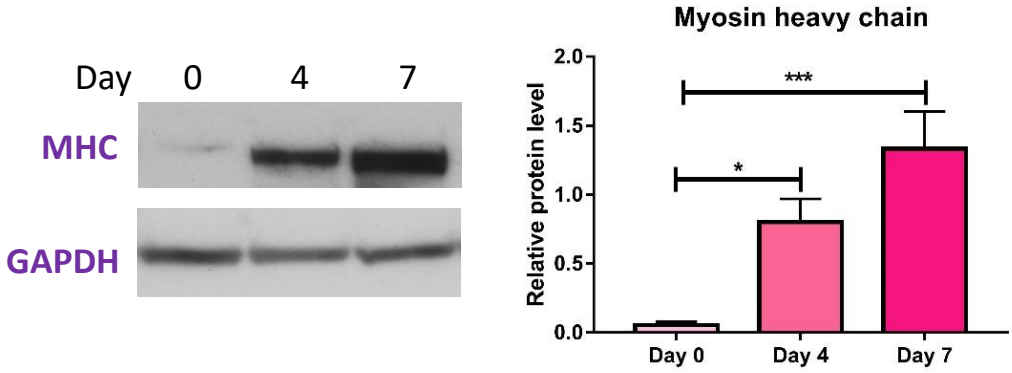

Figure 3.6 Myosin heavy chain during myogenesis. Myosin heavy chain (MHC) levels normalised to GAPDH. There was a significant difference between the three time points (one-way ANOVA, p = 0.0008). Myosin heavy chain levels are significantly higher on day 4 vs day 0, and on day 7 vs day 0 (Tukey's multiple comparisons, p = 0.0312 and p = 0.0006 respectively). There is no significant difference between day 4 and day 7 (p = 0.1395). n = 6 myogenic donors.

3.3.5 TDP-43 localisation was consistent and protein levels remained constant during myogenesis

To examine whether localisation of TDP-43 was affected by myogenesis, TDP-43 localisation was assessed using image analysis on days 0, 4, and 7 of differentiation. Examples of TDP-43 localisation in myotubes is shown in Figure 3.7. There was no difference in the localisation of TDP-43 between time points via two-way ANOVA. However, there was a significant difference in the distribution of TDP-43 between the subcellular compartments regardless of time points (two-way ANOVA $p < 0.0001$) showing TDP-43 is not distributed evenly between the subcellular localisations. Regardless of differentiation time point, the localisation with the highest TDP-43 expression was nucleus only with 51 ± 9 % (two-way ANOVA with Tukey's post-hoc test) (Figure 3.8 A-B). TDP-43 protein expression during myogenesis was assessed using Western blotting. There was no difference in TDP-43 protein expression between the three time points examined (Figure 3.8 C).

3.3.6 p62 levels did not change during differentiation

To test whether p62 is altered during myogenesis, p62 protein levels were assessed using fluorescent microscopy and Western blotting on days 0, 4, and 7 of differentiation. The strongest p62 staining appeared on day 7. For all time points, typical punctate staining in the sarcoplasm could be observed, although this was less pronounced on day 4 (Figure 3.9 A). At all time points, diffuse sarcoplasmic and nuclear expression were also observed. Total p62 protein levels during myogenesis were assessed using Western blotting (Figure 3.9 B), which showed no difference in p62 protein expression between any of the time points assessed.

3.3.7 Sestrin-2 was highest on day 7 of differentiation

To assess whether sestrin-2 was influenced by myogenic differentiation, immunofluorescence was used to examine distribution, and Western blotting was used to compare protein expression on days 0, 4, and 7 of differentiation. Sestrin-2 localisation was diffuse throughout the sarcoplasm on all days of differentiation, with some puncta of increased staining. There was no sestrin-2 localisation to the nucleus

(Figure 3.10 A). Sestrin-2 protein levels were not different between day 0 and day 4, however there was increased sestrin-2 protein expression on day 7 of differentiation compared to day 0 (Figure 3.10 B). Expression was 4.5 times higher on day 7 compared to day 0.

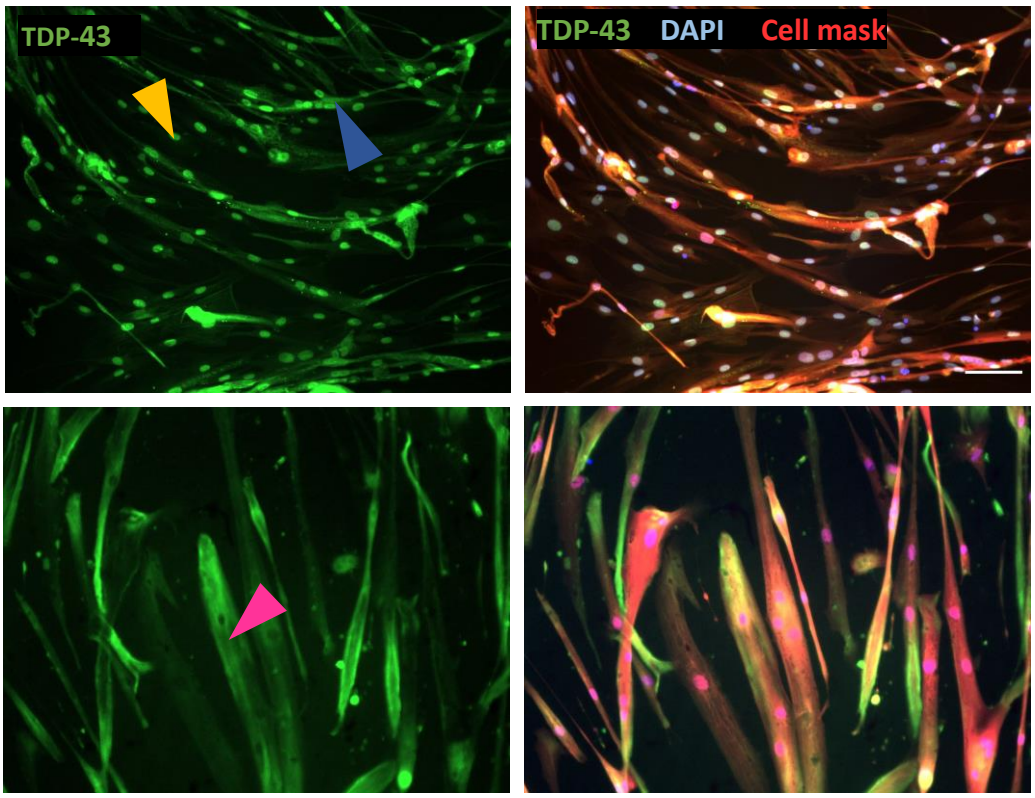

Figure 3.7 Examples of TDP-43 localisation classification. TDP-43 immunofluorescent images showing examples of myogenic cells with nuclear only TDP-43 (yellow arrowhead), nuclear and sarcoplasmic TDP-43 (blue arrowhead), and sarcoplasmic only TDP-43 (pink arrowhead). Scalebar = 100 µm.

3.3.8 Sestrin-1 protein levels were highest on day 4 of myogenesis

To better understand the role of sestrin-1 during myogenesis, its protein levels were compared via Western blotting on day 0, 4, and 7 of differentiation. Sestrin-1 levels were highest on day 4 of differentiation, before decreasing on day 7 to similar levels as day 0 (Figure 3.10 C). Sestrin-1 expression was 71 % higher on day 4 compared to day 0, and 40 % higher compared to day 7.

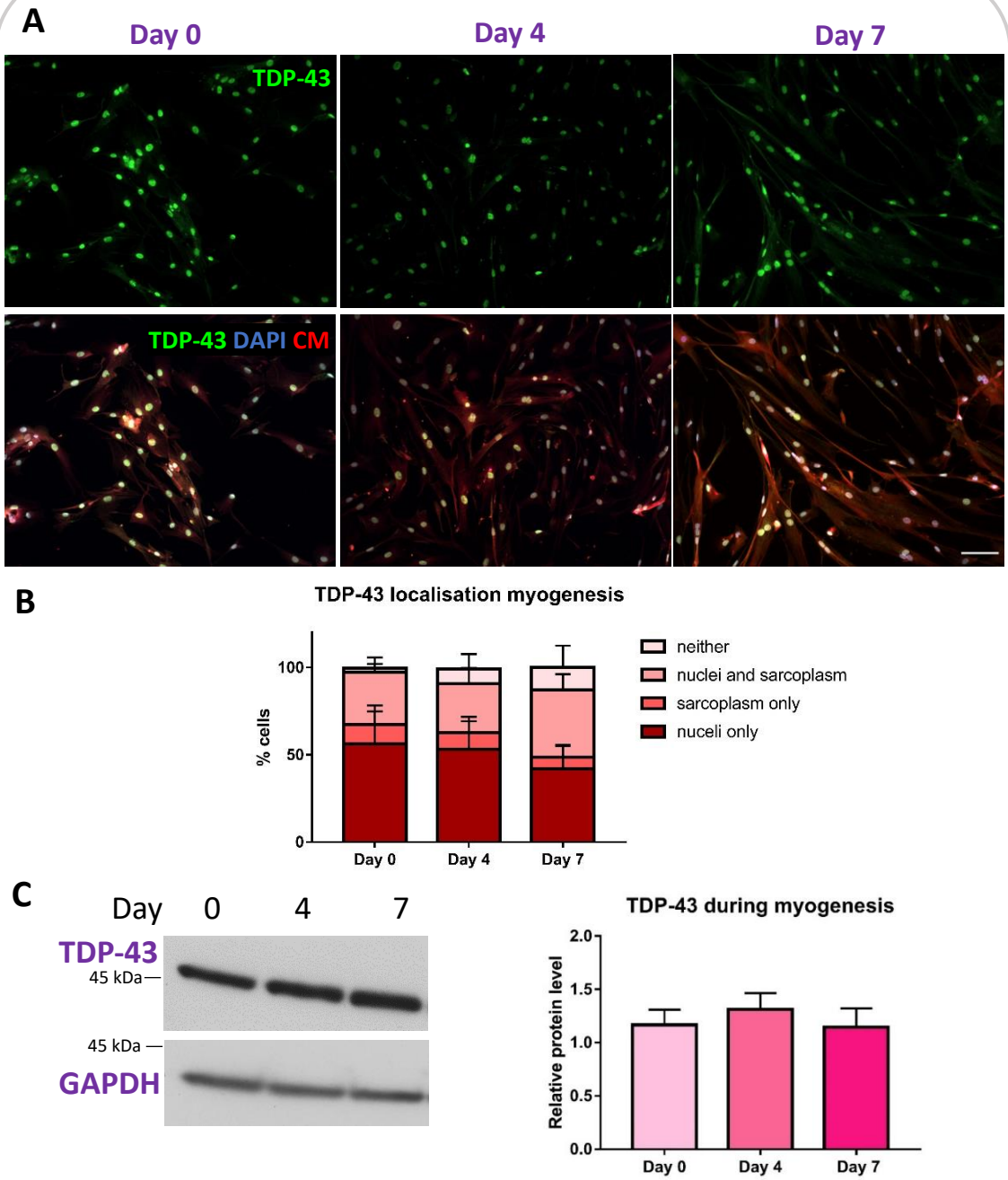

Figure 3.8 TDP-43 localisation and expression during myogenesis. (A) Images of TDP-43 distribution on day 0, 4, and 7 of differentiation. CM- cell mask. Scale bar = 100 µm. (B) TDP-43 distribution n = 4 myogenic donors. There was no difference in TDP-43 localisation between timepoints (two-way ANOVA, p = 0.999). (C) Total TDP-43 expression levels during myogenesis normalised to GAPDH. There was no difference in expression between time points (one-way ANOVA, p = 0.716). n = 6 donors.

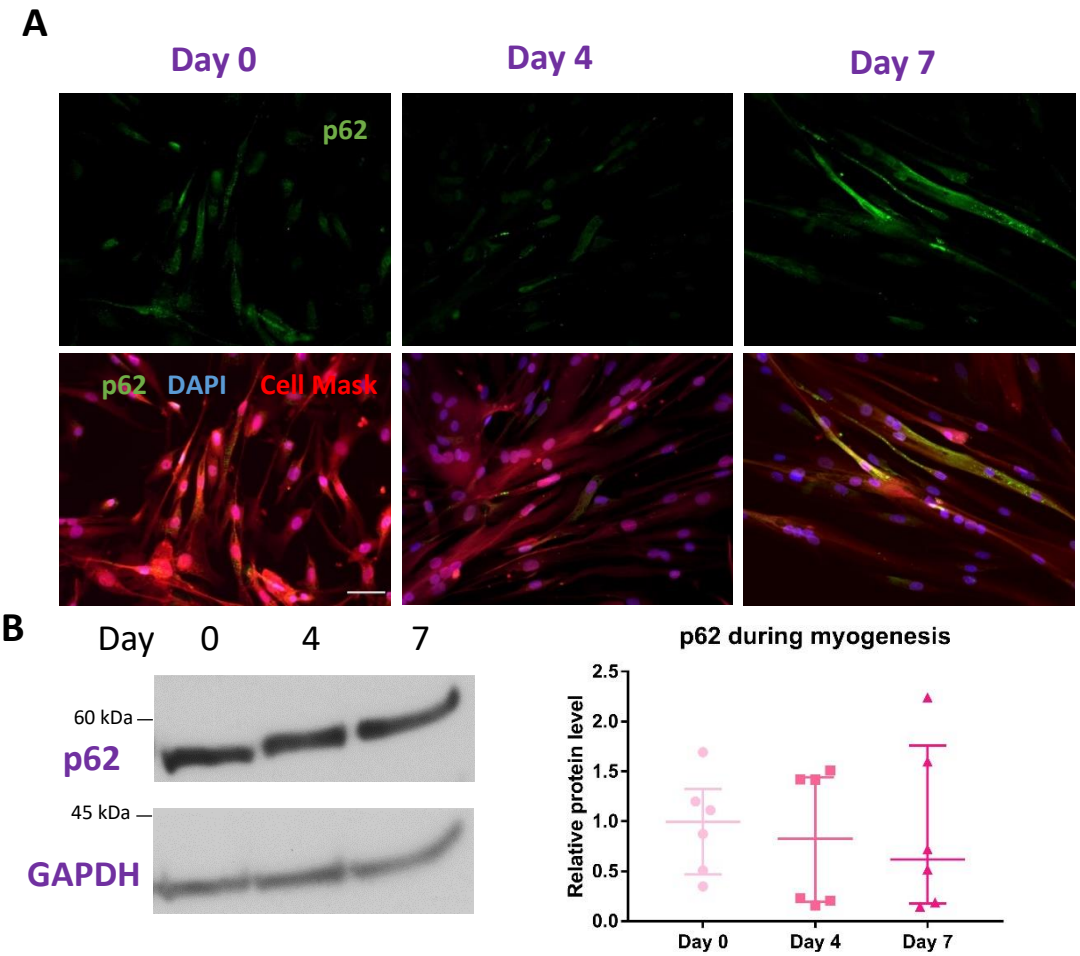

Figure 3.9 p62 during myogenesis. (A) Fluorescent microscopy images of p62 localisation during myogenesis, scale bar 50 µm. (B) Total protein levels of p62 during myogenesis normalised to GAPDH levels. There was no difference between the time points (Kruskal-Wallis test p = 0.863). n = 6 donors.

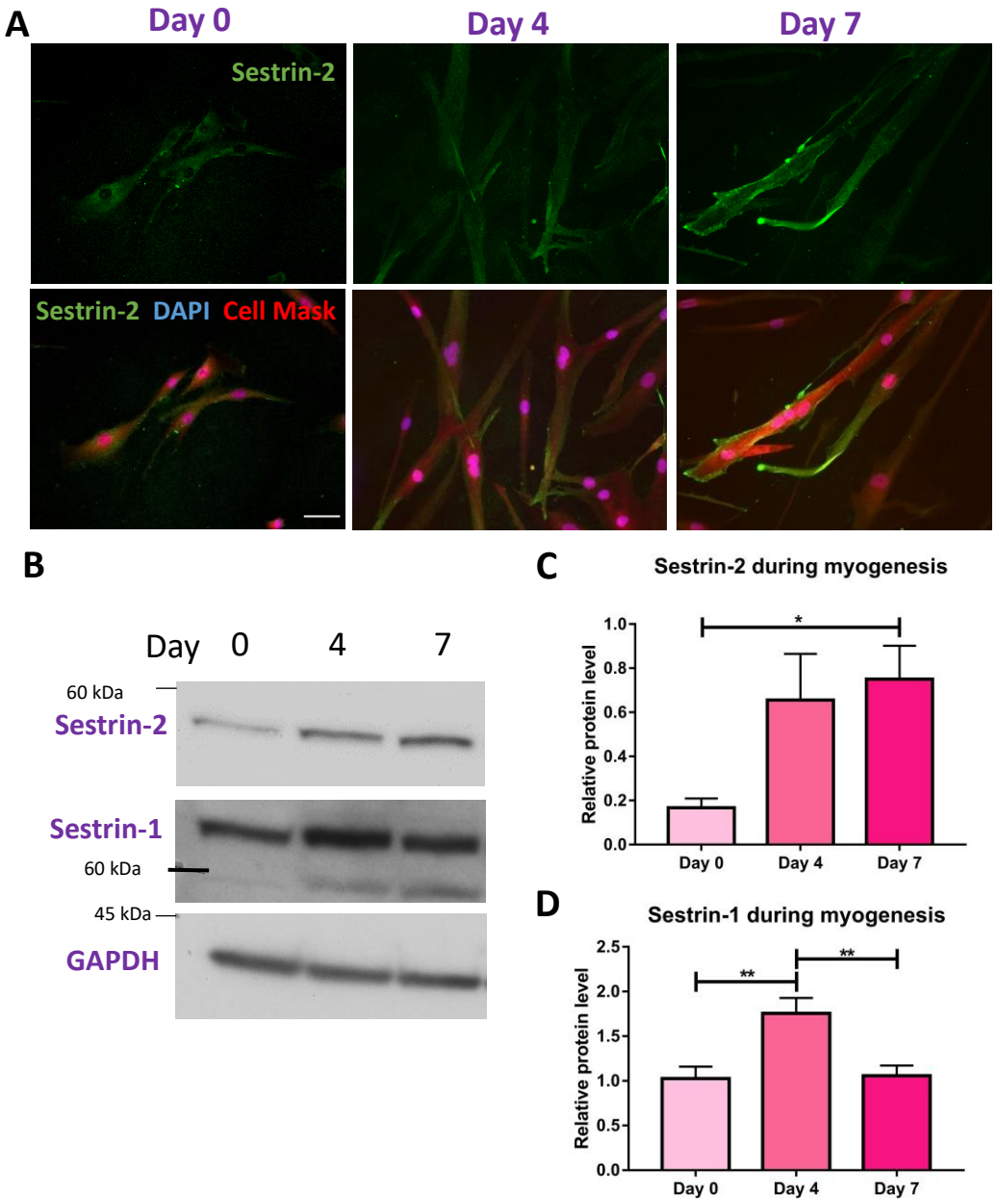

Figure 3.10 Sestrin-2 and sestrin-1 follow different expression patterns during myogenesis. (A) Fluorescent microscopy images of sestrin-2 localisation throughout differentiation. Scale bar = 50 µm. (B) Representative blots of sestrin-2 and sestrin-1. (C) Total protein levels of sestrin-2 during myogenesis normalised to GAPDH levels. There was a difference between the days (one-way ANOVA p = 0.0342), with day 7 sestrin-2 protein levels higher than day 0 (Tukey's multiple comparisons, p = 0.0396). There was no difference between any other time point (day 0 vs day 4 p = 0.0898, day 4 vs day 7 p = 0.8994). (D) Sestrin-1 levels during myogenesis normalised to GAPDH. There was a significant difference between the three time points (one-way ANOVA, p = 0.0036). Sestrin-1 levels are significantly higher on day 4 than on day 0 or day 7 (Tukey's multiple comparisons, p = 0.0068 and p = 0.0092). n = 6 donors.

3.4 Discussion

The aim of this chapter was to characterise basic features of myogenesis in human cultured muscle cells, and to examine any changes to the proteins of interest TDP-43, p62, and sestrins during myogenesis. Some of the analyses in later chapters do not differentiate between myotubes and single nucleated cells (e.g TDP-43 localisation, Western blotting), therefore it is important to know whether differential differentiation impacts on these analyses. The time points of differentiation examined in this chapter were mostly day 0 during proliferation, day 4, and day 7 of differentiation. However, in subsequent chapters, many of the experimental time points were conducted at day 9 of differentiation (7+2 treatment). Therefore it would have been beneficial to extend all of the analyses to the time point of day 9 to ensure that there were no unexpected effects between day 7 to day 9 in TDP-43, p62, or differentiation markers.

Skeletal muscle cells were obtained from commercial sources. The donors did not have any reported muscle-related health conditions and were therefore classed as healthy. By using healthy skeletal muscle cells, the effect of certain inflammatory conditions on non-inflammatory features of sIBM can be examined. However, the demographics of the donors does not accurately reflect those of sIBM patients, for example all but one donors were below the age of 50 and half were female, whilst sIBM has a male predominance (37). An attempt was made to ensure donors were healthy, especially considering BMI as obesity may affect pathways relevant to myogenesis (332, 333) and skeletal muscle repair (334, 335). However, it was not possible to exclude all donors who had a high BMI due to limited availability of donor cell samples, and two donors had BMI over 30.

The skeletal muscle-derived cells were obtained from two separate commercial sources, which may mean myogenic cells from one company are different to the other due to different isolation and purification procedures. Ideally, myogenic donors would only be sourced from one commercial company. Colloquially, there was no obvious

differences in cells from the two commercial sources in terms of differentiation or proliferation.

Inter-donor variation also existed in these samples, both with the demographic characteristics and the cells themselves. It would have been beneficial to characterise the myogenicity of the starting population of cells for each donor, for example in terms of their CD56, desmin, and myoD expression to understand the purity and myogenicity of the cells. The presence of contaminating fibroblasts could also have been tested, for example with staining for TE-7. Furthermore, at the passages used, senescent markers such as senescence-associated β-galactosidase staining and p16 expression could have been examined (280). Another characterisation that could have been performed is testing how long each donor could proliferate in culture before reaching replicative senescence. This may have given greater understanding of the variability in some of the myogenic features examined here, and if the cells had entered senescence at the passages used.

There was a wide variety in myofusion indices between donors used. This makes it difficult to extrapolate between experiments where different donors were used for experiments that do not differentiate between myotubes and precursors. The decision was made to use multiple human donors instead of a robust cell line such as mouse C2C12 cells or one human donor, despite the fact that donor differences could influence the response of myogenic cells to inflammatory factors in subsequent chapters. This was to ensure that any significant effect was strong enough to occur across multiple donor cell populations and avoid results that are less generalisable to human cells, despite the small number of donors used here.

3.4.1 Myogenic differentiation

Previously, it was thought that human myotubes are not capable of contraction *in vitro* (336, 337), with multiple studies failing to culture contractile human myotubes (338, 339). Here, spontaneous myotube contraction was observed in multiple cultures without complex differentiation formulations (339) or micropatterned surfaces (340) that have been used previously. However, as noted by others, this contraction was

visible only for short periods before myotubes stopped twitching, indicating a probable temperature sensitive contractile response (339). Spontaneous contraction was observed in four myogenic donors, whilst others did not show any detectable signs of contraction.

Myogenic differentiation was not significantly different between the two differentiation timepoints examined of day 4 and day 7. This suggests maximal differentiation may be reached by day 4. However, testing of each day during differentiation would be needed to find the maximal differentiation timepoint. An important consideration is that some myotubes may be detaching from the surface and therefore not being counted in analyses of nuclei per myotube, MFI, and MHC expression. Whilst some of these myotubes may be undergoing apoptosis or necrosis, it is also possible that healthy myotubes detach from the culture substrate when they are spontaneously contracting. The similarity between day 4 and day 7 for differentiation markers show day 7 is an appropriate start point for experiments on mature myotubes (i.e. when inflammatory factors are administered). In this way, the effect on cells undergoing myogenesis should be limited.

Whilst MFI, nuclei per myotube and MHC expression reflected the difference between proliferating and differentiating myotubes, the detection of acetylcholinesterase was not an accurate measure of differentiation. Here, detection of myotubes was performed manually by eye with HCS CellMask™ and DAPI counterstaining. Usually, MFI calculations are based on staining with myosin heavy chain (341), which offers another layer of specificity toward differentiated myotubes. Perhaps, the MFI calculations performed here overestimated the differentiation of myotube cultures based on a general cell stain. There was not a detectable difference in acetylcholinesterase activity between myogenic precursors and myotubes. However, this may be due to the higher passage number used here (approximately passage 7). Previously, it has been shown that acetylcholinesterase levels in myotubes decrease with advanced passage (326). The aim of the original study was to examine the potency of myogenic cells for cell therapy applications, where measurements of AChE may be suitable, however as it is significantly impacted by passage, detection of AChE

should not be used as a replacement for more robust myofusion standards such as myofusion index and nuclei per myotube. Furthermore, the experiments by Thurner *et al* normalised AChE expression to protein quantification which was not performed here.

3.4.2 TDP-43, p62, and sestrins during myogenesis

TPD-43 localisation was not different between myoblasts and myotubes, with sarcoplasmic TDP-43 visible during proliferation. This is contrary to previous results with mouse primary skeletal muscle cells where there is no TDP-43 observed in the sarcoplasm in myoblasts (327). Potentially, this could be a result of increased passage of the human primary cells resulting in a drift towards a more differentiated phenotype in the myoblasts despite observed proliferation. Indeed, this was evidenced by the observation of cells containing multiple nuclei in proliferating cultures. TDP-43 expression was also not affected by differentiation timepoints, showing TDP-43 is equally important in proliferation and differentiation of skeletal muscle cells.

p62 protein expression was not different between the three myogenesis time points examined, contrary to previous results showing p62 expression decreased with myogenesis due to increased autophagic activity (329). This suggests that further investigations of p62 via Western blotting with inflammatory mediators in subsequent chapters will not be affected by different levels of differentiation. To determine whether autophagic flux also increases with myogenesis in the cells used here, other markers of autophagy such as LC3 could be utilised.

In subsequent chapters, TDP-43 and p62 were assessed for sarcoplasmic aggregation in myotubes with confocal microscopy, to see if inflammatory mediators trigger aggregation of these proteins similar to what is seen in sIBM. However, the aggregation of TDP-43 and p62 was not assessed during myogenic differentiation. Amyloid-like inclusions of TDP-43 have been found in the sarcoplasm during myogenic differentiation and are involved in regulating sarcomeric mRNA (327). Therefore, TDP-43 sarcoplasmic aggregation may be different under the differentiation time points examined here, which was not examined. In subsequent chapters, TDP-43

sarcoplasmic aggregation was selectively assessed in myotubes, therefore any effects of differentiation on TDP-43 aggregation should be minimised.

Sestrin-1 and sestrin-2 were both differentially regulated in myogenesis, however at different time points. Sestrin-1 is not maintained throughout myogenesis whilst sestrin-2 levels appear elevated at day 7, suggesting its continued presence is necessary for myotubes. Previously, sestrin-2 mRNA levels were only found to be significantly different from day 0 of differentiation after two days differentiation (330). Here, the results do not follow the same expression pattern. However, protein expression of sestrin-2 during myogenesis has not previously been examined, and it is possible that despite the peak mRNA at day 2, sestrin-2 protein continues to accumulate during differentiation at subsequent differentiation time points. The temporary upregulation of sestrin-1 during myogenic differentiation appears a novel finding, suggesting either sestrin-1 is important for myogenesis or is regulated by processes that are upregulated during myogenesis. Sestrin-1 knockout mice showed no difference in myofibre size or force generation, but have worsened disuse atrophy compared to wild type controls, but specific effects on differentiation or satellite cells were not examined (306).

3.4.3 Summary

Overall, this chapter shows that the features of TDP-43 and p62 that will be examined in later chapters are unlikely to be influenced by myogenesis. However, sestrin-1 and sestrin-2 are differentially expressed during myogenesis suggesting an importance for these proteins in myogenic differentiation. This, combined with the variability of myofusion between donors, may introduce some difficulty in interpreting results of sestrin expression with inflammatory treatments.

Chapter 4:
Effect of IL-1β and IFNγ on myotubes

Chapter 4. Effect of IL-1β and IFNγ on myotubes

4.1 Introduction

An overview of the inflammatory cytokines IL-1β and IFNγ and their potential involvement in sIBM can be found in Section 1.9 and Section 1.10 respectively. An overview of *in vitro* work where myotubes were treated with IL-1β and IFNγ can be found in Section 1.17. Many of these previous studies have had a main focus of amyloid β or APP accumulation in myotubes. The effect of IL-1β on TDP-43 has previously been investigated in primary rat myotubes (219), showing IL-1β contributes to TDP-43 sarcoplasmic mislocalisation. However, few previous studies have focussed on the effects of IL-1β and IFNγ on p62 in human myotubes, the relationship between TDP-43 and p62 in myotubes treated with inflammatory cytokines, and the effect of combined IL-1β and IFNγ treatment on TDP-43 in human myotubes.

Along with the fact IFNγ is upregulated in sIBM muscle and IL-1β and IFNγ have previously been used in sIBM *in vitro* investigations, adding these inflammatory cytokines to myotubes can more generally be used to investigate the response of muscle cells to inflammation. Furthermore, IFNγ and IL-1β may be secreted by immune cells that infiltrate into muscle in sIBM, namely CD8+ T cells and macrophages respectively (131, 147), so treatment with these cytokines may partially mimic the extracellular environment of sIBM.

4.1 Aims and hypotheses

The aim of this chapter is to build upon previous work with a stronger focus on TDP-43 and p62 using IL-1β and IFNγ to investigate sIBM-like characteristics in skeletal muscle-derived cells. Here the effect of IL-1β+IFNγ, or the two cytokines individually were investigated for effects on TDP-43 and p62 aggregation and expression, as well as TDP-43 localisation. To characterise the relationship between p62 and autophagy, expression of LC3 was also explored. Furthermore, the effect on sestrin-1 and sestrin-2 expression with inflammatory cytokine treatment was investigated. This chapter also

aims to address the more general question of whether inflammation such as here with addition of inflammatory cytokines, can preclude non-inflammatory features that are observed in sIBM.

Based on previous work in primary rat myotubes (219), it is hypothesised that IL-1β treatment will cause mislocalisation of TDP-43 to the sarcoplasm. Treatment with IFNγ or IL-1β+IFNγ will also have an effect on TDP-43 localisation. It is hypothesised that any treatment with inflammatory cytokines will cause the size and frequency of TDP-43 and p62 aggregates in the sarcoplasm to increase compared to control myotubes.

4.2 Methods

4.2.1 Treatment of myotubes with IL-1β and IFNγ

Treatment of skeletal muscle-derived cells with IL-1β, IFNγ, or these cytokines combined was performed as per Section 2.2. Cells were proliferated for two days before differentiation for seven days. Myotubes were treated with IL-1β (20 ng/mL), IFNγ (750 ng/mL) or IL-1β+IFNγ at the same concentrations for 48 hours.

4.2.2 Cytotoxicity assay

Cytotoxicity of IL-1β and/or IFNγ was assessed via LDH release as previously described in Section 2.3, except 2.32 $x10^4$ cells were grown in 48-well plates for the same length of time.

4.2.3 Immunofluorescent microscopy

Seeding of cells and staining for immunofluorescent microscopy was conducted as described in Section 2.4. Skeletal muscle-derived cells were differentiated for 7 days before addition of cytokines for 48 hours.

4.2.4 TDP-43 localisation with IL-1β + IFNγ treatment

TDP-43 subcellular localisation was assessed using widefield immunofluorescent images as described in Section 2.5.

4.2.5 p62 puncta and TDP-43 sarcoplasmic aggregate analysis

Immunofluorescent images obtained using confocal microscopy were used to analyse p62 and TDP-43 sarcoplasmic aggregation. p62 puncta analysis was performed as described in Section 2.6. TDP-43 sarcoplasmic aggregate analysis was performed as described in Section 2.7.

4.2.6 Nuclear p62 puncta analysis

As well as sarcoplasmic p62 analysis, for myotubes treated with IL-1β or IFNγ individually, nuclear p62 puncta size and frequency was assessed. The same images were used for analysis as in Section 4.2.5, except only the third slice in the six-slice z-

stack was used for nuclear p62 analysis. Using Image J, the DAPI channel was converted to a binary mask, and the p62 channel was manually thresholded. The two resulting channels were multiplied together using the "image calculator" function in Image J to obtain p62 puncta in the nuclei only. p62 puncta size was assessed as described in Section 2.6. p62 puncta frequency was assessed in a similar way to the methods described in Section 2.6, except instead of normalising to cell mask area, frequency results were normalised to area occupied by the DAPI channel (nuclei area) that was obtained via the "measure" function.

4.2.7 SDS PAGE and Western blotting

SDS PAGE and Western blotting for TDP-43, p62, sestrin-1, and sestrin-2 were performed as described in Section 2.8. LC3 densitometry results were expressed as the LC3II/LC3I ratio by dividing the densitometry readings of LC3II by LC3I. Total LC3II was also assessed by dividing LC3II by GAPDH.

4.3 Results

4.3.1 IL-1β and IFNγ alone or in combination are not cytotoxic to cultured myotubes

To assess whether the concentrations of IL-1β and IFNγ investigated were cytotoxic to cultured myotubes, LDH release was measured from myotubes treated with IL-1β, IFNγ, or IL-1β+IFNγ after 48 hours incubation. There was no difference in cytotoxicity between the control group and any of the cytokine treatment groups (Figure 4.1 B). Two of the six donors showed high levels of LDH release even in the control group with a mean cytotoxicity between them of 84 %. When these two donors were excluded, the mean of the cytotoxicity percentage in the control group was 43 %, and there was no difference between the control group and cytokine treatment groups (one-way ANOVA $p = 0.375$). Microscopic images of myotubes cultured under each treatment condition were captured in a separate experiment to those used in the LDH release assay. This showed no discernible differences in cell morphology between the control group and the cytokine treatment groups (Figure 4.1 A).

4.3.2 IL-1β and IFNγ combined caused increased p62 puncta size

Confocal microscopy was used to image p62 puncta in the sarcoplasm of myogenic cells. Sarcoplasmic p62 displayed as small puncta and all myogenic cells examined showed p62 expression. p62 was also observable in the nucleus and with weak diffuse staining in the sarcoplasm (Figure 4.2). The effect of IL-1β+IFNγ combined treatment on p62 puncta size, and frequency relative to cell area was measured to see if the combination of IL-1β+IFNγ affects p62 aggregation. The relative frequency of p62 particles was not affected by IL-1β+IFNγ compared to control (Figure 4.3 A). However, IL-1β+IFNγ treatment caused an increase in p62 puncta size compared to control (Figure 4.3 B). The mean size of p62 puncta in the control group was 0.28 ± 0.06 μm^2, and in the IL-1β+IFNγ treatment group was 0.49 ± 0.13 μm^2.

4.3.3 TDP-43 sarcoplasmic aggregation was not affected by IL-1β and IFNγ combined

From the same images used to analyse p62 puncta (Figure 4.2), TDP-43 was also assessed to examine if IL-1β+IFNγ affected TDP-43 sarcoplasmic aggregation or colocalisation with p62. Figure 4.2 shows TDP-43 in the sarcoplasm was mostly diffuse, with occasional areas of small aggregation shown as areas with increased

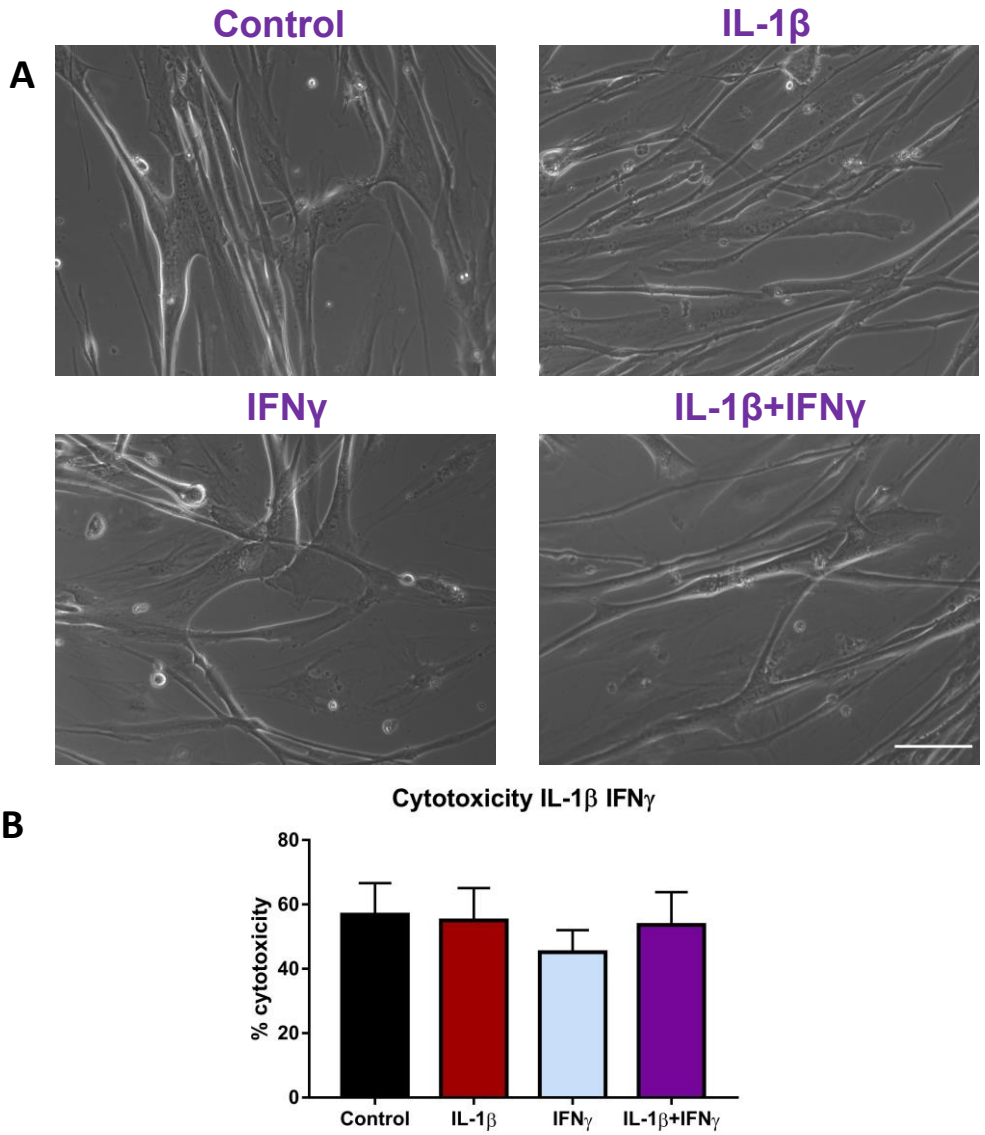

Figure 4.1 Cytotoxicity of IL-1β and IFNγ alone or in combination on myotubes.
(A) Phase contrast images of myotubes treated with cytokines. Scale bar = 100 µm. (B) Cytotoxicity relative to positive control. There was no difference in cytotoxicity between any of the conditions (one-way ANOVA p = 0.821). n = 6 myogenic donors.

fluorescent intensity. TDP-43 was also observable in the nucleus. The frequency of TDP-43 sarcoplasmic aggregates relative to cell area was not different between control and IL-1β+IFNγ treated myotubes (Figure 4.5 A). Furthermore, TDP-43 aggregate size was not affected by IL-1β+IFNγ treatment (Figure 4.5 B). The mean TDP-43 aggregate size in the control group was 3.35 ± 1.28 μm^2. Some TDP-43 aggregates were observed colocalised with p62 puncta. Any colocalisation was mostly partial, with only some of the TDP-43 aggregate area also showing p62 puncta staining (Figure 4.4). There was no difference in the percentage of TDP-43 aggregates that colocalised with p62 puncta between the control and IL-1β+IFNγ treatment group (Figure 4.5 C). The median percentage of TDP-43 aggregates that colocalised with p62 puncta was 10 ± 18 %. Not all images of myogenic cells showed TDP-43 aggregates. The frequency of images that contained any TDP-43 aggregates was not different between vehicle control and IL-1β+IFNγ treatment groups (Figure 4.5 D).

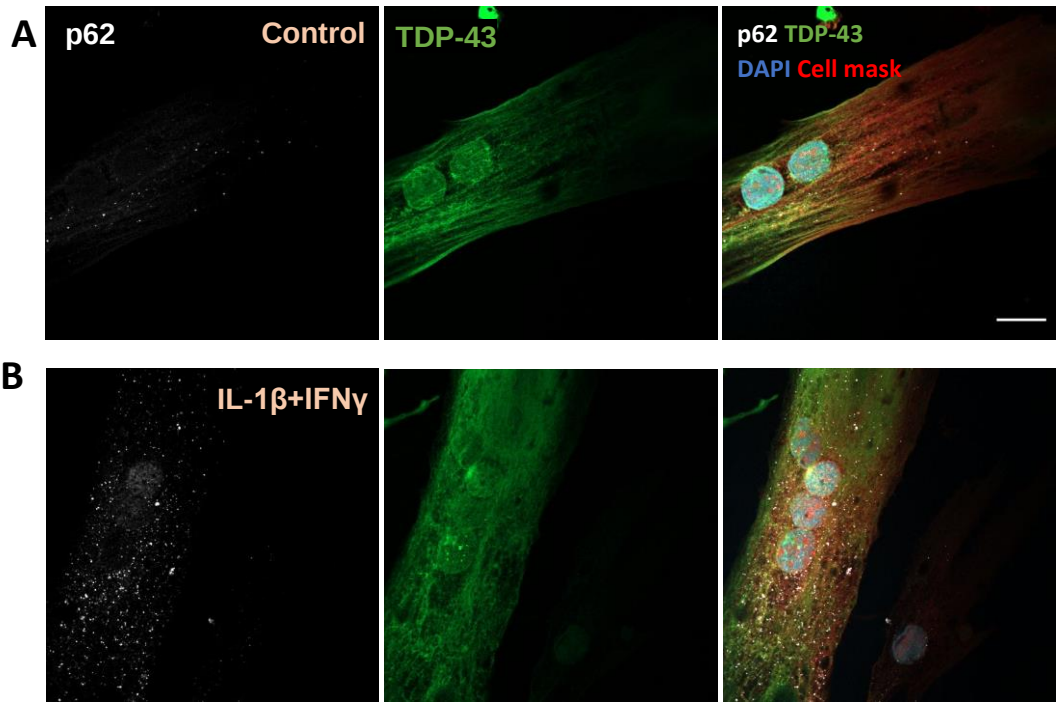

Figure 4.2 TDP-43 and p62 staining with IL-1β and IFNγ. Representative images of p62 and TDP-43 in myotubes with vehicle control (A) or IL-1β+IFNγ (B) treatment for 48 hours. Scale bar = 20 µm.

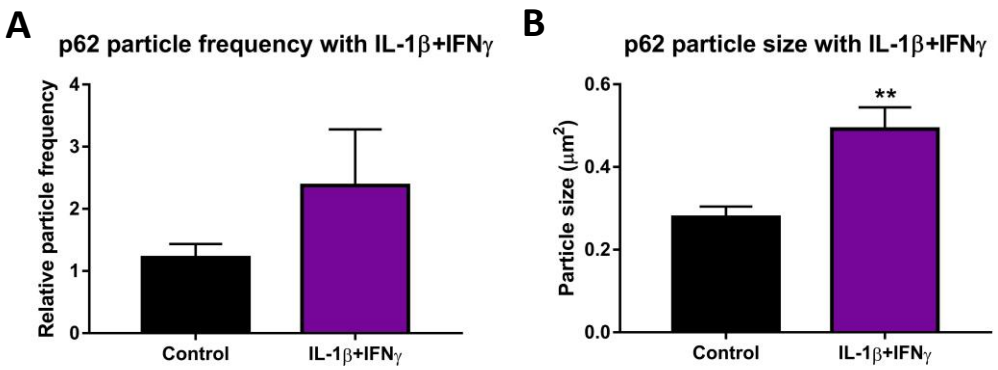

Figure 4.3 p62 puncta size was increased with IL-1β+IFNγ. (A) p62 particle frequency relative to cell mask (CM) area was not different between vehicle control and IL1-β+IFNγ (Student's T test p = 0.241). (B) p62 particle size increased compared to control for myotubes treated with IL-1β+IFNγ (Student's T test p = 0.0046). n = 6 myogenic donors.

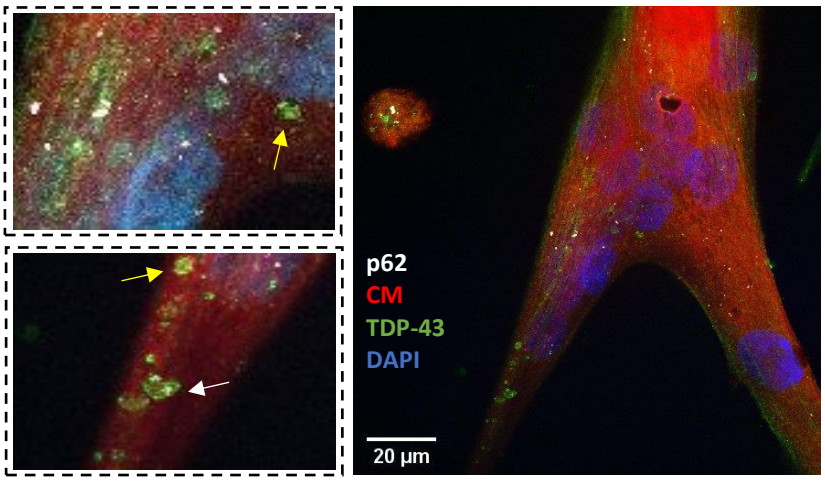

Figure 4.4 Examples of TDP-43 and p62 aggregates in myotubes. Image of a vehicle control treated myotube stained for p62 and TDP-43 under fluorescent microscopy. Arrows in insets show TDP-43 sarcoplasmic aggregates, with bottom inset showing a TDP-43 aggregate that colocalises with p62 puncta (white arrow). Scale bar = 20 μm.

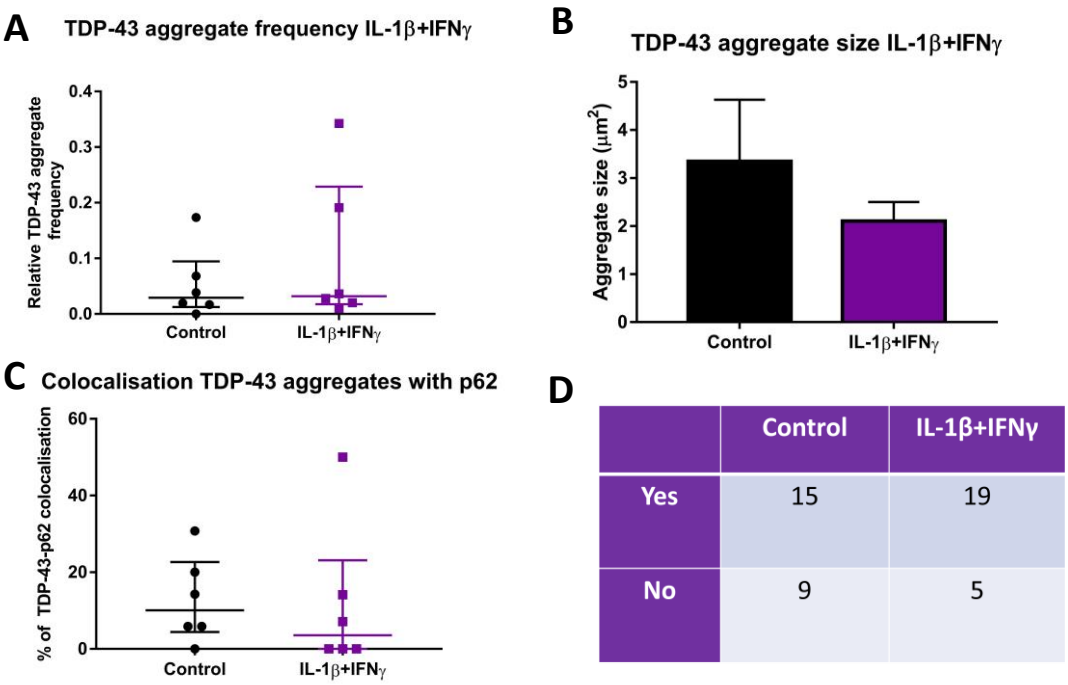

	Control	IL-1β+IFNγ
Yes	15	19
No	9	5

Figure 4.5 TDP-43 aggregate size or frequency was not affected by IL-1β+IFNγ.

(A) The frequency of TDP-43 aggregates when normalised to cell area through cell mask staining was not different between control and IL-1β +IFNγ treated myotubes (Mann-Whitney U test p = 0.589). (B) The size of TDP-43 aggregates was not different between control IL-1β+IFNγ treated myotubes, (Student's T test p = 0.376). TDP-43 aggregates were sometimes co-localised with p62 (C), but there was no difference in co-localisation between control and IL-1β+IFNγ treatment (Mann-Whitney U test p = 0.502). (D) There was no difference in the likelihood of images containing TDP-43 aggregates between treatment conditions (Fisher's exact test p = 0.341, four images (each with three z-stacks) for of six donors). n = 6 myogenic donors.

4.3.4 TDP-43 subcellular localisation was not altered by treatment with IL-1β and IFNγ combined

To examine whether TDP-43 localisation changed with combined IL-1β+IFNγ treatment, the subcellular localisation of TDP-43 was classified for each cell as either within the nucleus, sarcoplasm, nucleus and sarcoplasm, or neither (not expressed) using widefield immunofluorescent microscopy. There was no difference in TDP-43

localisation between the control group and IL-1β+IFNγ treatment group (Figure 4.6). There was also no difference in the distribution of TDP-43 within the subcellular compartments as assessed via two-way ANOVA ($p = 0.0812$), suggesting TDP-43 is spread evenly between these compartments.

4.3.5 p62 puncta size or frequency were not affected by IL-1β or IFNγ treatment individually

Following on from the finding that IL-1β+IFNγ treatment caused an increase in p62 sarcoplasmic puncta size, the effect of these cytokines individually was assessed to examine whether this size increase is due to one of these cytokines only. The TDP-43 analyses were also conducted for IL-1β or IFNγ individually. Three of the same myogenic donors were used that were used for IL-1β+IFNγ analysis, and two different donors that were not used for IL-1β+IFNγ analysis were assessed. This was due to limited stocks of some of the myogenic donors used for IL-1β+IFNγ experiments.

Confocal microscopy was used to assess p62 puncta in the sarcoplasm (Figure 4.7). All myogenic cells showed p62 expression which was localised both to distinct puncta and also showed weakly diffuse staining in the sarcoplasm. p62 frequency relative to cell area was not different between control and either IL-1β or IFNγ (Figure 4.8 A). Furthermore, the size of p62 puncta was not different between control and either IL-1β or IFNγ treatment (Figure 4.8 B). The mean p62 puncta size in the control group was $0.33 \pm 0.03\ \mu m^2$.

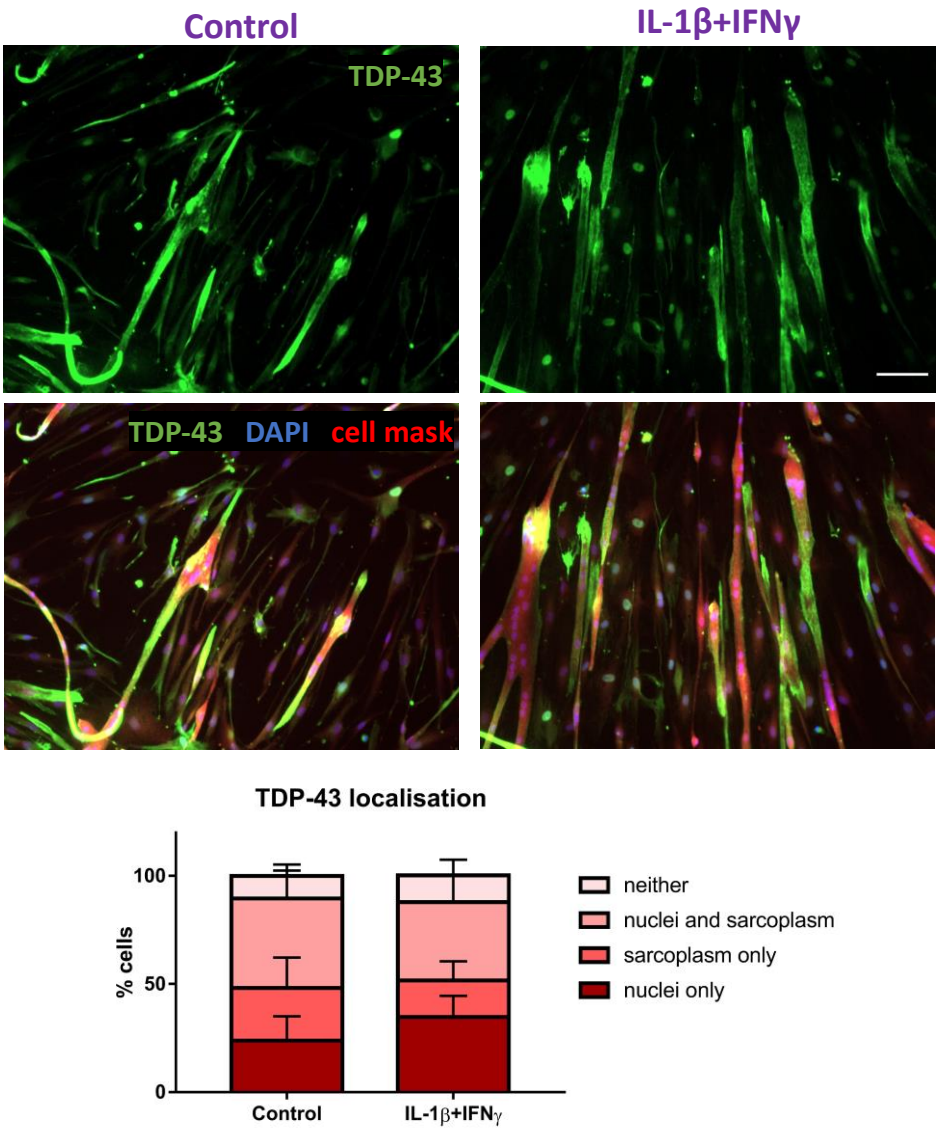

Figure 4.6 IL-1β+IFNγ does not affect TDP-43 localisation. Immunofluorescent images of TDP-43 distribution within myotubes. Scale bar = 100 µm. There was no difference in TDP-43 localisation between control myotubes and those treated with IL-1β+IFNγ (two-way ANOVA p 0.822). n = 5 myogenic donors.

4.3.6 TDP-43 sarcoplasmic aggregation was not affected by IL-1β or IFNγ

The effect of IL-1β or IFNγ treatment individually on TDP-43 sarcoplasmic aggregation was also assessed. Figure 4.7 shows TDP-43 within IL-1β, IFNγ or control myotubes. In the displayed images, TDP-43 was located diffusely throughout the sarcoplasm and

was either weakly present or mostly absent from the nucleus. There was no difference between the control group and IL-1β, or control and IFNγ for TDP-43 aggregate frequency relative to cell area (Figure 4.9 A). Furthermore, there was no difference between the control group and either IL-1β or IFNγ for TDP-43 aggregate size (Figure 4.9 B). The mean TDP-43 sarcoplasmic aggregate size in the control group was 0.89 ± 0.21 μm^2. Not all images of myogenic cells contained TDP-43 aggregates. There was no difference in the frequency of images that contained any TDP-43 aggregates between

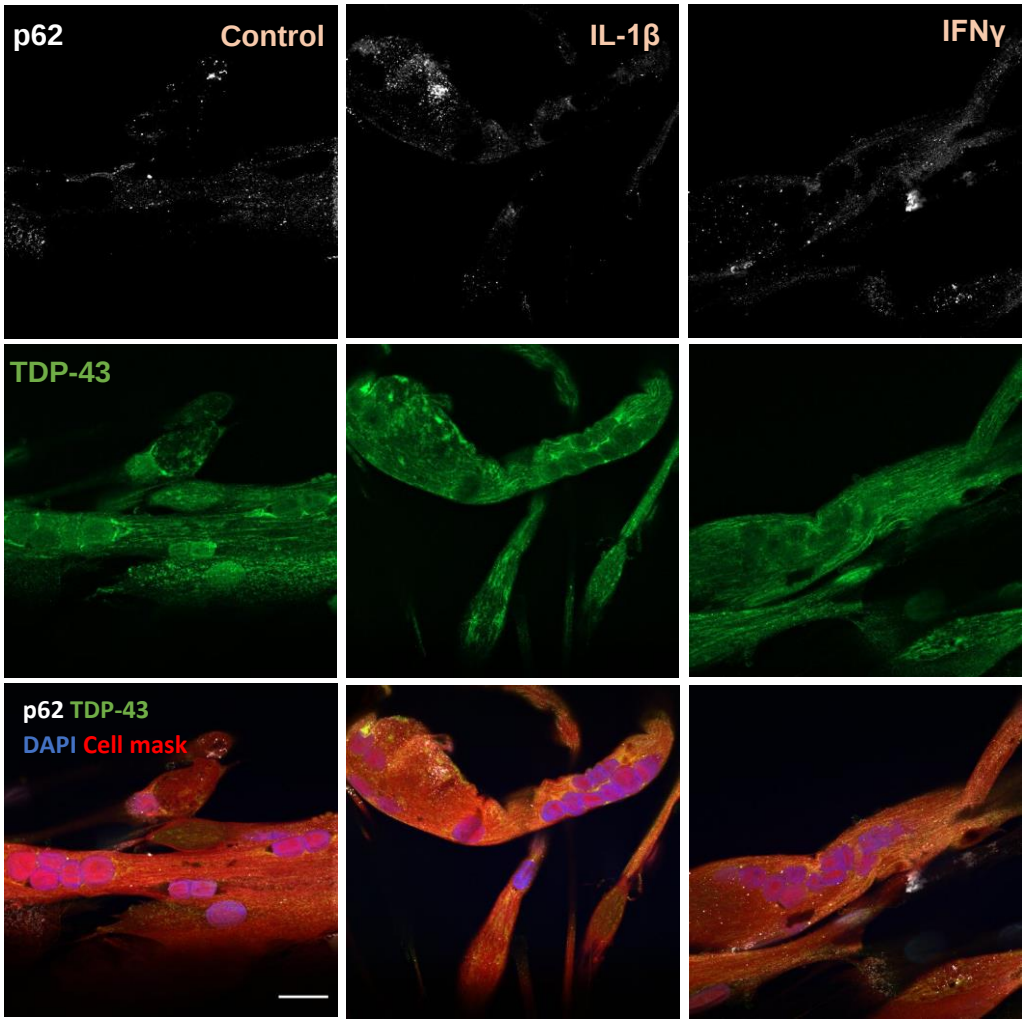

Figure 4.7 TDP-43 and p62 in IL-1β or IFNγ treated myotubes. Representative immunofluorescent images of p62 and TDP-43 in myotubes treated with IL-1β or IFNγ compared to vehicle control. Scale bar = 20 µm.

the three treatment conditions of control, IL-1β, or IFNγ (Figure 4.9 D). Some TDP-43 puncta colocalised with p62, however there was no difference between control myotubes and either IL-1β or IFNγ for the percentage of TDP-43 aggregates that colocalised with p62 puncta (Figure 4.9 C). The median percentage colocalisation in the control group was 4 ± 8 %.

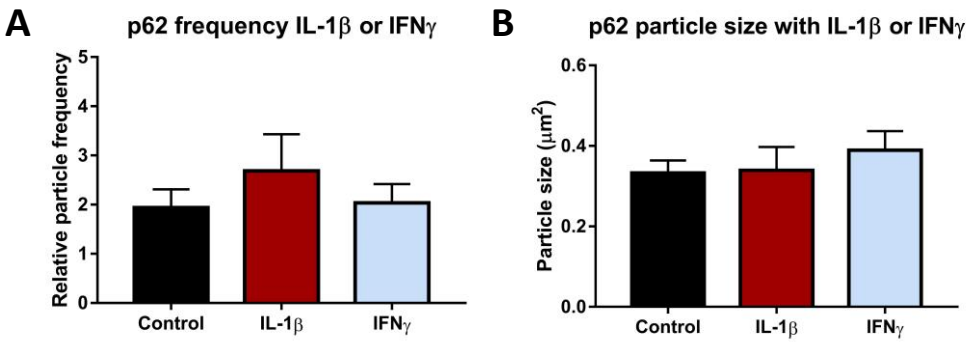

Figure 4.8 p62 puncta frequency or size was not affected by IL-1β or IFNγ treatment.
(A) There was no difference in p62 particle frequency relative to cell area between any condition (p = 0.587). (B) There was no difference in p62 puncta size between conditions (p = 0.660). n = 5 myogenic donors. One-way ANOVA.

4.3.7 TDP-43 subcellular localisation was not affected by IL-1β or IFNγ

To investigate whether IL-1β or IFNγ individual treatments affected TDP-43 localisation, immunofluorescent imaging was used to classify TDP-43 subcellular location. There was no difference between the control group and either IL-1β or IFNγ for the distribution of TDP-43 within the subcellular compartments (Figure 4.10). However, the distribution of TDP-43 between the subcellular compartments regardless of treatment condition was different (two-way ANOVA $p < 0.0001$), showing that TDP-43 was not distributed evenly within cells. The subcellular localisation that showed the highest percentage of TDP-43 was nuclei and sarcoplasm with 60 ± 8 % of cells (two-way ANOVA with Tukey's post-hoc test).

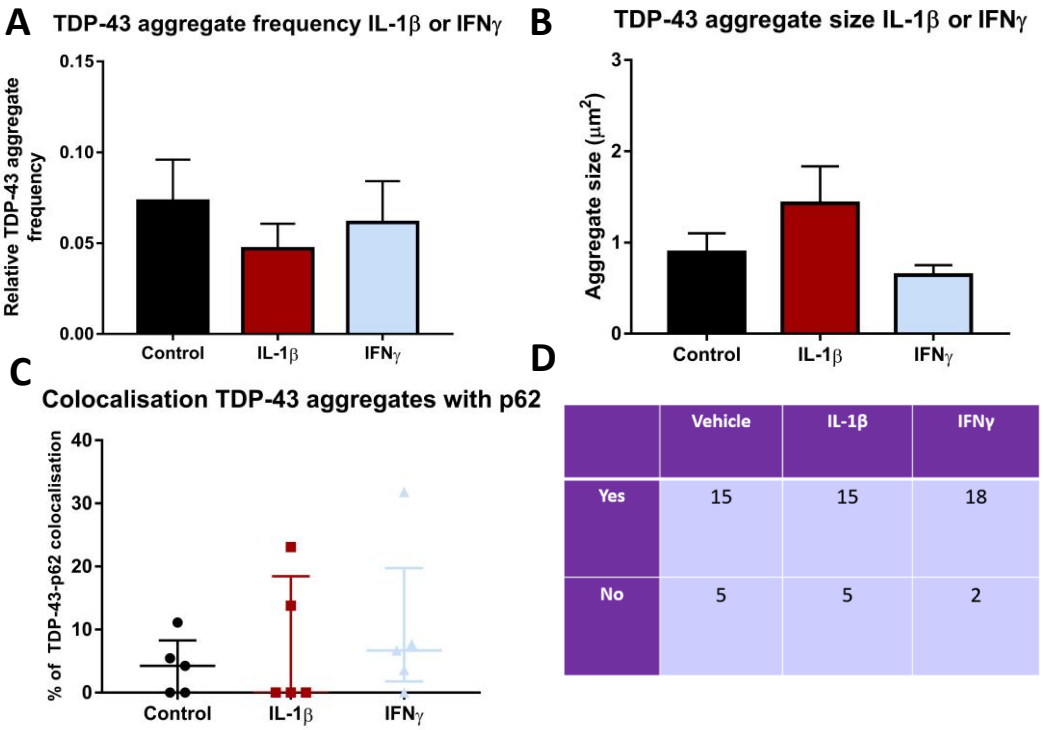

	Vehicle	IL-1β	IFNγ
Yes	15	15	18
No	5	5	2

Figure 4.9 TDP-43 aggregate size or frequency was not affected by IL-1β or IFNγ. (A) There was no difference in TDP-43 aggregate frequency relative to cell area (p = 0.421), or TDP-43 aggregate size (B, p = 0.152) between the treatment conditions. (C) The percentage of TDP-43 aggregates that colocalised with p62 particles was not different between any condition (p = 0.729). (D) There was no difference in the presence of TDP-43 aggregates within images between the conditions (Chi-square p = 0.392). n = 5 myogenic donors. One-way ANOVA or Kruskal-Wallis test.

4.3.8 p62 expression was increased with IL-1β and LC3II/LC3I ratio was increased with IL-1β+IFNγ

Following the discovery that combined IL-1β and IFNγ treatment caused increased p62 puncta size, the effect of IL-1β+IFNγ as well as these cytokines individually was assessed on p62, TDP-43, and LC3 protein expression using Western blotting (Figure 4.11 A). Densitometry analysis showed p62 protein expression normalised to GAPDH was not different compared to control for IL-1β+IFNγ or IFNγ. However, treatment with IL-1β increased p62 protein levels approximately 2.5-fold compared to control (Figure 4.11 B). There was no difference between any of the treatment conditions for TDP-43 protein expression relative to GAPDH (Figure 4.11 C).

To further understand changes in p62, the autophagic marker LC3 protein expression was also examined to see if p62 changes were due to autophagic flux. Compared to control, myogenic cells treated with IL-1β+IFNγ showed increased LC3II/LC3I ratio, whilst IL-1β or IFNγ individually showed no difference. The mean LC3II/LC3I ratio in control was 0.22 ± 0.04 and in IL-1β+IFNγ was 0.72 ± 0.15, a 3.2 fold increase. All LC3II/LC3I ratios were below 1 showing higher expression of LC3I than LC3II (Figure 4.11 D). However, when assessing LC3II expression normalised to GAPDH, there was no difference between any of the conditions (Figure 4.11 E).

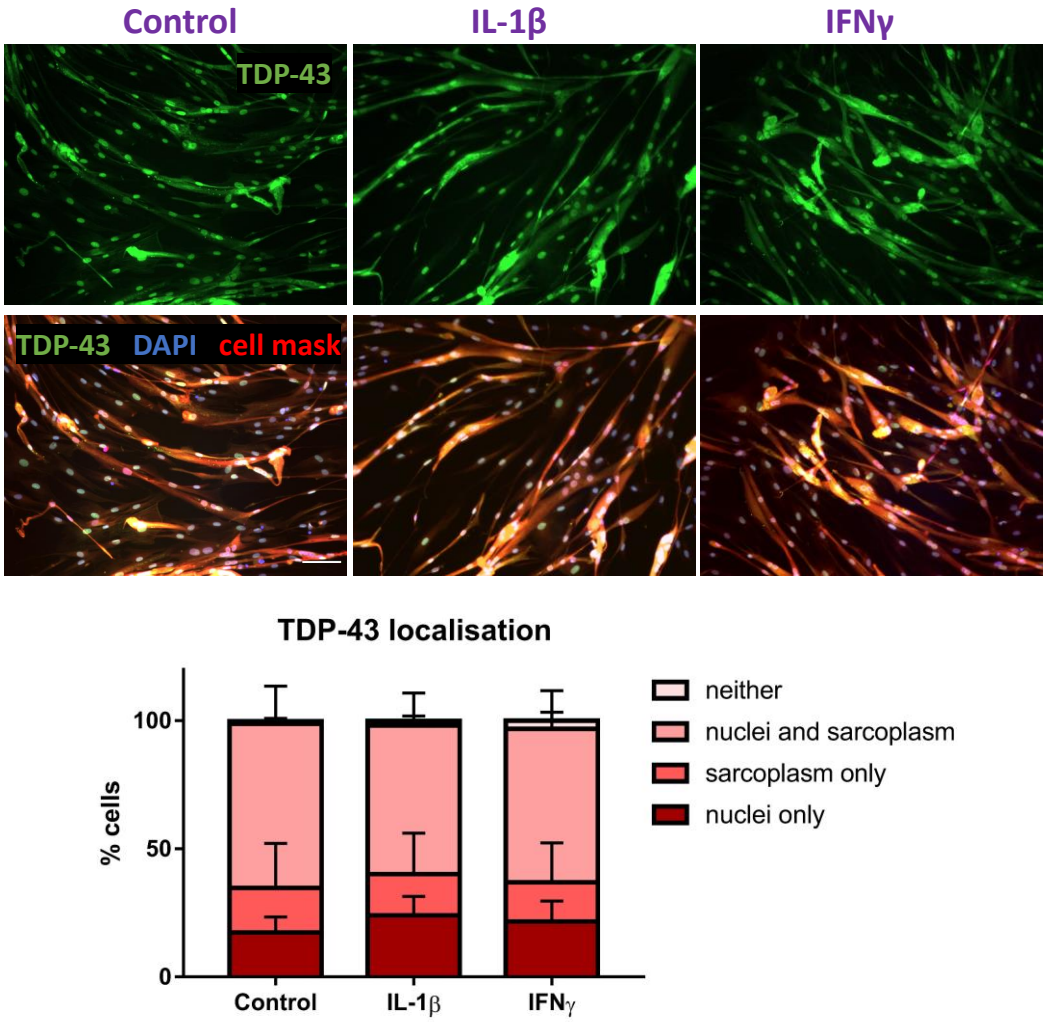

Figure 4.10 IL-1β or IFNγ does not affect TDP-43 localisation. Immunofluorescent images of TDP-43 distribution within myotubes. Scale bar = 100 µm. There was no difference in TDP-43 localisation between control myotubes and those treated with either IL-1β or IFNγ (two-way ANOVA p = 0.999). n = 5 myogenic donors.

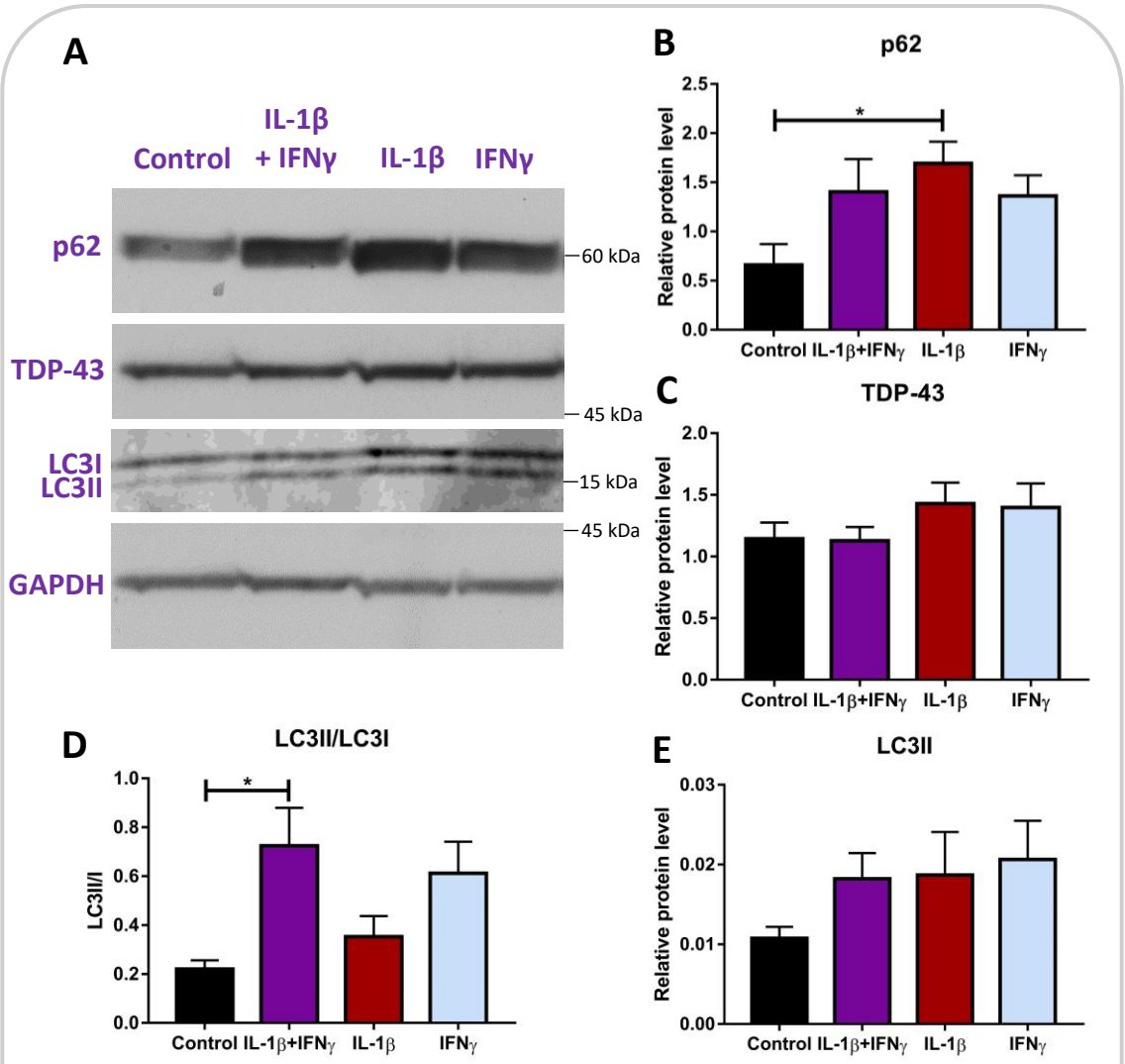

Figure 4.11 p62 expression was increased with IL-1β and LC3II/LC3I ratio increased with IL-1β+IFNγ. (A) Western blot of p62, TDP-43, and LC3 with GAPDH loading control. (B) p62 densitometry normalised to GAPDH. There was an increase compared to control for p62 protein expression with IL-1β treatment (p = 0.0223). There was no difference in p62 expression compared to control for IL-1β+IFNγ (p = 0.119) or IFNγ (p = 0.147). (C) Densitometry analysis of TDP-43 protein expression normalised to GAPDH. There was no difference in TDP-43 between any of the conditions (one way ANOVA p = 0.384). (D) Ratio of LC3II to LC3I expression. IL-1β+IFNγ increased LC3II/LC3I ratio compared to control (p = 0.0116). There was no difference compared to control for IL-1β (p = 0.737), but there was weak evidence that LC3II/I ratio increased with IFNγ (p = 0.0545). (E) Total LC3II relative to GAPDH. There was no difference between any of the conditions (one-way ANOVA p = 0.352). One-way ANOVA with Dunnett's multiple comparisons. n = 6 myogenic donors.

4.3.9 p62 nuclear puncta size or frequency was not affected by IL-1β or IFNγ

Following on from the discovery that p62 protein levels were increased with IL-1β treatment compared to control, without affecting p62 sarcoplasmic puncta size or frequency, nuclear p62 puncta were analysed to see if this accounts for the increase in p62 protein. It was noticed that a few p62 puncta were localised to the nucleus, whilst the majority of puncta were found in the sarcoplasm (Figure 4.12 A). p62 puncta frequency relative to nuclei area was not different between control and either IL-1β or IFNγ (Figure 4.12 B). Furthermore, the size of p62 puncta in the nucleus was not affected by IL-1β or IFNγ treatment compared to control (Figure 4.12 C). The mean size of p62 puncta in the nucleus was 0.22 ± 0.05 μm^2.

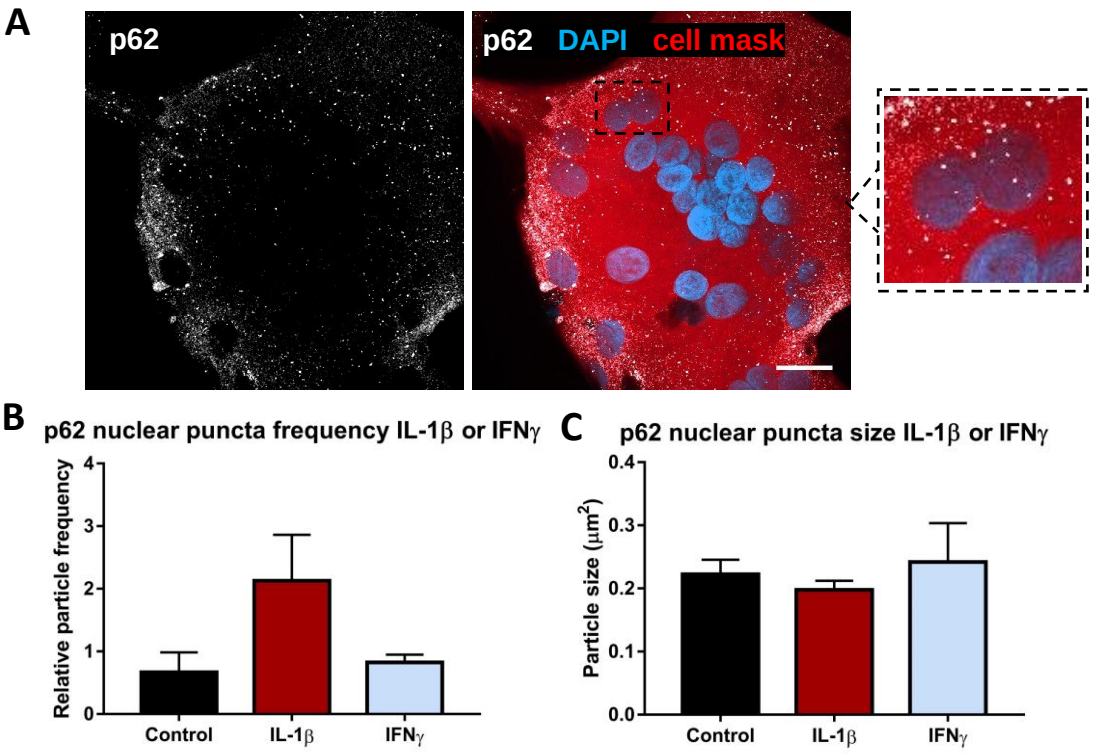

Figure 4.12 p62 nuclear puncta were not affected by IL-1β or IFNγ treatment. (A) Image of a myotube treated with IL-1β. Inset shows nuclear p62 puncta. (B) Frequency of p62 puncta normalised to nuclear area. There was no difference between any of the treatments for p62 nuclear puncta frequency (one-way ANOVA p = 0.186). (C) Size of nucleus-located p62 puncta was not different between treatment conditions (one-way ANOVA p = 0.731). n = 5 myogenic donors.

4.3.10 Sestrin-2 protein levels were increased with IFNγ, but not IL-1β or combined IL-1β and IFNγ treatment

To examine if cytokine treatment with IL-1β, IFNγ, or these cytokines combined affected sestrins, Western blotting was used to assess protein expression of sestrin-1 and sestrin-2. Densitometry analysis showed IL-1β+IFNγ or IL-1β alone did not change sestrin-2 protein levels relative to vehicle control. However, treatment with IFNγ alone caused an increase in sestrin-2 protein expression relative to control, with an approximate 2-fold increase between expression medians (Figure 4.13 A). It was noticed that sestrin-2 had two electrophoretic bands, termed here heavy (higher weight) and light (lower weight). For each of the six donors, the distribution of the electrophoretic bands was described (Figure 4.13 B). Between the treatment conditions, the sestrin-2 band distribution appeared different with IL-1β showing more donors with light band expression and IFNγ showing mostly heavy band expression. It was not possible to assess the relative distribution of these bands using densitometry as they were too close together. Sestrin-1 protein expression was also assessed using Western blotting. Densitometry analysis showed there was no difference in sestrin-1 protein expression between the control and any cytokine treatment (Figure 4.13 C).

4.3.11 Control conditions with IL-1β+IFNγ or IL-1β/IFNγ experiments were comparable

As previously mentioned, only three of the donors were the same for the two sets of experiments with IL-1β+IFNγ combined, or IL-1β or IFNγ individually. Six donors were used for IL-1β+IFNγ, whereas five donors were used for IL-1β or IFNγ for p62 and TDP-43 sarcoplasmic aggregation analysis. It is not possible to make direct comparisons between the two experiments due to the different donors and the fact the experiments were not conducted at the same time. However, to ensure a level of consistency between the two experiments was maintained, the results from the two control conditions were compared (using Student's T test). There was no difference between the controls for p62 frequency ($p = 0.116$), p62 size ($p = 0.208$), TDP-43 frequency ($p = 0.578$), TDP-43 size ($p = 0.120$), or TDP-43-p62 colocalisation ($p = 0.145$). There was also no difference in TDP-43 localisation between the two experimental controls (two-way ANOVA $p = 0.474$).

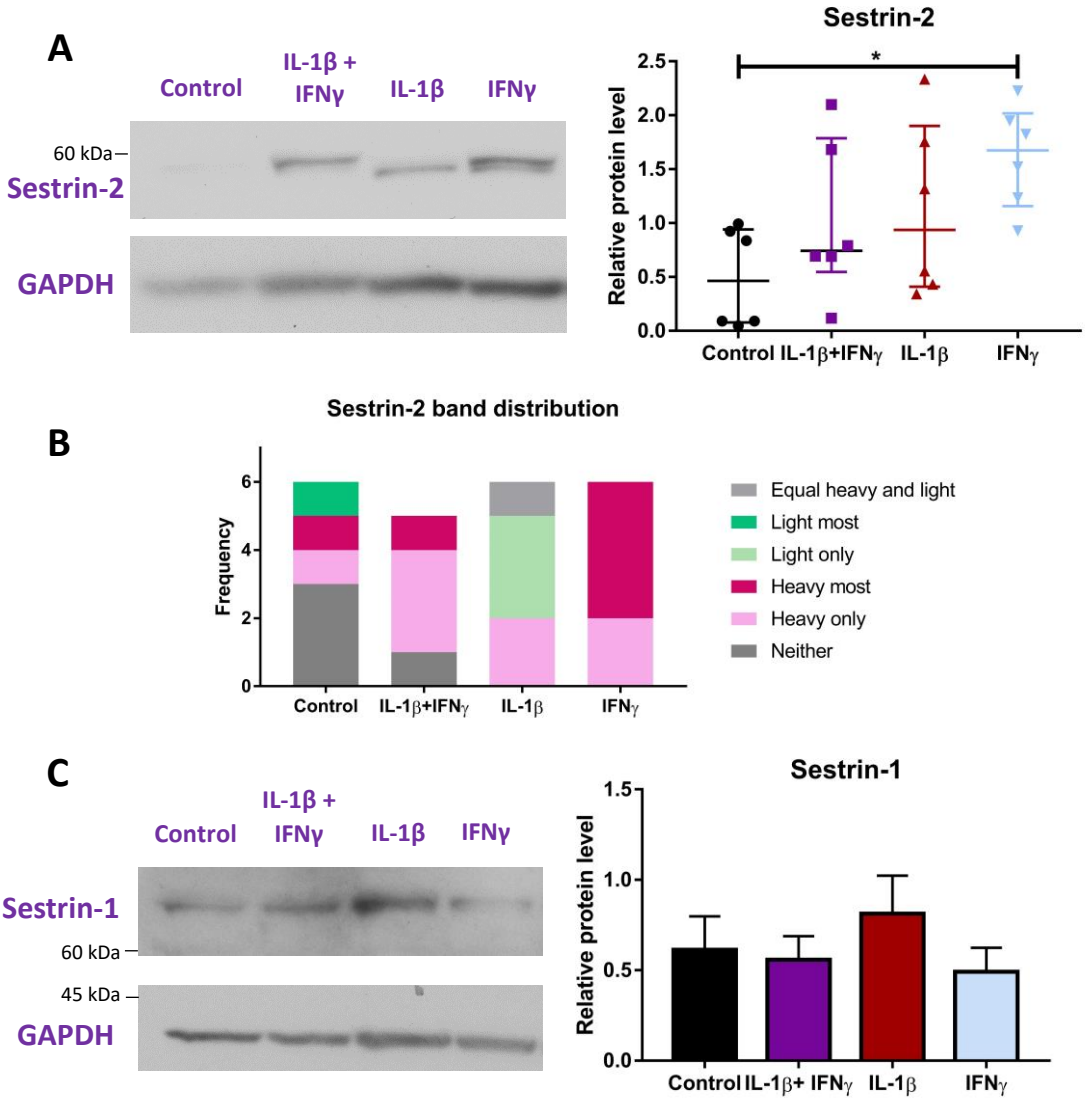

Figure 4.13 Sestrin-2 and sestrin-1 expression with IL-1β and IFNγ treatment. (A) Total sestrin-2 protein levels relative to GAPDH. There was increased sestrin-2 expression with IFNγ compared to control ($p = 0.0212$), but not with IL-1β+IFNγ ($p = 0.387$) or IL-1β ($p = 0.244$). (B) In some samples, two protein bands were visible with Western blotting, a heavy and light band. For IL-1β+IFNγ, one donor was not included as it was not clear which of the two bands was expressed. The presence and distribution of each band appeared variable between conditions and donors. (C) Sestrin-1 protein expression was not affected by any cytokine treatment ($p = 0.684$). Kruskal-Wallis with Dunn's multiple comparisons or one-way ANOVA with Dunnett's multiple comparisons, n = 6 myogenic donors.

4.4 Discussion

This chapter explored the effects of IL-1β and IFNγ on TDP-43, p62, and sestrins in cultured primary human myotubes, building upon previous work using these cytokines in cultured myogenic cells to investigate sIBM features, with a stronger focus on TDP-43 and p62. Treatment of myotubes with inflammatory cytokines IL-1β and IFNγ has been purported to increase protein aggregation based on increased generalised immunofluorescent signal of thioflavin-S (145, 290), a dye that binds amyloidogenic proteins (342). As well as IL-1β and IFNγ, TNFα and IFNγ combined treatment has also been used to investigate sIBM features *in vitro* (145, 219, 290, 295), which may be more representative of the sIBM inflammatory milieu as both of these cytokines are secreted by CD8+ T cells, the most abundant immune cells in sIBM muscle. However it has previously been shown that combined treatment of IFNγ and TNFα causes cytotoxicity to cultured human muscle cells, whilst individual treatments did not (343).

Overall the relationship between inflammation and non-inflammatory features in sIBM is currently poorly understood. The aim of this chapter was to understand whether inflammation in the form of IL-1β and/or IFNγ may be responsible for inclusion body formation containing TDP-43 and p62 in human myotubes.

Firstly, the cytotoxic effects of IL-1β and IFNγ either individually or combined was assessed. Even in the control group there was relatively high cytotoxicity. This may represent suboptimal culture conditions of myotubes, which may be due to the long duration of differentiation of nine days, or due to using smaller 48-well plates for this experiment. In subsequent chapters using the same culture length but larger 24-well plates, control cytotoxicity was not as high as observed in this chapter suggesting a larger surface area than 48-well plates may be needed for survival of myotubes. Despite this, IFNγ and/or IL-1β did not exhibit cytotoxicity when used alone or in combination compared to untreated cells. This corroborates previous findings showing IFNγ is not cytotoxic to cultured human muscle cells (343, 344). On the other hand, previous results show treatment of human myotubes with IL-1β and IFNγ combined caused increased staining with propidium iodide, indicating increased cell death (295),

which was not observed here with cytotoxicity assessment. IL-1β treatment has also been found to increase DNA breaks when added during human myoblast proliferation (136). These different cytotoxic responses of cytokines may be due to differences in experimental set up. For example differences in incubation time, with 48 hours used here and 72 hours used by Schmidt *et al* (295), or adding IL-1β during differentiation instead of proliferation (136). The concentration of IL-1β chosen here has been used in previous studies of sIBM using human muscle cells (145, 290, 295). However, the IFNγ concentration was very high which is unlikely to be representative of *in vivo* conditions. A range of IL-1β and IFNγ concentrations should have been tested for their effects on TDP-43 and p62 to ensure that no concentration-dependent effects were missed. Furthermore, it would have been beneficial to analyse a range of durations of cytokine administration. However, the image analysis required for p62 and TDP-43 analysis was a rate-limiting step so this was not undertaken.

4.4.1 TDP-43

Addition of IL-1β+IFNγ or these cytokines individually did not cause TDP-43 aggregation within the sarcoplasm. This suggests that IL-1β or IFNγ may not cause aggregation of p62 in these skeletal muscle cells. Previously, combined treatment of primary human myotubes with IL-β and IFNγ caused protein aggregation observed through increased immunostaining of thioflavin-S (145, 290), which stains aggregated amyloidogenic proteins (345). Whilst there was increased overall signal from thioflavin-S (145, 290), this appeared throughout the sarcoplasm of myotubes and was not localised to separate aggregates, so this may not be a comparable method for identifying individual aggregates that were analysed here. Treatment of primary rat myotubes with IL-1β and TNFα did not cause inclusion-like bodies when assessing amyloid-β, TDP-43, and ubiquitin aggregation (219). Whilst TDP-43 aggregates were identified here under all conditions. These differences between studies in the aggregation of proteins in the sarcoplasm with inflammatory cytokine treatment could be due to the different treatment cytokines used, the difference in source material (human vs rat), and/or the different methods of aggregation identification used.

Mislocalisation of TDP-43 into the sarcoplasm without apparent nuclear localisation has been described in sIBM skeletal muscle (100). This phenomenon has also been shown in previous *in vitro* sIBM investigations with overexpression of β-amyloid or treatment of primary rat myotubes with IL-1β (219). In ALS, loss of nuclear TDP-43 caused dysregulation of RNA splicing (346), and deficits in DNA repair mechanisms (347). Here, TDP-43 localisation was not affected by any treatment with IL-1β or IFNγ, contradictory to previous results with IL-1β treatment in primary rat muscle cells showing increased sarcoplasmic localisation (219). This may be due to different specificities of antibodies used, with a C-terminus-specific antibody showing TDP-43 mislocalisation in rat myotubes (219), whereas here a polyclonal antibody recognising N-terminus as well as a central TDP-43 epitope (348) that is contained within the truncated 35 kDa TDP-43 fragment (83, 349) was used. Both antibodies should also detect full-length TDP-43. Indeed, Ahmed *et al* (219) noted that staining with N-terminal TDP-43 was localised to the nucleus only under control and cytokine treatment conditions. This raises interesting questions about the cleavage state of TDP-43 after exposure to inflammatory cytokines.

The antibody used here has also previously been used to stain sIBM muscle showing sarcoplasmic aggregation and lack of nuclear localisation (100, 350), as well as loss of nuclear localisation in cultured sIBM myotubes (351). Some cells under control conditions also showed TDP-43 localisation to the sarcoplasm without clear nuclear expression, suggesting this may also be displayed in healthy myotubes. It is not clear why treatment of IL-1β failed to recapitulate TDP-43 localisation as previously described, potentially a species-specific difference may exist. Analysis was not restricted to multinucleated myotubes, but as TDP-43 localisation was not affected by myotube differentiation (see Section 3.3.5 and Figure 3.8) this should not interfere with interpretations. The effect of IL-1β and IFNγ combined or IFNγ alone on TDP-43 localisation has not previously been reported. This also showed no effect on TDP-43 localisation. All together, these results suggest that exposure to inflammatory cytokines does not cause TDP-43 mislocalisation in these muscle cells. However, to fully test this, it would be necessary to perform experiments with multiple concentrations of IL-1β and/or IFNγ for varying exposure times.

It has previously been found that compared to controls, sIBM patients have increased muscular expression of TDP-43 (97, 98). There was no truncated TDP-43 protein bands observed at 25-35 kDa, which are more cytotoxic and found in ALS inclusions (88) and increased in sIBM (98). Contrary, a separate study found no increased full-length TDP-43 in the soluble fraction with sIBM compared to healthy muscle, but an increase was observed in the SDS soluble fraction. Further, 35 and 25 kDa TDP-43 were observed in the soluble fraction with a higher expression in sIBM muscle (98). These C-terminal fragments are less soluble, so may not be sufficiently solubilised with the RIPA lysis buffer method used here. Another denaturant such as high concentration urea (352) could be used to assess 23-35 kDa TDP-43 fragments, which may show different results to the intact TDP-43 protein expression.

Alternative to the hypothesis tested here, it is also possible that non-inflammatory features of sIBM including TDP-43 and p62-containing inclusion bodies are capable of triggering inflammation. Much of the previous work investigating TDP-43 has been in the context of ALS, FTLD, and Alzheimer's disease. In fact, TDP-43 overexpression in astrocytes caused increased secretion of proinflammatory cytokines including IL-1β, IL-6, and TNFα (353). Further, exposure of microglia to extracellular TDP-43 aggregates lead to IL-1β secretion (354), and similarly extracellular exposure of microglia to wild type, truncated, or mutant TDP-43 activated microglia and upregulated TNFα and IL-1β expression (355). In iPSC-derived motor neurones, TDP-43 can trigger mitochondrial DNA release, which causes upregulation of type I IFN expression (IFNα and IFNβ) (356). In favour of inflammation precluding TDP-43 pathology it was found treatment of mouse astrocytes and microglia with TNFα or lipopolysaccharide (LPS) as inflammatory stimuli caused increased sarcoplasmic expression of TDP-43. Further, treatment with LPS/TNFα of wild type and transgenic mice expressing a fragment of TDP-43 A315T gene showed increased ratio of TDP-43 in the cytoplasm compared to nucleus in the spinal cord as well as increased insoluble fraction of TDP-43 protein (357). The involvement of TDP-43 in neuroinflammation has been reviewed (358). Potentially there exists a bidirectional or positive feedback relationship where TDP-43 promotes release of inflammatory cytokines which in turn promotes further TDP-43 pathology,

or inflammation triggers TDP-43 pathology which promotes further inflammation of surrounding immune cells.

Interestingly, IL-1β may be associated with amyloid plaque clearance in an APP overexpressing mouse model of Alzheimer's disease (359, 360). This anti-β amyloid effect is also seen for IFNγ (361), TNFα (362), and IL-6 (363) through activation of microglia. This suggests inflammatory cytokines play a beneficial role in regulating β amyloid aggregation. Potentially the two proteins TDP-43 and APP/β amyloid have different involvements with the immune system despite their shared propensity to aggregate. In the context of the central nervous system, there is evidence to the contrary of the hypothesis that inflammation triggers TDP-43 aggregation, and the relationship may be more nuanced. However, the pathology of TDP-43 in the CNS and skeletal muscle may not be easily transferrable, due to tissue-specific roles for TDP-43 (109). Fewer studies have focussed on the interaction of TDP-43 and the cytokines in skeletal muscle compared to the nervous system. In transgenic mice with muscle-specific expression of wild type TDP-43, aggregates of TDP-43 were observed as well as fibre size variation and upregulated endoplasmic reticulum stress. However, there was no infiltration of immune cells into the muscle, suggesting TDP-43 aggregation is insufficient to trigger the immune response observed in sIBM (364).

4.4.2 LC3

Autophagy is the process by which material is degraded through the use of lysosomes. As described in Section 1.7, p62 functions as a selective receptor in autophagy where it binds polyubiquitinated proteins for recognition by LC3 for autophagosome formation. LC3 exists in two forms, the cytosolic soluble LC3I and the phosphatidylethanolamine conjugated LC3II. During autophagy LC3I is converted to LC3II when it associates with the inside of autophagosome membranes. With fusion to the lysosome, LC3II is degraded along with the autophagosome contents (365). The ratio of LC3II to LC3I is sometimes used to monitor autophagic flux, with an increased ratio representing higher autophagic activity. Alternatively, measurement of LC3II expression between experimental conditions relative to a loading control is used, due to problems with calculating the LC3II/LC3I ratio including the higher affinity of LC3II compared to LC3I

for antibodies used to probe their expression (366, 367). Ideally, measurements of autophagic flux are compared to treatment with autophagy inhibitors such as bafilomycin A1 or chloroquine, to prevent lysosomal degradation of LC3II and thus accurately measure whether LC3II increases are due to autophagy blockade or increased autophagic flux (366). Here, LC3 protein expression was utilised to further understand changes in p62. LC3 itself is relevant to the disease phenotype of sIBM, where the number of muscle fibres expressing LC3 is higher than in polymyositis fibres (102, 242), increased LC3II expression is observed in sIBM muscle compared to control (368), and LC3 aggregates are larger in sIBM than other inflammatory myopathies (117).

4.4.3 IL-1β and p62

IL-1β significantly increased p62 protein expression. p62 degradation is often used as a marker of increased autophagic flux (369), thus its increased expression with IL-1β may suggest a disruption to the autophagic machinery. However, p62 protein increase was not accompanied by an increase in p62 puncta size or frequency or LC3II changes, which would be expected if autophagy was inhibited. Therefore, the increase in p62 expression may reflect alterations in pathways other than autophagy. p62 protein expression is increased when the proteasome is inhibited (114), which could be the cause of the observed p62 increase here. However, there is no current indication that IL-1β is able to inhibit proteasomal function.

Alternatively, IL-1β can increase p62 protein expression which may be independent of proteasomal or autophagic pathways. NF-κB which is downstream of the IL-1 receptor can activate p62 expression. p62 is itself an activator of NF-κB signalling, promoting a positive feedback loop for NF-κB activation (370). It has previously been shown that IL-1β can upregulate p62 expression in prostate cancer cell lines. However, this p62 increase was lower than that of cells treated with the autophagy inhibitor chloroquine, showing that p62 increase with IL-1β was not due to autophagy blockade, but it was not clear if increased p62 was due to autophagic flux. This also corresponded to an increase in diffuse staining pattern of p62 (371). The mechanism of p62 protein increase with IL-1β in this study may however be specific to pancreatic (and breast)

cancer cell lines where it plays a role in acquired hormone receptor independence through IL-1β signalling (372). On the other hand, in nucleus pulposus cells, treatment with IL-1β decreased p62 protein expression through activation of autophagy (373). In macrophages, treatment with LPS causes activation of NF-κB, which causes increased expression of p62 (374). In both microglia and tri-cultures of microglia, neurones, and astrocytes, treatment with IL-1β caused increased p62 protein expression without altering the LC3II/LC3I ratio compared to untreated cells. When treating with IL-1β in the presence of the autophagy inhibitor bafilomycin A1, LC3II/LC3I ratio and p62 expression was increased compared to non-IL-1β treated autophagy inhibited cells, suggesting IL-1β was activating autophagy (375). The role of IL-1β on p62 may be organ or cell line specific. It would be interesting to further probe the mechanism of IL-1β induced p62 upregulation in these muscle cells by investigating the expression of NF-κB proteins, as well as the effect of IL-1β treatment with NF-κB blockade on p62 expression levels.

To further investigate the increased protein expression of p62 with IL-1β, nuclear puncta analysis of p62 was conducted to see if non-sarcoplasmic changes were responsible for increased p62 expression. Nuclear analysis showed no change in p62 puncta size or frequency with IL-1β compared to control suggesting the increased protein expression was not due to non-sarcoplasmic changes. Therefore, it is not clear how the increase in p62 protein with IL-1β translates into a change in p62 in terms of its cellular distribution. Potentially this discrepancy could be due to different sensitivities of the two techniques, with Western blotting able to detect changes in protein levels better than analysis of p62 puncta immunofluorescent staining. Alternatively, myotubes also contained weak p62 staining diffusely throughout the sarcoplasm and occasionally in the nucleus, that was not included in puncta analysis as it was removed through thresholding which could account for this change. It is important to note that p62 Western blotting analysis included one extra donor that was not used for p62 (and TDP-43) immunofluorescence analysis with IL-1β or IFNγ. However, exclusion of this donor in p62 densitometry analysis does not influence the results.

4.4.4 IFNγ or IL-1β+IFNγ and p62

Unlike IL-1β, there was no effect of IFNγ individual treatment on p62 expression, puncta size or frequency. The relationship between IFNγ and p62 has previously been examined. In the liver epithelial tumourigenic Huh7 cell line, treatment with IFNγ induced autophagy resulting in a concentration and time-dependent decrease in p62 protein expression (376). On the other hand, in nasal epithelial cells, treatment with IFNγ caused increased autophagic flux as detected by LC3. However, this was accompanied by increased expression of p62 protein which was not due to autophagy deficiency as shown by bafilomycin A1 treatment. The authors concluded IFNγ increased autophagy in these cells but insufficiently, which contributed to increased apoptosis (377). Furthermore, in the mouse macrophage-like cell line Raw 264.7 IFNγ treatment after 24 hours caused increased p62 protein expression (378). IFNγ influenced the recruitment of p62 and ubiquitin to *Toxoplasma*-containing vacuoles in mouse embryonic fibroblasts (379). A similar effect was also seen for IFNγ treatment and recruitment of p62 to *Burholderia cenocepacia* co-localisation, with IFNγ treatment in infected cells accompanied by decreased p62 expression due to increased autophagy (380). Like IL-1β, there appears to be differential effects of IFNγ on p62 expression. This highlights the pleiotropic roles of p62, as well as potential cell type specific differences. The lack of effect of IFNγ treatment here on p62 may suggest that in skeletal muscle cells, there is no effect of IFNγ on autophagy.

IL-1β+IFNγ caused an increase in p62 puncta size without increasing total p62 protein expression of puncta frequency. IL-1β+IFNγ also increased LC3II/LC3I ratio without increasing total LC3II expression. An increase in LC3II/LC3I ratio suggests increased autophagic flux, however this would usually be accompanied with a decrease in p62 expression which was not seen here, as well as an increase in total LC3II protein. An increase in p62 puncta size could represent an increase in autophagic activity, a blockade of autophagy, or represent an unrelated process. Co-immunofluorescent staining of puncta with p62 and LC3 may help elucidate if the observed larger p62 puncta with IL-1β+IFNγ were autophagosomes. Co-treatment with IL-1β+IFNγ and autophagy inhibitors prior to Western blotting would also help answer the cause of

p62 puncta size increase. At present the relationship between IL-1β+IFNγ treatment and autophagy in these cells is not clear. However, the increase in p62 puncta size with IL-1β+IFNγ is unlikely to represent p62 aggregation or inclusion body formation as seen in sIBM, as these aggregates are much larger at up to 10 µm in diameter (118). Interestingly, the effect of IL-1β+IFNγ on p62 puncta size and LC3II/LC3I ratio appeared independent of the effects of these two cytokines used individually. This suggests a potential co-operative effect in the signalling pathways of these two cytokines.

There was some colocalisation of p62 puncta with TDP-43 aggregates under all conditions, however this was mostly partial with the rare occurrence of complete colocalisation between the two proteins. The frequency of TDP-43 puncta that colocalised with p62 with any cytokine treatment was low and not different to control, further suggesting a lack of induction of inclusion body formation with treatment of these cytokines.

4.4.5 Sestrins

Sestrins are proteins involved in stress sensing, skeletal muscle homeostasis and response to exercise (see Section 1.18). Sestrins have not previously been implicated in sIBM. However due to their stress-sensing and muscle homeostatic roles, their expression and activity in skeletal muscle may be beneficial in protecting against sIBM muscle damage. The effect of inflammatory cytokines IL-1β and/or IFNγ were examined on sestrin-2 protein expression here, with a two-tailed hypothesis.

Sestrin-1 protein levels were not affected by any cytokine treatment compared to control cells. However, sestrin-2 was increased with IFNγ treatment compared to controls, whilst IL-1β or combined IL-1β+IFNγ showed no effect. The influence of IFNγ on sestrin-2 expression has not previously been reported. The different effects of IFNγ on the two sestrins highlights that sestrin-1 and sestrin-2 expression are likely differentially regulated, which was also observed in myogenesis in Chapter 3 (Section 3.3.7 and Section 3.3.8). The differential effect of IFNγ on the two examined sestrins may mean sestrin-2 increase with IFNγ is caused by a function that is not shared with sestrin-1. Both sestrin-1 and sestrin-2 are pleiotropic proteins that have multiple

functions, some of which overlap. According to a recent review by Chen *et al* (302), compared to sestrin-1, sestrin-2 has additional effects of maintaining glucose and insulin homeostasis, and inhibiting DNA damage and ER stress. IFNγ has previously been shown to induce ER stress in lung cancer cells, whilst also causing apoptosis (381). IFNγ has been shown to cause decreased expression of genes related to metabolic homeostasis (170, 173). Sestrin-2 is necessary for the regulation of energy homeostasis where it is required for liver insulin responsiveness ang glucose tolerance (382). Potentially IFNγ induces either ER stress or metabolic disruption in muscle cells that leads to increased sestrin-2 expression, which would be interesting to examine further.

Two bands of sestrin-2 were observable with Western blotting. When resolved on a polyacrylamide gel with reduced bisacrylamide, sestrin-2 separates into electrophoretic bands based on its phosphorylation state. When leucine is added to cells, α, β, and γ bands are present. However, when cells are starved of leucine, a fourth electrophoretic band appears termed δ. As well as appearance of the δ band, leucine starvation causes a decrease in the α band. The amount of sestrin-2 in the δ band negatively correlates with mTORC1 activation, suggesting this electrophoretic shift may be responsible for repressing mTOR signalling in response to leucine levels as opposed to sestrin-2 protein upregulation (383). As not all five sestrin-2 bands were observable here it is not possible to determine which electrophoretic bands the two observed bands correspond to. It would be interesting to perform the Western blotting with 7.5 % polyacrylamide gels with 0.19 % bis-acrylamide (383) to examine the full range of sestrin-2 electrophoretic bands.

4.4.6 Summary

Overall, the addition of the inflammatory cytokines IL-1β and IFNγ either individually or combined at the concentrations tested failed to recapitulate the phenotype of sarcoplasmic TDP-43 and p62 aggregation observed in sIBM. Although the size of p62 puncta were increased with IL-1β+IFNγ treatment, this was not accompanied by increased protein expression and it was unclear whether the larger p62 puncta were due to increased autophagic flux. This suggests treating myotubes with IL-1β+IFNγ may

not be a useful model of sIBM. IL-1β increased expression of p62 protein without influencing p62 puncta, most likely through an autophagy-independent mechanism. The lack of effect on TDP-43 with some effects observed with p62, along with the lack of colocalisation suggests differential regulation of these two proteins under exposure to inflammatory cytokines. Equally, sestrin-1 and sestrin-2 had different responses to IFNγ, with no effect on sestrin-1 and upregulation of sestrin-2 protein expression, a novel finding in muscle cells.

Chapter 5: Effect of macrophage conditioned medium on myotubes

Chapter 5. Effect of macrophage conditioned medium on myotubes

5.1 Introduction

Other than cytotoxic CD8+ T cells, one of the other frequently detected immune cells in sIBM is macrophages. Macrophages are members of the innate immune system that phagocytose bacteria and apoptotic cells (384), secrete inflammatory cytokines including IL-1β, IL-6, and IL-12 (385), and perform antigen presentation (386). Different subsets of macrophages exist that are differentiated based on their location in the body. Tissue resident macrophages are located within the tissue itself whereas monocyte-derived macrophages arise from circulating monocytes, which infiltrate into the tissue and differentiate into macrophages based on physiological cues. Tissue resident macrophages are surveyors of their tissue, ensuring homeostasis (387, 388). Monocytes are recruited to tissues based on chemotactic cues, where they differentiate into effector macrophages based on the conditions in the tissue (389). Macrophages are a plastic cell type that can alter their phenotype based on environmental cues. Traditionally, macrophages were defined as either inflammatory (M1) or alternatively activated (M2). PBMC-derived monocytes and monocyte/macrophage cell lines can be induced to take on M1-like or M2-like phenotypes with the addition of exogenous mediators. To simulate inflammatory conditions, IFNγ either alone or combined with lipopolysaccharide (LPS) primes macrophages towards an M1-like phenotype. The addition of IL-4 and IL-13 is used to induce the M2 phenotype (390, 391). More recently, the complexity of macrophage plasticity has been realised, and macrophage phenotypes exist on a spectrum that is less binary and less easily defined (392, 393).

In skeletal muscle repair, neutrophils are the first immune cell to infiltrate into injured skeletal muscle within 2 hours post injury. These neutrophils phagocytose damaged muscle and release factors including cytokines to promote inflammation (394). The infiltration of monocytes closely follows neutrophils, which differentiate into

inflammatory macrophages where they phagocytose necrotic fibres, with peak numbers around one to three days post injury (394, 395). Inflammatory macrophages can also promote skeletal muscle cell proliferation (395). Towards the later stages of skeletal muscle repair, macrophages transition into a more anti-inflammatory phenotype (396) which promote skeletal muscle cell differentiation (395). The phagocytosis of material by inflammatory macrophages may encourage their switching to an anti-inflammatory cell type contributing to resolving inflammation by producing anti-inflammatory cytokines (IL-4, TGF-β1, and IGF-1) that neutralise inflammatory cytokines and block neutrophil responses (394).

In sIBM, macrophages may play a detrimental role by contributing to the inflammatory milieu and causing damage to skeletal muscle cells. Compared to cytotoxic T cells, there are limited studies characterising infiltrating macrophages in sIBM. Roos *et al* (122) showed sIBM muscle had an increased protein signature of macrophage markers CD74, STAT1, and CD163 compared to control muscle samples. Furthermore, different subsets of macrophages were identified, including siglec 1+ STAT1+ macrophages that were involved in active myophagocytosis (phagocytosis of muscle), and STAT6+ macrophages found infiltrating into the endomysium (122).

In a separate study that compared immune cell populations with blood flow restricted exercise in sIBM, there was a presence before treatment of both M1 (CD206-) and M2 (CD206+) macrophages in the muscle (123). This further demonstrates macrophages in sIBM muscle may present with multiple phenotypes. Nitric oxide synthase expression was observed in macrophages in sIBM muscle, showing an inflammatory phenotype (397). Furthermore, there was a correlation between the amount of invading macrophages (as well as the amount of invading CD3+ T cells) and number of respiratory-deficient myofibres with mitochondrial abnormalities in sIBM (70), suggesting inflammatory cell infiltration may affect myofibre respiratory defects. In mice injected with anti-cn1A antibodies, CD68+ macrophages infiltrated more frequently into muscle fibres than control, suggesting a potential link between anti-cn1A antibodies and macrophage activation and recruitment (261). Overall, there is evidence of macrophage infiltration in sIBM muscle, with macrophages displaying

varied phenotypes. However, their full role and mechanism of action of macrophages in sIBM is not fully understood. It is not clear whether macrophages in sIBM muscle contribute to the disease and muscle weakness, or if their presence is due to their roles in skeletal muscle repair and therefore not actively participating in sIBM pathology.

5.1.1 Aims and hypothesis

The overall aim of this chapter was to investigate whether macrophages can contribute to pathological features observed in sIBM muscle. More specifically, the aim was to investigate if secreted factors from inflammatory or unprimed macrophages affect TDP-43 and p62 sarcoplasmic aggregation, TDP-43-sarcoplasmic mislocalisation, or expression of sestrins. As M2-like macrophages are usually involved in resolution of tissue injury, this phenotype was not investigated as it is unlikely to be a causative factor in sIBM fibre damage. Instead, this chapter focusses on whether secreted factors from pro-inflammatory M1-like M(IFNγLPS) macrophages have a causative role in non-inflammatory sIBM-like features.

It is hypothesised that addition of conditioned medium from inflammatory primed macrophages, but not non-inflammatory primed macrophages will lead to TDP-43 and p62 sarcoplasmic aggregation, and TDP-43 mislocalisation to the sarcoplasm.

5.2 Methods

5.2.1 THP-1 cell culture

THP-1 cells are a suspension human mononuclear myeloid leukaemia cell line (398) that were chosen as a model cell for monocytes. THP-1 cells were a kind gift from Prof. Derek Gilroy, UCL Division of Medicine. THP-1 cells were used between passages 12-20 and were maintained in ATCC-modified RPMI medium with 10 % FBS, 1 % L-glutamine, and 1 % penicillin-streptomycin at 37 °C with 5 % CO_2 in a humidified incubator with a maximal cell density of approximately $1x10^6$ cells/mL. THP-1 cells were differentiated into unprimed adherent macrophages (M(PMA)) by treating $3x10^5$ THP-1 cells in 500 µL of media with 150 nM phorbol 12-myristate-acetate (PMA) for 24 hours, before resting in non-PMA media for 72 hours. M(IFNγLPS) which are similar to M1 inflammatory polarised macrophages were obtained from M(PMA) THP-1 cells by additional 48 hour incubation in 20 ng/mL IFNγ and 10 ng/mL LPS from *Escherichia coli* (Sigma Aldrich, UK L2630).

5.2.2 Treatment of myogenic cells with macrophage conditioned medium

Conditioned medium was collected from $6x10^5$ cells/mL from M(PMA) or M(IFNγLPS) THP-1 after additional 24 hour incubation in serum free medium without PMA, IFNγ, or LPS. Conditioned medium was centrifuged, re-aliquoted and stored at -80 °C until use. $4x10^4$ myogenic cells per well in a 24 well plate were grown for 2 days in Skeletal Muscle Growth Media, before differentiating in N2 medium for a further 7 days. Afterward, 20 % v/v THP-1 conditioned medium was added in fresh N2 medium for 48 hours. Unsupplemented RPMI at 20 % v/v in N2 differentiation medium was used as control.

5.2.3 Cytotoxicity assay

The release of LDH from myotubes was used to quantify cytotoxicity of THP-1 conditioned medium as described in Section 2.3.

5.2.4 Treatment of THP-1 cells with myotube conditioned medium

Cells from four myogenic donors were differentiated for 7 days, cells from one myogenic donor were differentiated for 5 days before addition of either IL-1β 20 ng/ml + IFNγ 750 ng/mL or vehicle (equal volume 0.1 % w/v BSA) control for 48 hours. Myotubes were washed with PBS before addition of fresh N2 differentiation medium. After 24 hours incubation, myotube conditioned medium (CM) was collected and centrifuged, re-aliquoted, and stored at -80 °C until use.

THP-1 cells were differentiated into M(PMA) or M(IFNγLPS) macrophages which were treated with 20 % myotube CM or N2 media control in 80 % complete THP-1 growth medium for 24 hours. For M(IFNγLPS), CM incubation included IFNγ and LPS. Afterwards, macrophages were washed and incubated in serum free RPMI for 24 hours, before centrifuging at 500 xg to remove debris and storing THP-1 conditioned medium at -80 °C before use in ELISA. See Figure 5.1 for a schematic of myotube-macrophage conditioned media experiments.

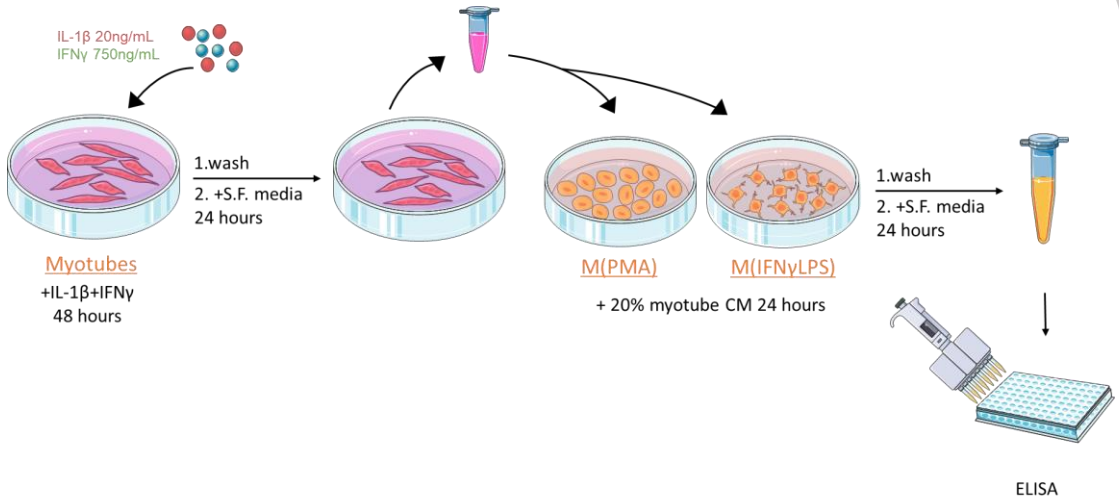

Figure 5.1 Schematic of method for secreted factors from macrophages treated with myotube conditioned medium. Myotubes were either unprimed or primed with IL-1β+IFNγ for 48 hours before washing and adding fresh myotube differentiation medium. Myotube CM was collected and 20 % added to macrophage growth medium for both M(PMA) and M(IFNγLPS) macrophages. After 24 hours incubation, macrophages were washed and fresh SF macrophage medium added for 24 hours before collecting CM for ELISA. SF – serum free, CM – conditioned medium, LPS – lipopolysaccharide, ELISA – enzyme-linked immunosorbent assay.

5.2.5 p62 particle analysis, TDP-43 sarcoplasmic aggregate analysis, and TDP-43 localisation

Myotubes were seeded at $4x10^4$ cells per 24 well, proliferated for two days, before differentiation for 7 days in N2 medium. 20 % v/v macrophage conditioned medium was added to myotubes in N2 medium for 48 hours. After this, myotubes were labelled with antibodies against p62 and TDP-43 as described in Section 2.4. p62 puncta analysis was performed as described in Section 2.6, and TDP-43 sarcoplasmic aggregate analysis was performed as described in Section 2.7. The same cultures for TDP-43 and p62 aggregate analysis were also used to assess TDP-43 subcellular localisation as described in Section 2.5.

5.2.6 ELISA for IL-6, IL-12 p70, IL-1β, and TNFα

THP-1 cells were seeded either in 6 well or 24 well plates at $6x10^5$ cells/mL. After differentiating into M(PMA) or M(IFNγLPS) macrophages, cells were incubated for an additional 24 hours in serum free medium. Macrophage CM was collected, centrifuged to remove debris , re-aliquotted and stored at -80 °C until use. ELISAs were also performed for myotube CM treated macrophages. DuoSet sandwich ELISAs for the human cytokines IL-6, IL-12 p70, IL-1β and TNFα were performed as described in Section 2.9. Serum free RPMI blanks were subtracted from standards and sample readings.

5.2.7 SDS PAGE and Western blotting

SDS-PAGE and Western blotting for TDP-43, p62, sestrin-2, sestrin-1 and GAPDH was performed as described in Section 2.8. For sestrin-1, membranes were stained as per Section 2.8 except membranes were cut when dry between 75 and 60 kDa molecular markers, and only this section was used for sestrin-1 detection.

5.3 Results

5.3.1 Morphology, IL-6 and TNFα levels were different between M(PMA) and M(IFNγLPS) macrophages

To ensure that inflammatory priming of macrophages with IFNγ and LPS was successful, the morphology of cells and the secretion of inflammatory mediators was compared between unprimed M(PMA) and M(IFNγLPS) macrophages. M(IFNγLPS) cells had a more spindle-like morphology and appear to contain more intracellular granules than non-inflammatory primed M(PMA) macrophages (Figure 5.2 A). Secreted levels of IL-6, IL-12p70, IL-1β, and TNFα were examined via ELISA (Figure 5.2 B-D). IL-12p70 was not consistently detected in either M(PMA) or M(IFNγLPS) cells. IL-1β secretion was highly variable between biological repeats, and there was no difference between the two macrophage types. The median amount of IL-1β secreted from M(PMA) was 0 ± 11 pg/ml. However, M(IFNγLPS) THP-1 had higher levels of IL-6 and TNFα than their unprimed M(PMA) counterparts (Figure 5.2 B,C). The mean IL-6 release from M(PMA) was 1 ± 0 pg/mL and 13 ± 2 pg/mL for M(IFNγLPS), and the mean TNFα release was 6 ± 3 pg/mL for M(PMA) and 30 ± 4 pg/mL for M(IFNγLPS). Taken together, this shows the inflammatory priming of M(IFNγLPS) cells was successful, with detectable biological differences compared to unprimed macrophages.

5.3.2 Macrophage conditioned media was not cytotoxic to myotubes

To investigate whether secreted factors from macrophages were cytotoxic to myotubes, LDH release was measured for myotubes treated with 20 % macrophage conditioned medium from M(PMA) and M(IFNγLPS) and compared to myotubes treated with 20 % RPMI. There was no change in cytotoxicity compared to myotubes treated with RPMI control for either M(PMA) or M(IFNγLPS) (Figure 5.3). The median cytotoxicity in the control group was 17 ± 24 %.

5.3.3 Macrophage conditioned medium did not cause p62 aggregation

To test whether macrophage secretory factors affect p62 aggregation, image analysis of p62 puncta was used. Figure 5.4 shows p62 puncta in myotubes treated with 20 % macrophage CM or RPMI control. p62 staining was mostly in puncta with some diffuse

sarcoplasmic staining present. When adding conditioned medium from M(PMA) or M(IFNγLPS) at 20 %, there was no change in p62 puncta size or relative frequency compared to RPMI media control (Figure 5.5 A,B). The mean p62 puncta size in the control group was 0.31 ± 0.04 μm^2. The effect of macrophage secreted factors on p62

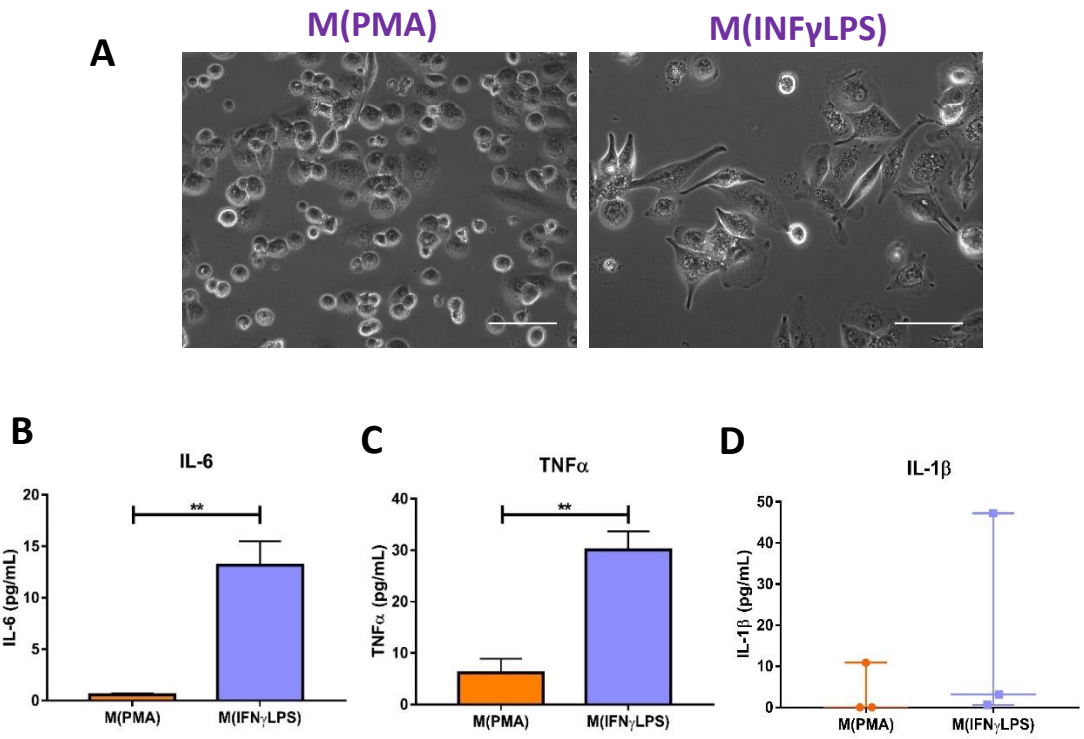

Figure 5.2 Characterisation of macrophage inflammatory priming. (A) Morphological differences between unprimed M(PMA) macrophages and inflammatory primed M(IFNγLPS) macrophages. Scale bar = 100 µm. (B) Secreted IL-6 levels were higher in M(IFNγLPS) macrophages than M(PMA) (Student's T test, p = 0.0055). (C) Secreted TNFα levels were higher in M(IFNγLPS) macrophages than M(PMA) (Student's T test, p = 0.006). (D) There was no difference in IL-1β secretion from M(PMA) and M(IFNγLPS) (Mann-Whitney U test p = 0.3). n = 3 biological repeats. PMA – phorbol 12-myristate-13 acetate, LPS – lipopolysaccharide IL-6 – interleukin-6, TNFα – tumour necrosis factor α.

protein expression were also examined via Western blotting. There was no change in p62 expression for either macrophage CM type (Figure 5.5 C) compared to myogenic cells treated with RPMI control.

5.3.4 Macrophage conditioned medium did not cause TDP-43 aggregation

To investigate whether secretory factors affected TDP-43 sarcoplasmic aggregation, image analysis was used to assess presence, size, frequency, and p62 colocalisation of TDP-43 aggregates. Figure 5.4 shows TDP-43 within myotubes treated with 20 % macrophage conditioned medium or RPMI control. TDP-43 was located diffusely throughout the sarcoplasm and was either present or absent from the nucleus. As with p62, there was no effect of either type of macrophage CM on TDP-43 aggregation in terms of size or relative aggregate frequency (Figure 5.6 A,B). The median size of TDP-43 aggregates in the control group was 0.40 ± 5.28 μm^2. Furthermore, co-localisation of TDP-43 aggregates with p62 was not affected by macrophage CM (Figure 5.6 C). The mean percentage of TDP-43 aggregates that colocalised with p62 in the control group was 28.75 ± 10.44 μm^2. Not all images contained TDP-43 sarcoplasmic aggregates. There was no difference in the likelihood of observing TDP-43 aggregates in images between the three treatment conditions (Chi-squared p = 0.478, Figure 5.6 D). Total protein expression of TDP-43 as assessed via Western blotting was not affected by addition of either macrophage CM relative to RPMI media control (Figure 5.6 E).

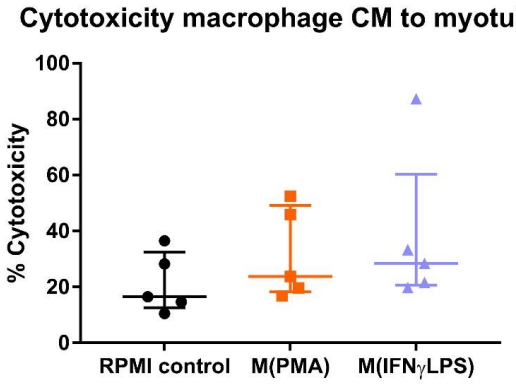

Figure 5.3 Cytotoxicity of macrophage conditioned medium to myotubes. There was no difference in cytotoxicity relative to RPMI control for M(PMA) or M(IFNγLPS) conditioned media Kruskal-Wallis p = 0.284). n = 5 myogenic donors.

5.3.5 TDP-43 subcellular localisation was not affected by macrophage conditioned medium

The effect of macrophage CM on the subcellular localisation of TDP-43 was examined and compared to myotubes treated with equivalent volume of RPMI. There was no difference in TDP-43 localisation between conditions via two-way ANOVA (Figure 5.7). There was a significant difference ($p < 0.0001$) regardless of treatment condition in the

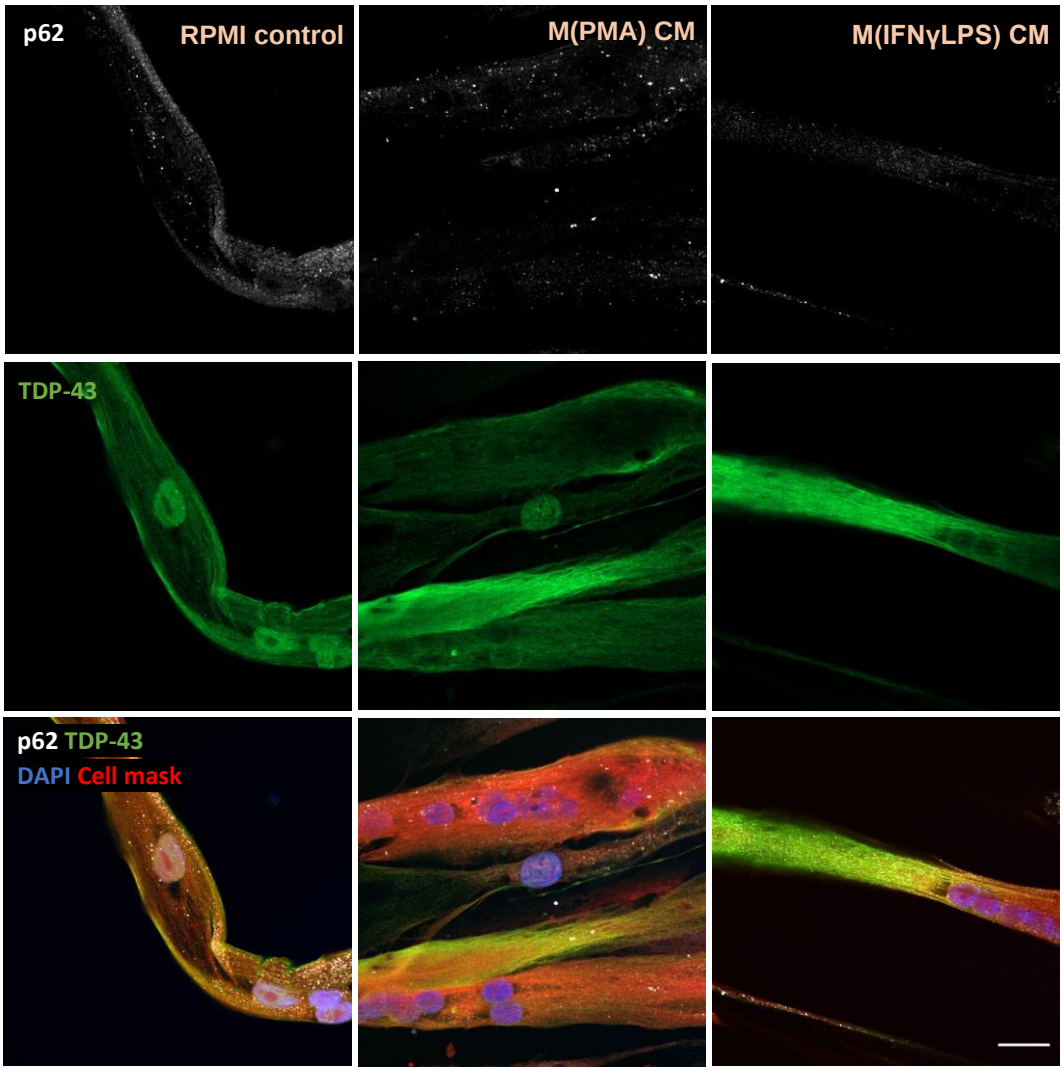

Figure 5.4 Images of p62 and TDP-43 in macrophage conditioned medium-treated myotubes. (A) Representative images of TDP-43 and p62 in myotubes. Scale bar = 20 µm.

divide of TDP-43 within the subcellular compartments, showing distribution was not split evenly between cellular areas within myotubes. The subcellular compartment with the highest percentage of TDP-43 localisation was nucleus and sarcoplasm with mean 60 ± 8 % (two-way ANOVA with Tukey's post-hoc test).

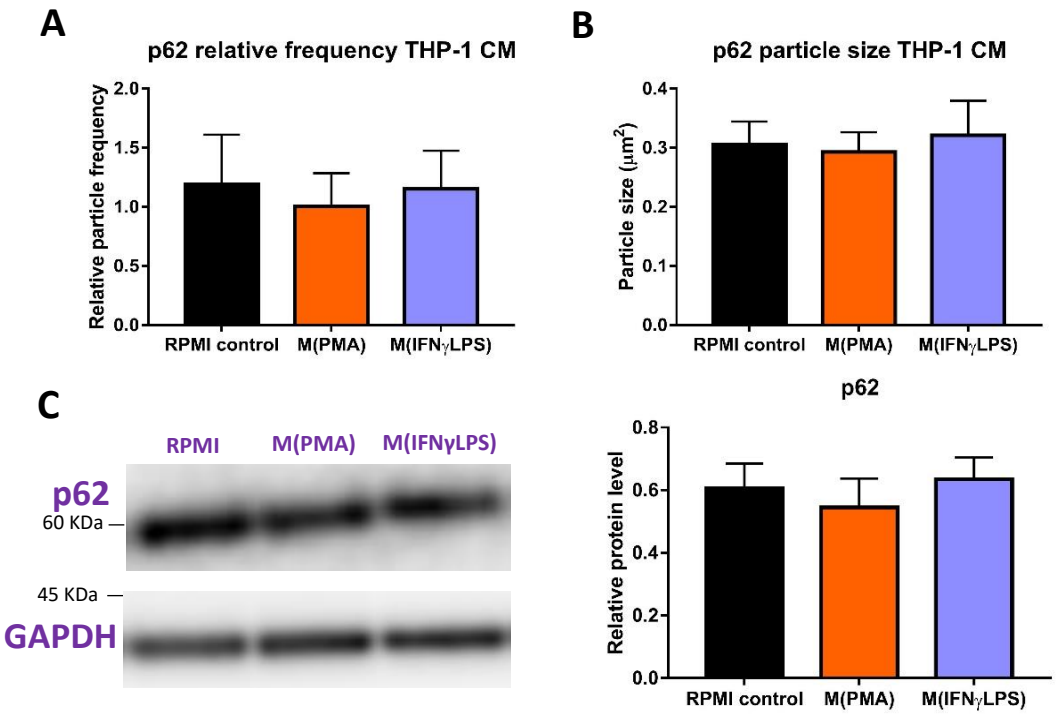

Figure 5.5 p62 puncta analysis and protein expression was not affected by macrophage conditioned medium. (A) The relative frequency of p62 puncta to cell area was not different with M(PMA) or M(IFNγLPS) conditioned media (CM) (p = 0.923). (B) There was no difference in p62 puncta size with M(PMA) or M(IFNγLPS) CM (p = 0.907). (C) Total p62 protein expression, representative blot from one donor. With densitometry analysis, there was no difference in p62 expression between myotubes treated with RPMI control or any macrophage CM (p = 0.733). One-way ANOVA, n = 4 myogenic donors.

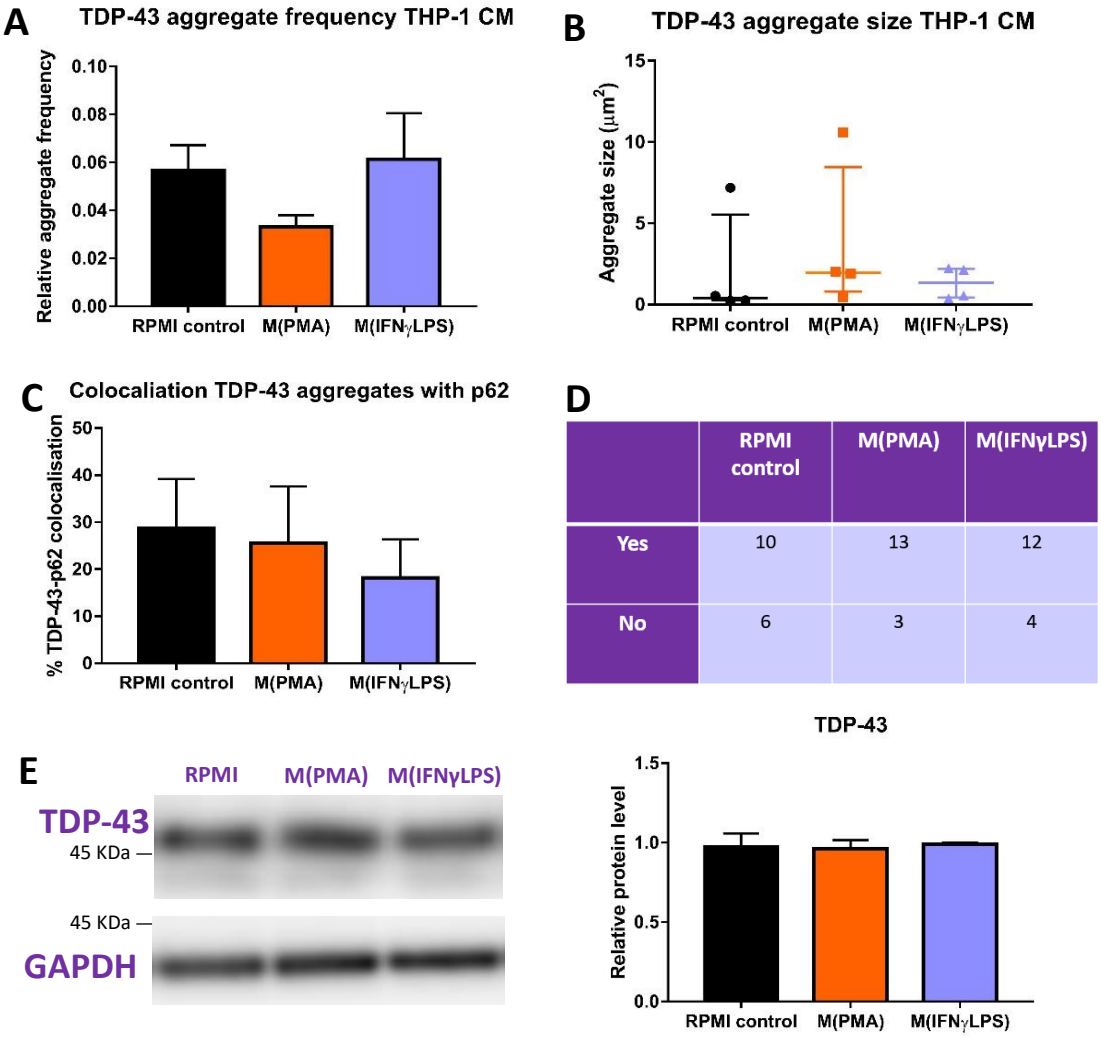

Figure 5.6 TDP-43 aggregation or protein expression was not affected by macrophage secreted factors. (A) TDP-43 aggregate frequency relative to cell area was not affected by M(PMA) or M(IFNγLPS) conditioned medium (CM) treatment ($p = 0.305$). (B) TDP-43 aggregate size was not different between control and M(PMA) or M(IFNγLPS) CM treatment ($p = 0.510$). (C) There was no difference in percentage co-localisation of TDP-43 aggregates with p62 puncta between control and M(PMA), or control and M(IFNγLPS) CM ($p = 0.768$). (D) There was no difference in presence of TDP-43 aggregates between conditions (Chi-squared $p = 0.478$, four images (each with 3 z-slices) for each of four donors). (E) Total TDP-43 protein expression for one myogenic donor. There was no difference between RPMI control and M(PMA), or RPMI control and M(IFNγLPS) ($p = 0.937$). One-way ANOVA or Kruskal-Wallis test, n = 4 donors.

5.3.6 Macrophage conditioned medium did not affect sestrin-1 or sestrin-2 expression

To examine whether secreted factors from macrophages affected sestrin expression, Western blotting of myotubes treated with macrophage CM or RPMI control was used. There was no difference compared to RPMI control for sestrin-2 expression for M(PMA) or M(IFNγLPS) treated myotubes (Figure 5.8 A). Similarly, sestrin-1 expression was not affected by incubation with conditioned medium from either macrophage type Figure 5.8 B).

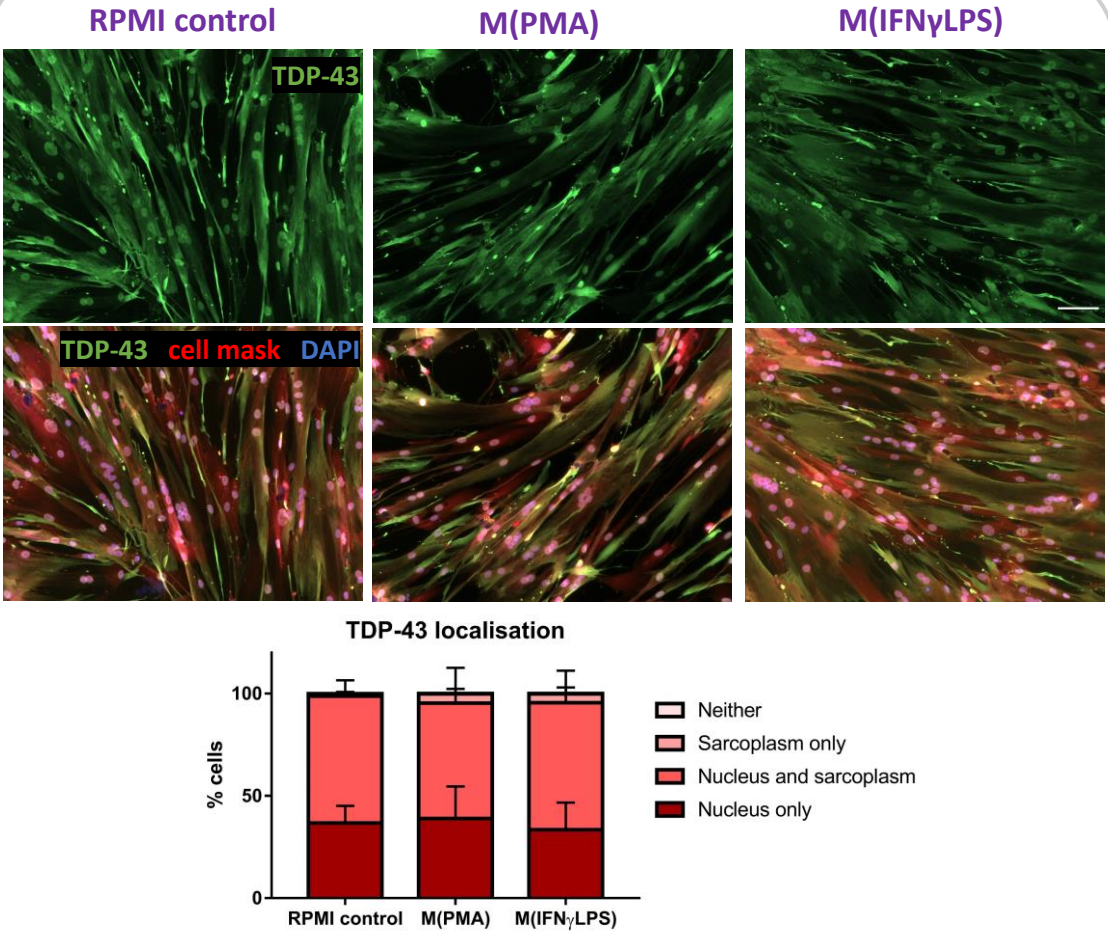

Figure 5.7 TDP-43 localisation with macrophage conditioned medium. Example images of TDP-43 staining in myotubes. Scale bar = 100 µm. TDP-43 localisation was not different between the three treatment conditions (two-way ANOVA, p = 0.998). n = 4 myogenic donors.

5.3.7 Treating macrophages with myotube differentiation medium abrogated cytokine release

To investigate if a feedback loop exists between myotubes exposed to inflammatory insult and subsequent macrophage responses, CM from unprimed or IL-1β+IFNγ inflammatory primed myotubes was added to M(PMA) and M(IFNγLPS), then macrophage cytokine secretion was quantified via ELISA. For each cytokine, a single control was also run for M(PMA) and M(IFNγLPS) where myotube N2 differentiation medium (not conditioned with myotubes) was added to macrophages (n = 1). For IL-6, TNFα, and IL-1β, incubation with N2 medium control resulted in cytokine levels below the detectable limits and below 1 pg/mL. For TNFα and IL-1β, the level of cytokine produced when either M(PMA) or M(IFNγLPS) were cultured with inflammatory-primed or unprimed macrophages was also below the detection limit and below 1 pg/mL (Figure 5.9 C-F). Treatment of M(PMA) and M(IFNγLPS) macrophages with umprimed myotube conditioned medium resulted in IL-6 levels below 1 pg/mL. However, when either macrophage type was treated with inflammatory primed myotube CM, the IL-6 levels were increased compared to macrophages treated with unprimed myotube conditioned medium (Figure 5.9 A,B). IL-6 levels were 6 ± 1 pg/mL for M(PMA) treated with inflammatory-primed myotube CM and 6 ± 2 pg/mL for M(IFNγLPS) under the same treatment. However, these cytokine levels were below the detection limit of 9 pg/mL. For M(IFNγLPS) treated with inflammatory primed myotube CM, this was lower than the IL-6 production of 13 ± 2 pg/mL for M(IFNγLPS) with no conditioned medium as shown in Figure 5.2 B.

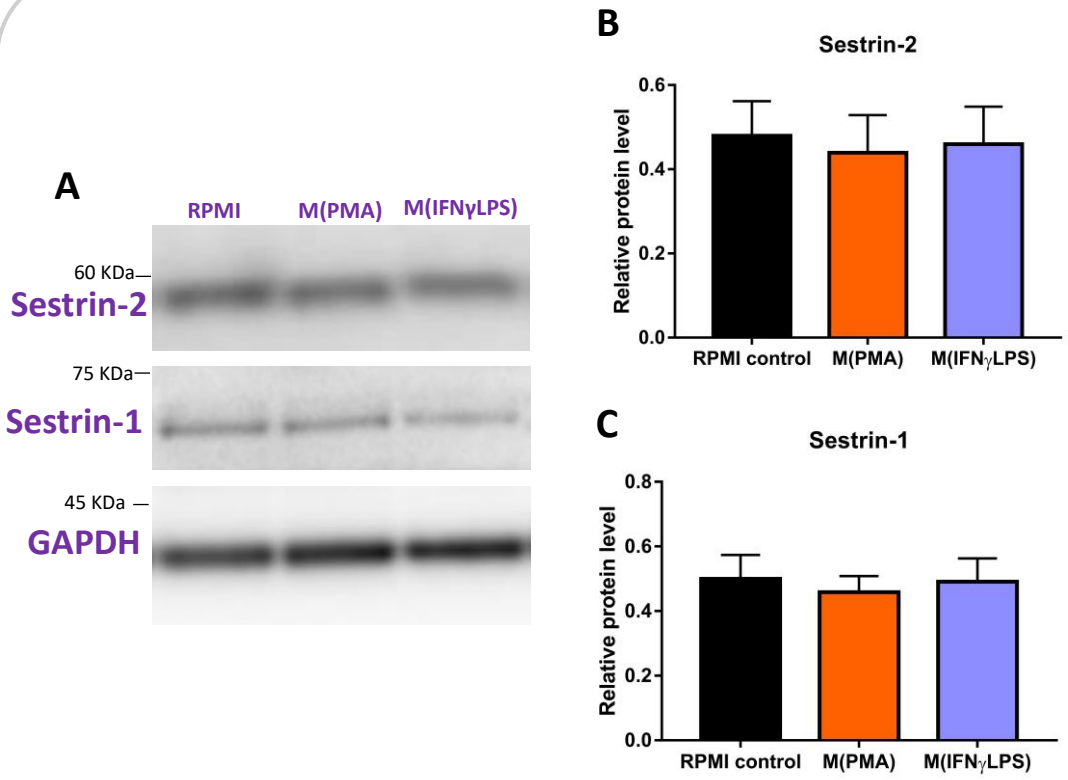

Figure 5.8 Sestrin-2 or sestrin-1 protein expression was not altered by conditioned medium from M(PMA) or M(IFNγLPS) macrophages. (A) Representative blots from one myogenic donor of sestrin-1 and sestrin-2 expression. (B) There were no differences in sestrin-2 expression in myotubes treated with 20 % RPMI control, M(PMA) or M(IFNγLPS) conditioned medium ($p = 0.947$). (C) There were no differences in sestrin-1 expression in myotubes treated with 20 % RPMI control, M(PMA) or M(IFNγLPS) conditioned medium($p = 0.899$). One-way ANOVA, n = 4 myogenic donors.

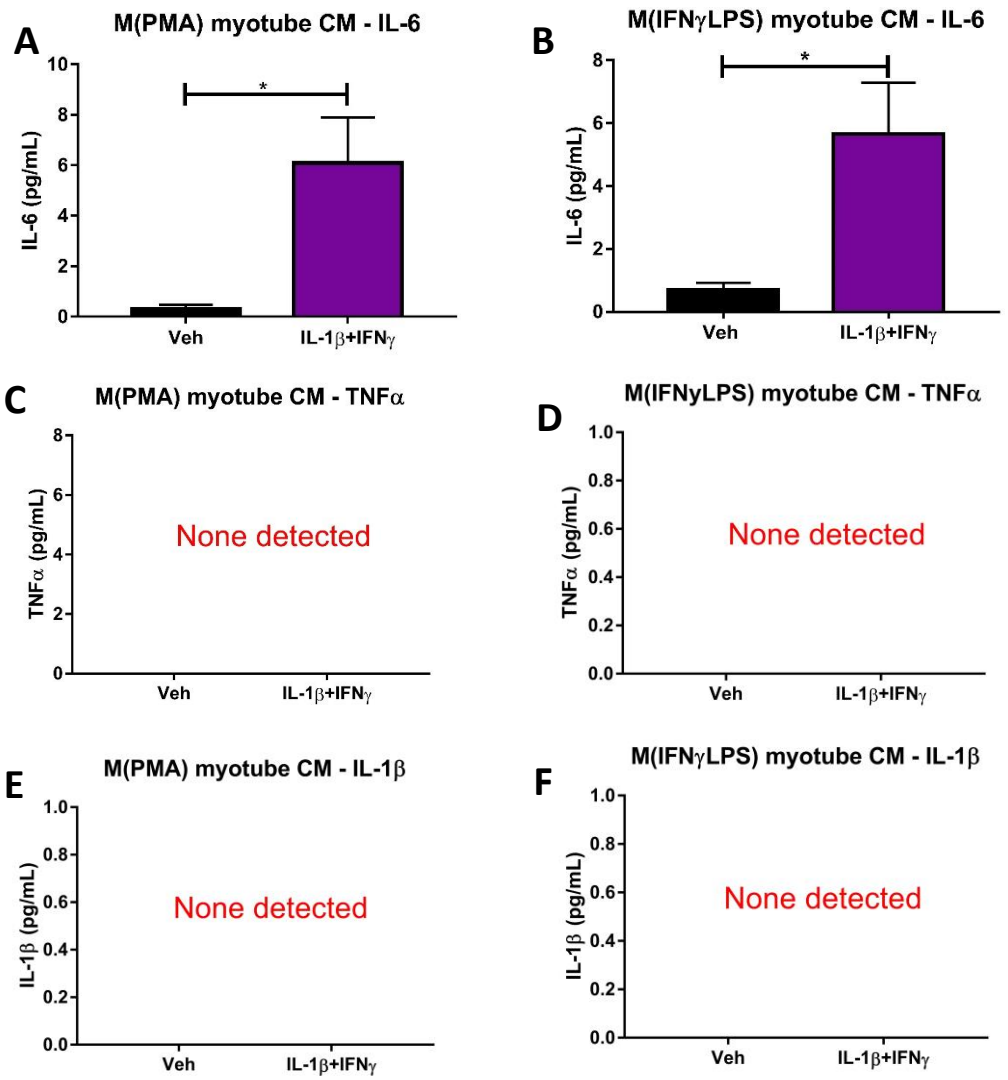

Figure 5.9 Inflammatory primed myotubes caused macrophages to secrete more IL-6 than unprimed myotubes. Myotubes were primed with vehicle (veh, equal volume 0.1 % bovine serum albumin) control or inflammatory primed (IL-1β+IFNγ). (A,B) Addition of inflammatory primed myotube media to M(PMA) or M(IFNγLPS) macrophages increased their production of IL-6 compared to control myotube conditioned medium (CM) ($p = 0.0129$ and 0.0166 respectively). (C, D) Addition of either unprimed or inflammatory primed myotube CM resulted in no detectable release of TNFα (C,D) or IL-1β (E,F) from either M(PMA) or M(IFNγLPS). n = 5 myogenic donors, displayed results from 1 of 2 independent macrophage experiments. Student's T-test.

5.4 Discussion

The aim of this chapter was to investigate whether secreted mediators from inflammatory macrophages can contribute to non-inflammatory features of TDP-43 and p62 aggregation and TDP-43 mislocalisation as seen in sIBM. This was compared to unprimed macrophages as a control. Firstly, the phenotype of inflammatory primed M(IFNγLPS) and unprimed M(PMA) macrophages was characterised. Secreted IL-1β showed highly variable levels in both unprimed M(PMA) and inflammatory primed M(IFNγLPS) macrophages suggesting this is not a cytokine that is consistently upregulated with inflammatory stimulation in this cell line. IL-12p70 was not detectable in either macrophage type. It has previously been found that mRNA levels of IL-1β were increased with IFNγLPS treatment in THP-1 cells (399, 400), however this may not translate to an increased IL-1β protein secretion. A separate study found that M(IFNγLPS) macrophages had higher secretory levels of IL-6, and weak evidence of higher IL-1β and TNFα ($0.07 < p < 0.05$) compared to M(PMA). However, IL-12 p70 was not different between M(IFNγLPS) and M(PMA) (401). Therefore, it is not clear why IL-1β was not increased here, but as previously shown IL-12 p70 may not be a sensitive marker for THP-1 inflammatory priming. Overall, there were changes in cell morphology, TNFα and IL-6 secretion between M(PMA) and M(IFNγLPS), showing successful inflammatory priming in M(IFNγLPS) macrophages. However, the levels of IL-6 and TNFα from M(IFNγLPS) were low in the range of tens of pg/mL.

Despite the higher secretion of TNFα with M(IFNγLPS) which is a cytotoxic cytokine (402), there was no increased cytotoxicity when culturing myotubes with M(IFNγLPS) conditioned medium. Previously, treatment of C2C12 myotubes with 20 ng/mL TNFα for 48 hours caused reduced viability and myotube diameter (403). Furthermore, treatment of C2C12 myotubes with 1 or 10 ng/mL TNFα resulted in cytotoxicity as shown by increased LDH release (404). It is likely that the low secretion of TNFα from M(IFNγLPS) compounded by the dilution of macrophage CM for treatment of myotubes was not sufficient to induce cell death in myotubes. This highlights that concentrations of macrophage secreted factors could be below levels required to elicit responses in myotubes.

5.4.1 p62, TDP-43, and sestrins

There was no effect of CM from either macrophage phenotype on any examined TDP-43 or p62 feature, suggesting that secretory factors from macrophages may not contribute to sIBM-like TDP-43 or p62 pathology in these cells at the concentrations examined here. This may also show there was no blockade or alteration of autophagy that would be represented by p62 changes. Potentially the cell number of macrophages from which CM was collected could have been increased to maximise any effects of the CM and increase secreted cytokine concentrations. However, there are relatively few macrophages found in sIBM muscle, especially compared to CD8+ T cell infiltrates. Therefore, the low concentrations of macrophage secreted factors used here may more accurately reflect those found in sIBM muscle. Protein levels of p62, TDP-43, and sestrin-1 or sestrin-2 were not affected by macrophage conditioned medium. This suggests that low concentrations of macrophage inflammatory mediators do not regulate production of these proteins. As sestrin-2 is upregulated by cell stress, this also suggests macrophage CM at low levels may not cause stress in myotubes.

5.4.2 Myotube secretory factors

Myotubes were inflammatory primed with IL-1β and IFNγ and the effect of CM from these myotubes on macrophage cytokine production was examined, to see whether a feedback loop exists between inflamed muscle/myotubes and macrophage inflammatory priming. Previously it has been found that CM from C2C12 myotubes suppressed the expression of IL-1β from murine macrophages (405). Although not biologically repeated, treatment of either macrophage type with 20 % N2 differentiation medium control abrogated IL-1β, TNFα, and IL-6 production. The lack of TNFα and IL-1β with myotube conditioned medium treatment is therefore likely due to unexpected effects of myotube differentiation medium on macrophages. Therefore, it was not possible to assess the effect of myotube CM on IL-1β and TNFα secretion.

Myotube differentiation medium is composed of DMEM/F12, 1 % N2, 1 % insulin-transferrin-selenium, 0.2 % penicillin-streptomycin, and 1 % L-glutamine. Compared to macrophage growth medium, the main differences in constituents of myotube

differentiation medium are: transferrin, insulin, progesterone, putrescine, selenite, alanine, thymidine, pyruvate, lipoic acid, linoleic acid, hypoxanthine, and more inorganic salts (based on supplier's formulation information (406-408)). In the J774A.1 murine macrophage line, it was found that cells cultured in RPMI maintained a suspension phenotype, whereas those cultured in DMEM/F12 were adherent. Furthermore, RPMI-macrophages upregulated IL-1β gene expression with LPS treatment whereas DMEM/F12 macrophages did not, whilst TNFα transcription was inducible via both media types (409). Other components in N2 media can also affect inflammatory priming of macrophages. Progesterone can downregulate IL-12 and nitric oxide production by macrophages (410), and putrescine impairs M1 gene transcription (411, 412). Treatment of macrophages with lipoic acid can alter their cytokine secretion, with increased IL-1β but decreased TNFα and IL-6 secretion (413). Therefore, it is possible that the components of myotube differentiation medium lead to a reversal of the M(IFNγLPS) phenotype, with less inflammatory cytokine secretion. However, direct comparisons between macrophages cultured in RPMI and myotube differentiation medium would be necessary to establish this.

Despite the inhibition of expression of IL-1β and TNFα with myotube conditioned medium, IL-6 was secreted with myotube CM treatment, albeit below the level of detection of 9 pg/mL. IL-6 secretion was higher when either macrophage phenotype was cultured in inflammatory primed myotube CM. This suggests inflammatory-primed myotubes secrete factors strong enough to influence macrophage cytokine secretion, overcoming the effects of N2 medium that could prevent IL-6 release. However, the factors secreted by myotubes primed by IL-1β and IFNγ were not investigated so it is not known what myotube secreted factor caused this result.

In skeletal muscle repair, damaged skeletal muscle secretes CCL2 which attracts circulating monocytes (414). Few studies have directly investigated the effect of inflammatory myotube-macrophage cross-talk. Myotubes treated with palmitate activated the NF-κB signalling pathway, which is also activated through IL-1β. Palmitate-treated myotubes secreted IL-6, TNFα and CCL2, and conditioned medium from these myotubes activated Raw264.7 macrophages towards an inflammatory

phenotype (415). In injured skeletal muscle, macrophages infiltrate and produce large amounts of IL-6 (416). The role of IL-6 in skeletal muscle is complex, as it is also a myokine secreted by the muscle itself. IL-6 promotes muscle repair and hypertrophy, however it is also conversely associated with atrophy under chronic exposure conditions (417). Subjecting myotubes to IL-1β may have caused activation of NF-κB and release of pro-inflammatory mediators, potentially IL-6 itself, that polarise macrophages to secrete IL-6 to promote muscle regeneration. It would be interesting to investigate the IL-6 secretion from myotubes primed with IL-1β+IFNγ. Furthermore, direct effects of IL-6 treatment on macrophages could be examined, as well as incubating macrophages in myotube CM containing IL-6 neutralising antibodies.

5.4.3 THP-1 cells as model macrophages

THP-1 cells are usually maintained in medium containing the reducing agent 2-mercaptoethanol which was not included here. It has been found that exclusion of 2-mercaptoethanol from THP-1 growth medium does not affect proliferation, metabolic activity, or differentiation of the cells. However, when THP-1 were deprived of both 2-mercaptoethanol and FBS, M(PMA) had increased metabolic activity and decreased secreted β-hexosaminidase (418), a lysosomal enzyme that can be secreted from macrophages important in control of mycobacteria (419). Therefore the omission of 2-mercaptoethanol here may have unduly influenced the conditioned medium collected for transfer to myotubes, as this was performed under serum-free conditions.

It is important to note that results from this chapter were obtained using a monocytic cell line derived from a myeloid leukaemia patient. This cell line was utilised due to its ability to proliferate for long periods during cell culture, as opposed to primary cells which have finite proliferative capacity and may have high inter-donor variability. THP-1 cells have been extensively used as models of macrophage-like cells. However, as with any transformed cell line, differences can exist in the phenotype and responses compared to non-transformed primary cells (420). Notably, THP-1 cells have been shown to have an altered cytokine release profile compared to PBMC monocyte derived macrophages (401). Furthermore, any sIBM-specific monocyte characteristics

would not be observable using THP-1 cells. To increase biological relevance of these experiments, the effect of sIBM PBMC-derived macrophages could be investigated.

5.4.4 Summary

This chapter aimed to investigate whether secreted factors from inflammatory macrophages can cause degenerative features of TDP-43 and p62 aggregation and TDP-43 mislocalisation in cultured healthy myotubes. Overall, the results from this chapter suggest secreted factors from inflammatory macrophages do not contribute to TDP-43 and p62 sIBM-like sarcoplasmic aggregation at the concentration tested in the cells examined. Sestrins may also not be affected by macrophage secreted factors. Unexpectedly, myotube differentiation medium abrogated release of inflammatory cytokines, but conditioned medium from IL-1β+IFNγ-treated myotubes increased the secretion of IL-6 from M(PMA) and M(IFNγLPS) macrophages, potentially due to an IL-6 positive feedback loop. This chapter did not extend to investigating the role of direct cell-cell interactions of macrophages with myotubes, which may show different effects.

Chapter 6: Effect of TALL-104 conditioned medium and co-culture on myotubes

Chapter 6. Effect of TALL-104 conditioned medium and co-culture on myotubes

6.1 Introduction

6.1.1 CD8+ T cells in sIBM

The role of CD8+ T cells in sIBM has been covered in Section 1.11. CD8+ T cells infiltrate into the endomysium and muscle fibres themselves in high quantities in sIBM. These CD8+ T cells are highly differentiated and cytotoxic, secreting high levels of cytotoxic mediators including perforins and granzymes. Further, the high expression of MHC I on sIBM muscle suggests that the muscle itself may be presenting antigens to CD8 cells. This is corroborated by evidence CTLs in sIBM are clonally or oligoclonally expanded (421-423) suggesting CD8+ T cells are reacting to a currently undetermined antigen(s) presented by sIBM muscle. Whilst there is a good body of work characterising the CD8+ T cell infiltrate observed in sIBM, there are fewer studies directly investigating the effects of cell-mediated cytotoxicity on myotubes in a manipulatable manner. There is a need to better understand the interactions between CD8+ T cells and other sIBM features such as TDP-43 and p62 sarcoplasmic aggregation to understand which, if any, pathological feature precludes the other.

6.1.2 Natural killer cells

Natural killer (NK) cells are members of the innate immune system that act in a similar way to cytotoxic T cells by killing infected and tumourigenic cells. NK cells cause target cell apoptosis in a similar way to CTLs, through formation of an immunological synapse and the use of cytotoxic granules containing granzymes and perforin, and through use of death receptor signalling including Fas/FasL and TRAIL. NK cells like CD8 T cells secrete cytostatic and cytotoxic cytokines including TNFα and IFNγ (424). The main difference between NK cells and CTLs lies in their activation. NK cells are activated by receptors that recognise molecules on infected and tumourigenic cells. Specifically, NK cells express inhibitory and activating receptors, and their activation depends on the balance of the signals from these receptors. Unlike CTLs, their cytotoxic capabilities do not require prior priming to the target antigen via APCs as they are activated by target

cells directly (425). The activation of natural killer cells is enhanced by proinflammatory cytokines in the surrounding environment including IFNα and β (426).

Natural killer cells can be subclassified as dim or bright based on their CD56 expression. CD3-CD56+dim natural killer cells are cytotoxic, whereas the less abundant CD3-CD56+bright NK cells are immunoregulatory via their cytokine production (427). Other than the differences in recognition between CD8 and NK cells, there are some differences in their cytotoxicity. CD56dim NK cells have higher expression of perforin and granzyme A, but lower expression of granzyme B compared to CD57+ CD8+ T cells. However, both cell types had similar ability to degranulate in response to target cells (428).

The proportion of natural killer cells in sIBM patient blood was found to be similar to that of healthy control patients (429). However, the estimated abundance of different immune cells in sIBM muscle has been investigated based on gene expression data, showing that after CD8+ T cells, the second most frequent immune signature in sIBM muscle belonged to natural killer cells (124).

6.1.3 TALL-104 cell line

TALL-104 is an IL-2 dependent cell line developed from a 2 year old T-ALL (T-cell acute lymphoblastic leukaemia) patient. These cells are positive for CD8, CD3 (a T cell lineage marker(430)), TCR α and β chains, as well as natural killer cell markers including CD56 (431) and CD161 (432). TALL-104 cells are cytotoxic towards target cells. Most research using TALL-104 has focussed on their cytotoxicity towards tumourigenic cells, where they specifically target transformed cells whilst sparing healthy cells (433-436). The mechanism of TALL-104 cytotoxicity has been investigated, showing that cytotoxicity is mediated through direct cell-cell contacts and not secreted factors. Addition of blocking antibodies against natural killer cell receptors NKp46, NKG2D, and 2B4 prevented TALL-104 mediated target lysis, showing TALL-104 activity against transformed cells is mediated through NK cell receptors (431). Furthermore, it was found that the cytotoxic mechanism employed by TALL-104 cells varied depending on the target cell, with combined killing via perforin and TRAIL pathways of B lymphoblast

lines, and Jurkat T lymphoblast lines killed through perforin and Fas pathways (432). However, a separate study found TALL-104 cells do not express FasL with glioma cells (431), further highlighting the complex activity of this cell line towards different targets.

There is an overlap between some of the markers of CTLs and NK cells. Subsets of natural killer cells can co-express CD8 (CD8+ CD3- CD56+) (437), and 30 % of blood natural killer cells express the CD8αα homodimer, whilst cytotoxic T cells usually express an αβ heterodimer (438, 439). A subset of immune cells termed natural killer T (NKT) cells also exist which express natural killer cell markers including CD161 (440) and CD56 (441). NKT cells also express a TCR with α and β chains, however unlike T cell TCRs that recognise MHC I antigens, NKT TCR recognise lipid antigens from CD1d that resembles MHC I (442). Other T cell markers are also expressed by NKT cells, including CD3 (441). NKT cells are capable of cytotoxicity through perforin, TRAIL, or FasL-mediated mechanisms (443-445), and some NKT subsets express CD8 (446). TALL-104 cells are not true CD8+ T cells and their mechanism of action is not dependent on MHC recognition. TALL-104 cells instead resemble a mixed lineage sharing features of NK, NKT and CD8 T cells.

Culturing primary CD8+ T cells can be a difficult process that usually requires access to donor blood samples, FACS or MACS mediated cell separation, and extensive characterisation. Further, primary CD8 T cells have a finite lifespan in culture. As TALL-104 cells are immortalised due to their neoplastic nature, this has benefits of easier use compared to continuous isolation and short-term culture of primary-derived CD8 T cells. Ideally, matched patient blood and muscle samples from sIBM patients could be utilised in culture to investigate whether CD8+ T cells directly contribute to non-inflammatory features in sIBM including TDP-43 and p62 sarcoplasmic aggregation. Here, TALL-104 cells were used as a proxy for cytotoxic immune cells to directly investigate effects of cell-mediated cytotoxicity on sIBM non-inflammatory features.

6.1.4 Aims and hypothesis

This chapter aimed to explore the effect of cytotoxic immune cells on non-inflammatory features of sIBM, focussing on the effects of secreted factors and direct coculture interactions of TALL-104 cells on TDP-43 and p62 in myotubes. The effects of conditioned medium transfer and addition of TALL-104 cells to myotube cultures were investigated for TDP-43 and p62 sarcoplasmic aggregation and TDP-43 mislocalisation.

It is hypothesised that TALL-104 coculture and conditioned medium will cause increased sarcoplasmic aggregation of TDP-43 and p62, as well as mislocalisation of TDP-43 to the sarcoplasm. Furthermore, it is hypothesised that addition of conditioned medium from myotubes primed with IL-1β+IFNγ will cause increased secretion of inflammatory cytokines IFNγ and TNFα from TALL-104 cells.

6.2 Methods

6.2.1 TALL-104 cell culture

TALL-104 cells were purchased from LGC standards, UK. TALL-104 cells were cultured in ATCC-modified RPMI with 20 % FBS and 20 ng/mL IL-2 premium grade (Milltenyi Biotec, UK 130-097-744) at 37 °C and 5 % CO_2 in a humidified incubator. The optimum cell density in culture was between 0.5 x 10^6 – 1 x 10^6 /mL. TALL-104 were used between passage 4 and 12 with the initial cryovial from the supplier taken as passage 1.

6.2.2 Collection of TALL-104 conditioned medium

TALL-104 cells were seeded at 7 x 10^5 cells/mL in fresh medium in T75 flasks. Cells were counted daily and conditioned medium was collected once cell count reached over 9 x 10^5 cells. This took approximately 3-5 days, with two rounds of conditioned media collection performed. As a control, the same volume of complete TALL-104 medium was incubated for the same duration, without cells.

6.2.3 Treatment of myotubes with TALL-104 conditioned medium and cytotoxicity assay

Myogenic cells were seeded at 4x10^4 cells per 24-well. Cytotoxicity was measured using a non-radioactive cytotoxicity kit as described in Section 2.3, via two overlapping experiments. First, increasing percentages of TALL-104 conditioned medium were added to myotubes between 5 – 50 % v/v in N2 differentiation medium and compared against a N2-differentiation medium control. Secondly three concentrations of TALL-104 CM (10 %, 20 %, and 30 % v/v) were compared against respective percentages of TALL-104 medium (RPMI + 20 % FBS + IL-2) which was incubated without cells for the same period as the conditioned medium. Myotubes were incubated in TALL-104 CM or relevant control for 48 hours before collecting media for cytotoxicity assay. For downstream experiments of TDP-43 and p62, 30 % v/v conditioned medium or IL-2 medium control were chosen.

6.2.4 TALL-104 myotube coculture and cytotoxicity assay

Myotubes were seeded at either $4x10^4$ cells per 24-well with two days proliferation or $5.5x10^4$ cells per well with one day proliferation followed by 5 days differentiation. TALL-104 cells were centrifuged at 170 xg and resuspended in N2 myotube differentiation medium with 20 ng/mL IL-2 for addition to myotube cultures. Different effector to target (E:T) ratios of 0.5:1, 1:1, 2.5:1, and 5:1 of TALL-104 cells were added based on the initial seeding density of myogenic cells for 4, 24, or 48 hours, and cytotoxicity was measured as described previously. For downstream experiments analysing TDP-43 and p62, 1:1 E:T ratio for 24 hours was chosen.

6.2.5 IFNγ and TNFα ELISA of cocultured TALL-104

Medium from TALL-104-myotube cocultures (Section 6.2.4) was also collected for ELISA analysis of IFNγ and TNFα levels. TALL-104 cells cultured in myotube N2-differentiation medium with IL-2, without myotubes were used as a TALL-104 only control. Media from 24 hour coculture or TALL-104 only control was used. Media samples were frozen at -80 °C until use. ELISA was conducted as previously described in Section 2.9 except conditioned medium was diluted to 70 % original concentration in reagent diluent before use, which was accounted for in final concentration calculations.

6.2.6 TDP-43 localisation with TALL-104 conditioned medium and coculture

TDP-43 localisation was imaged using widefield microscopy as described previously in Section 2.5.

6.2.7 TDP-43 aggregate and p62 puncta analysis with TALL-104 conditioned medium and coculture

The same samples used for TDP-43 localisation were used for TDP-43 aggregate and p62 puncta analysis imaged using a Zeiss LSM 800 confocal microscope using methods described previously in Section 2.6 and 2.7 with minor modifications. Eight images each of two z-stacks were captured per condition per donor. p62 aggregates were defined as 3 or more pixels in size using Image J “Analyse Particles”. TDP-43 and p62 sarcoplasmic aggregation analysis was conducted blind.

6.2.8 Treatment of TALL-104 with myotube conditioned medium

Conditioned medium from unprimed or inflammatory primed myotubes was collected as described in Section 2.2, with four donors differentiated for 7 days utilised. $7x10^5$ TALL-104 cells were seeded in 1 mL of complete TALL-104 growth medium containing 30 % v/v myotube conditioned medium for 48 hours, after which the medium was changed to serum free RPMI for 24 hours. Treated TALL-104 CM was collected, centrifuged at 500 xg to remove debris, re-aliquotted, and stored at -80 °C until use for ELISA.

6.3 Results

6.3.1 TALL-104 conditioned medium was not cytotoxic to myotubes

Cytotoxicity of TALL-104 conditioned medium (CM) was assessed to examine if secreted factors from TALL-104 cells were cytotoxic to myotubes as well as to choose a CM percentage for further experiments. Firstly, percentages of conditioned medium ranging from 5 – 50 % v/v were added to myotubes for 48 hours. There was no difference between the N2-medium control and any of the examined CM conditions (Figure 6.1 A). The mean cytotoxicity in the control group was 22 ± 6 %. For downstream experiments, 30 % v/v TALL-104 was chosen to ensure enough conditioned medium could be collected for the experiments. To ensure that there was no cytotoxic effect arising from addition of IL-2 in the TALL-104 CM that may mask cytotoxicity of TALL-104 secreted factors, 10, 20, and 30 % v/v CM was compared to respective percentages of RPMI + IL-2 only control. There was no difference in cytotoxicity with IL-2 control compared to TALL-104 CM at the three tested concentrations. There was also no difference in cytotoxicity for increasing concentration of IL-2 control, suggesting IL-2 is not cytotoxic to myotubes (Figure 6.1 B). The cytotoxicity with N2 control in Figure 6.1 A and the three percentages of IL-2 RPMI control in Figure 6.1 B were compared. There was no difference between these control conditions (one-way ANOVA $p = 0.766$) further showing IL-2 is not cytotoxic to cultured myotubes.

6.3.2 Inflammatory primed myotubes may affect activation of TALL-104 cells

To investigate whether a feedback loop exists between myotubes subjected to inflammatory insult and cytotoxic immune cell activation, TALL-104 cells were cultured with 30 % v/v conditioned medium from myotubes that were either unprimed or primed for two days with IL-1β+IFNγ (Figure 6.2). There was weak evidence that IFNγ secretion was higher when TALL-104 cells were cultured with inflammatory primed myotube conditioned medium compared to unprimed myotubes ($p = 0.0591$). The mean IFNγ released from TALL-104 with inflammatory primed myotube CM was 5 ± 1

pg/mL, compared to 2 ± 1 pg/mL for control primed myotube CM. However, IFNγ levels from both conditions were below the limit of detection of 9 pg/mL for the ELISA.

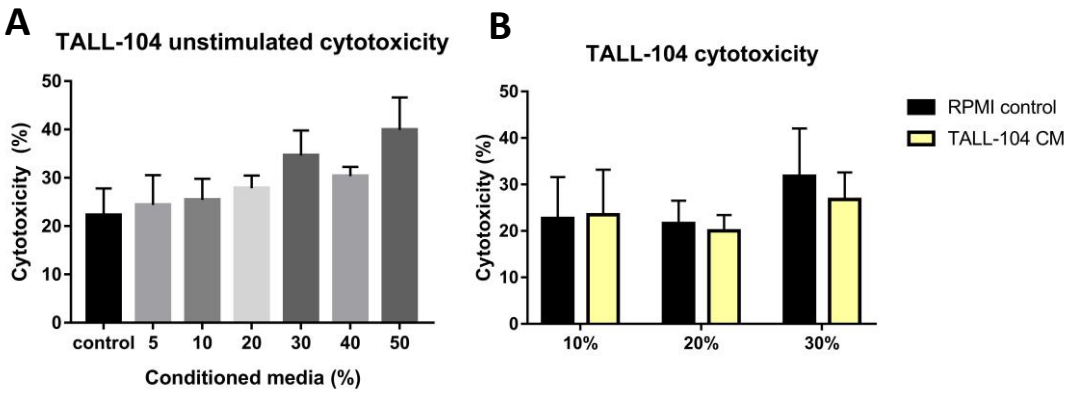

Figure 6.1 Cytotoxicity of TALL-104 conditioned medium on myotubes. (A) Cytotoxicity of different percentages of TALL-104 conditioned medium (CM). There was no difference between N2-medium control and any percentage of TALL-104 conditioned medium (One-way ANOVA p = 0.177). (B) Difference between three percentages of TALL-104 CM and the respective amount of RPMI + IL-2 control medium for myotube cytotoxicity. There was no difference between CM and RPMI control for any percentage (two-way ANOVA, RPMI vs conditioned medium p = 0.760, difference between percentages p = 0.760). n = 6 myogenic donors.

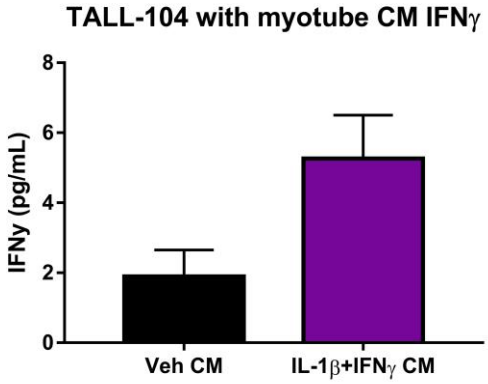

Figure 6.2 Effect of inflammatory conditioned myotube medium on TALL-104 IFNγ secretion. TALL-104 cells were treated with 30 % conditioned medium (CM) from either 0.1 % bovine serum albumin vehicle (veh)-treated myotubes or IL-1β+IFNγ treated myotubes. There was weak evidence of an increase in IFNγ secretion from TALL-104 cells with CM from IL-1β+IFNγ myotubes (Student's T-test, p = 0.0591). n = 4 myogenic donors.

6.3.3 p62 puncta frequency or size was not affected by TALL-104 secreted factors

To assess whether secreted factors from cytotoxic immune cells affect p62 sarcoplasmic aggregation, immunofluorescent analysis was used to assess p62 sarcoplasmic puncta size and frequency in myotubes treated with TALL-104 CM. Figure 6.3 shows immunofluorescent images of p62 in myotubes treated with 30 % v/v TALL-104 CM. p62 was found mostly in the sarcoplasm where it displayed both distinct small puncta staining as well as strong diffuse staining in the control and TALL-104 CM conditions. Some p62 staining could also be seen in the nuclei. The frequency of p62 puncta relative to cell area was not different between IL-2 control and 30 % TALL-104 conditioned medium condition (Figure 6.4 A). Furthermore, the size of p62 puncta was not affected by addition of TALL-104 conditioned medium (Figure 6.4 B). The mean p62 puncta size was 0.54 ± 0.11 μm^2 in the IL-2 control group.

6.3.4 TDP-43 aggregates were more likely in myotubes treated with TALL-104 CM, but aggregate size or frequency was not affected

To investigate whether secreted factors from cytotoxic immune cells influenced TDP-43 sarcoplasmic aggregation, 30 % conditioned medium from TALL-104 cells or IL-2 RPMI control was added to myotubes, before analysing TDP-43 aggregate size, frequency, and presence. Figure 6.3 shows TDP-43 immunofluorescent staining in myotubes treated with IL-2 control or TALL-104 CM. TDP-43 was expressed in the nuclei as well as diffusely in the sarcoplasm. There was no effect of TALL-104 CM on the size or relative frequency of TDP-43 aggregates (Figure 6.5 A,B). The mean size of TDP-43 aggregates was 0.72 ± 0.19 μm^2 in the IL-2 control group. Furthermore, there was no difference between IL-2 control and TALL-104 conditioned medium-treated myotubes for the percentage of TDP-43 aggregates that colocalised with p62 puncta (Figure 6.5 C). The mean percentage of TDP-43 aggregates that colocalised with p62 puncta in the IL-2 control group was 19 ± 7 %. When considering whether each image (of two z slices) contained TDP-43 aggregates, there was a higher frequency of TDP-43 aggregates in TALL-104 CM images compared to IL-2 control medium (Fisher's

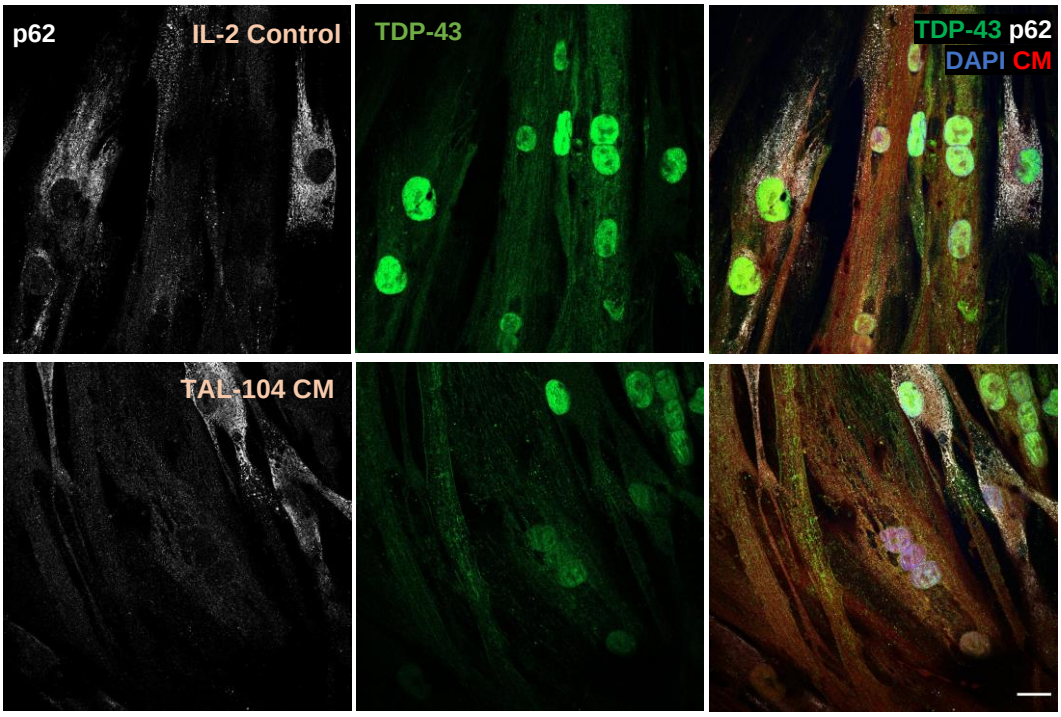

Figure 6.3 p62 and TDP-43 with TALL-104 conditioned medium. (A) Representative images of TDP-43 and p62 in myotubes treated with IL-2 control and TALL-104 conditioned medium (CM). Scale bar = 20 µm.

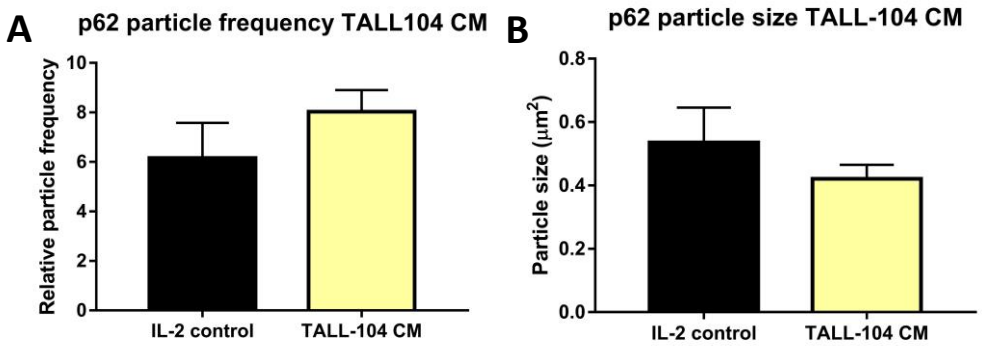

Figure 6.4 TALL-104 conditioned medium did not affect p62 puncta size or frequency. (A) There was no difference between IL-2 control and 30 % TALL-104 conditioned medium (CM) for p62 puncta frequency relative to cell area (p = 0.289), (B) or p62 puncta size (p = 0.357). Student's T-test, n = 6 myogenic donors.

exact test p = 0.0326, Figure 6.5 D). There was no difference in the number of cells imaged in each condition (p = 0.322, 3.1 ± 0.2 vs 3.6 ± 0.4 cells per image mean ± SEM for IL-2 control and TALL-104 CM respectively).

6.3.5 TDP-43 subcellular localisation was not affected by TALL-104 secreted factors

TDP-43 subcellular localisation was examined after incubation with 30 % v/v TALL-104 conditioned medium or IL-2 control. There was no difference in TDP-43 localisation between myotubes treated with IL-2 control and those treated with TALL-104 CM

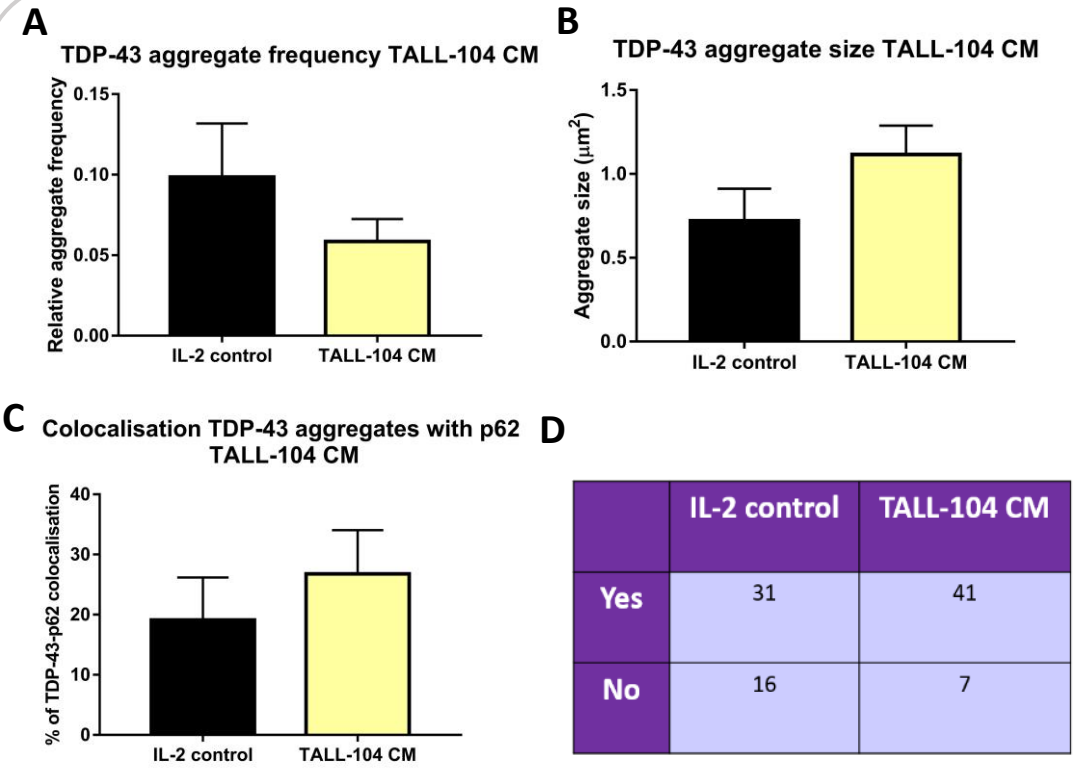

Figure 6.5 TALL-104 conditioned medium did not affect TDP-43 aggregate frequency, size, or colocalisation with p62. (A) There was no difference between IL-2 control and 30 % TALL-104 conditioned medium (CM) for TDP-43 aggregate frequency relative to cell area (p = 0.294), (B) TDP-43 aggregate size (p = 0.155), (C) or colocalisation with p62 puncta (p = 0.465). (D) There was a higher frequency of images containing TDP-43 aggregates in the TALL-104 CM group compared to IL-2 control (p = 0.0326, Fisher's exact test), 8 images for each of 6 donors per condition. A-C Student's T-test. n = 6 myogenic donors.

for TDP-43 localisation (Figure 6.6). There was a significant difference between localisation areas irrespective of treatment condition ($p < 0.0001$), showing that distribution of TALL-104 was not even between the different subcellular compartments. Regardless of treatment condition, the localisation areas with the highest percentage of TDP-43 were nucleus and sarcoplasm (mean 53 ± 4 %) closely followed by nucleus only (mean 47 ± 5 %) (two-way ANOVA with Tukey's post-hoc test).

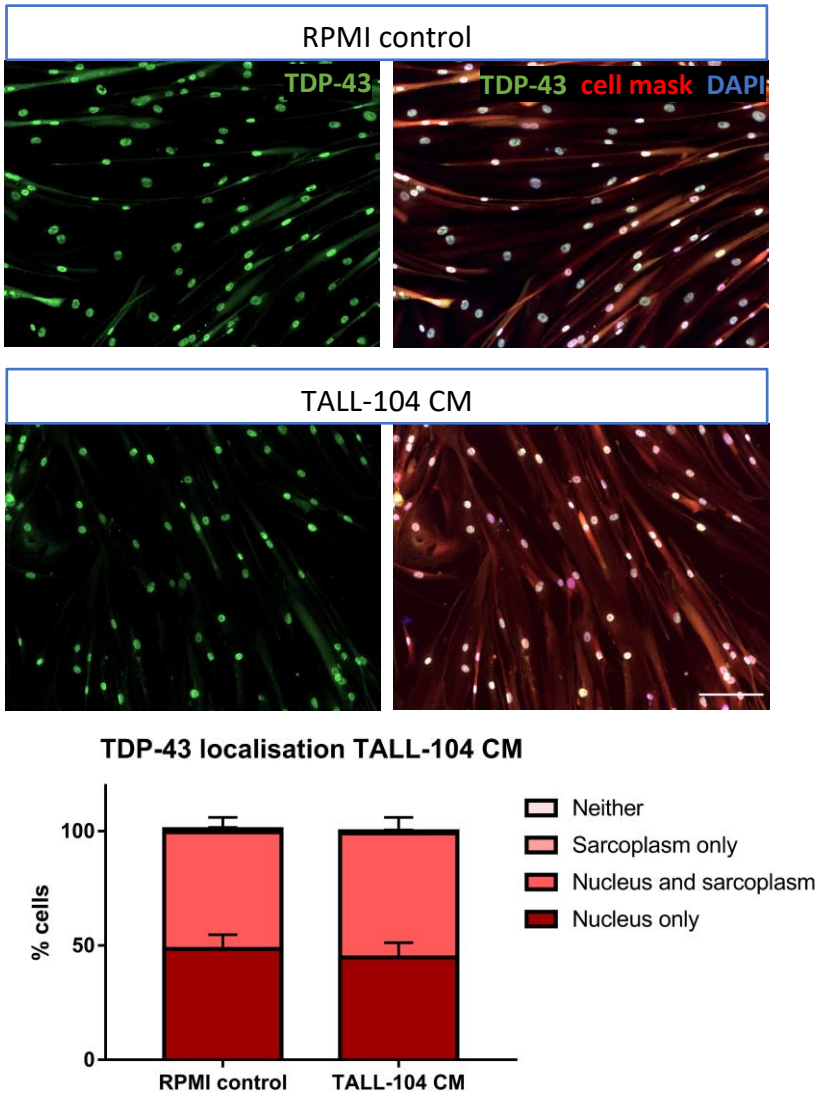

Figure 6.6 TDP-43 subcellular localisation was not affected by TALL-104 conditioned medium. Representative images of TDP-43 localisation with RPMI control or TALL-104 conditioned media (CM). Scale bar = 100 µm. There was no difference between RPMI control and TALL-104 conditioned media (CM) for subcellular localisation of TDP-43. Two-way ANOVA p = 0.906, n = 5 myogenic donors.

6.3.6 TALL-104 coculture was cytotoxic to myotubes

As well as conditioned medium from cytotoxic immune cells, direct coculture was investigated. To examine if direct coculture with TALL-104 cells was cytotoxic to myotubes, LDH release was measured from cocultures at different E:T (effector to target) ratios after 4, 24, and 48 hours. The E:T ratios used were 0.5:1, 1:1, 2.5:1, and 5:1. In cocultures, large areas of floating debris surrounded by TALL-104 cells were observed. Myotubes that remained attached to the surface appeared thinner than those in the control condition (Figure 6.7 A). At 4 hours, only the highest E:T ratio of 5:1 showed a significant increase in cytotoxicity compared to myotubes cultured with IL-2 control (Figure 6.7 B). By 24 hours, all E:T ratios showed increased cytotoxicity of myotubes compared to control, which was also true for 48 hours co-culture (Figure 6.7 C,D). At 24 hours, the mean percentage cytotoxicity was 13 ± 2 % in the control, 54 ± 3 % for 0.5:1, 69 ± 3 % 1:1, 75 ± 9 % 2.5:1, and 94 ± 9 % 5:1. When comparing cytotoxicity over time, all E:T ratios showed higher cytotoxicity at 24 hours compared to 4 hours, whereas only 5:1 ratio showed increased cytotoxicity from 24 hours to 48 hours, suggesting most cytotoxic effects occur between 4 and 24 hours (Figure 6.7 E).

6.3.7 Coculturing TALL-104 with myotubes lead to increased IFNγ and TNFα secretion from TALL-104 at higher E:T ratio

To examine whether coculturing TALL-104 cells with myotubes affected activation of TALL-104 cells, ELISA was used to measure secreted levels of IFNγ and TNFα in the culture medium. IFNγ and TNFα levels were measured after 24 hours TALL-104-myotube coculture. This was compared to TALL-104 cells cultured in myotube medium without myotubes as a negative control, where IFNγ and TNFα were not detected above 1 pg/mL. There was higher IFNγ and TNFα secretion at 2.5:1 and 5:1 compared to negative control TALL-104, but not at 0.5:1 and 1:1 (Figure 6.8 A,C). Furthermore, there was higher IFNγ and TNFα secretion at 5:1 compared to either 1:1 and 0.5:1 E:T ratio, and higher secretion of both cytokines at 2.5:1 than 0.5:1. The median IFNγ release was 7 ± 16, 29 ± 18, 91 ± 99, and 171 ± 119 pg/mL for 0.5:1, 1:1, 2.5:1, and 5:1

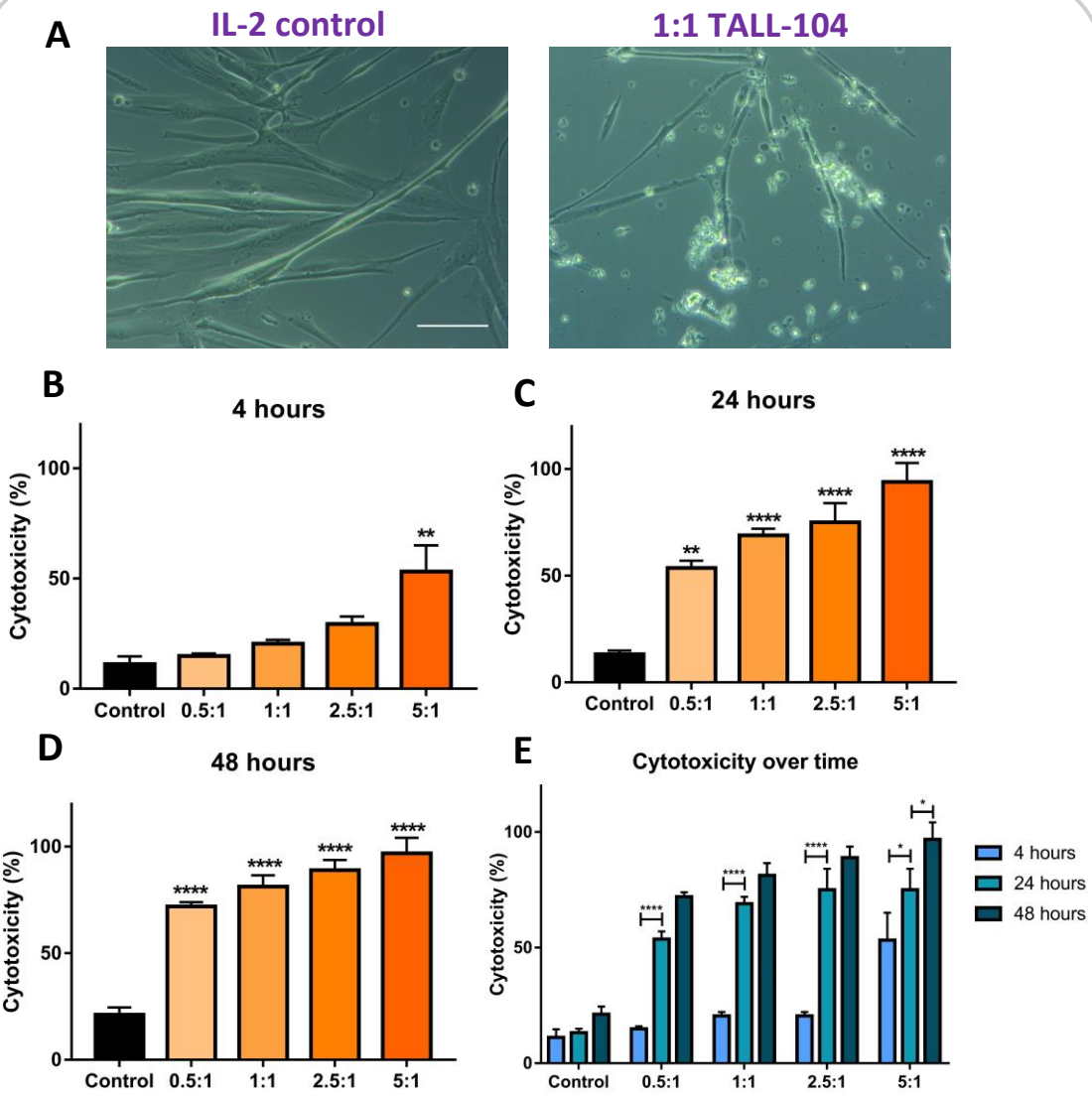

Figure 6.7 TALL-104 coculture was cytotoxic to myotubes. (A) Phase contrast images of myotubes under IL-2 control or 1:1 TALL-104 effector to target (E:T) ratio after 24 hours. Fewer myotubes were observed with coculture, and remaining myotubes appeared thinner. Scale bar = 100 µm. (B-D) Cytotoxicity of different E:T ratios compared to IL-2 control. (B) At 4 hours of coculture, there was higher cytotoxicity in the 5:1 E:T condition compared to control ($p = 0.0005$), but not for any other E:T ratio. (C) At 24 hours there was higher cytotoxicity for 0.5:1, 1:1, 2.5:1, and 5:1 compared to control ($p = 0.001$ 0.5:1, $p = 0.0001$ all other comparisons). (D) At 48 hours, there was higher cytotoxicity for 0.5:1, 1:1, 2.5:1, and 5:1 compared to control ($p = 0.0001$ for all comparisons). (E) For each E:T ratio, comparison of cytotoxicity between timepoints. There was no difference in cytotoxicity over time in the control group. Cytotoxicity was higher at 24 hours than 4 hours for 0.5:1, 1:1, 2.5:1 ($p < 0.0001$), and 5:1 ($p = 0.0223$). Cytotoxicity was also higher at 48 hours than 24 hours for 5:1 ($p = 0.0226$). For all E:T ratios 48 hours had higher cytotoxicity than 4 hours. (B-D) One-way ANOVA with Dunnett's multiple comparisons. (E) Two-way ANOVA with Tukey's multiple comparisons. n = 4 myogenic donors.

respectively. The median TNFα release was 0 ± 20, 18 ± 14, 53 ± 28, and 78 ± 50 pg/mL for 0.5:1, 1:1, 2.5:1, 5:1 respectively. Figure 6.8 B and D show the same results as Figure 6.8 A and C as a linear regression. This shows linearity of IFNγ (r^2 = 0.9245) and TNFα (r^2 = 0.9335) secretion with increasing E:T ratio when considering only the

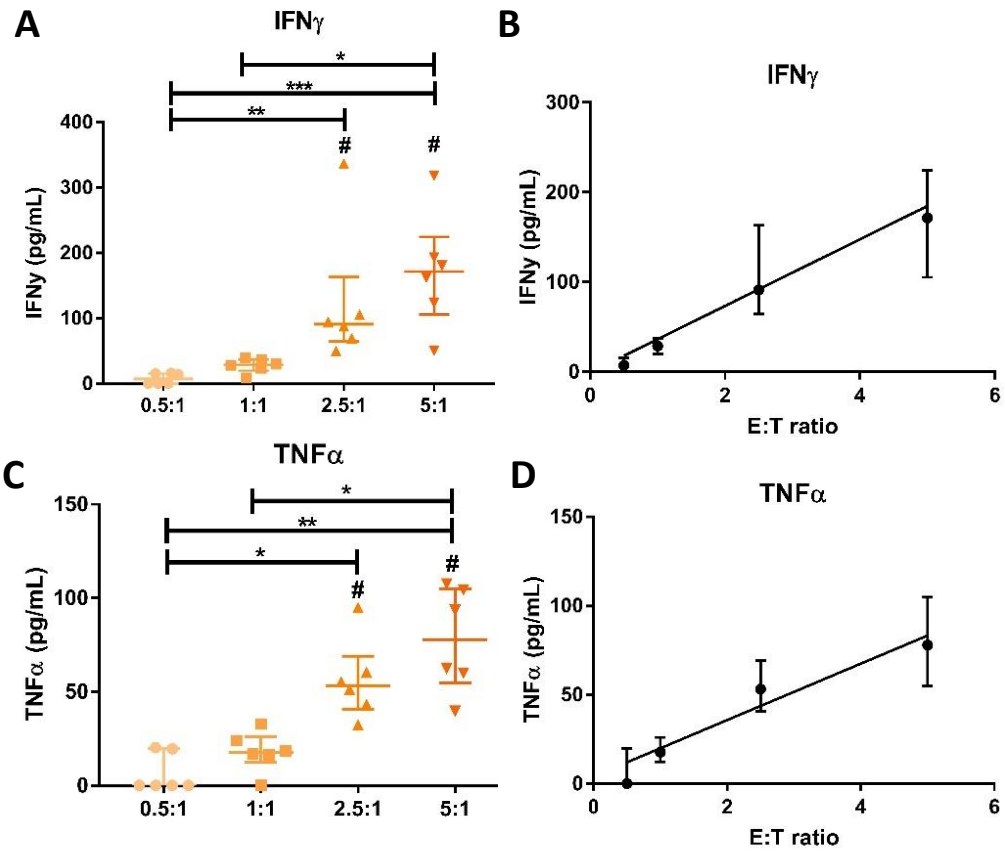

Figure 6.8 IFNγ and TNFα secretion from TALL-104 cells co-cultured with myotubes. Different effector (TALL-104):target (myotube) ratios were used. (A) IFNγ secretion was higher when cocultured with myotubes than with TALL-104 alone for 2.5:1 and 5:1 ratios (#, p = 0.0196 2.5:1, p = 0.0009 5:1. Two-way ANOVA with Sidak multiple comparisons). No IFNγ was detected from any ratio of TALL-104 cultured alone (data not shown). IFNγ secretion was higher in 5:1 vs 0.5:1 (p = 0.0006), 5:1 vs 1:1 (p = 0.0475), and 2.5:1 vs 0.5:1 (p = 0.0075). Kruskal-Wallis test with Dunn's multiple comparisons. (B) The increase in IFNγ with increasing E:T ratio was mostly linear (r^2 = 0.9245). (C) TNFα secretion was higher when cocultured with myotubes than with TALL-104 alone for 2.5:1 and 5:1 ratios (#, p = 0.0001 2.5:1, p < 0.0001 5:1. Two-way ANOVA with Sidak multiple comparisons). TNFα secretion was higher for 5:1 than 0.5:1 (p = 0.0016), 5:1 vs 1:1 (p = 0.0189), and 2.5:1 vs 0.5:1 p = 0.0246). Kruskal-Wallis test with Dunn's multiple comparisons. (D) The increase in TNFα with increasing E:T ratio was mostly linear (r^2 = 0.9335). n = 6 myogenic donors. Median ± IQR.

median concentration value for each condition.

6.3.8 TALL-104 cells attached to and invaded myotubes

TDP-43 and p62 immunofluorescent staining was conducted in myotube TALL-104 cocultures. In some immunofluorescent images of cocultures, small rounded cells with a high nuclear to cytoplasm ratio were observed which were likely TALL-104 cells. TALL-104 cells were observed attaching to myotubes (Figure 6.9 A). They were also seen in the sarcoplasm of myotubes, with a halo of darkness surrounding them, which may show localised myotube destruction (Figure 6.9 B). Furthermore, TDP-43 and p62 were visible in TALL-104 cells. TDP-43 was observed in the nucleus of TALL-104 cells, as well as strongly staining the edges of the cells. p62 was less pronounced but was also localised towards the periphery of the cell cytoplasm.

6.3.9 TALL-104 coculture did not affect p62 puncta size or frequency

To examine if direct coculture with cytotoxic immune cells caused p62 aggregation in myotubes, immunofluorescent microscopy was used to quantify size and frequency of p62 puncta. 24 hours coculture with 1:1 E:T ratio of TALL-104 cells was used. Figure 6.10 shows immunofluorescent images of p62 in myotubes. p62 was mostly located in the sarcoplasm with variable sized puncta and some areas of diffuse staining, occasional p62 puncta in the nucleus could also be observed. p62 puncta frequency relative to cell area was not affected by TALL-104 coculture compared to IL-2 control (Figure 6.11 A). There was also no difference in p62 puncta size between IL-2 control and TALL-104 coculture (Figure 6.11 B) with mean p62 puncta size of 0.27 ± 0.02 μm^2 in the IL-2 control group.

6.3.10 TDP-43 aggregates were less likely in TALL-104 cocultured myotubes, but TDP-43 aggregate size or frequency was not affected

To assess if coculturing TALL-104 cells with myotubes affected TDP-43 sarcoplasmic aggregation in myotubes, immunofluorescent image analysis was used to quantify TDP-43 aggregate size and frequency. Figure 6.10 shows TDP-43 staining in myotubes. TDP-43 was diffusely located throughout the cytoplasm. Some myotubes showed

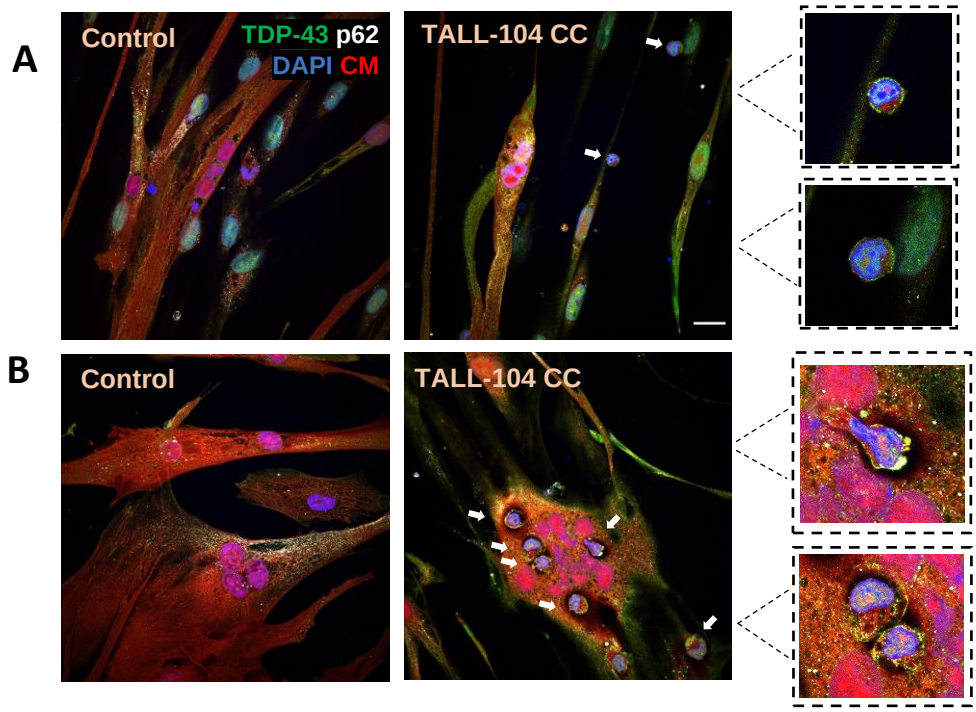

Figure 6.9 Attachment and invasion of myotubes by TALL-104 cells. (A) TALL-104 cells attached to myotubes (B) TALL-104 cells invading the sarcoplasm of myotubes, some showing morphological changes (top inset). Scale bar = 20 µm. White arrows indicate TALL-104 cells. CM – cell mask, CC - coculture.

nuclear TDP-43 staining whereas others showed an absence of TDP-43 in the nucleus. The frequency of sarcoplasmic TDP-43 aggregates relative to myotube area was not different between myotubes cultured with IL-2 control or TALL-104 cells (Figure 6.12 A). There was also no difference in TDP-43 aggregate size (Figure 6.12 B) or co-localisation with p62 puncta (Figure 6.12 C) between control and TALL-104 coculture. The median TDP-43 aggregate size in the IL-2 control group was 0.65 ± 0.45 µm^2. TDP-43 aggregates were not observed in all images. There was a lower frequency of images containing any TDP-43 aggregates in the TALL-104 coculture group than the IL-2 control group (Fisher's exact test p = 0.0018 Figure 6.12 D). There was no difference in the median number of cells imaged in each condition (p = 0.651, 3 ± 2 vs 3 ± 3 for IL-2 control and TALL-104 coculture respectively).

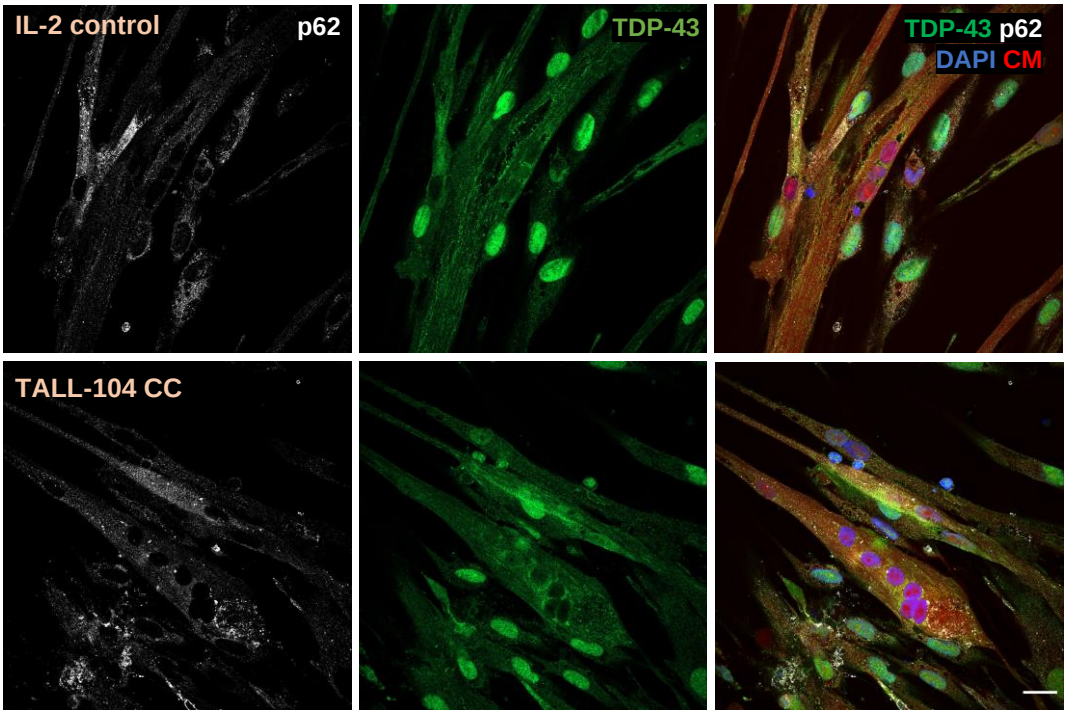

Figure 6.10 p62 and TDP-43 in myotubes treated with IL-2 control or TALL-104 coculture. Representative images of TDP-43 and p62 in IL-2 control or TALL-104 coculture (CC) treated myotubes. CM- cell mask. Scale bar = 20 µm.

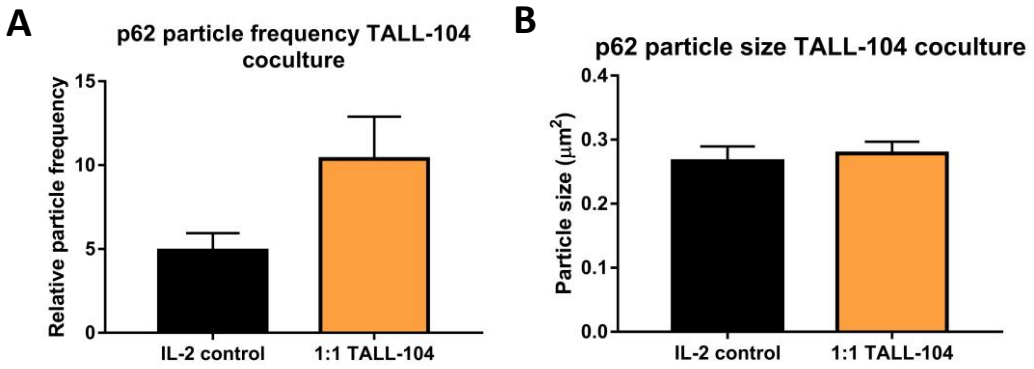

Figure 6.11 Coculture of TALL-104 cells with myotubes did not affect p62 particle size or frequency. (A) There was no difference in p62 puncta frequency between IL-2 control and TALL-104 coculture at 1:1 effector to target ratio (p = 0.0796). (B) There was no difference in p62 puncta size between IL-2 control and TALL-104 coculture (p = 0.697). Student's T-test, n = 5 myogenic donors.

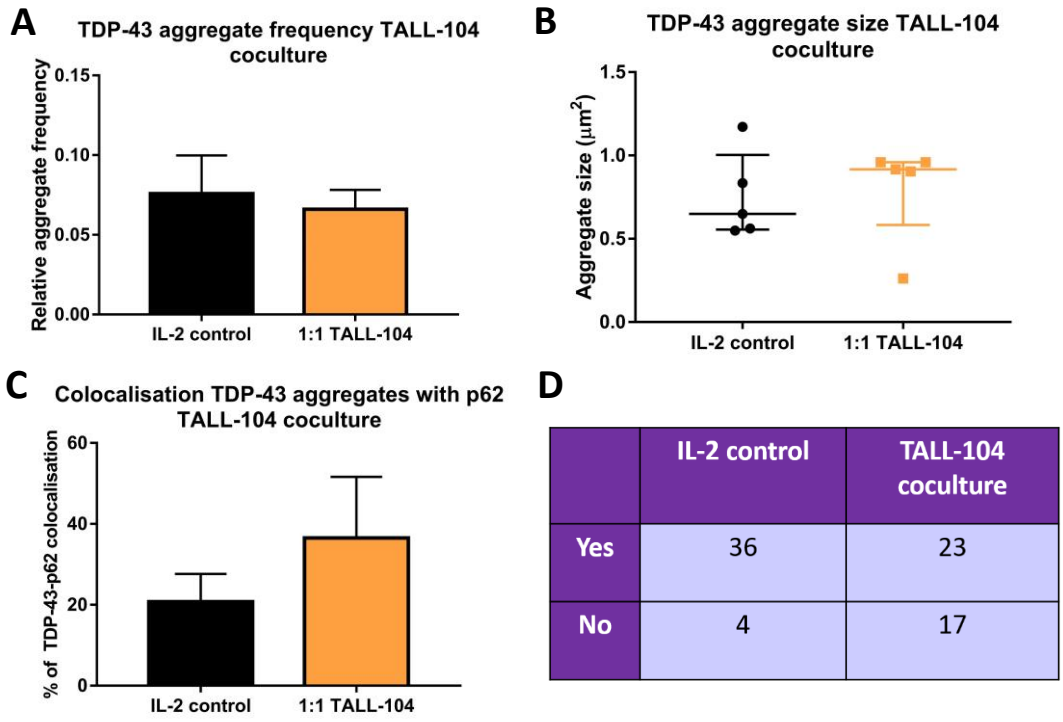

	IL-2 control	TALL-104 coculture
Yes	36	23
No	4	17

Figure 6.12 TDP-43 aggregate frequency or size was not affected by TALL-104 coculture. (A) There was no difference between IL-2 control and TALL-104 co-culture for TDP-43 aggregate frequency relative to cell area (p = 0.728), (B) aggregate size (p = 0.548), (C) or colocalisation with p62 puncta (p = 0.369). (D) There was a higher frequency of images containing TDP-43 aggregates in the IL-2 control group compared to TALL-104 coculture (Fisher's exact test p = 0.0018, eight images (with two z-stacks) for each of 5 donors). Student's T-test or Mann-Whitney U test. n = 5 myogenic donors.

6.3.11 TDP-43 subcellular localisation was affected by TALL-104 coculture

The localisation of TDP-43 within cells was assessed when cells were cultured with 1:1 E:T ratio of TALL-104 cells for 24 hours and compared to myotubes treated with IL-2-containing media for the same length of time. There was a significant difference in the interaction between TDP-43 localisation category and treatment condition, showing TDP-43 localisation was altered with TALL-104 coculture (two-way ANOVA) (Figure 6.13). The only subcellular localisation that showed a difference between IL-2 control and TALL-104 coculture with Tukey's post-hoc testing was nucleus only, showing fewer cells with TDP-43 only in the nucleus in TALL-104 coculture compared to IL-2 control. In the immunofluorescent images, in the TALL-104 coculture group there appeared more

cells with weak TDP-43 sarcoplasmic (and nuclear) expression. There was also a significant difference in the localisation of TDP-43 between the subcellular compartments (two-way ANOVA $p < 0.0001$). The localisation with the largest percentage of TDP-43 regardless of treatment condition was nucleus and sarcoplasm with mean 83 ± 4 % (Tukey's post-hoc test).

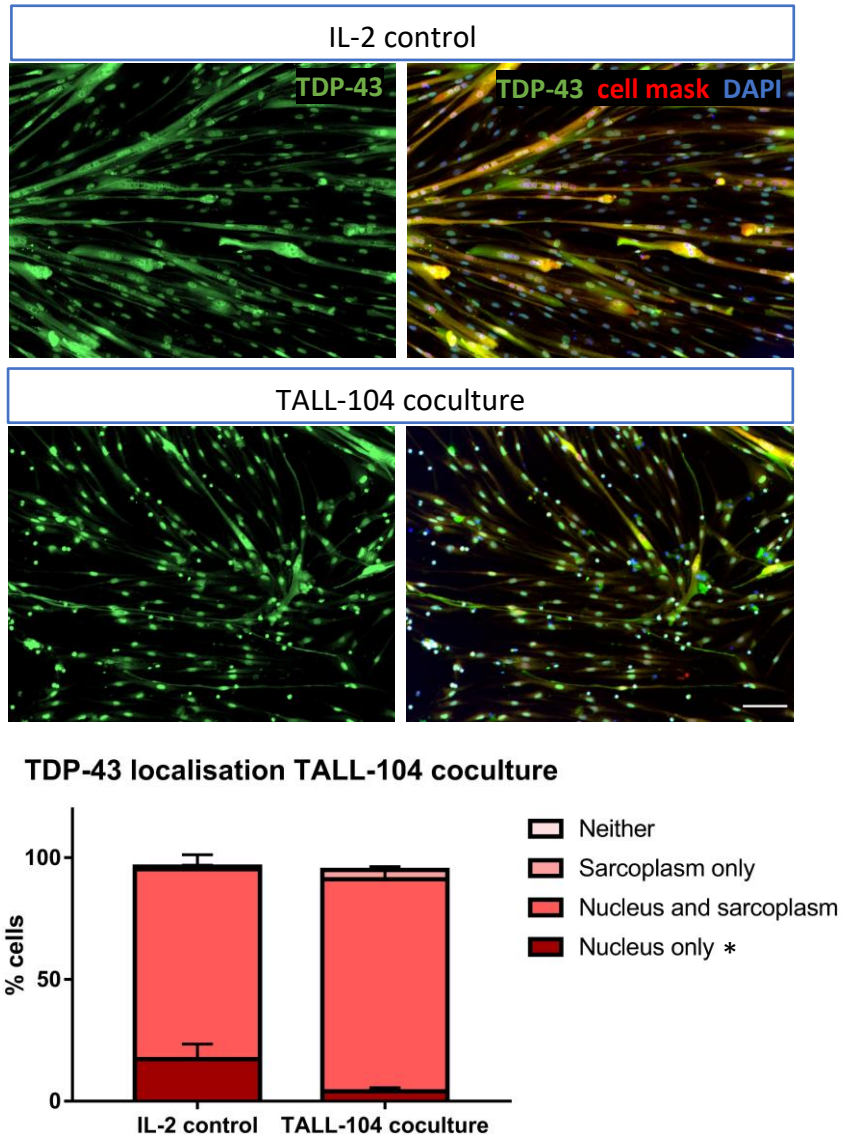

Figure 6.13 TDP-43 subcellular localisation was affected by TALL-104 coculture.
Representative images of TDP-43 localisation with IL-2 control and TALL-104 coculture. Scale bar = 100 µm. There was a difference in the distribution of TDP-43 between the subcellular compartments between the two treatment conditions (two-way ANOVA interaction factor p = 0.02). There was a decrease in nuclear only expression of TDP-43 with TALL-104 coculture compared to IL-2 control (p = 0.0401), but there was no difference for the nuclei and sarcoplasm (p = 0.241), sarcoplasm only (p = 0.974), or neither (p > 0.999) groups. Two-way ANOVA with Sidak's multiple comparisons. n = 5 myogenic donors.

6.4 Discussion

The aim of this chapter was to investigate the effect of cytotoxic immune cells on sIBM-like features of TDP-43 and p62 aggregation, as well as TDP-43 localisation. The cytotoxic cell line TALL-104 has features of both CD8+ T cells and natural killer cells and is capable of inducing cell-mediated cytotoxicity through release of perforins and granzymes and induction of extrinsic apoptotic pathways. The effect of secreted factors from cytotoxic immune cells via conditioned medium transfer as well as the effect of direct coculture with TALL-104 cells was tested. Initially, the cytotoxicity of both CM and co-culture was tested. IL-2-containing medium was used with or without RPMI for CM and coculture respectively in the control conditions. IL-2 is a cytokine whose main roles are within the immune system (447), therefore it was not expected that the inclusion of IL-2 in the controls would have any detrimental effect on myogenic cells. IL-2 has been found to reversibly inhibit sodium influx upon 1 Hz electrical stimulation in human muscle cells (448, 449), but this is unlikely to affect experiments in this chapter. Here, it was found that IL-2-containing medium was not cytotoxic to myotubes.

6.4.1 TALL-104 cytotoxicity and activity with myotubes

It was expected that TALL-104 coculture with myotubes would not be cytotoxic as there should not be any epitopes expressed by myogenic cells that trigger TALL-104 cytotoxic effects. Furthermore, it has previously been shown that TALL-104 cells spare normal cells whilst targeting tumourigenic cells (433-436). Therefore, the overwhelming cytotoxicity here was unexpected. The activation of TALL-104 cells is MHC-independent, instead relying on combined inhibitory and activation signals from natural killer cell receptors (431). Previously, it has been shown that PBMCs containing natural killer cells target autologous skeletal muscle cultures from healthy patients. This cytotoxicity was caused by PBMCs depleted of macrophages and expressing CD16 (expressed on NK cells, neutrophils, and macrophages (450-452)), as neutralising antibodies against CD16 prevented cytotoxicity. However, the mechanism causing natural killer cell mediated auto-cytotoxicity was not tested. On the other hand,

autologous myotubes were not targeted or killed by isolated CD8 cytotoxic T cells (453). This suggests the culture of myogenic cells may reveal epitopes or receptor expression in myotubes that is usually hidden or absent *in vivo.* Contrary to this, another study examining co-culture of rhabdomyosarcoma cells with the natural killer cell line NK-92 did not observe high cytotoxicity, suggesting a lack of natural killer-mediated muscle cell lysis (454). Thus, there are contradicting effects of NK-mediated lysis of cultured myotubes. The reasons why TALL-104 cells were reactive to myogenic cultures here remains unclear. Potentially, myogenic cells express a high amount of activating ligands or a low amount of inhibitory ligands that bind receptors on TALL-104 cells, causing them to become reactive. Only coculture with myogenic cells was used here. The specificity of TALL-104 cells could be tested by co-culturing them with other normal cells that have previously not shown reactivity, such as PBMCs (436). The lack of reactivity of TALL-104 cells to normal cells such as allogeneic mixed population normal brain cells (435) indicates that cytotoxicity against myotubes is unlikely to be due to HLA-mismatching or anti-self recognition.

Previous studies have investigated *in vitro* myositis models of CD8 T cell mediated myotube lysis. Coculture of antigen-specific CD8+ T cells and myotubes has been conducted by Kamiya *et al* to model polymyositis, in which C2C12 cells were transduced to express an ovalbumin peptide and MHC I, and cocultured with CD8+ cells from transgenic mice that have ovalbumin-specific TCR expression. Myotubes that were not transduced to express the ovalbumin target experienced no cytotoxicity when cocultured with the CD8+ T cells. However, myotubes expressing ovalbumin died with increasing lysis at increasing densities of CTLs. The CD8+ cells infiltrated into the myotubes, and myotubes that had CTL invasion died quicker than uninvaded myotubes (455). The results from the CD8+ C2C12 coculture supports the notion that TALL-104 cells mediate cytotoxicity in an antigen-independent and NK cell-like manner, as CD8+ cells did not attack normal C2C12 myotubes. This is also an example of a coculture method that could be utilised to study muscle-intrinsic pathological features of sIBM with disease-relevant cell types. It would be interesting to utilise this approach to investigate TDP-43 and p62 pathology and compare it to the TALL-104 coculture here.

The effect of coculturing isolated CD8+ T cells from sIBM with autologous myotubes has previously been investigated. 1 out of 4 sIBM patient's CTLs showed cytotoxicity against autologous myotubes, whereas 3 of 6 polymyositis and 1 of 5 dermatomyositis T cell isolates showed myotube autoreactivity (456). This shows that some sIBM patient CTLs may be primed to react to skeletal muscle antigens, however the majority of sIBM T cells did not detrimentally target autologous myotubes. In a study (457) investigating polymyositis patients only, autologous polymyositis myotubes cultured with CD8+CD28- cells had higher cell death compared to coculture with CD8+CD28+ cells which was mediated through perforin and granzyme B. Myotubes were more susceptible to this cell death than myogenic precursors. Further, CD4+CD28- polymyositis cells were also cytotoxic to autologous myotubes. Lack of the costimulatory CD28 molecule in CD8 cells is associated with a cytotoxic inflammatory phenotype with some resistance to glucocorticoid suppression (457).

Under coculture of TALL-104 with myogenic cells, there was a higher expression of IFNγ and TNFα in the higher E:T ratios of 2.5:1 and 5:1 compared to TALL-104 cells alone. This suggests that direct contact of myotubes with TALL-104 caused activation of TALL-104 cells, which is also shown through their cytotoxicity. Another method of examining TALL-104 activation in the presence of myogenic cells would be to examine their proliferation rate, with a higher proliferation showing activation.

6.4.2 Secreted factors from TALL-104

Conditioned medium from TALL-104 cells did not affect TDP-43 or p62 aggregate size or frequency, showing in these myotubes secreted factors from cytotoxic cells may not trigger this sIBM-like feature. However, there was no detectable secretion of IFNγ or TNFα from TALL-104 when cultured alone. This suggests TALL-104 cells are not activated under basal culture conditions, and therefore conditioned medium from these cells may not accurately reflect the secretory phenotype of invading T cells in sIBM. This is in accordance with previous results showing no detection of TNFα or IFNγ in TALL-104 cells cultured alone (434, 435, 458). However, this is contrary to another study showing TALL-104 cells cultured in the presence of IL-2 secreted IFNγ at 54.7 U/mL and TNFα at 1.8 U/mL (459). The measurement of TALL-104 IFNγ and TNFα here

was conducted in N2 differentiation medium to act as a control for coculture experiments. Potentially, as may be the case with macrophage cytokine secretion (see Figure 5.9 and Section 5.3.7), culture with N2 medium as opposed to RPMI may abrogate cytokine production. Unfortunately, TNFα and IFNγ levels were not quantified from TALL-104 cells cultured in basal TALL-104 medium, therefore it is not known whether conditioned medium contained these cytokines.

To ameliorate the potential lack of cytokines in TALL-104 CM, TALL-104 cells could be activated via addition of compounds such as PMA, thapsigargin, or ionomycin for collection of CM (460, 461). Thapsigargin and ionomycin increase the cytoplasmic concentration of calcium ions, forcing binding of cytotoxic granules with the T cell membrane and release of their contents (460, 462). PMA activates protein kinase C due to its similar structure to diacyl glycerol, the natural ligand of protein kinase C, which is involved in a plethora of T cell activation steps including exocytosis of lytic granules (463).

6.4.3 p62

There was no effect of TALL-104 conditioned medium on p62 puncta size or frequency, suggesting that there was no blockade or activation of selective autophagy. With TALL-104 coculture, there was also no alteration of p62 puncta size or frequency. Therefore, sarcoplasmic aggregation of p62 in human myogenic cells may not be triggered by exposure to TALL-104 cells . During coculture conditions, it is likely that imaged myotubes were experiencing a pro-apoptotic environment as marked by the high cytotoxicity. Autophagy is able to occur concurrently or precede apoptotic cell death (464), however the lack of p62 puncta alterations here may suggest upregulated autophagy accompanied by apoptosis was not occurring. It is also possible that the myotubes observed for TDP-43 and p62 sarcoplasmic aggregation with TALL-104 coculture were not undergoing apoptosis, as they were adhered to the culture surface and few myotubes showed characteristics of apoptosis such as membrane blebbing or nuclear condensation (465), although this was not quantified. Further staining, for example with phosphatidylserine which is present on the membrane of cells undergoing the early stages of apoptosis, would help elucidate the viability of these

cells. To confirm that no changes in p62 were present with coculture or TALL-104 conditioned medium, protein expression of p62 could be investigated. To further assess the involvement of autophagy, expression of LC3 could also be assessed.

6.4.4 A role for cytotoxic immune cells in TDP-43 localisation?

As with the results from other chapters, not all cells or images examined contained TDP-43 aggregates. However, both conditioned medium and coculture affected the likelihood of finding cells containing any TDP-43 sarcoplasmic aggregates within an image, with opposing effects between the two conditions. TALL-104 conditioned medium treatment led to an increased likelihood of TDP-43 aggregates compared to IL-2 control, whilst coculture lead to a decreased likelihood. These results are different to finding a higher frequency of aggregates, but instead reflects a change in the number of cells containing any TDP-43 aggregates. Importantly, for CM or coculture changes in TDP-43 likelihood were not due to a difference in number of cells per image. As there was no accompanying effect on TDP-43 aggregate size for either coculture or conditioned medium, these aggregates may represent a change in a basal role of TDP-43, such as its role in RNA processing in myo-granules (327). This suggests that CM from resting cytotoxic T cells may increase the number of cells that are producing myo-granules. This result also highlights that despite the low detection of inflammatory cytokines in TALL-104 CM, these cells were secreting soluble mediators capable of affecting myogenic cells.

On the other hand, the decrease in myotubes with TALL-104 coculture may represent fewer cells forming myo-granules, potentially as the myogenic cells were in a highly cytotoxic environment that triggers apoptosis. When cells are undergoing apoptosis there is a rapid degradation of mRNA (466), which may be why fewer cells show TDP-43 aggregates as TDP-43 is an RNA binding protein. However, with the current results, it is not possible to know whether any TDP-43 aggregates represent myo-granules. With further investigations it would be interesting to see if under the same treatment conditions mRNA molecules of sarcomeric proteins co-localised with these TDP-43 aggregates which would shed light on the function of these TDP-43 aggregates. TDP-43 is also localised to stress granules in conditions of cellular stress to aid cell survival

(90). To examine if TDP-43 aggregates here are stress granules, the co-localisation of TDP-43 with stress granule-specific markers such as G3BP1 (327) could be undertaken. However, it would be expected that more stress granules would form under TALL-104 coculture conditions due to the high cytotoxicity in this environment.

TALL-104 CM had no effect on TDP-43 localisation, whereas direct coculture resulted in a decrease in cells showing nuclear only TDP-43 expression. However, there was not a significant change in any other subcellular localisation compartment, therefore it is not clear where this TDP-43 localisation had shifted. This also shows that a "mislocalisation" of TDP-43 towards the sarcoplasm away from the nucleus as seen in sIBM and other *in vitro* investigations of sIBM with cytokine treatment was not recapitulated with TALL-104 coculture, as nuclear expression was still observed. There may be a variable effect of TALL-104 targeting towards single nucleated or multinucleated myogenic cells which was not explored here. These results could be further classified for single and multinucleated cells to examine if TDP-43 nuclear expression is differentially affected in these cell types. As Section 3.3.5 shows, there was no effect of differentiation on TDP-43 localisation or difference in myotubes and myoblasts under basal conditions. The decreased frequency of TDP-43 aggregates in images and the decreased nuclear localisation with TALL-104 coculture could be influenced by selection bias where only surviving cells were analysed as dead cells detach from culture surfaces. The remaining myogenic cells may therefore represent a more robust population that are resistant to TALL-104 killing. To help answer if this is the case, TDP-43 localisation and aggregation could be analysed after 4 hours of coculture at 1:1 E:T ratio, which did not show increased cytotoxicity compared to control.

Western blotting for proteins with TALL-104 CM or coculture was not performed. It would be interesting to examine protein levels of TDP-43, p62, and sestrins in TALL-104 CM cultured myotubes, to see if TALL-104 secreted factors can regulate expression of these proteins. Because myotubes underwent cell death with coculture, and the TALL-104 cells were observed to directly interact with the myotubes, this would make any protein measurements difficult in the coculture condition. Under immunofluorescence

TALL-104 cells were visualised with both p62 and TDP-43 antibodies, so Western blotting of these proteins would highlight expression in both myogenic and TALL-104 cells. A potential solution to this problem could involve FACS or MACS sorting of myogenic cells and TALL-104 after coculture, for example with CD3/CD7 for TALL-104 depletion prior to Western blotting.

It is important to note that TALL-104 cells are unlikely to be representative of the CD8+ T cells found infiltrating into sIBM muscle. TALL-104 were chosen due to their proliferative capacity in culture, cytotoxic effects, and commercial availability over other cell sources such as primary CD8+ T cells. However, their mixed CD8+ natural killer cell characteristics and transformed nature mean they are likely to respond differently to healthy or sIBM-derived CD8+ cells. TALL-104 cells are a neoplastic, proliferative cell line whereas sIBM CTLs are highly differentiated and display a senescent-like phenotype. However, TALL-104 are capable of inducing cell-mediated lysis with mechanisms also used by CD8+ T cells. To improve the biological relevance of these experiments, autologous primary human skeletal muscle cells and CD8+ cells from multiple healthy or even sIBM donors could be investigated.

6.4.5 Summary

Secreted factors from unstimulated TALL-104 cells did not influence TDP-43 or p62 sarcoplasmic aggregation in myogenic cells. TALL-104 cocultured with myogenic cells at higher E:T ratios showed high cytokine secretion, and even at low E:T ratios were unexpectedly cytotoxic to myogenic cells. Coculture of myogenic cells with TALL-104 cells did not affect TDP-43 or p62 aggregate size, however there was a decrease in nuclear only TDP-43 staining with coculture. Overall, TALL-104 secreted factors or coculture failed to illicit the sIBM-like phenotype of sarcoplasmic inclusion bodies containing TDP-43 and p62, but did trigger changes in TDP-43 localisation.

Chapter 7: Myobundle culture with cytokine treatment or TALL-104 coculture

Chapter 7. Myobundle culture with cytokine treatment or TALL-104 coculture

7.1 Introduction

7.1.1 3D models of skeletal muscle

Multiple 3D culture models of skeletal muscle have been created. In the human muscle, myofibres are surrounded by the basal lamina that is rich in collagen IV and laminin, which is further surrounded by the perimysium and epimysium that are rich in collagen I (467). 3D culture models of skeletal muscle have been extensively reviewed (468-471), and studies highlighting some of the most commonly used methods are included here. Many 3D skeletal muscle cultures use hydrogel-based culture. Originally, collagen I was one of the most widely used extracellular matrix proteins for this purpose. However, collagen I is a relatively stiff material compared to native muscle basal lamina, which affects muscle cell differentiation and contractile force generation (467). Alignment of myotubes within 3D skeletal muscle cultures is important for biological relevance and force generation.

One method for generating 3D skeletal muscle cultures is utilising micropatterned surfaces to aid alignment of myotubes. Laminin-coated channels inside a silicone mould with stiffness-tuned hydrogels were utilised to create 3D muscle constructs of C2C12 cells and primary human muscle cells (472). Myofiber sheets have been created on thermoresponsive polymer micropatterned substrates. By reducing the temperature of cultures on the thermoresponsive substrate, whole intact sheets of muscle cells could be harvested (473). Methacrylated gelatine hydrogels have been patterned with microgrooves for seeding of C2C12 cells to create engineered myofibres (474). This has further been expanded by coculturing C2C12 cells with PC12 neuronal cells with electrical pulse stimulation (475). Other micropatterned surfaces have been used including parallel lanes of regularly spaced rectangles (476).

Other 3D culture techniques are more suitable to generate skeletal muscle constructs for therapeutic use. This includes the use of 3D printing and electrospinning (477). Electrospinning is a technique for producing nanofibers from a biomimetic scaffold solution via extrusion under high voltage (471). Electrospinning has been used to create nanofibre yarn cores and hydrogel shells which allowed for C2C12 alignment amenable to long term culture (478). Electrospun fibrin hydrogels have been used as a scaffold for C2C12 culture for regeneration in a volumetric muscle loss model (479). Electrospinning can also be used with cell-containing gels, with cells undergoing electrospin extrusion. Cell-laden electrospinning has the benefit of the cells being incorporated into the fibres as opposed to seeding on top. This approach was utilised for C2C12 cells in an alginate/poly(ethylene) oxide fibre (480). 3D bioprinting has been used to generate skeletal muscle constructs consisting of human muscle progenitor cells in hydrogel with supporting polymer microchannels formed from poly(ε-caprolactone). These constructed were implanted into rats with defective muscles formed by excision of original muscle mass. Implantation of the 3D bioprinted muscle constructs restored 82 % of normal muscle force (481). 3D bioprinting has been used with C2C12 cell-laden collagen-based bioink combined with uniaxially aligned microfibrous bundles coated with collagen (482).

Many 3D myogenic culture techniques utilise cells cultured in hydrogel with the use of tether points that act like artificial tendons. Tethering the hydrogel allows for anisotropic alignment and structural organisation of myotubes, as well as contraction of the construct through its width. Flexible posts such of those made of silicone have been utilised in 3D muscle cultures, and measuring the deformation of the culture posts is used to examine force generation by muscle cultures. The use of flexible posts has been used in a 96 well format to create a high throughput platform for generating 3D skeletal muscle cultures for drug testing, called human skeletal muscle microtissue array device to investigate force or MyoTACTIC. Using this system, it was possible to monitor force generated *in situ* during culture via deflection of the micro-posts, without the need for a sacrificial end-point force measurement (483). Similar methods in 96 well format using deflectable posts have been created with mouse cells, using image-based motion detection to measure force (484). Another use of tethering posts

to generate 3D muscle cultures utilised a method previously created for culture of engineered heart tissue in which cells are seeded inside fibrin and Matrigel between flexible silicone posts (485). Using this method, it was possible to culture human induced pluripotent stem cells (iPSC) from patients with muscular dystrophies (486). Other flexible post-based methods have been developed with increased complexity, such as with integration into microfluidic devices with iPSC-derived motor neurone spheroids for ALS modelling (487). Larger 6 well formats have also been employed (488).

Myobundles are a hydrogel-based tethered culture system developed by the Bursac group (489). They consist of myogenic cultures suspended in a mix of Matrigel and fibrinogen, tethered at their longitudinal ends for anisotropic alignment of myotubes. The myobundles are seeded in a silicone mould in which a frame made of spunbond non-woven nylon (Cerex®) is placed (see Figure 7.1 F). The quantities of cells, Matrigel and fibrinogen concentrations were previously optimised for the measurement of force generation by the myobundles (490). The original myobundle design was developed using halved silicone tubing and Velcro® anchors (490) for rat cells, with nylon anchors and custom-made silicone moulds being used at a later stage for culture of human muscle cells (489). The myobundle design has also been utilised by other groups. For example, muscle cells cultured with the addition of stem cell derived motor neurones that self-assembled into neuromuscular junctions (491), and to evaluate the release of skeletal muscle injury biomarkers (492). The myobundles cultures were the first 3D cell culture method that successfully showed force generation using human cells, whereas previous models only showed success with rodent cells (489). Due to their ability to be used with human cells, the relative lack of specialist equipment, the fact they have previously been characterised in depth, and their large size amenable to force testing, the Velcro®/Cerex myobundle design was chosen as a functional 3D muscle cell culture model in this chapter.

sIBM-relevant treatments have been investigated in myobundles. The Bursac group have previously used IFNγ treatment of myobundles to investigate the effect of this cytokine on muscle wasting, and the restorative effect of electrical stimulation as an

exercise-like treatment throughout culture (159). This showed that treatment of myobundles with IFNγ (20 ng/mL) for seven days resulted in decreased specific force generation. Furthermore, IFNγ caused increased half relaxation time and time to peak tension showing slower force kinetics and potential fatigue, and myotubes with disorganised sarcomeric alpha actinin showing poor sarcomere spacing. The effects of TNFα on myobundles has also been studied. This showed that twitch and tetanic force were decreased with high concentrations of TNFα. Half relaxation time was also increased, but time to peak twitch was not affected when myobundles were stimulated 5 days after differentiation. It was suggested the decrease in force with TNFα could be due to inhibition of myogenesis or decreased sensitivity to calcium (493).

7.1.2 Aims and hypotheses

The overarching aim of this chapter was to investigate whether inflammation is capable of causing muscle weakness. More specifically, this chapter aimed to investigate whether IL-1β and/or IFNγ, or separately TALL-104 co-culture affects the amount of active force generated by myobundles with electrical stimulation. As secondary aims, this chapter investigated whether cytokine or TALL-104 treatments affect force kinetics, markers of atrophy through cross sectional or myotube area changes, or sarcomere organisation.

Based on previously published work with IFNγ treatment of myobundles described above, it is hypothesised that treatment with IFNγ will cause decreased active force. Furthermore, it is hypothesised that IFNγ will decrease myotube diameter, decrease myotube cross striation frequency, and increase half relaxation time. For treatment with IL-1β or IL-1β+IFNγ, it is hypothesised that there will be an effect of treatment on active force, myotube diameter, cross striation frequency, and force kinetics.

Based on the high cytotoxicity of TALL-104 coculture to myotubes described in Chapter 6, it is hypothesised that TALL-104 coculture will cause decreased active force generation of myobundles. It is hypothesised that there will be an effect of TALL-104

coculture on myobundle force kinetics, myotube or cross sectional area, and cross striation frequency.

7.2 Methods

7.2.1 CAD positive moulds

Autodesk fusion 360 was used to design positive moulds for fabrication of indented silicone moulds (Figure 7.1 A,D). Two moulds were designed, termed “Velcro” and “Cerex”. Both designs consisted of a rectangular base of dimensions: length 23.7 mm, width 19.5 mm, and depth 2 mm. Both designs also contained an inner channel protruding from the base with dimensions: length 12 mm, width 2.5 mm, and depth 2.52 mm. For the Velcro® design, two shorter protruding side channels positioned perpendicular to the inner channel above and below had dimensions of length 6.23 mm, width 2.5 mm, and depth 2.52 mm. For the Cerex design, a rectangular outer channel positioned surrounding the inner channel was used so that the central space encompassed by the outer channel (and containing the inner channel) was a 13 mm square. The rectangular outer channel has apical/basal width of 2.5 mm and lateral widths of 2 mm, and depth 2.52 mm (Figure 7.1). Positive moulds were printed by B.Made (UCL School of Architecture) using VeroClear with glossy finish on the protruding face design.

7.2.2 Generation of silicone moulds for myobundle culture

The 3D-printed positive moulds were used to generate reusable silicone moulds for myobundle culture. The positive mould faces were rubbed with a light layer of warmed petroleum jelly (Vaseline®, Unilever) to aid removal and to prevent curing difficulties caused by the 3D printed material. The positive moulds were placed face up in a 6 cm dish. SYLGARD™ 184 silicone elastomer kit (polydimethyl siloxane, PDMS from Dow, USA) was used, thoroughly mixing 9 parts elastomer base with 1 part curing agent. The mix was left at room temperature without vacuum in a shallow dish for 30 minutes to degas, with any large bubbles popped with a needle. 4 mL of elastomer mix was added to the face-up positive moulds using a 5 mL syringe, avoiding adding the mix directly to the mould face. After another 30 minutes to 1 hour additional degassing without vacuum, the silicone was cured at 60 °C overnight. After curing, the positive moulds were removed from the silicone, and negative silicone moulds were checked for

deformities with imperfect negative silicone moulds discarded. On the bottom of the silicone moulds, a scalpel was used to remove any raised corners to provide a flat base. For some negative silicone moulds with a thick base, the corners of the top of the mould were cut to reduce surface tension during culture and allow media to enter the mould.

7.2.3 Preparation of Velcro® anchors and Cerex® frames

Velcro® anchors were hand-cut to 5 mm length with width cut to 1 row of Velcro® hooks. Nylon spunbond fabric with weight 68 grams/cm^2 (Cerex®, product code 23200) was a kind sample from the manufacturer (Cerex Advanced Fabrics Inc, USA), and was hand-cut using a rounded scalpel blade into frames, with inner square diameter 13 mm, apical/basal widths of 1.5 mm, and lateral widths of 1 mm.

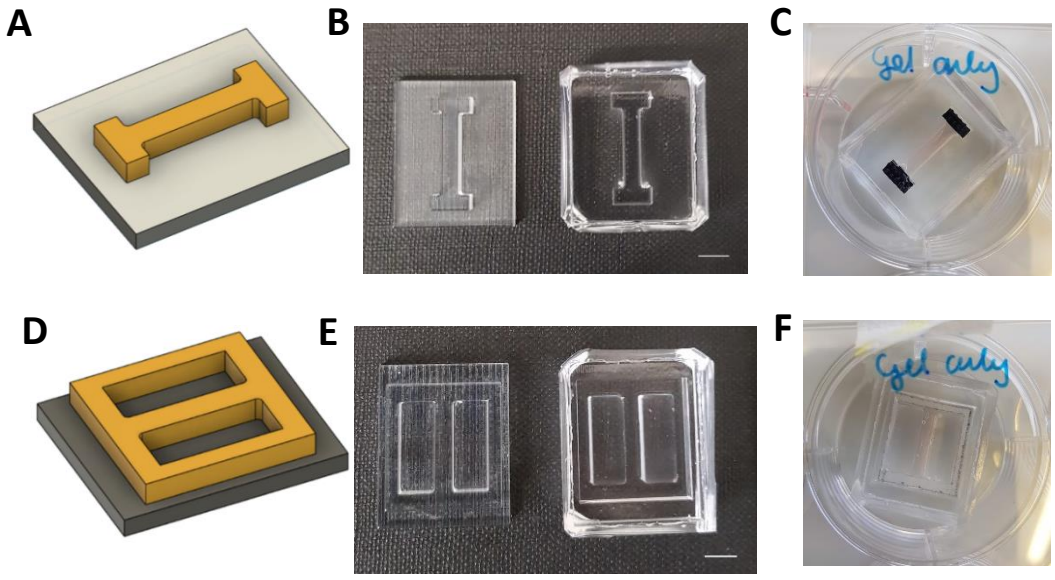

Figure 7.1 Design and fabrication of negative and positive Velcro and Cerex myobundle moulds. Computer-aided design software was used to create positive Velcro (A) or Cerex (D) moulds. (B,E) 3D-printed plastic positive moulds (left) were used to create an impression in polydimethyl silaxane (PDMS) (right) to form negative moulds for cell culture. Scale bar = 5 mm. (C, F) Demonstration of gel without cells in central channel anchored to Velcro® pieces (black,D) or Cerex° frame (white square, F) inside a 6 well plate.

7.2.4 Processing of silicone moulds and anchors/frames for cell culture

To prevent excessive spreading of hydrogel mixture along the Cerex® frame, wax dots were drawn with an ImmEdge® barrier pen (Vector Laboratories, USA) either side of the inner channel positioning. Velcro® anchors, Cerex® frames, and silicone culture moulds were sterilised in 70 % ethanol for at least 30 minutes, after which frames and anchors were washed with PBS then air-dried. Silicone moulds were coated with 0.2 %, 0.5 %, or 1 % w/v Pluronic® F127 (Sigma Aldrich, UK) in distilled water for 1 hour to minimise myobundle attachment to PDMS, after which moulds were rinsed with PBS and left to air-dry. Once anchors/frames and silicone moulds were dry, the Velcro® anchors or Cerex® frames were placed in the appropriate channels in the silicone mould.

7.2.5 Myobundle preparation and culture

Myobundles were prepared following a previously published method (489). Bovine thrombin (T7513 Sigma Aldrich, UK) stock solution at 50 U/mL was made in 0.1 % w/v BSA in PBS. Bovine fibrinogen (F8630 Sigma Aldrich, UK) stock solution at 20 mg/mL was made in PBS. Aliquots of thrombin and fibrinogen stock were stored at –20 ° C.

After typsinising cells following methods described in Section 2.1, myobundles were prepared on ice. 1,725,000 myogenic cells were resuspended in 39.1 µL low glucose DMEM, to which 4.6 µL thrombin stock and additional 25.3 µL low glucose DMEM were added. In a separate 0.5 mL microcentrifuge tube, 23 µL Matrigel was mixed with 23 µL fibrinogen. The contents of the two separate tubes were mixed initiating gelation and 92 µL mixture was added to the inner channel of the PDMS mould with Velcro anchors or Cerex frames placed inside. The final cell number in the myobundle was 1,380,000. The cell mixture was allowed to set at 37 °C for 30 minutes before addition of myobundle growth medium (F-10, 20 % FBS, 1 % penicillin-streptomycin, 1 % L-glutamine, 1 µM dexamethasone, and 1.5 mg/mL aminocaproic acid (Sigma Aldrich, UK A2504 in distilled water).

Myobundles were maintained in myobundle growth medium at 37 °C 5 % CO_2 for 48 hours before switching to myobundle differentiation medium (low glucose DMEM, 2 %

horse serum, 1 % penicillin-streptomycin, 1 % insulin-transferrin-selenium, and 2 mg/mL aminocaproic acid in distilled water). When myobundles were switched to differentiation medium, the culture conditions were switched from static to dynamic using constant, low frequency shaking. If after two days of differentiation the myobundles were sticking to the PDMS moulds, a thin syringe needle was used to gently detach myobundles from the mould. Cultures were maintained in differentiation medium for a total of 14 days. Cultures were observed frequently for spontaneous twitching, a sign of successful differentiation. Some cultures detached from the frames at later stages of differentiation, which were discarded.

7.2.6 Myobundle treatment

Three myogenic donors were used for treatment. For force testing, 2-3 myobundles per donor per condition were used. For IL-1β and IFNγ treatments, myobundles were treated on day 10 until day 14 of differentiation, with complete medium change with fresh cytokines on day 12. Myobundles were treated under continued dynamic conditions. 20 ng/mL IL-1β and 750 ng/mL IFNγ were used in 5 mL myobundle differentiation medium.

For TALL-104 coculture, two conditions were tested. For both conditions TALL-104 cells were added to fresh myobundle differentiation medium containing 20 ng/mL IL-2. Firstly, $1.3x10^6$ million TALL-104 cells were added to myobundles under dynamic conditions. Secondly, $1.4x10^6$ TALL-104 were added directly to the mould face in 1 mL of media, left for 4 hours under stationary conditions, before addition of remaining medium and continuing to culture under static conditions. Myobundle differentiation medium containing 20 ng/mL IL-2 was used as control. Under both conditions, TALL-104 cells were cocultured with myobundles for 48 hours.

In a few experiments, acetylcholine was added to myobundles under microscopic observation. Acetylcholine chloride (Sigma, UK) was reconstituted to a stock solution to 550 mM in distilled water. A volume of acetylcholine stock was added directly onto the centre of the myobundle in culture medium so that the final concentration of acetylcholine diluted in medium was 10 mM. Live microscopy under phase contrast

was used to monitor acetylcholine effects using an Olympus IX81-ZDC inverted widefield fluorescent microscope.

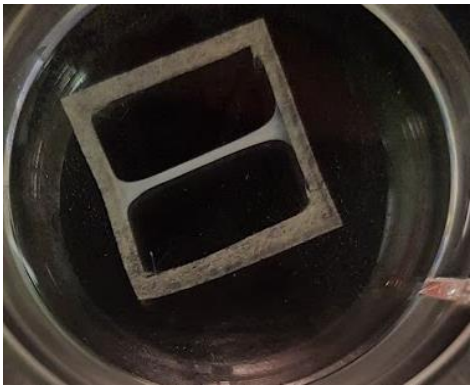

Figure 7.2 Myobundle attached to Cerex frame. At the end point of differentiation, myobundles can be removed from PDMS moulds and maintain their length attached to the Cerex frames.

7.2.7 Set up of organ bath hardware and software

An 8-chamber organ bath with 10 mL tissue vessels (Panlab, Spain) was used set to 37 ^{o}C. The organ bath cavity was filled with distilled water with anti-algae treatment, and a thermostat (Panlab, Spain) was used to heat the water. An MP150 data acquisition system (Biopac, UK) was used to record electrode stimulation patterns as digital input and force transducer readings as analogue input. The MP150 unit was composed of a UIM100C component, and multiple DA100C units to which the TR1201HS model force transducers (Panlab, Spain) were connected via TC113 adaptors (Biopac, UK). Each individual DA100C unit was calibrated for maximal voltage output with gain set to maximal (5000 Hz). The electrode stimulator was connected to the digital input of the UIM100C component via a NL952 cable (Digitimer, UK) for measuring the timing and duration of electrode stimulation. AcqKnowledge 4.4 was used to record and manually analyse force transducer readings. Force transducers were calibrated with a handmade weight in the AcqKnowledge software before each day's experiments.

Handmade platinum electrodes were constructed and designed by Steve Amos and Dr. Tim West, Royal Veterinary College. Electrodes were designed based on dimensions of a double ring stimulating electrode (Panlab, Spain) with parallel straight electrode probes made of platinum wire (0.3 mm diameter, Merck, UK). Electrodes were connected to an electrode stimulator (model D330 Digitimer, UK). The electrode stimulator was composed of the following units: D331 sync+gate, D332 pulse, D335 meter, and 8 D333H dual stim modules. A silk thread (Barnyarns Ripon, UK) was attached to one end of the Cerex frame near the myobundle attachment. The other end of this thread was wrapped around the force transducer spool. The bottom end of the myobundle was secured onto the electrode by threading the electrode mounting hook through the Cerex frame. The frame was cut away leaving only the attachment points to the electrode and thread to the force transducer (Figure 7.3), and the myobundle was submerged in CO_2 independent medium (product code 18045054) in the organ bath chamber without carbogen bubbling, and left to equilibrate for 15-20 minutes before commencing stimulation studies.

7.2.8 Measurement of contractile myobundle force

Isometric myobundle contractile force with electrical stimulation was tested on day 14 of culture. Tetanic contractions were measured at 30 Hz, approximately 40 V, 1.5 second duration and 1.1 ms width and 0.5 mm stretch. Twitch contractions were measured at approximately 40 V with a single pulse and 0.5 mm stretch. A minimum of 2 minutes was left between successive stimulations, and 3 minutes between elongation periods. Stretch was applied by movement of the force transducer via the inbuilt micromanipulator. For myobundle cultures with TALL-104, a fatigue stimulation condition was also used with the same conditions as tetanic contraction, but stimulation duration increased to 15 seconds.

7.2.9 Analysis of active force

Passive force was taken as the mean force in mN before stimulation. Average total force was taken as the mean at the highest point of force curve during electrical stimulation. Active force was expressed as total force minus passive force. Specific

force was defined as active force normalised to cross sectional area (CSA) of myobundles in mN/mm^2, measured via dystrophin staining (see Section 7.2.13 and Section 7.2.14). Force plots of active force over time are displayed with results normalised to average passive force so that passive force is roughly equivalent to 0 mN.

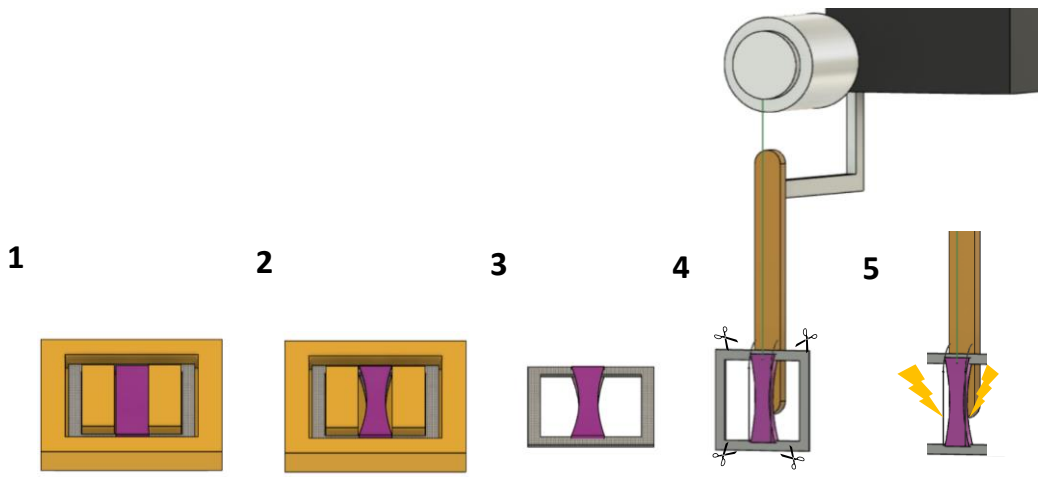

Figure 7.3 Schematic of myobundle preparation and stimulation. (1) Myobundles (pink) are seeded onto Cerex frames (grey) inside a silicone mould (yellow). (2) During myotube differentiation, the myobundle contracts anisotropically. (3) The myobundle attached to the Cerex is removed from the silicone mould at the end point. (4) Myobundle is attached to a vertical force transducer by attaching the Cerex frame to the hook at the bottom of the electrode, and via a silk thread (green) wrapped around the force transducer at the top. The Cerex frame is cut away leaving only the attachment points. (5) Myobundle is stimulated to contract via the electrodes placed lengthways either side of the myobundle. Image prepared in Autodesk Fusion 360.

7.2.10 Analysis of force kinetics

Kinetic properties of tetanic contractions were measured (Figure 7.4). Kinetic properties were measured manually on the force curves in AcqKnowledge 4.4. Time to peak force was measured as the time in seconds from the beginning of the force to the highest point of the force curve. Stimulation to force latency was the time in ms from the first pulse of stimulation to the beginning of the force initiation. Half contraction

time was the time in seconds from the start of contraction until the half value in mN between the passive force and force value at end of contraction. Half relaxation time was the time in seconds from the end of the force curve (i.e. the beginning of relaxation phase) to the time at which the force value during relaxation is half the difference between the end force value and the initial mean passive force value. Tetanus-twitch ratio was the active tetanus force divided by active twitch force. For TALL-104 cocultured myobundles, time to fatigue was also calculated under 15

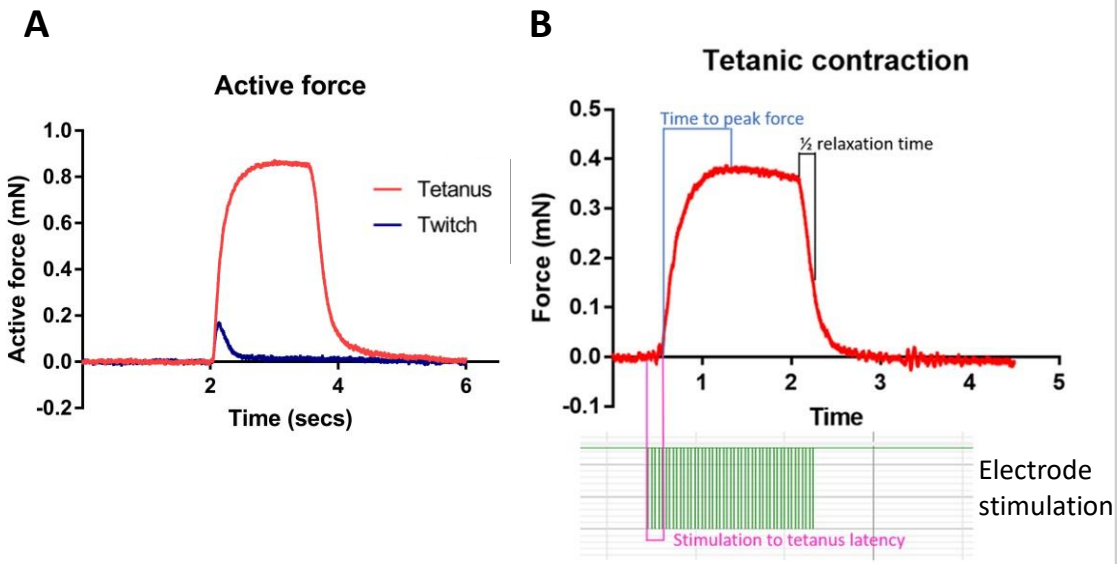

Figure 7.4 Examples of force characteristics. (A) A twitch response to a single pulse stimulus generates lower active force than a tetanic contraction with continuous stimulation for 1.5 seconds. (B) Example of kinetic characteristics of tetanic contraction. Time to peak force is the time from initiation of tetanus to the highest point of contraction. Stimulation to tetanus latency is the time difference between the electrode stimulation initiation and the beginning of the tetanic contraction. ½ relaxation time during relaxation is the time taken to reach ½ the force value between the end of the tetanus and the mean passive force. Not shown: ½ contraction time.

seconds continuous tetanic stimulation. This was the time in seconds from the initiation of contraction to the time at which the force began to decrease linearly whilst electrode stimulation was still applied. Furthermore measurements of fatigue half relaxation time were made, defined as the time to reach half the force value

between that recorded at 1.8 seconds after the initial increase in force in the contraction and the mean passive force before stimulation.

7.2.11 Embedding and sectioning myobundles

After force testing, myobundles were fixed in 4 % PFA solution for 24-48 hours at 4 °C before washing in PBS and maintaining in PBS at 4 °C until use up to 1 month later. Myobundles were cut into two sections along their width and added to Q path microstar III tissue cassettes (VWR, UK). For TALL-104 coculture myobundles, biopsy sponges (VWR, UK) were added to histology cassettes. Myobundles were embedded using a Shandon Duplex processor overnight with a hold at the first step in 70 % ethanol, followed by the steps below:

95 % ethanol 5 % methanol 1 hour

Four rounds of 100 % ethanol at 1, 1.5, 1.5, and 2 hours progressively

Two rounds of Histo-Clear™, 1 hour each

Paraffin wax 1 hour

Second paraffin wax 30 minutes to 1 hour

Myobundles were positioned within the wax with one myobundle half oriented along its longitudinal axis, and one myobundle half orientated along its transverse axis. 5 µm sections were cut with a microtome, floated in a water bath at 37 °C, and mounted on silanised microscope slides. For silanisation, slides were degreased in acetone for 5 minutes, silanated for 5 minutes in 2 % v/v (3-aminopropyl)triethoxysilane in acetone for 5 minutes, washed once in acetone and once in water, 5 minutes each, and dried before use.

7.2.12 Preparation of myobundle sections for immunofluorescent staining

Myobundles were dewaxed and rehydrated after sectioning. Dried slides were placed at approximately 65 °C for 1 hour to melt paraffin wax before the following dewaxing in Histo-Clear™ and rehydration in ethanol steps with vigorous agitation every 30 seconds:

Histo-Clear™ 5 minutes

Histo-Clear™ 10-15 minutes

100 % ethanol 3 minutes

90 % ethanol 3 minutes

70 % ethanol 3 minutes

50 % ethanol 3 minutes

Two distilled water washes, 3 minutes each.

After rehydration, sections underwent antigen retrieval in citrate buffer pH 6 (10 mM trisodium citrate (BDH, UK) in distilled water with 0.05 % v/v tween 20 (Sigma Aldrich, UK), correct pH obtained with addition of dropwise hydrochloric acid) at approximately 85 °C for 30 minutes followed by 20 minutes at room temperature. Slides were washed in water. An ImmEdge® pen (Vector Laboratories, USA) was used to create an island around the myobundle sections for addition of solutions.

7.2.13 Immunofluorescent labelling of myobundle sections

Sections were prepared and stained using immunofluorescent-conjugated secondary antibodies following a previously published protocol (494). Sections were blocked in FFPE (formalin-fixed, paraffin embedded) blocking buffer (1 % w/v BSA, 2 % FBS in PBS, 0.2 µm sterile filtered) for a minimum of 30 minutes. Approximately 60 µL of primary antibody (dystrophin 1:250 Abcam ab275391, sarcomeric alpha actinin 1:400 Abcam ab137346, and CD7 1:275 Proteintech 60209-1-Ig) were added overnight at 4 °C in a humidified chamber. Slides were washed three times 5 minutes each in PBS and Alexa Fluor™-conjugated (546 anti-mouse or 488 anti-rabbit, Invitrogen UK) secondary antibodies were added for 1 hour at room temperature, 1:500 dilution. 10 µM DAPI was added for 5 minutes before mounting coverslips (VWR, UK) with DAKO fluorescent mounting medium. After mounting medium dried, coverslip edges were sealed with clear nail varnish. Slides were stored at 4 °C until imaging using a Zeiss LSM980 confocal microscope.

7.2.14 Analysis of myobundle sections

Confocal microscopy was used to image myobundle sections. Whole cross-sectional area (CSA) was obtained from dystrophin stained cross sections using 10 X images stitched together with 10 % overlap. Dystrophin staining was also used to calculate

myotube area by measuring myotubes in four regions of the CSA, with region size chosen depending on size of myobundle CSA. Sarcomeric alpha actinin staining was used to observe organisation of sarcomeres within myotubes in longitudinal myobundle sections. For three 20 X magnification regions per myobundle, myotubes were classified as having either striated actinin staining or no clear striation pattern. Striated myotubes were expressed as a percentage of total observed myotubes. Dystrophin and sarcomeric alpha actinin staining analysis was conducted blinded.

7.3 Results

7.3.1 Discontinuation of Velcro mould design

Early on in the optimisation process for generating myobundles, it was decided to discontinue the use of the Velcro design in favour of Cerex frame design. This was due to the preferential handling properties of Cerex-based myobundles. Once removed from the mould, Cerex-based myobundles are able to maintain their original length through the tension of the Cerex frame, as opposed to Velcro-based myobundles which contract to a shorter length once removed from the silicone mould. For mounting onto the vertical electrode/organ bath set up, the design of the Cerex frame was also better suited, as a needle could easily be passed through the Cerex® fabric to thread the silk for suspension from the force transducer spool.

7.3.2 Myobundles exhibited standard responses to voltage and frequency changes

To ensure that prepared myobundles were capable of responding to stimulation in a physiological manner, their response to altered frequency and voltage was tested. Under single pulse stimulation (1 Hz), myobundles exhibited twitch responses (Figure 7.4 A, Figure 7.5 A). Between 5 Hz and 10 Hz, an unfused tetanus response was created. At 15 Hz and above, tetanic contractions became fused. Increasing frequency increased active force until 30 Hz were there was no observed increase in active force (Figure 7.5 A). At a constant tetanic frequency of 30 Hz, and altering voltage, there was minimal active force observable at 11 V. Increasing voltage increased active force production, until 37 V where only slight increases in force were observed to 46 V (Figure 7.5 B).

During the optimisation stage of myobundle design and preparation, the effect of chemical mediation of contraction was also tested on some myobundles with the addition of acetylcholine. After addition of acetylcholine the myobundles strongly contracted. Under microscopic analysis this was observed as a movement of the myobundles towards their centre point and an increase in their width (Figure 7.6).

During this experiment, myobundles remained in culture with acetylcholine as there was no washing or media changing. Despite this, myobundles began to slowly relax in the presence of acetylcholine, suggesting a desensitisation response.

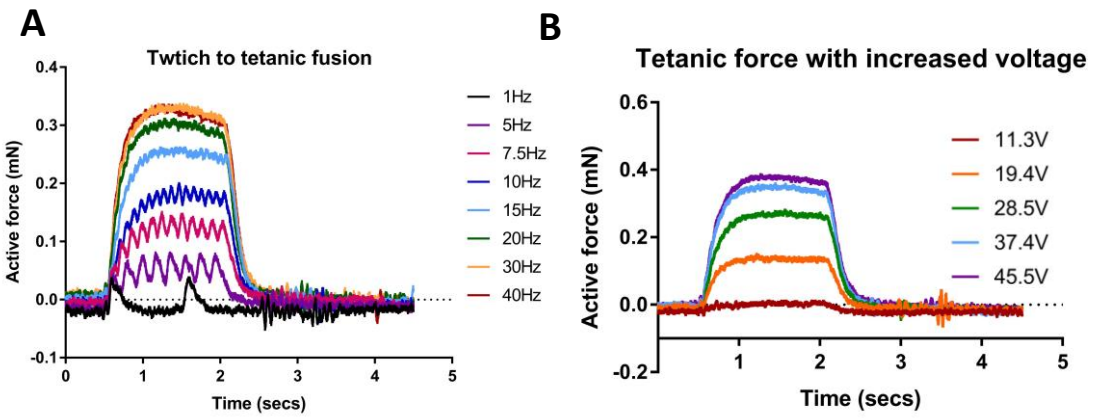

Figure 7.5 Force characteristics of myobundles. (A) At the same voltage (30V) and with increasing frequency of stimulation, the twitch response (1Hz, black line) turns into an unfused tetanus (5-10Hz), before becoming a fused tetanus around 15Hz (light blue line). (B) At the same frequency (20 Hz) and with increasing voltage, the active force increased.

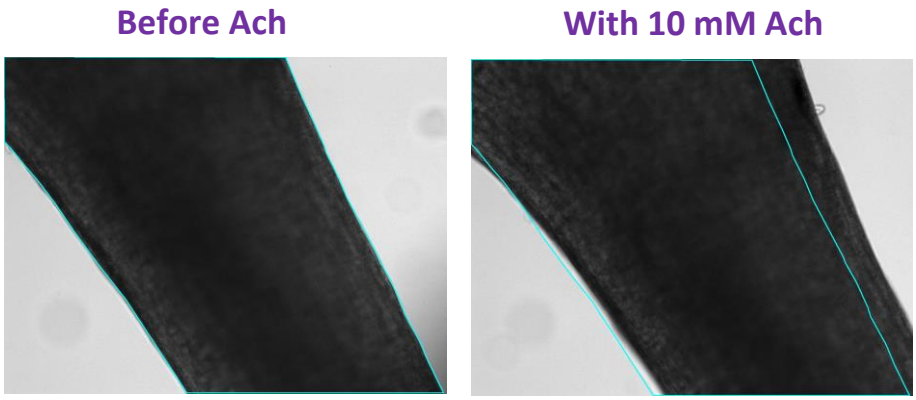

Figure 7.6 Myobundles respond to acetylcholine stimulation. Images of Myobundles (attached to Cerex frame) at basal tension (left) and after addition of 10 mM acetylcholine (Ach) during the contractile phase (right). On both images the blue shows the outline of the myobundle at passive tension, showing an increase in width of the myobundle after Ach stimulation.

7.3.3 Active force was not affected by IL-1β or IFNγ treatment

To assess whether IL-1β and IFNγ treatment individually or combined affects skeletal muscle force generation, active twitch and tetanus were measured after myobundles were cultured with cytokines for four days. Compared to untreated myotubes, there was no difference in active twitch (Figure 7.7 A) or active tetanic force (Figure 7.7 B) with any cytokine treatment condition. The mean active twitch force in the control group was 0.09 ± 0.04 mN, and for tetanic contraction was 0.51 ± 0.16 mN.

7.3.4 Tetanus kinetics were affected by IL-1β and IFNγ combined treatment

The effect of IL-1β and IFNγ incubation separately or combined on the kinetic properties of tetanic contractions was assessed to examine if these cytokines influence the speed of contraction. There was no difference in the ratio of tetanus to twitch active force between control myobundles and any cytokine treatment (Figure 7.8 A). There was also no difference in the time taken to respond to electrical stimulation to initiation of tetanic force (stimulation to tetanus force latency, Figure 7.8 D). The mean stimulation latency in the control group was 41.3 ± 2.5 ms. However, half relaxation time was increased with combined IL-1β and IFNγ treatment compared to control

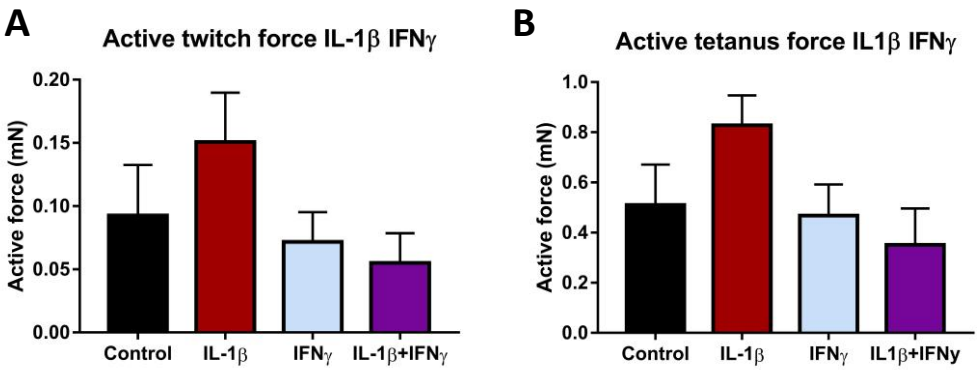

Figure 7.7 Active twitch and tetanus force with IL-1β, IFNγ or combined. There was no difference in active twitch (A) or tetanus (B) force with any cytokine treatment compared to control (p = 0.169 and p = 0.252 respectively). One-way ANOVA, n = 3 myogenic donors average of 2-3 myobundles per donor.

(0.35 ± 0.05 s IL-1β+IFNγ vs 0.20 ± 0.01 s control), and there was weak evidence that IFNγ increased half relaxation time (0.34 ± 0.05 s, p = 0.0553) (Figure 7.8 B). The time to peak force was decreased compared to control with IL-1β only (0.94 ± 0.03 s control vs 0.72 ± 0.03 s IL-1β only) (Figure 7.8 C). However, time to peak force was increased compared to control for IL-1β and IFNγ combined (1.2 ± 0.03 s IL-1β+IFNγ). Treatment with IFNγ showed no difference in time to peak force compared to control (p = 0.0755) (Figure 7.8 C). There was no difference compared to control and any treatment group for half contraction time (Figure 7.8 E) with median half contraction time of 0.13 seconds in the control group.

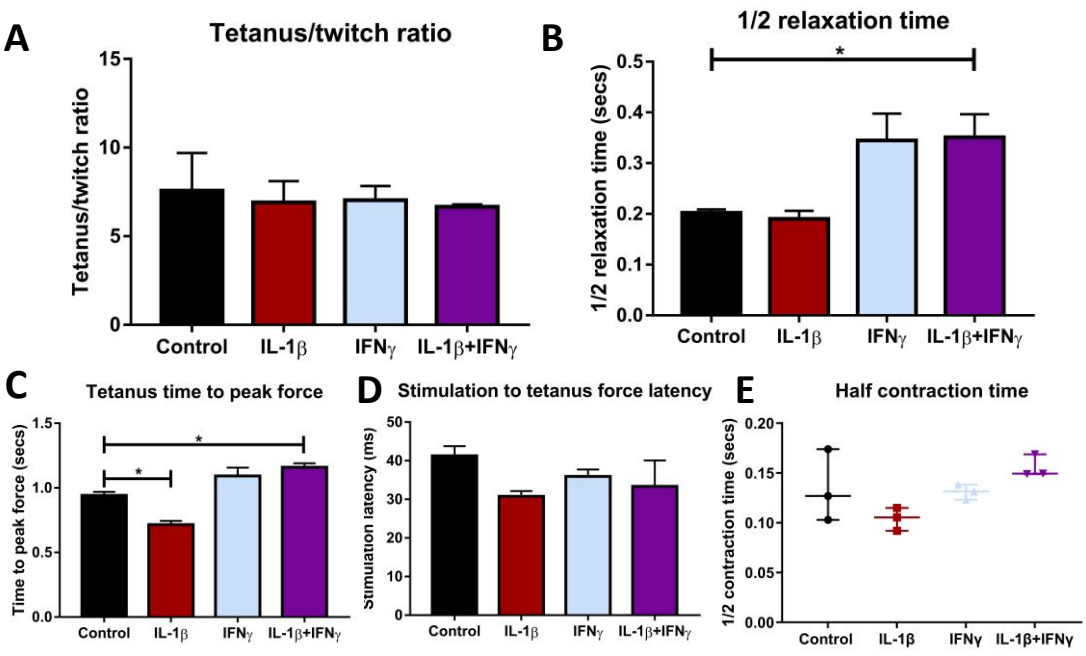

Figure 7.8 Tetanus kinetics with IL-1β, IFNγ or combined. (A) Tetanus-twitch ratio was not different between control and any cytokine treatment (one-way ANOVA p = 0.903). (B) Half relaxation time was increased with IL-1β+IFNγ treatment (p = 0.046) compared to control, and there was weak evidence that IFNγ increased half relaxation time (p = 0.0553). There was no difference with IL-1β (p = 0.990). (C) Time to peak force was decreased with IL-1β compared to control (p = 0.0116) and increased with IL-1β+IFNγ (p = 0.0139), and was not different with IFNγ (p = 0.0755). (D) There was no difference compared to control for stimulation to tetanus latency for any treatment (one-way ANOVA p = 0.304). (E) There was no difference compared to control for half contraction time (p = 0.0877). One-way ANOVA or Kruskal-Wallis test with Dunnett's multiple comparisons, n = 3 myogenic donors, average of 2-3 myobundles per donor per condition.

7.3.5 Cross sectional area or myotube area was not affected by cytokine treatment

As a measure of hypertrophy/atrophy, CSA and myotube area of transverse myobundle sections were analysed with dystrophin immunofluorescent staining. CSA analysis showed myobundles had variable shapes and sizes (Figure 7.9 A), however there was no difference in total CSA between control and any cytokine treated myobundles. The average CSA in the control group was 0.448 ± 0.034 mm^2. Dystrophin is located near the sarcolemma of individual myotubes (495) (Figure 7.9 B). There was a significant difference in myotube area between the treatment conditions (one-way ANOVA p = 0.0494), however this difference was between IFNγ and IL-1β+IFNγ (Tukey's multiple comparisons p = 0.042), and not between cytokine treatment and control. The mean myotube area in the control group was 266 ± 8 μm^2.

7.3.6 IFNγ treatment decreased actinin striation frequency of myotubes in myobundles

The effect of IL-1β and IFNγ cytokine treatment on myotube structural disorganisation was assessed. Myotubes were stained with sarcomeric alpha actinin (SAA) antibody to visualise sarcomeric structure. This also visualised the alignment of myotubes within myobundles, showing under all conditions there is mostly one directional alignment of myotubes following the length of the myobundle (Figure 7.10 A, Figure 7.16 A). Individual myotubes were classified as having either striated SAA staining or no clear striated SAA pattern (Figure 7.10 B). There was no difference between control myotubes and IL-1β treatment, however both IFNγ and IL-1β+IFNγ decreased the percentage of myotubes that showed clear SAA striation pattern compared to control (Figure 7.10 C). The mean percentage of myotubes showing striated SAA in the control group was 42 ± 5 %, for IFNγ alone was 19 ± 7 %, and for IL-1β+IFNγ was 20 ± 2 %.

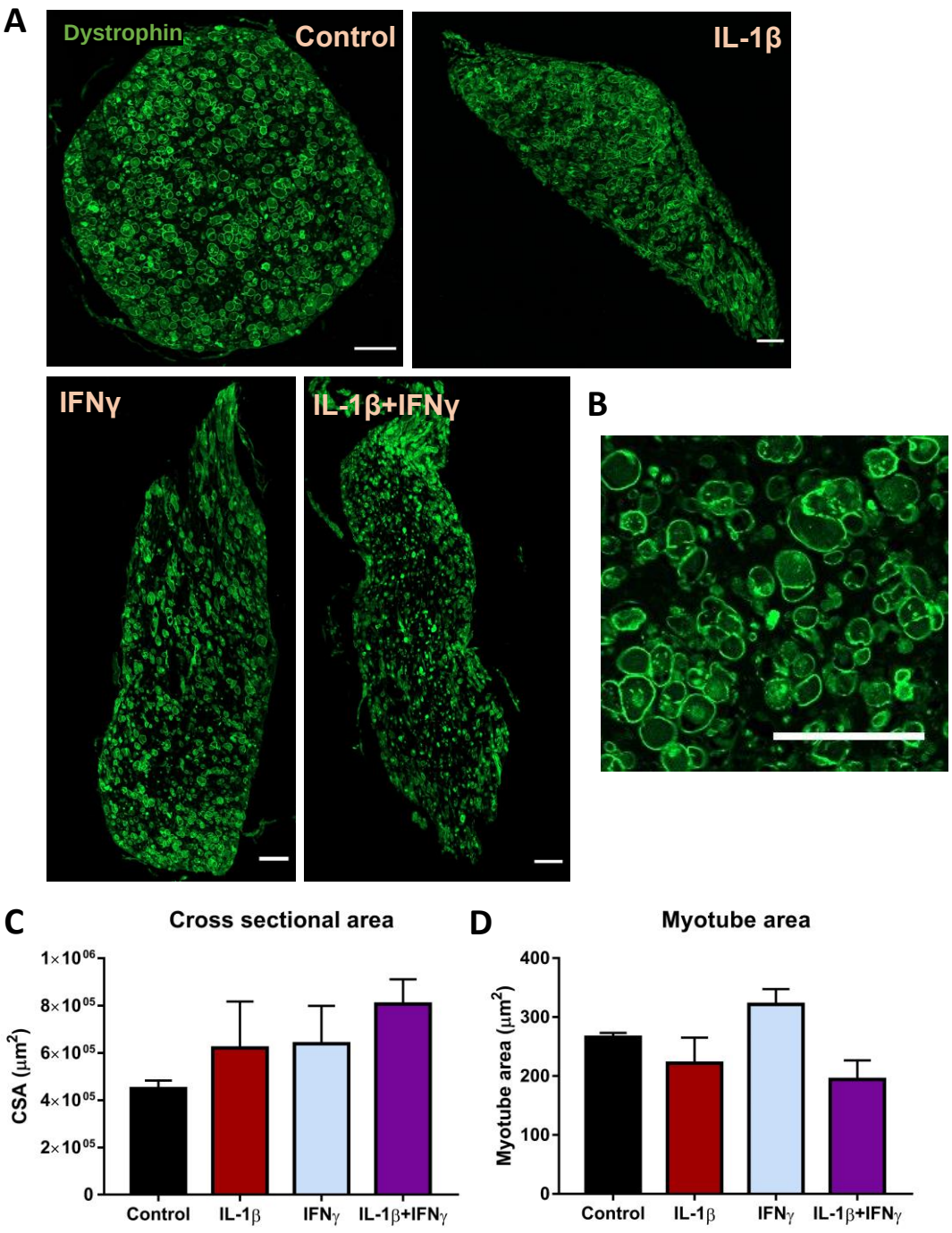

Figure 7.9 Cross sectional area and myotube area of myobundles was not affected by cytokine treatment. (A) Representative images of myotube cross sections stained with dystrophin. (B) Enlarged area of control cross section showing individual myotubes. A and B scale bar = 100 μm. (C) Total cross sectional area is not affected by any cytokine treatment (one-way ANOVA p = 0.300). (D) Myotube area was affected by cytokine treatment (p = 0.0494) but no cytokine to control comparison was significant (Dunnett's multiple-comparisons). Mean ± SEM. n = 3 myogenic donors except IL-1β n = 2, 1-3 myobundles per donor per condition.

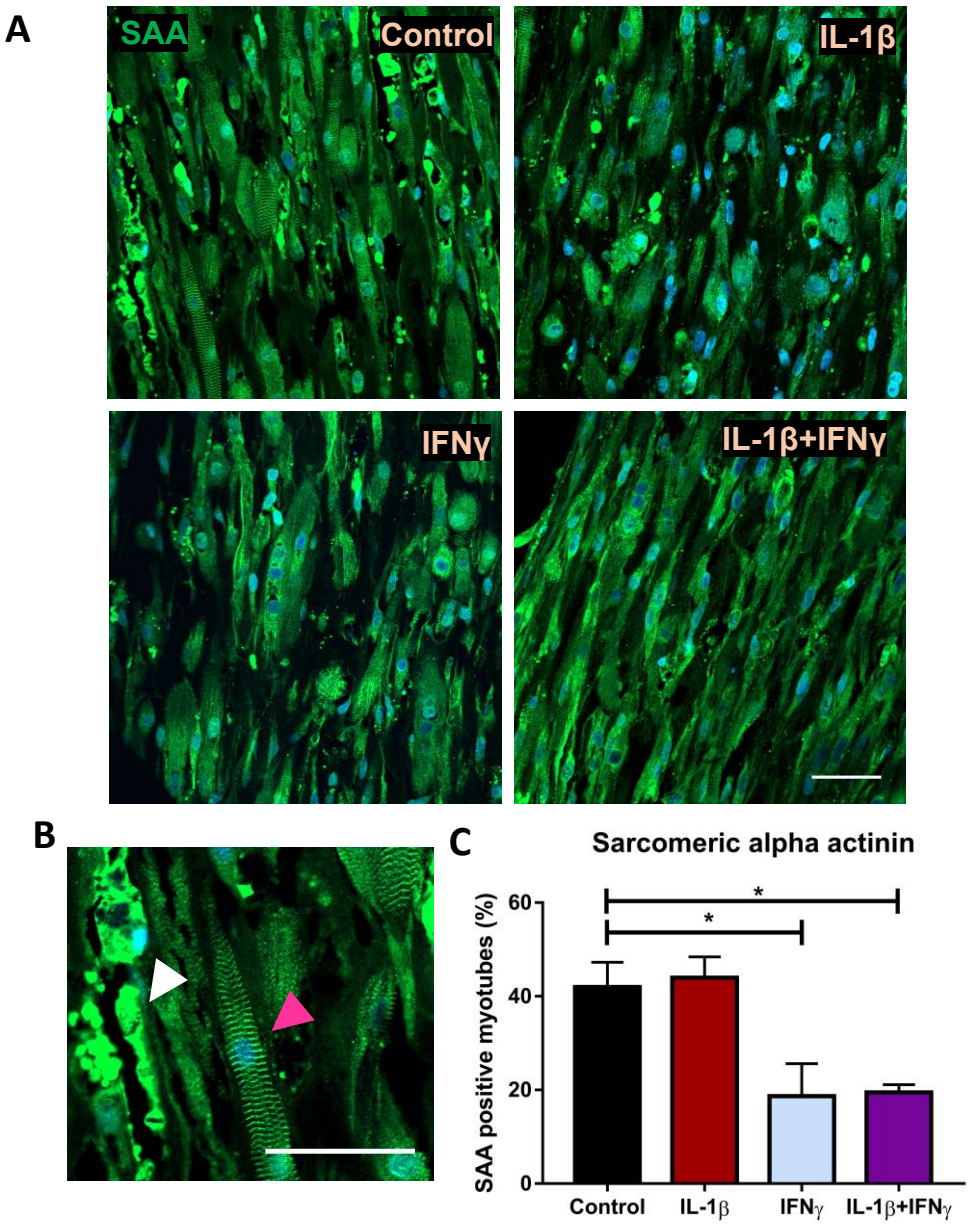

Figure 7.10 Striated sarcomeric alpha actinin was lower with IFNγ and IL-1β+IFNγ treatment. (A) Representative images of sarcomeric alpha actinin (SAA) staining with cytokine treatment (B) Enlarged area of control, showing myotube with clear banded actinin organisation (pink arrowhead), and myotube without clearly banded actinin organisation (white arrowhead). A and B scale bar = 50 µm. (C) There were fewer myotubes or cells with clear SAA banding in myobundles treated with IFNγ and IL-1β+IFNγ compared to control ($p = 0.0312$ and $p = 0.0363$ respectively). One-way ANOVA with Dunnett's multiple comparisons. Mean ± SEM. n = 3 myogenic donors except IL-1β n = 2, 1-3 myobundles per donor per condition.

7.3.7 Active twitch or tetanic force was not altered by TALL-104 coculture

The influence of cytotoxic immune cell culture on the ability of myobundles to generate force was investigated. Two experiments were conducted for coculture of TALL-104 cells with myobundles. In the first, $1.3x10^6$ TALL-104 cells were cocultured with myobundles for 48 hours with continuous shaking. Two myogenic donors were tested. In this condition, there was no observable difference in active tetanic or twitch force between myobundles treated with IL-2 control and those with TALL-104 coculture (Figure 7.11), although statistical analysis was not performed as n = 2. Under light microscopy it was observed that TALL-104 cells were dispersed throughout the culture well, including outside of the PDMS mould.

In the second set of experiments, $1.4x10^6$ TALL-104 cells were cultured with myobundles for 48 hours under static conditions. Active twitch or tetanus was not different in myobundles cocultured with TALL-104 cells compared to IL-2 control myobundles (Figure 7.12 A, B). The mean active twitch force in the IL-2 control condition was 0.13 ± 0.04 mN, and active tetanus was 0.71 ± 0.21 mN. Active specific force was also measured, defined as the active tetanic force divided by the CSA for each myobundle. There was no difference in active specific tetanic force between IL-2 control and myobundles cocultured with TALL-104 (Figure 7.12 C). The average specific force in the control group was 1.49 mN/mm^2.

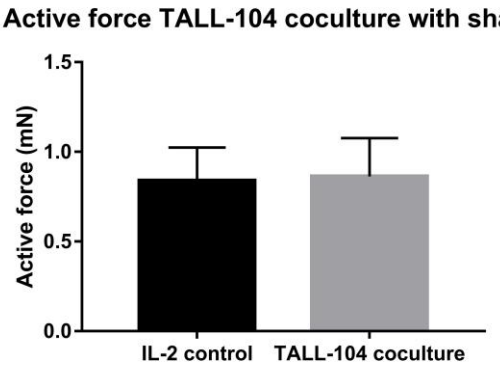

Figure 7.11 Active tetanus force with TALL-104 coculture with shaking. There was no observable difference in active force from myobundles treated with IL-2 control or cocultured with $1.3x10^6$ TALL-104 cells when cultured under constant shaking conditions. n = 2 myogenic donors (no statistical tests performed).

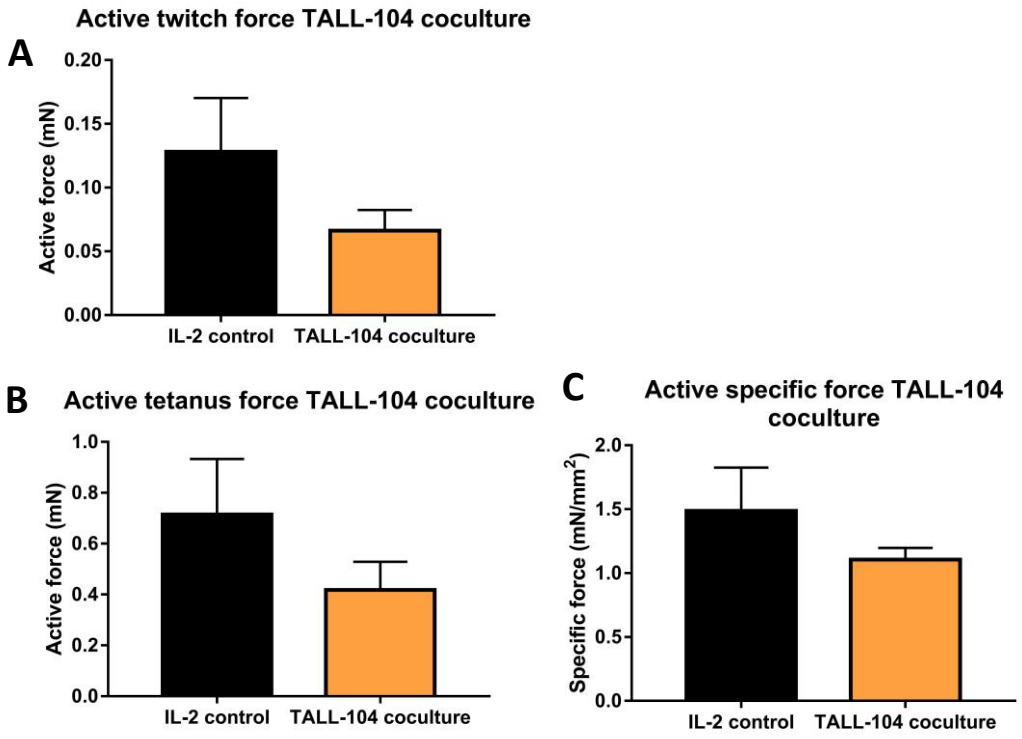

Figure 7.12 Active twitch or tetanus force was not affected by TALL-104 coculture.

There was no difference in active force between IL-2 control and TALL-104 coculture for twitch (A, p = 0.242), or tetanus (B, 0.293). (C) There was no difference in specific tetanus force defined as the active force per mm^2 of cross-sectional area between control and TALL-104 coculture (p = 0.337). Student's T-test, n = 3 myogenic donors, 2-3 myobundles per donor per condition.

7.3.8 TALL-104 coculture did not affect tetanus kinetics

The effect of cytotoxic immune cells on myobundle electrically-stimulated tetanus kinetics was assessed to see if TALL-104 cells influenced speed of contraction. The ratio of tetanus to twitch active force, half relaxation time, time to peak force, and stimulation to force latency were compared between myobundles treated with 48 hour IL-2 control or TALL-104 coculture. There was no difference in the ratio of tetanus to twitch active force between control and coculture myobundles (Figure 7.13 A). There was no difference in half relaxation time between control and coculture conditions (Figure 7.13 B). The mean half relaxation time in the IL-2 control group was

0.24 ± 0.02 s. Time to peak force was also not different between TALL-104 coculture and IL-2 control (Figure 7.13 C). The mean time to peak force in the IL-2 control group was 0.95 ± 0.05 s. The stimulation to force initiation (stimulation to force latency) was not affected by TALL-104 coculture (Figure 7.13 D), with the mean latency period in the control group 39.7 ± 1.1 ms. Half contraction time was not affected by TALL-104 coculture (Figure 7.13 E) with median half contraction time of 0.13 seconds in the IL-2 control group.

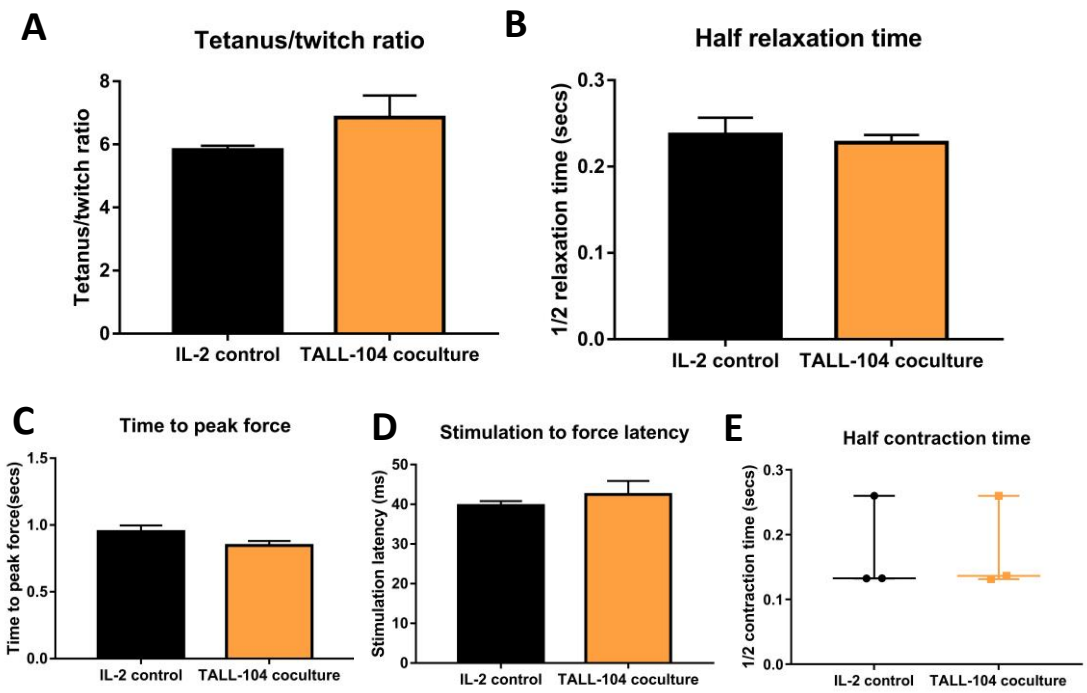

Figure 7.13 Force kinetics were not affected by TALL-104 coculture. (A) There was no difference between IL-2 control and TALL-104 coculture for tetanus to twitch ratio (p = 0.221), (B) half relaxation time (p = 0.689), (C) time to peak force (p = 0.148), (D) stimulation to force latency (p = 0.484), (E) or half contraction time (p = 0.999). Student's T-test or Mann-Whitney U test, n = 3 myogenic donors, 2-3 myobundles per donor per condition.

7.3.9 TALL-104 coculture did not affect fatigue responses

As well as twitch and tetanic stimulation, a fatigue condition was tested for TALL-104 cocultured myobundles to examine if coculture with cytotoxic immune cells causes fatigue in myobundles. This involved continuous stimulation at approximately 40 V and

30 Hz for 15 seconds. The myobundles in the IL-2 control and TALL-104 coculture condition were not capable of continued force production and the active force gradually began decreasing towards the level of the passive force (Figure 7.14 A). Two measurements of the fatigue response were made. The first was the time after initial increase in tetanic contraction until force began to decrease linearly, termed time to fatigue. There was no difference between myobundles treated with IL-2 control and TALL-104 coculture for time taken to reach fatigue (Figure 7.14 B). The mean time to fatigue in the control group was 2.13 ± 0.09 s. The second measurement of fatigue response was fatigue half relaxation time, defined as the time to reach half the difference between the force value recorded 1.8 seconds after the initial increase in force and the passive force. There was no difference in fatigue half relaxation time between IL-2 control myobundles and those with TALL-104 coculture (Figure 7.14 C). The median half relaxation time during the fatigue protocol was 3.99 ± 0.17 s.

7.3.10 Cross sectional area was not affected by TALL-104 coculture but myotube area may decrease

To investigate whether coculturing myobundles with cytotoxic immune cells caused hypertrophy or atrophy, dystrophin staining was used to quantify CSA and myotube area in IL-2 control treated or TALL-104 cocultured myobundles. There was no difference in cross sectional area between control and TALL-104 coculture myobundles (Figure 7.15 A,B). The median CSA in the IL-2 control group was 0.63 ± 0.33 mm^2. There was weak evidence that myotube area decreased with TALL-104 coculture compared to IL-2 control (Figure 7.15 C, $p = 0.064$), suggesting culturing myobundles with TALL-104 cells may lead to atrophy. The mean myotube area in the IL-2 control group was 216 ± 42 μm^2 and with TALL-104 coculture was 104 ± 12 μm^2.

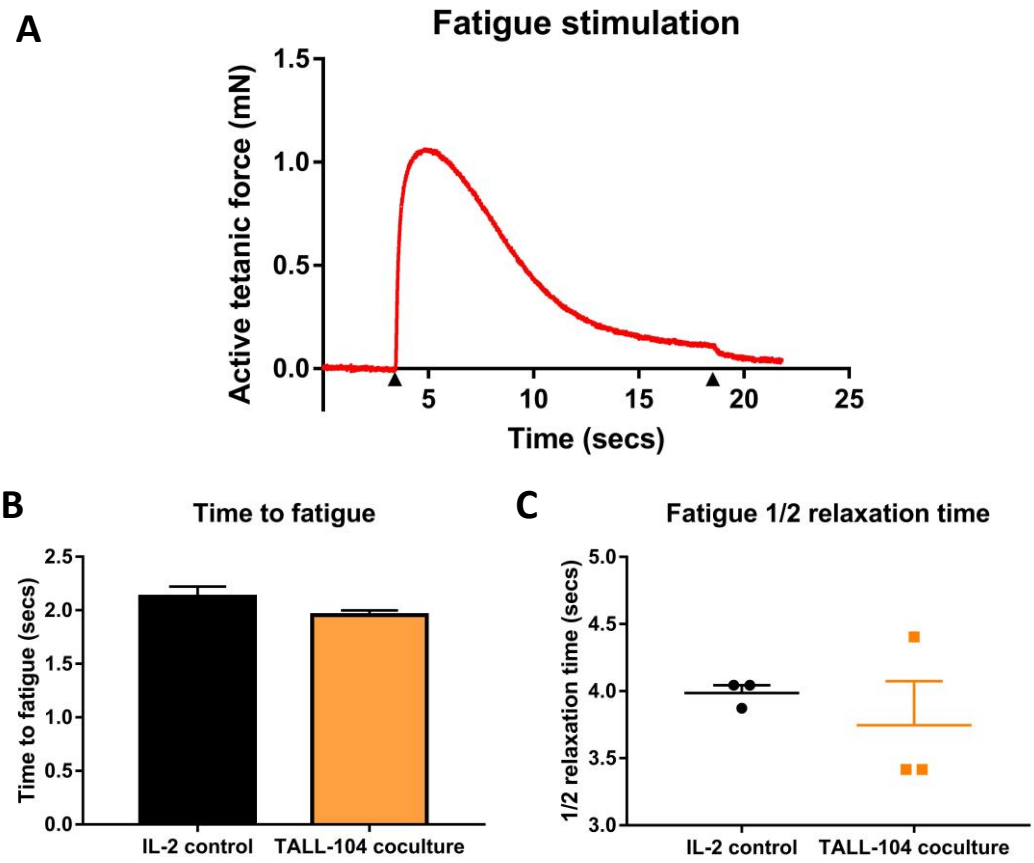

Figure 7.14 Fatigue with continuous tetanic stimulation was not affected by TALL-104 coculture. (A) Representative force curve with 15 seconds stimulation at 40 V and 30 Hz. Black arrows indicate start and finish of stimulation. (B) There was no difference in the time from beginning of contraction until force begins decreasing between IL-2 control and TALL-104 coculture ($p = 0.174$). (C) There was no difference in half relaxation time in the fatigue condition between control and TALL-104 coculture ($p = 0.800$). Student's T-test or Mann-Whitney U test, n = 3 myogenic donors, 2-3 myobundles per donor per condition.

7.3.11 Few TALL-104 cells infiltrated into myobundles

As there was no change in active force with TALL-104 coculture, the invasion of myobundles by TALL-104 cells was investigated by staining myobundle cross sections with CD7, a marker of thymocytes and T cells that is expressed on both natural killer cells and CD8+ cytotoxic T cells (496). TALL-104 cells should be 94 % positive for CD7 (459). CD7 staining in myobundle CSA showed some lack of specificity with some patchy staining without association to a nuclear region. In 7 CSAs of myobundles

treated with TALL-104 coculture, TALL-104 cells were detectable in 5 CSAs. The mean number of TALL-104 cells detected in one CSA per myobundle was 7 ± 3 cells. The TALL-104 cells were mostly located near the periphery of the myobundles (Figure 7.15 A inset), the mean distance travelled from the myobundle edge by TALL-104 cells was 40.2 ± 5.3 µm.

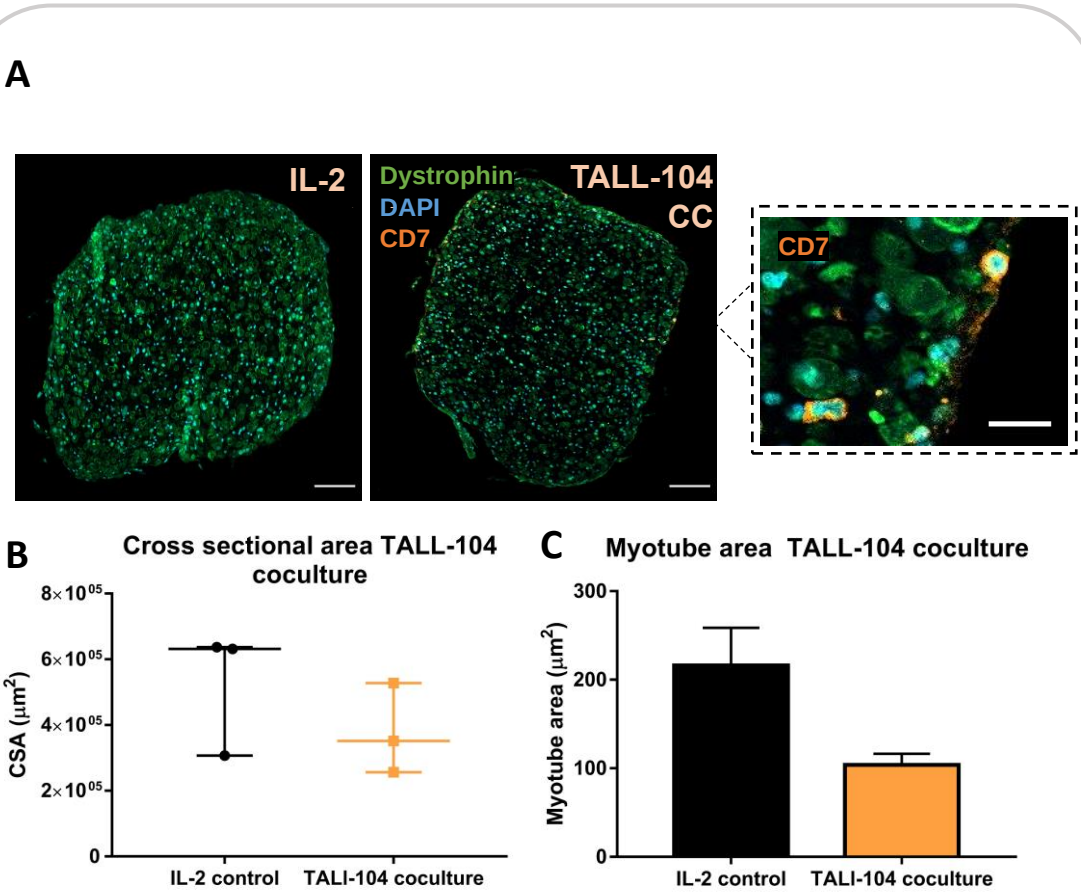

Figure 7.15 TALL-104 coculture does not affect cross sectional area but may affect myotube area. (A) Dystrophin staining of myobundles and inset of TALL-104 coculture showing TALL-104 cells labelled with CD7. Cross sectional area scale bars = 100 µm, inset scalebar = 20 µm. (B) There was no difference in cross sectional area of myobundles cultured with IL-2 or TALL-104 coculture (Mann-Whitney U test p = 0.400). (C) There was weak evidence of a decrease in myotube area with TALL-104 coculture compared to IL-2 control (Student's T-test p = 0.064). n = 3 myogenic donors, 2-3 myobundles per donor per condition.

7.3.12 Actinin striation frequency was not affected by TALL-104 coculture

Longitudinal sections of myobundles were stained for SAA to assess whether culturing myobundles with cytotoxic immune cells disrupted myotube structure. There was no difference in the percentage of myotubes that showed clear SAA striation between IL-2 control and TALL-104 coculture (Figure 7.16). The mean SAA striation percentage in the control group was 35 ± 7 %.

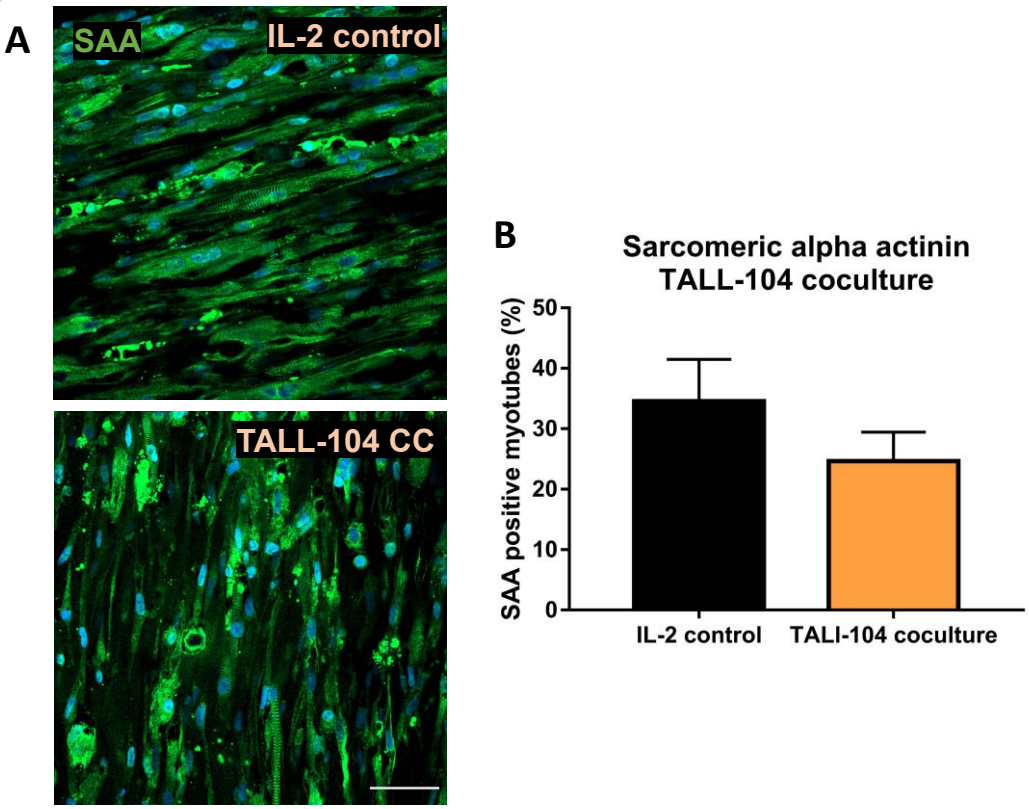

Figure 7.16 Sarcomeric alpha actinin striations in myotubes were not affected by TALL-104 coculture. (A) Sarcomeric alpha actinin (SAA) staining of myotubes treated with IL-2 control or TALL-104 coculture (CC). Scale bar = 20 µm. (B) There was no difference in percentage of myotubes with striated SAA when myobundles were treated with IL-2 control or TALL-104 coculture (Student's T-test p = 0.302). n = 3 myogenic donors, 2-3 myobundles per donor per condition.

7.4 Discussion

7.4.1 Myobundles responded in a physiological manner with similar parameters to previous results

This chapter aimed to explore the effect of inflammatory mediators that may be relevant to sIBM on the ability of skeletal muscle to generate force, to examine if these inflammatory factors can contribute to skeletal muscle weakness. From the previous chapters, two inflammatory conditions were examined: treatment with the inflammatory cytokines IL-1β and IFNγ, and coculture with the cytotoxic immune cell line TALL-104. Cytokine culture was chosen as this condition has previously been extensively used as a means of inducing sIBM-like features *in vitro*, but it is not known whether combined cytokine treatment was relevant to the clinical feature of muscle weakness in sIBM. Coculture with TALL-104 cells was also chosen as it was the most disease-relevant to the invasion of sIBM muscle by cytotoxic CD8 T cells out of the inflammatory factors investigated here.

Firstly, the basal characteristics of myobundles were examined to ensure they were physiologically relevant and similar to previously published work. The myobundles prepared here had similar responses to increased frequency as previously prepared myobundles by Madden *et al* (489), who showed near-fused tetanus at 10 Hz, with fused tetanus at 20 Hz. Here, fused tetanus was achieved at 15 Hz and above. Active force production increased with increasing voltage with an apparent non-linear fashion, with a lower increase in force between higher stimulation voltages. This relationship was used to choose a stimulation voltage for further experiments to maximise force output (40 V).

The myobundles were designed to be larger than those described by Madden *et al* (489) with the myobundle liquid mix volume approximately 1.8 times higher, and PDMS moulds designed larger to accommodate this. The stimulation conditions here (approximately 40 V and 30 Hz) were similar to those used previously of 20 Hz and 40V/cm. Despite this, the myobundles in this thesis appeared to produce lower active tetanic force than Madden *et al*'s myobundles at the same differentiation endpoint of

two weeks (0.5 mN vs ~ 1 mN). This is likely due to the fact this chapter's myobundles are generated from myogenic cells cultured in Ham's F10 medium supplemented with FGF and 20 % FBS. Madden *et al* showed that cells and myobundles prepared in F10 medium produce significantly lower active force than those cultured in 10 % FBS and supplemented with epidermal growth factor. Myogenic cells cultured in F10 + 20 % FBS + FGF had an approximate active tetanic force of 0.1 mN (489), whereas here the active force was higher (0.5 mN), which may be due to the increased size of the myobundles.

Myobundles responded as expected to both electrical stimulation and chemical stimulation with acetylcholine. Stimulation with acetylcholine under microscopy showed a long, strong contraction before the myobundle eventually began relaxing again. This relaxation in the continued presence of acetylcholine is likely due to desensitisation of the nicotinic acetylcholine receptor. In desensitisation, continuous binding of the receptor to acetylcholine causes deactivation of the associated ion channel, preventing prolonged depolarisation of the sarcolemma with eventual repolarisation which halts muscle contraction. In this way, skeletal muscle no longer responds to continuous acetylcholine stimulation, but when the stimulus (acetylcholine) is removed, the nicotinic acetylcholine receptors return back to a sensitised state (497, 498). Repeat stimulation with acetylcholine was not explored here so it is not known whether myobundles become re-sensitised.

Here, cross sectional area of control (untreated) myobundles was 0.448 mm^2. This is similar to the CSA of 0.5 mm observed for myobundles cultured by Chen *et al* (159). Myotube area here in the untreated control group was 265.7 μm^2 which is approximately double the myotube area found by Chen *et al* of 130 μm^2. However, it is similar to the myotube area of 234.5 μm^2 when myobundles were cultured with electrical stimulation (159). The myobundles here were stained after force testing which may contribute to this discrepancy, although CSA more accurately resembled measurements without electrical stimulation during culture. Myobundles here were created with a larger mould and volume of myobundle mixture than those previously

published. The similarity in CSA suggests that regardless of length and mould width, myobundles remodel the matrix and compact a similar amount.

Sarcomeric alpha actinin staining was used to visualise sarcomeric organisation within myotubes. Alpha actinin is associated with the z-line (499) and is involved in the attachment of actin filaments to the z-line (500). Here, cross striation frequency measured by sarcomeric alpha actinin staining was 42 % in the control group, which is very similar to the approximately 45 % cross striation frequency in untreated myobundles in Chen *et al* (159). Overall, the myobundles responded as expected to electrical and chemical stimulation, with similar characteristics to previously published work, except with lower active force generation likely due to suboptimal culture media conditions.

7.4.2 IL-1β and IFNγ treatment of myobundles

Active force was not affected by any cytokine treatment. This is contrary to previously published results where myobundle treatment with IFNγ caused a decrease in active force compared to untreated myobundles as seen by Chen *et al* (159). This discrepancy may be due to the shorter time period of four days for IFNγ incubation used here compared to seven days incubation used by Chen *et al*. This suggests only extended IFNγ exposure can affect active force. The time point at which IFNγ is added during differentiation was slightly different. Here, IFNγ is added after 10 days differentiation, whereas previously it was added after 7 days differentiation. The additional three days differentiation may provide a protective effect to IFNγ insult, potentially due to increased differentiation or maturity of myotubes.

Another possibility to differences in active force with IFNγ treatment could be that the equipment used here is not sensitive enough to detect small changes in force. The force transducer range is 5 mg-25 g (lower limit approximately equates to 0.049 mN). The ~ 0.5 mN recorded for control myobundles is within this range so the system sensitivity should be high enough. A degree of error is introduced with the Digitimer electrode stimulation system which relies on analogue manual controls for voltage and frequency, and consistently generating the same voltage between measurements and

channels was difficult. This may have influenced the consistency of results between myobundle measurements, in turn making it difficult to observe small changes in active force generation between treatment conditions. Alternatively, there is a difference in the concentration of IFNγ with 750 ng/mL used here and 20 ng/mL used by Chen *et al* (159). Potentially dose-dependent effects of IFNγ on muscle force exist, however this does not currently appear to have been investigated.

Kinetic properties of tetanic contractions were also assessed with cytokine treatment. Time to peak force and stimulation to tetanus latency are measurements of the speed at which myobundles can respond to the electrical stimulus. Increased half relaxation time is a sign of muscle fatigue (501). For example, multiple voluntary maximal contractions of a muscle can cause an increase in ½ relaxation time compared to pre-exercise as the muscle fatigues (502). The relaxation period involves active transport of calcium into the sarcoplasmic reticulum and re-covering of myosin binding sites by tropomyosin. The latency period between stimulation and onset of contraction is governed by the depolarisation of the sarcolemma and movement of the action potential along it, as well as the release of calcium from the sarcoplasmic reticulum (5). Time to peak force is affected by the kinetics of the cross-bridge formation during the power stroke, as well as the rate of calcium transients (503, 504).

In Chen *et al* (159) time to peak tension (force) and ½ relaxation time were both increased with IFNγ treatment. Here, there was weak evidence that ½ relaxation time was also increased with IFNγ treatment. However, there was no difference between control and IFNγ for time to peak force, showing only partial recapitulation of IFNγ treatment kinetic properties of tetanic contractions. Combined IL-1β+IFNγ or IL-1β treatment on myobundles has not previously been investigated. Time to peak force was increased compared to control for IL-1β+IFNγ, whereas treatment with IL-1β caused a decrease in time to peak force. These opposing results suggest a potential combined effect of IL-1β+IFNγ that is not seen with these cytokines individually. However, without considering statistical analyses of these results, IL-1β+IFNγ treatment more closely followed the same trends in tetanus kinetic responses as IFNγ individually which may suggest out of the two cytokines, IFNγ has the dominant effect

in combined cytokine treatment. Whilst there were no differences in ½ contraction time suggesting the rate of contraction is similar amongst conditions, the results followed a similar pattern to those of time to peak force.

Overall, IL-1β+IFNγ treatment slowed tetanic contraction during both the contraction and relaxation phase. However, time taken to respond to electrical stimulation was not affected, suggesting the ability of the sarcolemma to depolarise and cause release of calcium from sarcoplasmic reticulum stores is not affected. The lack of effect on active force but the longer duration of tetanus kinetics shows short durations of IL-1β+IFNγ treatment may cause fatigue without triggering weakness.

The decrease in time to peak force for IL-1β shows IL-1β can speed up response times for tetanic contractions. To the best of the author's knowledge, this is a previously undescribed phenomenon and it is not clear what mechanisms underpin this result. Treatment of human myometrial smooth muscle cells with IL-1β has been shown to increase the expression of SERCA (sarco/endoplasmic reticulum calcium-ATPase) 2b protein, which is responsible for transporting calcium ions into the sarcoplasmic reticulum from the cytosol. This was accompanied by an increase in cytosolic calcium ions when cells were triggered to release their intracellular stores, as well as an increased uptake of calcium into the cytoplasm from the media (505). Despite the difference in cell type here, potentially IL-1β triggers increased SERCA expression which increases the total pool of calcium ions that can be released as well as the excitability of myobundles with increased uptake of calcium, which may decrease the time to peak force. However if this were the case, it would be expected that increased SERCA expression would also lead to a decrease in half relaxation time due to its role in sequestering calcium, which was not observed with IL-1β treatment.

Cross sectional area and myotube area were measured as a proxy for hypertrophy or atrophy in whole myobundles and individual myotubes respectively. No cytokine treatment affected CSA or myotube area, showing no cytokine treatment induced either hypertrophic or atrophic effects. Chen *et al* (159) found IFNγ treatment caused no change in F-actin CSA, an increase in CSA with sarcomeric alpha actinin staining, a decrease in myotube density, and a decrease in myotube diameter. They concluded

that IFNγ treatment caused myotube atrophy. This is therefore another example of the differential responses of IFNγ found here to previous results, potentially due to temporal differences in treatment. It has previously been shown that in 2D cultures of skeletal muscle cells, treatment with IFNγ at 60 ng/mL for 72 hours does not alter fast-type myosin heavy chain content or the ratio of protein to DNA, suggesting that during this period IFNγ did not promote skeletal muscle catabolism (506), which is in accordance with the results observed here. IL-1β has previously been shown to have catabolic and atrophic effects on cultured muscle cells. Exposure of C2C12 cells to exogenous IL-1β caused reduced myotube width (139, 507), upregulation of atrophic genes (139), and reduced sarcomeric actin protein (507). It is not known why IL-1β did not illicit atrophic responses here, potentially the duration of treatment was not sufficient for these effects to arise. Alternatively, ECM or spatial considerations of the myobundle culture may confer a protective effect.

Sarcomeric alpha actinin staining was used to visualise cross striations of sarcomeres in myotubes. There was a significant decrease in the percentage of myotubes that showed clear actinin striation in the IFNγ (as well as IL-1β+IFNγ group), which was also observed by Chen *et al* (159). This indicates that there was a disorganisation of sarcomere structure within myotubes, with irregular spacing of the z-line. However, this observation did not translate into a measurable decrease in active force generation in the IFNγ treatment group. Furthermore, no compensatory mechanisms with IFNγ treatment seem to be in play such as myotube/myobundle hypertrophy. Therefore it is not clear why the decrease in sarcomeric structure did not result in decreased active force generation. Potentially, this was due to sarcomeric alpha actinin staining being performed on the same myobundles after force testing. The processing of myobundles for force testing may have therefore affected myotube integrity.

7.4.3 TALL-104 coculture with myobundles

CD8+ T cells are the most prevalent immune cell infiltrating into sIBM muscle. A plethora of work has characterised these cells as oligoclonal or clonally expanded, highly differentiated and cytotoxic effector cells. However, it still remains unknown whether CD8 T cells are responsible for the clinical symptoms of muscle weakness in

sIBM. TALL-104 cells were used as a proxy for cytotoxic immune cells, and the effect of coculturing these cells with myobundles was investigated to see whether direct immune-cell mediated cytotoxicity can contribute to muscle weakness. As a control, myobundles were incubated with IL-2, as this was also included in the coculture for activation of the TALL-104 cells. IL-2 can affect the activity of sodium channels in skeletal muscle (448, 449). However, this effect is reversible with removal of IL-2. Here, there was no IL-2 in the CO_2 independent medium with force testing, so there should not be any confounding effects of IL-2 in the control group. Indeed, there was no difference in active tetanus force between the two controls from the cytokine experiments (no treatment) and the controls from the TALL-104 coculture (IL-2 treatment, $p = 0.494$).

As previously noted in Chapter 6, TALL-104 have characteristics of both CD8 T cells and natural killer cells. Their mechanism of target recognition is MHC-independent, meaning their activation is not triggered through the same pathways as CD8 T cells. Therefore, any investigations into the mechanism of TALL-104 cell activation with myobundle coculture would not be representative of sIBM conditions. However despite this difference, the effector function of CD8 T cells and natural killer cells, as well as TALL-104 cells, are largely similar and based on release of cytotoxic granules or activation of extrinsic apoptotic pathways upon target cell contact.

The number of TALL-104 cells and duration of coculture was chosen based on results obtained in Chapter 6 showing high cytotoxicity for all E:T ratios after 48 hours. The number of TALL-104 cells with myobundles in the stationary culture condition represents an E:T ratio of approximately 0.8:1. It was expected that active force would be decreased or even completely ablated with TALL-104 coculture, with the potential of the myobundle disintegrating before the end point. However, this was not observed. Few TALL-104 cells were found infiltrated into myobundles, and there was no difference in active force.

Although cytotoxicity was not tested in myobundles, it can be presumed that due to the lack of effect of TALL-104 coculture on active force, there was limited cytotoxic effect on myotubes contained within myobundles. This potential difference in

cytotoxicity between 2D myotubes and myobundles may be due to three causes. The first, that the Matrigel and fibrin matrix in the myobundles impedes the detection of myotubes by TALL-104 cells, or limits their accessibility. Secondly, in 2D cultures there exists a passive effect that brings TALL-104 cells in close contact with cultured myotubes, namely gravity causing the sedimentation of the TALL-104 cells. This passive effect is lacking in myobundle cultures as the myobundles are not positioned flat at the surface of the PDMS mould, but slightly raised in suspension. Therefore, the TALL-104 cells only have a short period during sedimentation to attach to myobundles and interact via cell-cell contacts. After the initial experiments with dynamic coculture of myobundles showing no effect on active force, it was chosen to move to static conditions with a reduced medium incubation to try to maximise contact of TALL-104 cells with myobundles. The coculture-myobundle condition may more accurately reflect the effects of secreted factors from cytotoxic immune cells. However, no characterisation of secreted factors from cocultured TALL-104 cells was performed, therefore the activation state of these cells is not known. The final potential reason for lack of effects with myobundles compared to 2D culture is that the myobundle differentiation medium used may have negatively affected the viability or activation of TALL-104 cells, which was not tested.

Testing the viability of TALL-104 cells as well as their cytotoxicity against myotubes in myobundle differentiation medium compared to N2 or RPMI medium would help elucidate the lack of effect of TALL-104 in myobundles compared to 2D cultures. Further testing with longer exposure times and higher concentrations of TALL-104 cells are warranted, which may show different effects to the conditions used here. Despite TALL-104 showing activation via increased secretion of TNFα and IFNγ when cocultured in 2D, it is possible that this activation did not transfer to myobundle cocultures. TALL-104 could be pre-incubated with activating factors such as ionomycin and PMA (460, 461) before myobundle coculture to ensure their activity. TALL-104 sedimentation problems could be alleviated by creating adapted PDMS moulds for coculture that are designed to have a shallower inner channel in which the myobundle lies. Myobundles could be grown as described until the coculture point where they are transferred to the new PDMS moulds, which may allow the myobundle to sit flush against the base of

the PDMS inner channel. Small metal pins may be required to hold the Cerex frame in place and prevent the whole construct floating. Overall, TALL-104 coculture did not affect active force, although as described this may be due to poorly optimised conditions. It would be necessary to conduct further experiments of TALL-104 coculture with myobundles before any conclusions on the effect of these cells on muscle weakness can be drawn.

There was weak evidence that myotube area decreased with TALL-104 cells, showing myotube atrophy (with no myobundle atrophy). This shows that despite the sub-optimal culture conditions, TALL-104 cells may exhibit detrimental effects on myotubes. sIBM muscle fibres have been shown to have a lower mean diameter compared to healthy controls (72), therefore this feature of sIBM was recapitulated via myobundle TALL-104 coculture. It would be greatly interesting to optimise the preliminary experiments here to examine if atrophic effects are exacerbated, for example with higher TALL-104 concentrations.

7.4.4 Fatigue in sIBM

Kinetics of contractile force were measured here, showing IL-1β+IFNy treatment showed signs of increased muscle fatigue. In sIBM, it appears less is known about muscle fatigue specifically compared to weakness. Muscle fatigue can be defined as a reduction in maximal voluntary force induced by exercise, whereas endurance can be defined as the duration that a constant force output can be maintained (508). When sIBM patients underwent a clinical trial of blood flow restricted exercise, two patients withdrew from the exercise condition citing severe fatigue due to the training (221). Generalised fatigue has also been described in three Japanese sIBM patients (509). It has been recommended to use the two-minute walk test as opposed to the six-minute walk test in sIBM patients due to 7 % of patients becoming too fatigued in the longer condition (510). However, these effects may refer to fatigue more generally and not the ability of muscle to contract in response to multiple or sustained stimulations. Endurance may be decreased in sIBM patients when measured by functional testing. The 30-second chair stand test is a functional test which can measure a patient's leg muscle strength and endurance (511). In a small group of sIBM patients, the mean

number of times to stand up from sitting down in 30 seconds was 5-7 with an average age of 68-70 (221), which is below average for this age group (511), suggesting decreased endurance.

A fatigue stimulation condition was used with TALL-104 coculture where myobundles were stimulated at high frequency for 15 continuous seconds. This showed there was no difference in the time to fatigue or half relaxation time with TALL-104 coculture compared to control, which is corroborated by the force kinetics with standard tetanic contraction indicating no signs of fatigue. The time to fatigue was a measurement of time under continuous stimulation which therefore more accurately represents a measure of endurance. To better measure fatigue in myobundles, a condition of multiple tetanic contractions with minimal rest time between could be used, and measurement of active force changes between contractions tested. Overall, short-term exposure to TALL-104 cells in myobundles failed to induce weakness or fatigue, showing this condition does not recapitulate sIBM-like features.

7.4.5 Previous models of muscle weakness in sIBM

Previous investigations of muscle weakness in models of sIBM have been performed, and models that are amenable to strength testing have been developed. The strengths and weaknesses of these methods are summarised in Table 7.1. Transgenic mice carrying mutated human VCP have been used to model sIBM as they present with inclusion body myopathy, muscle inflammatory infiltrates and develop progressive muscle weakness (described in Section 1.15). Mutant VCP mice had decreased grip strength and decreased maximal tetanic force at 14 months. Treatment with arimoclomol for 10 months showed an amelioration in muscle weakness (219). Whilst VCP transgenic mice are a good model of the proteinopathy in sIBM, they also present with muscle extrinsic multi-system pathology including Paget's disease of bone and frontotemporal dementia. VCP transgenic mice offer a good platform for testing potential treatments to improve muscle weakness in sIBM, but they are not suitable for investigating causes of muscle weakness as VCP mutations are not universally present in sIBM cases (78).

Muscle-specific APP transgenic overexpression in mice has been investigated (269), as well as double transgenic APP and presenilin-1 mice (273) as models of sIBM. In the rotarod motor test where mice walk forwards to prevent falling off a rotating rod, APP transgenic and double APP presenilin-1 transgenic mice had decreased motor performance compared to controls, representing decreased strength and endurance. CD8+ cells can also be observed in the muscle of this model (270, 273). Whilst functional impairment of sIBM was reproduced in this model, specific strength tests were not conducted. Further, the relevance of APP to sIBM has been questioned.

A method of culturing sIBM-derived muscle cells in 2D with murine fibroblast feeder cells and exercise-like conditions with electrical stimulation during culture has been investigated. The contraction of sIBM myotubes compared to control donors was compared using image analysis to calculate the movement index of myotubes. Both control and sIBM myotubes were only observed contracting when cultured with electrical pulse stimulation. This showed no difference in contraction between sIBM and healthy myotubes (351), suggesting sIBM weakness may not be a muscle-intrinsic phenomenon, but may instead depend on *in situ* microenvironmental queues or inflammatory infiltration. This model of sIBM force benefits from the use of patient-derived muscle cells, allowing for direct investigations of sIBM muscle pathology. However, it fails to recapitulate the full complexity of sIBM such as the immune system involvement.

The mouse sIBM xenograft model developed by Britson *et al* (110) uses xenografts from sIBM patients engrafted into immunodeficient mice. The xenografts also carry over immune cells to the host, so that muscle intrinsic and inflammatory features of sIBM are incorporated. Therefore this model comes very close to recapitulating the native sIBM environment. Functional and force testing, for example with grip strength measurements and tetanic contraction of isolated muscle, could be utilised to examine if decreased strength is present in this model, however this has not currently been investigated.

Model	Pros	Cons
Transgenic VCP mice	• Recapitulates muscle-intrinsic pathology • Recapitulates weakness	• Lacks CD8+ specific pathology • Multi-system pathology not representative of sIBM
MCK-APP mice	• Decreased motor performance • APP and presenilin 1 mice show CD8+ infiltrates	• No direct strength testing • APP relevance to sIBM questionable
Electrical stimulation, feeder based primary sIBM cultures	• sIBM patient-derived • Animal-free	• Muscle weakness not recapitulated • Does not recapitulate inflammatory involvement
Xenograft model	• Relevant to sIBM phenotype; recapitulates muscle intrinsic and inflammatory features • Patient-derived	• Muscle strength not investigated • Limited by availability of sIBM muscle biopsies • Potential compensatory mechanisms from host
Myobundles	• Allows causes of muscle weakness to be examined • Animal-free	• Muscle weakness not recapitulated • Not patient-derived • Limited relevance of inflammatory conditions to sIBM pathology

Table 7.1 Models for sIBM strength testing. Summary of sIBM models that have either previously been investigated for muscle weakness or are amenable to strength/force testing. Myobundle strengths and weaknesses refer to results presented in this thesis. See in text (Section 7.4.5) for citations.

7.4.6 Summary

Neither cytokines nor coculture with cytotoxic immune cells at the concentrations and durations tested elicited weakness in myobundles. However, some alterations in secondary measures of myobundles were observed. IFNγ caused fatigue-like effects in myobundles and disrupted sarcomeric structure. TALL-104 coculture may have contributed to myotube atrophy without affecting active force. Optimised experiments

such as longer incubation time for cytokines or higher numbers of TALL-104 cells could be investigated. At present, the results in this chapter indicate under the conditions tested, neither cytokine treatment nor cytotoxic immune cell interactions affect myobundle weakness.

Chapter 8: General discussion and future work

Chapter 8. General discussion and future work

8.1 Discussion

sIBM is a complex disease presenting with diverse inflammatory features including infiltration of cytotoxic T cells, macrophages, and other immune cells, as well as elevated cytokine expression in the muscle. Furthermore, there is a wide range of non-inflammatory features observed in sIBM such as the presence of sarcoplasmic inclusion bodies, mitochondrial abnormalities, variable fibre size, and rimmed vacuoles.

The main clinical symptom of sIBM is progressive muscle weakness associated with decreased mobility at later stages of the disease. Unfortunately there are currently no effective treatments for sIBM patients. It is not clear what triggers muscle weakness in sIBM; whether it is a result of the inflammation, the non-inflammatory features, an interplay between inflammation and degeneration, or something else entirely. To help understand potential mechanisms in sIBM pathology, this thesis aimed to investigate the effects of the inflammatory environment on non-inflammatory sIBM-like features, mainly focussing on TDP-43 and p62, as sarcoplasmic aggregation of these two proteins has been suggested as a potentially specific marker for sIBM. The second main aim of this thesis was to examine whether inflammatory factors can contribute to muscle weakness. This was achieved by using a previously established 3D functional muscle culture system.

8.1 Experimental considerations

It was chosen to use primary human myogenic cells from different healthy donors as a culture material. As shown in Chapter 3, there was a wide range of demographic characteristics of these donors, as well as basic characteristics of the cells including their differentiation capabilities. This meant the starting point of all analyses already contained variability between the samples. The different demographic characteristics of the skeletal muscle cell donors is likely to influence their performance in cell culture conditions. It has been found younger (20-39 years old) as well as female donors had faster growing myogenic cells compared to older or male donors, however a higher

percentage of male donor myogenic cells were positive for MyoD (512). Another factor that was not controlled for was which muscle the cells were derived from. Four donors had cells isolated from abdominus rectus, one donor from vastus lateralis, and for the donors sourced from Lonza the source material was unknown. As the fibre type (slow or fast) from which muscle cells are derived influences the isoforms of myosin heavy chain that are expressed and different muscle groups differ in fibre composition (513), this may have introduced variability between the cells from different donors. Furthermore, the overall number of donors used for each experiment was relatively low, so any outlier responses to the inflammatory treatments may have affected the overall results. To alleviate some of this variability, the samples could be taken from donors of similar age and BMI, from the same muscle, and the total number of donor samples used could be increased.

Whilst the aforementioned donor characteristics can cause heterogeneity and large variance in results, this also means that any detected effects even in the small sample sizes used here, are more robust as they are reproducible across a variety of muscle cell phenotypes and donors. However, the high passage of cells used and the potential drift to a more differentiated phenotype is a possible confounding factor. Although not assessed, it is possible that these cells, whilst still proliferating, may have slowed down their growth rate. There is also the risk that some cultures may contain an unduly amount of senescent cells which could affect cellular responses to inflammatory treatments. On the other hand, this could work in favour of mimicking sIBM conditions more than early passage cells as sIBM is associated with ageing, and studies of sIBM cultured cells show decreased proliferation and earlier senescence (514).

It should be noted that whilst p62 and TDP-43 sarcoplasmic aberrations have been suggested as specific to sIBM, the inflammatory stimulations tested in this thesis are not specific to sIBM. For example, other inflammatory myopathies including polymyositis present with CD8+ T cell involvement (233), and elevated muscle cytokine levels may occur due to many diseases including sepsis (515). Furthermore, TDP-43 and p62 aberrations are also observed in other diseases, for example p62 aggregates in

IMNM (75) and TDP-43 myogranules in regenerating muscle (327). Therefore whilst the aim was to investigate sIBM-like characteristics, the factors investigated here do not specifically recapitulate the sIBM phenotype. The results presented here may also have wider applicability to muscle inflammation more generally.

As well as the lack of specificity and potentially lack of relevance of the inflammatory conditions used here to sIBM, the artificial and reductionist nature of using healthy human myotubes to model sIBM also needs to be considered. The treatment with high levels of inflammatory mediators on healthy human cells in culture for short time periods does not mirror the complexity, potential genetic aspects, time course, or inherent pathology of sIBM. Therefore, whilst an attempt was made to investigate sIBM-relevant pathological features, the results in this thesis cannot be more broadly applied to the condition of sIBM. However, this work may serve to inform future pre-clinical investigations or models of sIBM.

Throughout this thesis, the effects of inflammatory treatments were analysed on differentiated cultures of myotubes. The choice to use differentiated myotubes as opposed to myogenic precursors was taken as most previous *in vitro* sIBM investigations have also used myotube cultures, and because sIBM is an adult-onset disease in which the pathological hallmarks accumulate in mature skeletal muscle fibres. However, this approach may overlook the importance of proliferating cells, especially satellite cells, in sIBM. Satellite cells usually remain quiescent until activated by hypertrophic conditions or muscle damage for muscle growth and repair. It has been found that compared to healthy controls, sIBM muscle had increased nuclei expressing Pax7 as well as myoD and myogenin, showing increased number of satellite cells that were activated for myogenic regeneration. Furthermore, there was an increased percentage of fibres expressing neonatal myosin and CD56 suggesting fibres were regenerating in areas with inflammatory infiltrates (516). However, a separate study found there was no difference between control and sIBM muscle for the number of Ki-67+ Pax7+ nuclei, showing no increased proliferation of satellite cells in sIBM (72). At present, the role of satellite cell dysregulation in sIBM pathology remains unclear.

The effect of the inflammatory mediators investigated in this thesis are likely to have differential effects on proliferating cultures compared to myotubes. As an example, IFNγ treatment of proliferating myogenic cells causes decreased proliferation and differentiation into myotubes (156, 344, 517). Therefore, the importance of the inflammatory factors investigated here influencing muscle regeneration, which may also be altered in sIBM, was overlooked.

Inflammation has been investigated in this thesis as a potential causative factor in sIBM pathology and weakness. However, as noted in Chapter 5, inflammation also plays an important role in muscle regeneration and repair. This usually involves members of the innate immune system including neutrophils and macrophages. Therefore the presence of these cells in sIBM may not be a causative factor for pathology. Instead, the presence of macrophages may represent a continual attempt at repair of damaged muscle in sIBM.

8.2 Sestrins

Sestrins were investigated with inflammatory cytokine treatment, showing that IFNγ caused increased expression of sestrin-2. This may show activation of cell stress responses under this cytokine treatment. IFNγ is one of the most abundant cytokines released in sIBM muscle (124). It is possible there is a role for sestrins in sIBM muscle responses to IFNγ. The sestrin family are also implicated in muscle and energy homeostasis. The role of these proteins in sIBM has not previously been determined, however it would be interesting to compare the protein expression of sestrin-1 and sestrin-2 between sIBM and healthy control patients as the results shown here suggest inflammation can alter muscle sestrin-2 expression.

Whilst it was beyond the scope of this project, it would be interesting to investigate the overexpression of sestrins in CD8+ T cells and the effect coculture and secreted factors from these cells has on cultured myotubes, as it has previously been shown that expression of sestrin-2 in cytotoxic T cells was associated with an innate-like non-specific cytotoxicity response (311). As TALL-104 cells already mediate cytotoxic effects through innate pathways, this cell line would not be a suitable model for sestrin

investigations. Instead, primary CD8 T cells would be necessary. It would also be interesting to investigate the expression of sestrins in CD8 T cells from sIBM patients compared to healthy controls.

8.3 Inflammatory cytokines

The inflammatory factors investigated here included cytokine treatment with IL-1β and IFNγ. This has previously been utilised in *in vitro* treatment of myotubes to investigate sIBM features. Here, some of these investigations were replicated and expanded upon with human muscle cells, focussing on the effects of TDP-43 and p62. Overall, the results obtained did not suggest treatment with these cytokines recapitulated the phenotype of inclusion body formation as seen in sIBM. However, effects on p62 puncta size were observed with IL-1β+IFNγ. Instead of representing the large p62 aggregates seen in sIBM fibres which can be up to 10 µm in length (118), these aggregates were relatively small and may instead represent changes in autophagic pathways. IMNM also displays with p62 in the sarcoplasm, except with a more diffuse pattern than in sIBM. This in combination with the fact there were no observed changes in TDP-43 may mean the addition of IL-1β+IFNγ to myotubes more accurately recapitulates some IMNM pathological features as opposed to sIBM. No inflammatory treatments examined here showed a high percentage of colocalisation between TDP-43 aggregates and p62 puncta. In sIBM, these two proteins can be found colocalised in sIBM muscle fibres (98), therefore it is likely that the aggregates of either protein observed here do not accurately reflect inclusion bodies as found in sIBM. Whilst there were no effects of inflammatory conditions on TDP-43 aggregation, IL-1β+IFNγ caused p62 aggregation, suggesting TDP-43 and p62 may be under differential regulation in these muscle cells.

8.4 Inflammatory cells

The largest subset of immune cells infiltrating into sIBM muscle is cytotoxic T cells. Other immune cells are also implicated, including macrophages. The effect of secreted factors from cell lines serving as a proxy for these two cell types were investigated for effects on TDP-43 and p62 in myotubes. Like the treatment with inflammatory

cytokines IL-1β and IFNγ, there was no recapitulation of the sIBM phenotype of sarcomeric inclusion bodies containing TDP-43 and/or p62 for either macrophage or cytotoxic cell conditioned medium. Low levels of secreted factors from macrophages had no effect on p62 or TDP-43, suggesting macrophage secreted factors at the concentrations tested do not influence these proteins.

There was a need to better characterise the secretory phenotype of TALL-104 cells under basal culture conditions. Regardless, treatment with conditioned medium from the cytotoxic immune cell line TALL-104 did not affect p62 or TDP-43 aggregation in individual cells showing no formation of structures resembling inclusion bodies in sIBM. However, there was an increased number of images containing TDP-43 aggregates when myogenic cells were treated with TALL-104 conditioned medium. This is unlikely to reflect TDP-43 features in sIBM, but instead may represent an effect of TALL-104 secreted factors on TDP-43 myo-granules, which are involved in sarcomeric mRNA processing.

As well as investigating the effect of secretory factors of cytotoxic immune cells on TDP-43 and p62, the effect of direct coculture with cytotoxic immune cells was investigated. This showed TALL-104 cells had unexpected cytotoxic effects against cultured myogenic cells. TALL-104 cells were observed attaching and invading myotubes. Despite the strong cytotoxicity of cell contacts between myotubes and TALL-104 cells, there were no effects on TDP-43 or p62 that would reflect inclusion body formation. However, coculture with TALL-104 caused muscle cultures to have a reduction in TDP-43 localised exclusively to the nucleus. Whilst this is unlikely to reflect the mislocalisation of TDP-43 observed in sIBM and previously with other *in vitro* experiments, this is the closest of any inflammatory treatment investigated here to showing a shift in TDP-43 localisation. Importantly, this highlights that inflammation in the form of cytotoxic immune cells is capable of precluding and causing changes in TDP-43. It would be interesting to expand the myotube coculture experiments, for example by examining earlier coculture timepoints to visualise more myotubes before they succumb to TALL-104-mediated cytotoxicity.

The influence of inflammatory priming myotubes on the activity of macrophages and cytotoxic immune cells was investigated, showing that both macrophages and TALL-104 cells may modify their cytokine secretion in the presence of secreted factors from inflammatory myotubes. This suggests a positive feedback loop may exist where muscle undergoing inflammatory damage themselves trigger further inflammation. In sIBM, the exposure of muscle to infiltrating immune cells may cause the muscle to secrete cytokines which further encourages the infiltration and activation of immune cells in a self-perpetuating cycle. This also highlights the importance of skeletal muscle as a mediator of the immune system. However, the cytokines secreted from inflammatory-primed muscle cells were not examined, therefore it is not known what specific factors regulate this positive feedback.

8.5 A role for TDP-43 "pathology" in healthy muscle?

Under every condition, myotubes were detected that contained small p62 puncta and TDP-43 aggregates in the sarcoplasm. Furthermore, all conditions showed some colocalisation of p62 and TDP-43. This suggests a basal role for TDP-43 and p62 as well as their association in healthy myotubes. The presence of p62 puncta in all myotubes suggests a basal level of autophagy activation in these cells. Phosphorylation of p62 is important in mediating antioxidant protein production in response to exercise, showing physiological functions of p62 in muscle exist (518).

Previous *in vitro* characterisations of TDP-43 have shown its expression in the nucleus, and sometimes also diffusely in the sarcoplasm (219). Under every condition examined in this thesis including under untreated control conditions, myotubes that were negative for nuclear TDP-43 but positive for sarcoplasmic TDP-43 could be observed. TDP-43 mislocalisation out of the nucleus is usually described as a pathological process in conditions including sIBM, FTLD, and ALS. In these conditions, TDP-43 in the cytoplasm is abnormally phosphorylated, ubiquitinated, and cleaved into insoluble 35 and 25 kDa fragments which lose their nuclear localisation signal (519) required for transport into the nucleus. However, cleaved TDP-43 may not be an exclusively pathological process. A study has shown detectable levels of 25 and 35 kDa TDP-43 in

age matched healthy control muscle, although the expression was higher in sIBM samples (98), suggesting presence of these TDP-43 cleavage fragments may not necessitate muscle pathology. Furthermore, whilst most studies report nuclear TDP-43 localisation in muscle, a study culturing healthy control myotubes on feeder fibroblasts found approximately 60 % of myogenic nuclei contained TDP-43 (351). This corroborates the results here suggesting not all healthy cultured myotubes universally express nuclear TDP-43. This study also found that sIBM myotubes had an increase in sarcoplasmic TDP-43 accumulation and decreased nuclei containing TDP-43 compared to controls, but only when myotubes were cultured under electrical stimulation. This raises the interesting possibility that TDP-43 pathology in sIBM precipitates due to exercise/muscle use. Furthermore, the results presented by Li *et al* (351) show that TDP-43 pathology can be present without the presence of inflammation, providing evidence that non-inflammatory sIBM features may preclude or occur independently of inflammatory features.

Unfortunately, analysis of insoluble TDP-43 fractions via urea-based solubilisation of lysates was not performed here. It would be interesting to know whether 35 and 25 kDa fragments of TDP-43 existed in the control conditions, which would explain the occurrence of myotubes without nuclear TDP-43. As opposed to TDP-43 being cleaved in the sarcoplasm and losing its nuclear localisation, it is possible TDP-43 simply diffused out of the nucleus, as passive diffusion is the likely mechanism of nuclear to cytoplasmic TDP-43 shuttling (84, 85). The lack of nuclear TDP-43 in myotubes may mean that the myogenic cells here were not representative of a healthy population, potentially due to changes introduced through multiple passages. However, in some preliminary experiments, early passage (p3) myotubes and single nucleated cells also showed lack of nuclear TDP-43 staining (Appendix Figure 0.2), although no quantification between different passages was made. In one myogenic donor (HSKMDC 4), there were no cells quantified as having sarcoplasmic only TDP-43 expression, suggesting variability in normal TDP-43 localisation between donors.

8.6 Considerations for future preclinical sIBM research

As described previously, a study has investigated sIBM myotubes compared to healthy donor myotubes on a fibroblast feeder layer under electrical stimulation conditions. Very interestingly, there was no difference in contraction of myotubes from sIBM and control patients suggesting a muscle-extrinsic cause such as inflammation of weakness in sIBM (351). Alternatively, this could also suggest that sIBM muscle weakness does not arise from inherent myofibre dysfunction but could be due to global muscle quality problems such as fatty infiltration and loss of muscle mass. This result also highlights that myogenic precursors in sIBM are not predisposed to weakness. This study raises important questions about the biological relevance of myotube culture to represent sIBM pathology, as patient's own muscle cells may not show sIBM features under standard culture conditions. To investigate if the inflammatory component in sIBM evokes weakness, these results (351) could be expanded by co-culturing with matched patient immune cells.

Many of the non-inflammatory/degenerative features that have received the most attention in sIBM are those that share similarities with neurodegenerative diseases including ALS and Alzheimer's disease. This includes TDP-43, amyloid β, tau, and p62. This is likely due to the similarities between the presentations of protein aggregation in these two diseases (520). However, it is important that other non-inflammatory features, proteins, or pathways are not overlooked in favour of those that already have a clinical basis in other diseases, and the relevance of using other disease markers in sIBM research has been called into question (49).

The use of less biased approaches such as non-targeted proteomics or transcriptomics can serve as a useful tool for identifying strongly dysregulated pathways in sIBM. Indeed, a transcriptomic approach for analysing pathways involved in sIBM muscle compared to amputee controls showed genes involved in dendritic cell maturation were highly dysregulated in sIBM (201). The involvement of dendritic cells in sIBM has been poorly studied compared to other inflammatory cells like CD8 T cells (121, 124). This study (201) also identified disruption in calcium handling linked to T cell apoptosis,

showing the importance of immune dysregulation in sIBM. A separate transcriptomic analysis of myositis patient biopsies (521) found shared upregulated networks between myositis subgroups including muscle regeneration, as well as shared downregulated pathways such as humanin, an anti-apoptotic protein. sIBM-specific pathways were also found including upregulation of vasculogenesis and extracellular matrix genes. The authors suggested global transcriptomic analysis can highlight pathways that are not indicated by current clinical subtypes, which may be useful for predicting therapeutic responses.

The results presented here in Chapter 7 do not point to either short-term exposure to inflammatory cytokines or cytotoxic immune cells contributing to muscle weakness, however the approach of using myobundles deserves further attention as a manipulatable platform that may serve as a steppingstone to help elucidate causes of muscle weakness in sIBM and potential therapeutic targets.

The use of myobundles here in preliminary experiments failed to find a link between inflammation that may be relevant to sIBM and muscle weakness, in contradiction to previous results with longer term exposure to IFNγ. There was also no effect of TALL-104 coculture on force generation of myobundles. It is likely that insufficient TALL-104 numbers, time, or gravitational effects hampered the interaction of TALL-104 cells with myobundles. Further investigations into treatments or phenotypes relevant to sIBM for myobundle force testing are needed. Myobundles offer a reductionist approach in which a single factor can be manipulated at a time, which may make them more suitable to initial experiments for treatment testing over using animal models. The approach of using other similar 3D functional *in vitro* muscle constructs in myositis research is currently being investigated. At the 4th Global Conference on Myositis 2022 (522), work by M. Franken *et al* showed use of a 3D functional culture system to grow induced pluripotent stem cell-derived myotubes with addition of anti-cN1A antibodies from sIBM patients to investigate effects on force generation. At the same meeting, work by L. Covert *et al* showed use of myobundles treated with type I IFNs to investigate force generation in juvenile dermatomyositis. It is hoped that the interest

of using *in vitro* 3D functional models of skeletal muscle in myositis research will continue to grow.

8.7 Summary

To conclude, the results presented in this thesis hint that inflammation may not trigger TDP-43 aggregation in cultured human skeletal muscle cells. p62 can be influenced by addition of inflammatory cytokines, however this failed to recapitulate sIBM-like p62 pathology. Furthermore, the preliminary investigations presented in this thesis suggest that short durations of inflammatory cytokines or exposure to cytotoxic immune cells do not cause weakness in myobundles, although further investigations over longer time periods are warranted.

8.2 Future work

8.2.1 IL-1β and IFNγ signalling

To confirm addition of IL-1β and IFNγ can exert a response within the cultured skeletal muscle cells, proteins in the signalling pathways of these cytokines could be investigated. CIITA is increases upon IFNγ stimulation (156, 517). CIITA levels in the control and cytokine treatment groups could be measured via Western blotting with an expected increase in protein expression with IFNγ. To ensure skeletal muscle cells are capable of transducing IL-1β effects, the expression of the IL-1β receptor 1 (IL-1R1) or downstream effectors such as NF-κB proteins could be checked.

8.2.2 Analysis of autophagy with IL-1β+IFNγ

It was found that treatment with IL-1β+IFNγ caused an increase in the size of p62 puncta accompanied by a higher LC3II/LC3I ratio but without a total increase in LC3II protein. It is hypothesised that the treatment with IL-1β+IFNγ increased autophagic flux in myotubes, but more work is needed to confirm this. As LC3II (and p62) are both degraded during the autophagic process, it is necessary to run parallel experiments with all cytokine treatment groups and autophagy inhibitors such as chloroquine or bafilomycin-A1 to confirm increased autophagic flux. Analysis of protein levels via Western blotting could then be used to reveal whether changes in p62 aggregates and LC3II ratio are due to an increase in autophagic flux or a blockade of the autophagic process.

8.2.3 TDP-43 protein detection in the insoluble fraction and subcellular fractionation

The protein expression of TDP-43 was investigated here in the RIPA-soluble fraction. However, TDP-43 inclusions in the cytoplasm are largely composed of insoluble protein isoforms, including the 25-35 kDa cleaved C-terminal fragments. To investigate expression of these proteins, the insoluble protein fraction after RIPA lysis can be extracted using a urea-based buffer. This may more accurately reflect the TDP-43 isoforms found within sIBM inclusion bodies. Similarly, different primary antibodies

could be used for immunofluorescent detection of TDP-43 aggregates that better recognise cleaved or post-translationally modified TDP-43, such as phosphorylated TDP-43 (Ser409/410) (Proteintech UK, 80007-1-RR) and TDP-43 (C-terminal) (Proteintech UK, 12892-1-AP).

To complement the immunofluorescent analysis of TDP-43 localisation with inflammatory treatments, Western blotting of TDP-43 using subcellular fractionation could be conducted to examine the organelle-specific expression of TDP-43. This would be especially useful for comparing TDP-43 expression in whole cell lysates, the nucleus, and the cytoplasm.

8.2.4 Testing mitochondrial structure and function

One of the non-inflammatory features observed in sIBM skeletal muscle is abnormal mitochondria, seen as ragged red and COX-negative fibres. To test whether the inflammatory conditions examined here affects mitochondria in myotubes, the bioenergetic function of mitochondria could be assessed using a Seahorse XF analyser (524). Further, dyes such as MitoTracker™ or tetramethylrhodamine could be used for analysis of mitochondrial network structure. Mitophagy may also be affected in sIBM (63). The effect of inflammatory mediators on mitophagy may be analysed by assessing translocation of parkin to the mitochondria. Sestrin-2 has recently been found to localise to the mitochondria, both under normal conditions and when mitochondrial uncoupling is induced (525). The extent of localisation of sestrin-2 to mitochondria could be assessed under inflammatory conditions, as well as under mitochondrial stress conditions.

8.2.5 Macrophage coculture

Here, the effect of M(PMA) or M(IFNγLPS) conditioned media on TDP-43 and p62 aggregation was investigated. To further understand the role of macrophages on TDP-43 and p62, direct coculture of macrophages could be carried out. The effect of conditioned medium or direct coculture was not investigated in myobundles. Treating myobundles with conditioned medium and coculture could shed light on whether

macrophages secretory factors or direct cell interactions are capable of producing muscle weakness as seen in sIBM.

8.2.6 Combined treatment of conditioned media

Conditioned medium from macrophages and TALL-104 cells were used individually. However, as combined treatment of IL-1β and IFNγ affected p62 puncta size, it would be interesting to investigate the effect of combined treatment of macrophage and TALL-104 conditioned media, as this represents a more diverse and potentially more sIBM-relevant secretory phenotype. Further, as the conditioned medium from TALL-104 cells was found to contain minimal levels of IFNγ, conditioned medium from activated TALL-104 cells, for example with PMA and ionomycin that causes release of cytotoxic granules, should be investigated. To complement this, targeted analysis of the secretory phenotype of both TALL-104 and THP-1 cells could be carried out, for example with a Luminex® Assay or Proteome Profiler cytokine array.

8.2.7 Expanding coculture of myobundles with cytotoxic cells

Despite the high cytotoxicity of TALL-104 cells to myotubes in 2D conditions, there was no effect on active force when similar timeframes and cell ratios were used. Further experiments could be conducted to elucidate whether different conditions lead to changes in myobundle force production. Firstly, to prevent any issues of reduced TALL-104-myobundle interactions due to sedimentation of TALL-104 cells below the myobundle, the myobundles could be transferred to new PDMS moulds before addition of TALL-104 cells that have a lower depth of the inner channel, therefore causing the myobundle to sit on the bottom of the mould and facilitate TALL-104-myobundle interactions. Secondly, different quantities of TALL-104 cells and incubation time periods could be utilised to maximise any coculture effects.

In this study, TALL-104 cells were used as a proxy for cytotoxic T cells. However, these cells resemble both CD8+ T cells and natural killer cells. From biopsy samples, it is possible to culture sIBM myogenic cells (351), which could be expanded and cultured as myobundles. It would be interesting to investigate whether myobundles from sIBM

patient cells generated lower active force than matched healthy controls. Furthermore, with access to blood samples from the same sIBM patients, CD8+ T cells could be isolated and cocultured with myobundles to examine effects of inflammation on force generation. If a reduction in active force is found intrinsically within sIBM myobundles or with autologous CD8+ coculture, this setup could be utilised to test effects of drug candidates in a preclinical setting.

8.2.8 Analysis of calcium handling in myobundles

Some of the cytokine treatments used here, namely IL-1β+IFNγ, and IL-1β, affected tetanus kinetics without affecting force generation. It would be interesting to study the calcium handling properties of these myobundles to investigate whether this is responsible for altered force kinetics. Calcium binding dyes such as Fluo-8 can be added to myotubes before electrical stimulation. Under fluorescent microscopy, the calcium signal upon electrical stimulation can be measured. The ratio of calcium dye intensity after activation can be compared to the intensity at resting (ΔF/F), which can be plotted over time. It is hypothesised that the rate of calcium release, but not signal intensity, will be lower in IL-1β+IFNγ treated myobundles which showed increased time to peak force.

8.2.9 TDP-43 and p62 analysis in myobundles

TDP-43 and p62 sarcoplasmic aggregation was analysed in 2D cultured myotubes. However, to further characterise the effects of inflammatory mediators on TDP-43 and p62, it would be interesting to investigate sarcoplasmic aggregation in myobundles as well. Myobundles represent a more native, biologically relevant environment in which to observe p62 and TDP-43 than in 2D cultures. It would be especially interesting to see whether p62 puncta size increase with IL-1β+IFNγ carries over into myobundle cultures. Furthermore, in sIBM-patient myotubes it was found that pathological features of TDP-43 only precipitated with culture under electrical pulse stimulation (351), therefore results in myobundles after force testing may differ from 2D cultures.

8.2.10 TDP-43/p62 overexpression

The relationship between sIBM-like features of inflammation and protein aggregation remains uncertain. Here, the stance that inflammation precludes degenerative features of sIBM was taken, showing limited effect of the examined inflammatory milieu on TDP-43 and p62 protein aggregation. It could also be possible to investigate the effects of TDP-43 or p62 overexpression in muscle cells on responses such as proliferation and cytokine secretion of co-cultured or CM-treated inflammatory cells. TDP-43 or p62 overexpression models could be used to investigate the relationship between these two proteins and other features in sIBM such as mitochondrial abnormalities, as well as force testing in myobundles.

8.2.11 Manipulation of sestrins in cytotoxic T cells

The effect of some of the inflammatory conditions used here on sestrin-1 and 2 expression were examined. Previous work suggests that an increased expression of sestrins in CD8+ T cells in aged patients can lead to a senescent-like, highly cytotoxic phenotype (311). This may be similar to the highly differentiated cytotoxic CD8 T cells in sIBM. Primary human CD8+ cells could be manipulated to over-express sestrins, and co-culture or conditioned medium from these cells tested for effects on TDP-43 and p62 in myotubes.

References

1. Powers JD, Malingen SA, Regnier M, Daniel TL. The Sliding Filament Theory Since Andrew Huxley: Multiscale and Multidisciplinary Muscle Research. Annu Rev Biophys. 2021;50:373-400.
2. Betts JG, Young KA, Wise JA, Poe B, Kruse DH, Korol O. Anatomy and Physiology. Openstax.org available at: https://openstax.org/details/books/anatomy-and-physiology: Openstax.org; 2013. Available from: Openstax.org.
3. Sherwood L. Human physiology : from cells to systems. 7th ed. United Kingdom2010.
4. Al-Qusairi L, Laporte J. T-tubule biogenesis and triad formation in skeletal muscle and implication in human diseases. Skelet Muscle. 2011;1(1):26.
5. Tortora GJ, Derrickson, Bryan. Principles of anatomy and physiology. 12th edition. Hoboken, New Jersey, USA: John Wiley & Sons, Inc; 2009.
6. Ward CL, Corona BT, Yoo JJ, Harrison BS, Christ GJ. Oxygen generating biomaterials preserve skeletal muscle homeostasis under hypoxic and ischemic conditions. PloS one. 2013;8(8):e72485.
7. Dzangué-Tchoupou G, Mariampillai K, Bolko L, Amelin D, Mauhin W, Corneau A, et al. CD8+(T-bet+) cells as a predominant biomarker for inclusion body myositis. Autoimmun Rev. 2019;18(4):325-33.
8. Naddaf E, Barohn RJ, Dimachkie MM. Inclusion Body Myositis: Update on Pathogenesis and Treatment. Neurotherapeutics. 2018;15(4):995-1005.
9. Phillips BA, Zilko PJ, Mastaglia FL. Prevalence of sporadic inclusion body myositis in Western Australia. Muscle & nerve. 2000;23(6):970-2.
10. Shelly S, Mielke MM, Mandrekar J, Milone M, Ernste FC, Naddaf E, et al. Epidemiology and Natural History of Inclusion Body Myositis: A 40-Year Population-Based Study. Neurology. 2021.
11. Needham M, Corbett A, Day T, Christiansen F, Fabian V, Mastaglia FL. Prevalence of sporadic inclusion body myositis and factors contributing to delayed diagnosis. J Clin Neurosci. 2008;15(12):1350-3.
12. Machado PM, Ahmed M, Brady S, Gang Q, Healy E, Morrow JM, et al. Ongoing developments in sporadic inclusion body myositis. Curr Rheumatol Rep. 2014;16(12):477.
13. Cortese A, Machado P, Morrow J, Dewar L, Hiscock A, Miller A, et al. Longitudinal observational study of sporadic inclusion body myositis: implications for clinical trials. Neuromuscul Disord. 2013;23(5):404-12.
14. Keller CW, Schmidt J, Lünemann JD. Immune and myodegenerative pathomechanisms in inclusion body myositis. Ann Clin Transl Neurol. 2017;4(6):422-45.
15. Dimachkie MM, Barohn RJ. Inclusion body myositis. Semin Neurol. 2012;32(3):237-45.
16. Griggs RC, Askanas V, DiMauro S, Engel A, Karpati G, Mendell JR, et al. Inclusion body myositis and myopathies. Ann Neurol. 1995;38(5):705-13.
17. Brady S, Squier W, Hilton-Jones D. Clinical assessment determines the diagnosis of inclusion body myositis independently of pathological features. J Neurol Neurosurg Psychiatry. 2013;84(11):1240-6.
18. Hilton-Jones D, Miller A, Parton M, Holton J, Sewry C, Hanna MG. Inclusion body myositis: MRC Centre for Neuromuscular Diseases, IBM workshop, London, 13 June 2008. Neuromuscul Disord. 20. England2010. p. 142-7.
19. Rose MR. 188th ENMC International Workshop: Inclusion Body Myositis, 2-4 December 2011, Naarden, The Netherlands. Neuromuscul Disord. 2013;23(12):1044-55.

20. Rosina S, Varnier GC, Pistorio A, Pilkington C, Maillard S, Civino A, et al. Development and Testing of Reduced Versions of the Manual Muscle Test-8 in Juvenile Dermatomyositis. J Rheumatol. 2021;48(6):898-906.
21. Cox FM, Titulaer MJ, Sont JK, Wintzen AR, Verschuuren JJ, Badrising UA. A 12-year follow-up in sporadic inclusion body myositis: an end stage with major disabilities. Brain. 2011;134(Pt 11):3167-75.
22. Stark T, Walker B, Phillips JK, Fejer R, Beck R. Hand-held dynamometry correlation with the gold standard isokinetic dynamometry: a systematic review. Pm r. 2011;3(5):472-9.
23. Jørgensen AN, Aagaard P, Nielsen JL, Christiansen M, Hvid LG, Frandsen U, et al. Physical function and muscle strength in sporadic inclusion body myositis. Muscle & nerve. 2017;56(6):E50-e8.
24. Dunlap HV, Macneil LG, Tarnopolsky MA. Functional impairment in patients with sporadic Inclusion Body Myositis. Can J Neurol Sci. 2014;41(2):253-9.
25. Anatomy and Physiology I & II - Open & Free. https://oli.cmu.edu/courses/anatomy-physiology-i-ii-v2-academic/: Carnegie Mellon University.
26. Fitts RH, McDonald KS, Schluter JM. The determinants of skeletal muscle force and power: their adaptability with changes in activity pattern. J Biomech. 1991;24 Suppl 1:111-22.
27. Suchomel TJ, Nimphius S, Bellon CR, Stone MH. The Importance of Muscular Strength: Training Considerations. Sports Med. 2018;48(4):765-85.
28. Mills KR. The basics of electromyography. J Neurol Neurosurg Psychiatry. 2005;76 Suppl 2(Suppl 2):ii32-5.
29. Noda S, Murakami A, Kazuta T, Hirano S, Kimura S, Nakanishi H, et al. Clinical implication of denervation in sporadic inclusion body myositis. J Neurol Sci. 2022;439:120317.
30. Dabby R, Lange DJ, Trojaborg W, Hays AP, Lovelace RE, Brannagan TH, et al. Inclusion body myositis mimicking motor neuron disease. Arch Neurol. 2001;58(8):1253-6.
31. Hokkoku K, Sonoo M, Higashihara M, Stålberg E, Shimizu T. Electromyographs of the flexor digitorum profundus muscle are useful for the diagnosis of inclusion body myositis. Muscle & nerve. 2012;46(2):181-6.
32. Nojszewska M, Gawel M, Kierdaszuk B, Sierdziński J, Szmidt-Sałkowska E, Seroka A, et al. Electromyographic findings in sporadic inclusion body myositis. J Electromyogr Kinesiol. 2018;39:114-9.
33. Paganoni S, Amato A. Electrodiagnostic evaluation of myopathies. Phys Med Rehabil Clin N Am. 2013;24(1):193-207.
34. Naddaf E, Shelly S, Mandrekar J, Chamberlain AM, Hoffman EM, Ernste FC, et al. Survival and associated comorbidities in inclusion body myositis. Rheumatology (Oxford). 2021.
35. Dobloug GC, Garen T, Brunborg C, Gran JT, Molberg Ø. Survival and cancer risk in an unselected and complete Norwegian idiopathic inflammatory myopathy cohort. Semin Arthritis Rheum. 2015;45(3):301-8.
36. Oh TH, Brumfield KA, Hoskin TL, Kasperbauer JL, Basford JR. Dysphagia in inclusion body myositis: clinical features, management, and clinical outcome. Am J Phys Med Rehabil. 2008;87(11):883-9.
37. de Camargo LV, de Carvalho MS, Shinjo SK, de Oliveira ASB, Zanoteli E. Clinical, Histological, and Immunohistochemical Findings in Inclusion Body Myositis. Biomed Res Int. 2018;2018:5069042.
38. Elmansy M, Morrow JM, Shah S, Fischmann A, Wastling S, Reilly MM, et al. Evidence of nerve hypertrophy in patients with inclusion body myositis on lower limb MRI. Muscle & nerve. 2022.

39. Keshishian A, Greenberg SA, Agashivala N, Baser O, Johnson K. Health care costs and comorbidities for patients with inclusion body myositis. Curr Med Res Opin. 2018;34(9):1679-85.
40. Misterska-Skóra M, Sebastian A, Dzięgiel P, Sebastian M, Wiland P. Inclusion body myositis associated with Sjögren's syndrome. Rheumatol Int. 2013;33(12):3083-6.
41. Limaye VS, Cash K, Smith C, Koszyca B, Patel S, Greenberg SA, et al. Inclusion-body myositis and primary Sjögren syndrome: mechanisms for shared etiologies. Muscle & nerve. 2020;61(5):570-4.
42. Dieudonné Y, Allenbach Y, Benveniste O, Leonard-Louis S, Hervier B, Mariampillai K, et al. Granulomatosis-associated myositis: High prevalence of sporadic inclusion body myositis. Neurology. 2020;94(9):e910-e20.
43. Kusaoi M, Fukazawa T, Hirashima M, Morita Y, Yamaji C, Takai S, et al. A case of inclusion body myositis with systemic sclerosis. Mod Rheumatol. 2003;13(1):87-9.
44. Vemulapalli S, Sharer LR, Hsu VM. Inclusion body myositis in a patient with RNA polymerase III antibody-positive systemic sclerosis. J Rheumatol. 42. Canada2015. p. 730-2.
45. Haczkiewicz K, Sebastian A, Piotrowska A, Misterska-Skóra M, Hałoń A, Skoczyńska M, et al. Immunohistochemical and ultrastructural analysis of sporadic inclusion body myositis: a case series. Rheumatol Int. 2019;39(7):1291-301.
46. Moignet A, Lamy T. Latest Advances in the Diagnosis and Treatment of Large Granular Lymphocytic Leukemia. Am Soc Clin Oncol Educ Book. 2018;38:616-25.
47. Greenberg SA, Pinkus JL, Amato AA, Kristensen T, Dorfman DM. Association of inclusion body myositis with T cell large granular lymphocytic leukaemia. Brain. 2016;139(Pt 5):1348-60.
48. Villanova M, Kawai M, Lübke U, Oh SJ, Perry G, Six J, et al. Rimmed vacuoles of inclusion body myositis and oculopharyngeal muscular dystrophy contain amyloid precursor protein and lysosomal markers. Brain Res. 1993;603(2):343-7.
49. Greenberg SA. Theories of the pathogenesis of inclusion body myositis. Curr Rheumatol Rep. 2010;12(3):221-8.
50. Güttsches AK, Brady S, Krause K, Maerkens A, Uszkoreit J, Eisenacher M, et al. Proteomics of rimmed vacuoles define new risk allele in inclusion body myositis. Ann Neurol. 2017;81(2):227-39.
51. Brady S, Squier W, Sewry C, Hanna M, Hilton-Jones D, Holton JL. A retrospective cohort study identifying the principal pathological features useful in the diagnosis of inclusion body myositis. BMJ Open. 2014;4(4):e004552.
52. Greenberg SA, Pinkus JL, Amato AA. Nuclear membrane proteins are present within rimmed vacuoles in inclusion-body myositis. Muscle & nerve. 2006;34(4):406-16.
53. Chahin N, Engel AG. Correlation of muscle biopsy, clinical course, and outcome in PM and sporadic IBM. Neurology. 2008;70(6):418-24.
54. Amato AA, Gronseth GS, Jackson CE, Wolfe GI, Katz JS, Bryan WW, et al. Inclusion body myositis: clinical and pathological boundaries. Ann Neurol. 1996;40(4):581-6.
55. Askanas V, Alvarez RB, Engel WK. beta-Amyloid precursor epitopes in muscle fibers of inclusion body myositis. Ann Neurol. 1993;34(4):551-60.
56. Vattemi G, Nogalska A, King Engel W, D'Agostino C, Checler F, Askanas V. Amyloid-beta42 is preferentially accumulated in muscle fibers of patients with sporadic inclusion-body myositis. Acta Neuropathol. 2009;117(5):569-74.
57. Nogalska A, D'Agostino C, Engel WK, Klein WL, Askanas V. Novel demonstration of amyloid-β oligomers in sporadic inclusion-body myositis muscle fibers. Acta Neuropathol. 2010;120(5):661-6.
58. Greenberg SA. How citation distortions create unfounded authority: analysis of a citation network. Bmj. 2009;339:b2680.

59. Sherriff FE, Joachim CL, Squier MV, Esiri MM. Ubiquitinated inclusions in inclusion-body myositis patients are immunoreactive for cathepsin D but not beta-amyloid. Neurosci Lett. 1995;194(1-2):37-40.
60. Pruitt JN, 2nd, Showalter CJ, Engel AG. Sporadic inclusion body myositis: counts of different types of abnormal fibers. Ann Neurol. 1996;39(1):139-43.
61. Greenberg SA. Inclusion body myositis: clinical features and pathogenesis. Nat Rev Rheumatol. 2019;15(5):257-72.
62. Sarkozi E, Askanas V, Johnson SA, McFerrin J, Engel WK. Expression of beta-amyloid precursor protein gene is developmentally regulated in human muscle fibers in vivo and in vitro. Exp Neurol. 1994;128(1):27-33.
63. De Paepe B. Sporadic Inclusion Body Myositis: An Acquired Mitochondrial Disease with Extras. Biomolecules. 2019;9(1).
64. Reichmann H, Vogler L, Seibel P. Ragged red or ragged blue fibers. Eur Neurol. 1996;36(2):98-102.
65. Oldfors A, Moslemi AR, Jonasson L, Ohlsson M, Kollberg G, Lindberg C. Mitochondrial abnormalities in inclusion-body myositis. Neurology. 2006;66(2 Suppl 1):S49-55.
66. Watson SA, McStay GP. Functions of Cytochrome c oxidase Assembly Factors. Int J Mol Sci. 2020;21(19).
67. Rustin P, Munnich A, Rötig A. Succinate dehydrogenase and human diseases: new insights into a well-known enzyme. Eur J Hum Genet. 2002;10(5):289-91.
68. Murphy JL, Ratnaike TE, Shang E, Falkous G, Blakely EL, Alston CL, et al. Cytochrome c oxidase-intermediate fibres: importance in understanding the pathogenesis and treatment of mitochondrial myopathy. Neuromuscul Disord. 2012;22(8):690-8.
69. Oldfors A, Moslemi AR, Fyhr IM, Holme E, Larsson NG, Lindberg C. Mitochondrial DNA deletions in muscle fibers in inclusion body myositis. J Neuropathol Exp Neurol. 1995;54(4):581-7.
70. Rygiel KA, Miller J, Grady JP, Rocha MC, Taylor RW, Turnbull DM. Mitochondrial and inflammatory changes in sporadic inclusion body myositis. Neuropathol Appl Neurobiol. 2015;41(3):288-303.
71. Dahadhah FW, Jaweesh MS, Al Zoubi MS, Alarjah MIA, Hammadeh ME, Amor H. Mitochondrial nicotinamide adenine dinucleotide hydride dehydrogenase (NADH) subunit 4 (MTND4) polymorphisms and their association with male infertility. J Assist Reprod Genet. 2021;38(8):2021-9.
72. Kwon B, Kumar P, Lee HK, Zeng L, Walsh K, Fu Q, et al. Aberrant cell cycle reentry in human and experimental inclusion body myositis and polymyositis. Hum Mol Genet. 2014;23(14):3681-94.
73. Ivanidze J, Hoffmann R, Lochmuller H, Engel AG, Hohlfeld R, Dornmair K. Inclusion body myositis: laser microdissection reveals differential up-regulation of IFN-gamma signaling cascade in attacked versus nonattacked myofibers. The American journal of pathology. 2011;179(3):1347-59.
74. Ferrer I, Martín B, Castaño JG, Lucas JJ, Moreno D, Olivé M. Proteasomal expression, induction of immunoproteasome subunits, and local MHC class I presentation in myofibrillar myopathy and inclusion body myositis. J Neuropathol Exp Neurol. 2004;63(5):484-98.
75. Fischer N, Preuße C, Radke J, Pehl D, Allenbach Y, Schneider U, et al. Sequestosome-1 (p62) expression reveals chaperone-assisted selective autophagy in immune-mediated necrotizing myopathies. Brain Pathol. 2020;30(2):261-71.
76. Nagy S, Khan A, Machado PM, Houlden H. Inclusion body myositis: from genetics to clinical trials. J Neurol. 2022.

77. Rothwell S, Cooper RG, Lundberg IE, Gregersen PK, Hanna MG, Machado PM, et al. Immune-Array Analysis in Sporadic Inclusion Body Myositis Reveals HLA-DRB1 Amino Acid Heterogeneity Across the Myositis Spectrum. Arthritis Rheumatol. 2017;69(5):1090-9.
78. Gang Q, Bettencourt C, Machado PM, Brady S, Holton JL, Pittman AM, et al. Rare variants in SQSTM1 and VCP genes and risk of sporadic inclusion body myositis. Neurobiol Aging. 2016;47:218.e1-.e9.
79. Weihl CC, Baloh RH, Lee Y, Chou TF, Pittman SK, Lopate G, et al. Targeted sequencing and identification of genetic variants in sporadic inclusion body myositis. Neuromuscul Disord. 2015;25(4):289-96.
80. Hedberg-Oldfors C, Lindgren U, Basu S, Visuttijai K, Lindberg C, Falkenberg M, et al. Mitochondrial DNA variants in inclusion body myositis characterized by deep sequencing. Brain Pathol. 2021;31(3):e12931.
81. Scofield RH, Lewis VM, Cavitt J, Kurien BT, Assassi S, Martin J, et al. 47XXY and 47XXX in Scleroderma and Myositis. ACR Open Rheumatol. 2022;4(6):528-33.
82. de Boer EMJ, Orie VK, Williams T, Baker MR, De Oliveira HM, Polvikoski T, et al. TDP-43 proteinopathies: a new wave of neurodegenerative diseases. J Neurol Neurosurg Psychiatry. 2020;92(1):86-95.
83. Takagi S, Iguchi Y, Katsuno M, Ishigaki S, Ikenaka K, Fujioka Y, et al. RNP2 of RNA recognition motif 1 plays a central role in the aberrant modification of TDP-43. PloS one. 2013;8(6):e66966.
84. Ederle H, Funk C, Abou-Ajram C, Hutten S, Funk EBE, Kehlenbach RH, et al. Nuclear egress of TDP-43 and FUS occurs independently of Exportin-1/CRM1. Sci Rep. 2018;8(1):7084.
85. Pinarbasi ES, Cağatay T, Fung HYJ, Li YC, Chook YM, Thomas PJ. Active nuclear import and passive nuclear export are the primary determinants of TDP-43 localization. Sci Rep. 2018;8(1):7083.
86. Nishimura AL, Zupunski V, Troakes C, Kathe C, Fratta P, Howell M, et al. Nuclear import impairment causes cytoplasmic trans-activation response DNA-binding protein accumulation and is associated with frontotemporal lobar degeneration. Brain. 2010;133(Pt 6):1763-71.
87. Winton MJ, Igaz LM, Wong MM, Kwong LK, Trojanowski JQ, Lee VM. Disturbance of nuclear and cytoplasmic TAR DNA-binding protein (TDP-43) induces disease-like redistribution, sequestration, and aggregate formation. J Biol Chem. 2008;283(19):13302-9.
88. Prasad A, Bharathi V, Sivalingam V, Girdhar A, Patel BK. Molecular Mechanisms of TDP-43 Misfolding and Pathology in Amyotrophic Lateral Sclerosis. Front Mol Neurosci. 2019;12:25.
89. Palomo V, Tosat-Bitrian C, Nozal V, Nagaraj S, Martin-Requero A, Martinez A. TDP-43: A Key Therapeutic Target beyond Amyotrophic Lateral Sclerosis. ACS Chem Neurosci. 2019;10(3):1183-96.
90. Khalfallah Y, Kuta R, Grasmuck C, Prat A, Durham HD, Vande Velde C. TDP-43 regulation of stress granule dynamics in neurodegenerative disease-relevant cell types. Sci Rep. 2018;8(1):7551.
91. Ayala YM, De Conti L, Avendaño-Vázquez SE, Dhir A, Romano M, D'Ambrogio A, et al. TDP-43 regulates its mRNA levels through a negative feedback loop. Embo j. 2011;30(2):277-88.
92. Avendaño-Vázquez SE, Dhir A, Bembich S, Buratti E, Proudfoot N, Baralle FE. Autoregulation of TDP-43 mRNA levels involves interplay between transcription, splicing, and alternative polyA site selection. Genes Dev. 2012;26(15):1679-84.
93. Sreedharan J, Blair IP, Tripathi VB, Hu X, Vance C, Rogelj B, et al. TDP-43 mutations in familial and sporadic amyotrophic lateral sclerosis. Science. 2008;319(5870):1668-72.
94. Su XW, Broach JR, Connor JR, Gerhard GS, Simmons Z. Genetic heterogeneity of amyotrophic lateral sclerosis: implications for clinical practice and research. Muscle & nerve. 2014;49(6):786-803.

95. Dubourg O, Wanschitz J, Maisonobe T, Béhin A, Allenbach Y, Herson S, et al. Diagnostic value of markers of muscle degeneration in sporadic inclusion body myositis. Acta Myol. 2011;30(2):103-8.
96. Olivé M, Janué A, Moreno D, Gámez J, Torrejón-Escribano B, Ferrer I. TAR DNA-Binding protein 43 accumulation in protein aggregate myopathies. J Neuropathol Exp Neurol. 2009;68(3):262-73.
97. Weihl CC, Temiz P, Miller SE, Watts G, Smith C, Forman M, et al. TDP-43 accumulation in inclusion body myopathy muscle suggests a common pathogenic mechanism with frontotemporal dementia. J Neurol Neurosurg Psychiatry. 2008;79(10):1186-9.
98. Huntley ML, Gao J, Termsarasab P, Wang L, Zeng S, Thammongkolchai T, et al. Association between TDP-43 and mitochondria in inclusion body myositis. Lab Invest. 2019;99(7):1041-8.
99. Cortese A, Plagnol V, Brady S, Simone R, Lashley T, Acevedo-Arozena A, et al. Widespread RNA metabolism impairment in sporadic inclusion body myositis TDP43-proteinopathy. Neurobiol Aging. 2014;35(6):1491-8.
100. Salajegheh M, Pinkus JL, Taylor JP, Amato AA, Nazareno R, Baloh RH, et al. Sarcoplasmic redistribution of nuclear TDP-43 in inclusion body myositis. Muscle & nerve. 2009;40(1):19-31.
101. Pesiridis GS, Lee VM, Trojanowski JQ. Mutations in TDP-43 link glycine-rich domain functions to amyotrophic lateral sclerosis. Hum Mol Genet. 2009;18(R2):R156-62.
102. Hiniker A, Daniels BH, Lee HS, Margeta M. Comparative utility of LC3, p62 and TDP-43 immunohistochemistry in differentiation of inclusion body myositis from polymyositis and related inflammatory myopathies. Acta Neuropathol Commun. 2013;1:29-.
103. Versluys L, Ervilha Pereira P, Schuermans N, De Paepe B, De Bleecker JL, Bogaert E, et al. Expanding the TDP-43 Proteinopathy Pathway From Neurons to Muscle: Physiological and Pathophysiological Functions. Front Neurosci. 2022;16:815765.
104. Igaz LM, Kwong LK, Lee EB, Chen-Plotkin A, Swanson E, Unger T, et al. Dysregulation of the ALS-associated gene TDP-43 leads to neuronal death and degeneration in mice. The Journal of clinical investigation. 2011;121(2):726-38.
105. Ma XR, Prudencio M, Koike Y, Vatsavayai SC, Kim G, Harbinski F, et al. TDP-43 represses cryptic exon inclusion in the FTD-ALS gene UNC13A. Nature. 2022;603(7899):124-30.
106. Torres P, Ramírez-Núñez O, Romero-Guevara R, Barés G, Granado-Serrano AB, Ayala V, et al. Cryptic exon splicing function of TARDBP interacts with autophagy in nervous tissue. Autophagy. 2018;14(8):1398-403.
107. Ling JP, Pletnikova O, Troncoso JC, Wong PC. TDP-43 repression of nonconserved cryptic exons is compromised in ALS-FTD. Science. 2015;349(6248):650-5.
108. Jeong YH, Ling JP, Lin SZ, Donde AN, Braunstein KE, Majounie E, et al. Tdp-43 cryptic exons are highly variable between cell types. Mol Neurodegener. 2017;12(1):13.
109. Šušnjar U, Škrabar N, Brown AL, Abbassi Y, Phatnani H, Cortese A, et al. Cell environment shapes TDP-43 function with implications in neuronal and muscle disease. Commun Biol. 2022;5(1):314.
110. Britson KA, Ling JP, Braunstein KE, Montagne JM, Kastenschmidt JM, Wilson A, et al. Loss of TDP-43 function and rimmed vacuoles persist after T cell depletion in a xenograft model of sporadic inclusion body myositis. Sci Transl Med. 2022;14(628):eabi9196.
111. Liu WJ, Ye L, Huang WF, Guo LJ, Xu ZG, Wu HL, et al. p62 links the autophagy pathway and the ubiqutin-proteasome system upon ubiquitinated protein degradation. Cell Mol Biol Lett. 2016;21:29.
112. Tanaka K. The proteasome: overview of structure and functions. Proc Jpn Acad Ser B Phys Biol Sci. 2009;85(1):12-36.

113. Babu JR, Geetha T, Wooten MW. Sequestosome 1/p62 shuttles polyubiquitinated tau for proteasomal degradation. J Neurochem. 2005;94(1):192-203.
114. Shin WH, Park JH, Chung KC. The central regulator p62 between ubiquitin proteasome system and autophagy and its role in the mitophagy and Parkinson's disease. BMB Rep. 2020;53(1):56-63.
115. Zaffagnini G, Savova A, Danieli A, Romanov J, Tremel S, Ebner M, et al. p62 filaments capture and present ubiquitinated cargos for autophagy. Embo j. 2018;37(5).
116. Nogalska A, Terracciano C, D'Agostino C, King Engel W, Askanas V. p62/SQSTM1 is overexpressed and prominently accumulated in inclusions of sporadic inclusion-body myositis muscle fibers, and can help differentiating it from polymyositis and dermatomyositis. Acta Neuropathol. 2009;118(3):407-13.
117. Girolamo F, Lia A, Annese T, Giannini M, Amati A, D'Abbicco D, et al. Autophagy markers LC3 and p62 accumulate in immune-mediated necrotizing myopathy. Muscle & nerve. 2019;60(3):315-27.
118. Nakano S, Oki M, Kusaka H. The role of p62/SQSTM1 in sporadic inclusion body myositis. Neuromuscul Disord. 2017;27(4):363-9.
119. Milisenda JC, Pinal-Fernandez I, Lloyd TE, Grau JM, Miller FW, Selva-O'Callaghan A, et al. Accumulation of autophagosome cargo protein p62 is common in idiopathic inflammatory myopathies. Clin Exp Rheumatol. 2021;39(2):351-6.
120. Naddaf E. Inclusion body myositis: Update on the diagnostic and therapeutic landscape. Front Neurol. 2022;13:1020113.
121. Greenberg SA, Pinkus GS, Amato AA, Pinkus JL. Myeloid dendritic cells in inclusion-body myositis and polymyositis. Muscle Nerve. 2007;35(1):17-23.
122. Roos A, Preusse C, Hathazi D, Goebel H-H, Stenzel W. Proteomic Profiling Unravels a Key Role of Specific Macrophage Subtypes in Sporadic Inclusion Body Myositis. Front Immunol. 2019;10:1040-.
123. Jensen KY, Jacobsen M, Schrøder HD, Aagaard P, Nielsen JL, Jørgensen AN, et al. The immune system in sporadic inclusion body myositis patients is not compromised by blood-flow restricted exercise training. Arthritis Res Ther. 2019;21(1):293-.
124. Greenberg SA, Pinkus JL, Kong SW, Baecher-Allan C, Amato AA, Dorfman DM. Highly differentiated cytotoxic T cells in inclusion body myositis. Brain. 2019;142(9):2590-604.
125. Allenbach Y, Chaara W, Rosenzwajg M, Six A, Prevel N, Mingozzi F, et al. Th1 response and systemic treg deficiency in inclusion body myositis. PloS one. 2014;9(3):e88788.
126. Tau GZ, Cowan SN, Weisburg J, Braunstein NS, Rothman PB. Regulation of IFN-gamma signaling is essential for the cytotoxic activity of CD8(+) T cells. J Immunol. 2001;167(10):5574-82.
127. Tokunaga R, Zhang W, Naseem M, Puccini A, Berger MD, Soni S, et al. CXCL9, CXCL10, CXCL11/CXCR3 axis for immune activation - A target for novel cancer therapy. Cancer Treat Rev. 2018;63:40-7.
128. Mendez-Enriquez E, García-Zepeda EA. The multiple faces of CCL13 in immunity and inflammation. Inflammopharmacology. 2013;21(6):397-406.
129. Gschwandtner M, Derler R, Midwood KS. More Than Just Attractive: How CCL2 Influences Myeloid Cell Behavior Beyond Chemotaxis. Front Immunol. 2019;10:2759.
130. Dayer JM, Oliviero F, Punzi L. A Brief History of IL-1 and IL-1 Ra in Rheumatology. Front Pharmacol. 2017;8:293.
131. Mantovani A, Dinarello CA, Molgora M, Garlanda C. Interleukin-1 and Related Cytokines in the Regulation of Inflammation and Immunity. Immunity. 2019;50(4):778-95.
132. Dinarello CA. Overview of the IL-1 family in innate inflammation and acquired immunity. Immunol Rev. 2018;281(1):8-27.

133. Davis CN, Mann E, Behrens MM, Gaidarova S, Rebek M, Rebek J, Jr., et al. MyD88-dependent and -independent signaling by IL-1 in neurons probed by bifunctional Toll/IL-1 receptor domain/BB-loop mimetics. Proc Natl Acad Sci U S A. 2006;103(8):2953-8.
134. Liu T, Zhang L, Joo D, Sun SC. NF-κB signaling in inflammation. Signal Transduct Target Ther. 2017;2:17023-.
135. Grundtman C, Salomonsson S, Dorph C, Bruton J, Andersson U, Lundberg IE. Immunolocalization of interleukin-1 receptors in the sarcolemma and nuclei of skeletal muscle in patients with idiopathic inflammatory myopathies. Arthritis Rheum. 2007;56(2):674-87.
136. Authier FJ, Chazaud B, Plonquet A, Eliezer-Vanerot MC, Poron F, Belec L, et al. Differential expression of the IL-1 system components during in vitro myogenesis: implication of IL-1beta in induction of myogenic cell apoptosis. Cell Death Differ. 1999;6(10):1012-21.
137. Cerqueira É, Marinho DA, Neiva HP, Lourenço O. Inflammatory Effects of High and Moderate Intensity Exercise-A Systematic Review. Frontiers in physiology. 2019;10:1550.
138. Luo G, Hershko DD, Robb BW, Wray CJ, Hasselgren PO. IL-1beta stimulates IL-6 production in cultured skeletal muscle cells through activation of MAP kinase signaling pathway and NF-kappa B. Am J Physiol Regul Integr Comp Physiol. 2003;284(5):R1249-54.
139. Huang N, Kny M, Riediger F, Busch K, Schmidt S, Luft FC, et al. Deletion of Nlrp3 protects from inflammation-induced skeletal muscle atrophy. Intensive Care Med Exp. 2017;5(1):3.
140. Grabiec K, Tokarska J, Milewska M, Błaszczyk M, Gajewska M, Grzelkowska-Kowalczyk K. Interleukin-1beta stimulates early myogenesis of mouse C2C12 myoblasts: the impact on myogenic regulatory factors, extracellular matrix components, IGF binding proteins and protein kinases. Pol J Vet Sci. 2013;16(2):255-64.
141. Otis JS, Niccoli S, Hawdon N, Sarvas JL, Frye MA, Chicco AJ, et al. Pro-inflammatory mediation of myoblast proliferation. PloS one. 2014;9(3):e92363.
142. Tews DS, Goebel HH. Cytokine expression profile in idiopathic inflammatory myopathies. J Neuropathol Exp Neurol. 1996;55(3):342-7.
143. Lepidi H, Frances V, Figarella-Branger D, Bartoli C, Machado-Baeta A, Pellissier JF. Local expression of cytokines in idiopathic inflammatory myopathies. Neuropathol Appl Neurobiol. 1998;24(1):73-9.
144. Authier FJ, Mhiri C, Chazaud B, Christov C, Cherin P, Barlovatz-Meimon G, et al. Interleukin-1 expression in inflammatory myopathies: evidence of marked immunoreactivity in sarcoid granulomas and muscle fibres showing ischaemic and regenerative changes. Neuropathol Appl Neurobiol. 1997;23(2):132-40.
145. Schmidt J, Barthel K, Wrede A, Salajegheh M, Bähr M, Dalakas MC. Interrelation of inflammation and APP in sIBM: IL-1 beta induces accumulation of beta-amyloid in skeletal muscle. Brain. 2008;131(Pt 5):1228-40.
146. Netea MG, Simon A, van de Veerdonk F, Kullberg BJ, Van der Meer JW, Joosten LA. IL-1beta processing in host defense: beyond the inflammasomes. PLoS Pathog. 2010;6(2):e1000661.
147. Schroder K, Hertzog PJ, Ravasi T, Hume DA. Interferon-gamma: an overview of signals, mechanisms and functions. J Leukoc Biol. 2004;75(2):163-89.
148. Castro F, Cardoso AP, Gonçalves RM, Serre K, Oliveira MJ. Interferon-Gamma at the Crossroads of Tumor Immune Surveillance or Evasion. Front Immunol. 2018;9:847.
149. Platanias LC. Mechanisms of type-I- and type-II-interferon-mediated signalling. Nat Rev Immunol. 2005;5(5):375-86.
150. Majoros A, Platanitis E, Kernbauer-Hölzl E, Rosebrock F, Müller M, Decker T. Canonical and Non-Canonical Aspects of JAK-STAT Signaling: Lessons from Interferons for Cytokine Responses. Front Immunol. 2017;8:29.

151. Green DS, Young HA, Valencia JC. Current prospects of type II interferon γ signaling and autoimmunity. J Biol Chem. 2017;292(34):13925-33.
152. Cheng M, Nguyen MH, Fantuzzi G, Koh TJ. Endogenous interferon-gamma is required for efficient skeletal muscle regeneration. American journal of physiology Cell physiology. 2008;294(5):C1183-91.
153. Lipski DA, Dewispelaere R, Foucart V, Caspers LE, Defrance M, Bruyns C, et al. MHC class II expression and potential antigen-presenting cells in the retina during experimental autoimmune uveitis. J Neuroinflammation. 2017;14(1):136.
154. Steimle V, Siegrist CA, Mottet A, Lisowska-Grospierre B, Mach B. Regulation of MHC class II expression by interferon-gamma mediated by the transactivator gene CIITA. Science. 1994;265(5168):106-9.
155. Reith W, LeibundGut-Landmann S, Waldburger JM. Regulation of MHC class II gene expression by the class II transactivator. Nat Rev Immunol. 2005;5(10):793-806.
156. Londhe P, Davie JK. Gamma interferon modulates myogenesis through the major histocompatibility complex class II transactivator, CIITA. Molecular and cellular biology. 2011;31(14):2854-66.
157. Mantegazza R, Hughes SM, Mitchell D, Travis M, Blau HM, Steinman L. Modulation of MHC class II antigen expression in human myoblasts after treatment with IFN-gamma. Neurology. 1991;41(7):1128-32.
158. Foster W, Li Y, Usas A, Somogyi G, Huard J. Gamma interferon as an antifibrosis agent in skeletal muscle. J Orthop Res. 2003;21(5):798-804.
159. Chen Z, Li B, Zhan RZ, Rao L, Bursac N. Exercise mimetics and JAK inhibition attenuate IFN-γ-induced wasting in engineered human skeletal muscle. Sci Adv. 2021;7(4).
160. Ferrington DA, Gregerson DS. Immunoproteasomes: structure, function, and antigen presentation. Prog Mol Biol Transl Sci. 2012;109:75-112.
161. Liu HM, Ferrington DA, Baumann CW, Thompson LV. Denervation-Induced Activation of the Standard Proteasome and Immunoproteasome. PloS one. 2016;11(11):e0166831.
162. Cui Z, Hwang SM, Gomes AV. Identification of the immunoproteasome as a novel regulator of skeletal muscle differentiation. Molecular and cellular biology. 2014;34(1):96-109.
163. Ferrington DA, Husom AD, Thompson LV. Altered proteasome structure, function, and oxidation in aged muscle. Faseb j. 2005;19(6):644-6.
164. Farini A, Sitzia C, Cassani B, Cassinelli L, Rigoni R, Colleoni F, et al. Therapeutic Potential of Immunoproteasome Inhibition in Duchenne Muscular Dystrophy. Mol Ther. 2016;24(11):1898-912.
165. Racioppi L, Means AR. Calcium/calmodulin-dependent kinase IV in immune and inflammatory responses: novel routes for an ancient traveller. Trends Immunol. 2008;29(12):600-7.
166. Naz H, Islam A, Ahmad F, Hassan MI. Calcium/calmodulin-dependent protein kinase IV: A multifunctional enzyme and potential therapeutic target. Prog Biophys Mol Biol. 2016;121(1):54-65.
167. Gu R, Ding M, Shi D, Huang T, Guo M, Yu L, et al. Calcium/Calmodulin-Dependent Protein Kinase IV Mediates IFN-γ-Induced Immune Behaviors in Skeletal Muscle Cells. Cell Physiol Biochem. 2018;46(1):351-64.
168. Ding M, Huang T, Zhu R, Gu R, Shi D, Xiao J, et al. Immunological Behavior Analysis of Muscle Cells under IFN-γ Stimulation in Vitro and in Vivo. Anat Rec (Hoboken). 2018;301(9):1551-63.
169. Adhikari A, Cobb B, Eddington S, Becerra N, Kohli P, Pond A, et al. IFN-γ and CIITA modulate IL-6 expression in skeletal muscle. Cytokine X. 2020;2(2):100023.

170. Li P, Zhao Y, Wu X, Xia M, Fang M, Iwasaki Y, et al. Interferon gamma (IFN-γ) disrupts energy expenditure and metabolic homeostasis by suppressing SIRT1 transcription. Nucleic Acids Res. 2012;40(4):1609-20.
171. Elibol B, Kilic U. High Levels of SIRT1 Expression as a Protective Mechanism Against Disease-Related Conditions. Front Endocrinol (Lausanne). 2018;9:614.
172. Rahman S, Islam R. Mammalian Sirt1: insights on its biological functions. Cell Commun Signal. 2011;9:11.
173. Fang M, Fan Z, Tian W, Zhao Y, Li P, Xu H, et al. HDAC4 mediates IFN-γ induced disruption of energy expenditure-related gene expression by repressing SIRT1 transcription in skeletal muscle cells. Biochim Biophys Acta. 2016;1859(2):294-305.
174. Rigolet M, Hou C, Baba Amer Y, Aouizerate J, Periou B, Gherardi RK, et al. Distinct interferon signatures stratify inflammatory and dysimmune myopathies. RMD Open. 2019;5(1):e000811.
175. Kim BH, Shenoy AR, Kumar P, Das R, Tiwari S, MacMicking JD. A family of IFN-γ-inducible 65-kD GTPases protects against bacterial infection. Science. 2011;332(6030):717-21.
176. Pinal-Fernandez I, Casal-Dominguez M, Derfoul A, Pak K, Miller FW, Milisenda JC, et al. Machine learning algorithms reveal unique gene expression profiles in muscle biopsies from patients with different types of myositis. Ann Rheum Dis. 2020;79(9):1234-42.
177. Bhattarai S, Ghannam K, Krause S, Benveniste O, Marg A, de Bruin G, et al. The immunoproteasomes are key to regulate myokines and MHC class I expression in idiopathic inflammatory myopathies. J Autoimmun. 2016;75:118-29.
178. Murphy K, Weaver C. Janeway's Immunobiology 9th edition. New York and London: Garland Science, Taylor & Francis Group, LLC; 2017.
179. Raskov H, Orhan A, Christensen JP, Gögenur I. Cytotoxic CD8(+) T cells in cancer and cancer immunotherapy. Br J Cancer. 2021;124(2):359-67.
180. Stinchcombe JC, Bossi G, Booth S, Griffiths GM. The immunological synapse of CTL contains a secretory domain and membrane bridges. Immunity. 2001;15(5):751-61.
181. Basu R, Whitlock BM, Husson J, Le Floc'h A, Jin W, Oyler-Yaniv A, et al. Cytotoxic T Cells Use Mechanical Force to Potentiate Target Cell Killing. Cell. 2016;165(1):100-10.
182. van Daalen KR, Reijneveld JF, Bovenschen N. Modulation of Inflammation by Extracellular Granzyme A. Front Immunol. 2020;11:931.
183. Chávez-Galán L, Arenas-Del Angel MC, Zenteno E, Chávez R, Lascurain R. Cell death mechanisms induced by cytotoxic lymphocytes. Cell Mol Immunol. 2009;6(1):15-25.
184. Bouwman AC, van Daalen KR, Crnko S, Ten Broeke T, Bovenschen N. Intracellular and Extracellular Roles of Granzyme K. Front Immunol. 2021;12:677707.
185. Wei MC, Lindsten T, Mootha VK, Weiler S, Gross A, Ashiya M, et al. tBID, a membrane-targeted death ligand, oligomerizes BAK to release cytochrome c. Genes Dev. 2000;14(16):2060-71.
186. Enari M, Sakahira H, Yokoyama H, Okawa K, Iwamatsu A, Nagata S. A caspase-activated DNase that degrades DNA during apoptosis, and its inhibitor ICAD. Nature. 1998;391(6662):43-50.
187. Slee EA, Adrain C, Martin SJ. Executioner caspase-3, -6, and -7 perform distinct, non-redundant roles during the demolition phase of apoptosis. J Biol Chem. 2001;276(10):7320-6.
188. בסלו ס. File:CTL killing strategies.png Wikimedia Commons: Wikimedia Commons; [Available from: https://commons.wikimedia.org/wiki/File:CTL_killing_strategies.png.
189. Hassin D, Garber OG, Meiraz A, Schiffenbauer YS, Berke G. Cytotoxic T lymphocyte perforin and Fas ligand working in concert even when Fas ligand lytic action is still not detectable. Immunology. 2011;133(2):190-6.

190. Mirandola P, Ponti C, Gobbi G, Sponzilli I, Vaccarezza M, Cocco L, et al. Activated human NK and CD8+ T cells express both TNF-related apoptosis-inducing ligand (TRAIL) and TRAIL receptors but are resistant to TRAIL-mediated cytotoxicity. Blood. 2004;104(8):2418-24.
191. Martin MD, Badovinac VP. Defining Memory CD8 T Cell. Front Immunol. 2018;9:2692.
192. Lee SW, Choi HY, Lee GW, Kim T, Cho HJ, Oh IJ, et al. CD8(+) TILs in NSCLC differentiate into TEMRA via a bifurcated trajectory: deciphering immunogenicity of tumor antigens. J Immunother Cancer. 2021;9(9).
193. Larbi A, Fulop T. From "truly naïve" to "exhausted senescent" T cells: when markers predict functionality. Cytometry A. 2014;85(1):25-35.
194. Janeway CA Jr TP, Walport M, et al. Immunobiology: The Immune System in Health and Disease. 5th edition. New York: Garland Science; 2001.
195. Barnhart BC, Peter ME. The TNF receptor 1: a split personality complex. Cell. 2003;114(2):148-50.
196. Borys SM, Bag AK, Brossay L, Adeegbe DO. The Yin and Yang of Targeting KLRG1(+) Tregs and Effector Cells. Front Immunol. 2022;13:894508.
197. Herndler-Brandstetter D, Ishigame H, Shinnakasu R, Plajer V, Stecher C, Zhao J, et al. KLRG1(+) Effector CD8(+) T Cells Lose KLRG1, Differentiate into All Memory T Cell Lineages, and Convey Enhanced Protective Immunity. Immunity. 2018;48(4):716-29.e8.
198. Matsubara S, Suzuki S, Komori T. Immunohistochemical Phenotype of T Cells Invading Muscle in Inclusion Body Myositis. J Neuropathol Exp Neurol. 2022;81(10):825-35.
199. Kared H, Martelli S, Ng TP, Pender SL, Larbi A. CD57 in human natural killer cells and T-lymphocytes. Cancer Immunol Immunother. 2016;65(4):441-52.
200. Koch S, Larbi A, Derhovanessian E, Ozcelik D, Naumova E, Pawelec G. Multiparameter flow cytometric analysis of CD4 and CD8 T cell subsets in young and old people. Immun Ageing. 2008;5:6.
201. Johari M, Vihola A, Palmio J, Jokela M, Jonson PH, Sarparanta J, et al. Comprehensive transcriptomic analysis shows disturbed calcium homeostasis and deregulation of T lymphocyte apoptosis in inclusion body myositis. J Neurol. 2022;269(8):4161-73.
202. Nelke C, Pawlitzki M, Schroeter CB, Huntemann N, Räuber S, Dobelmann V, et al. High-Dimensional Cytometry Dissects Immunological Fingerprints of Idiopathic Inflammatory Myopathies. Cells. 2022;11(20).
203. Benveniste O, Guiguet M, Freebody J, Dubourg O, Squier W, Maisonobe T, et al. Long-term observational study of sporadic inclusion body myositis. Brain. 2011;134(Pt 11):3176-84.
204. Dobloug C, Walle-Hansen R, Gran JT, Molberg Ø. Long-term follow-up of sporadic inclusion body myositis treated with intravenous immunoglobulin: a retrospective study of 16 patients. Clin Exp Rheumatol. 2012;30(6):838-42.
205. Dalakas MC, Sonies B, Dambrosia J, Sekul E, Cupler E, Sivakumar K. Treatment of inclusion-body myositis with IVIg: a double-blind, placebo-controlled study. Neurology. 1997;48(3):712-6.
206. Dalakas MC, Koffman B, Fujii M, Spector S, Sivakumar K, Cupler E. A controlled study of intravenous immunoglobulin combined with prednisone in the treatment of IBM. Neurology. 2001;56(3):323-7.
207. Ryan DH. Next Generation Antiobesity Medications: Setmelanotide, Semaglutide, Tirzepatide and Bimagrumab: What do They Mean for Clinical Practice? J Obes Metab Syndr. 2021;30(3):196-208.
208. Rooks DS, Laurent D, Praestgaard J, Rasmussen S, Bartlett M, Tankó LB. Effect of bimagrumab on thigh muscle volume and composition in men with casting-induced atrophy. J Cachexia Sarcopenia Muscle. 2017;8(5):727-34.

209. Lach-Trifilieff E, Minetti GC, Sheppard K, Ibebunjo C, Feige JN, Hartmann S, et al. An antibody blocking activin type II receptors induces strong skeletal muscle hypertrophy and protects from atrophy. Molecular and cellular biology. 2014;34(4):606-18.
210. Hanna MG, Badrising UA, Benveniste O, Lloyd TE, Needham M, Chinoy H, et al. Safety and efficacy of intravenous bimagrumab in inclusion body myositis (RESILIENT): a randomised, double-blind, placebo-controlled phase 2b trial. Lancet Neurol. 2019;18(9):834-44.
211. Amato AA, Hanna MG, Machado PM, Badrising UA, Chinoy H, Benveniste O, et al. Efficacy and Safety of Bimagrumab in Sporadic Inclusion Body Myositis: Long-term Extension of RESILIENT. Neurology. 2021;96(12):e1595-e607.
212. Mariot V, Joubert R, Hourdé C, Féasson L, Hanna M, Muntoni F, et al. Downregulation of myostatin pathway in neuromuscular diseases may explain challenges of anti-myostatin therapeutic approaches. Nat Commun. 2017;8(1):1859.
213. Sachdev R, Kappes-Horn K, Paulsen L, Duernberger Y, Pleschka C, Denner P, et al. Endoplasmic Reticulum Stress Induces Myostatin High Molecular Weight Aggregates and Impairs Mature Myostatin Secretion. Mol Neurobiol. 2018;55(11):8355-73.
214. Mahoudeau A, Anquetil C, Tawara N, Khademian H, Amelin D, Bolko L, et al. Myostatin in idiopathic inflammatory myopathies: Serum assessment and disease activity. Neuropathol Appl Neurobiol. 2022:e12849.
215. Lilleker JB, Bukhari M, Chinoy H. Rapamycin for inclusion body myositis: targeting non-inflammatory mechanisms. Rheumatology (Oxford). 58. England2019. p. 375-6.
216. Benveniste O, Hogrel J-Y, Belin L, Annoussamy M, Bachasson D, Rigolet A, et al. Sirolimus for treatment of patients with inclusion body myositis: a randomised, double-blind, placebo-controlled, proof-of-concept, phase 2b trial. The Lancet Rheumatology. 2021;3(1):e40-e8.
217. Pawlitzki M, Nelke C, Korsen M, Meuth SG, Ruck T. Sirolimus leads to rapid and sustained clinical improvement of motor deficits in a patient with inclusion body myositis. Eur J Neurol. 2022;29(4):1284-7.
218. Mengel E, Patterson MC, Da Riol RM, Del Toro M, Deodato F, Gautschi M, et al. Efficacy and safety of arimoclomol in Niemann-Pick disease type C: Results from a double-blind, randomised, placebo-controlled, multinational phase 2/3 trial of a novel treatment. J Inherit Metab Dis. 2021;44(6):1463-80.
219. Ahmed M, Machado PM, Miller A, Spicer C, Herbelin L, He J, et al. Targeting protein homeostasis in sporadic inclusion body myositis. Sci Transl Med. 2016;8(331):331ra41.
220. Orphazyme announces topline results from pivotal trial of

arimoclomol for Inclusion Body Myositis (IBM) [press release]. Orphazyme, 12/2021 2021.
221. Jørgensen AN, Aagaard P, Frandsen U, Boyle E, Diederichsen LP. Blood-flow restricted resistance training in patients with sporadic inclusion body myositis: a randomized controlled trial. Scand J Rheumatol. 2018;47(5):400-9.
222. Jensen KY, Nielsen JL, Schrøder HD, Jacobsen M, Boyle E, Jørgensen AN, et al. Lack of muscle stem cell proliferation and myocellular hypertrophy in sIBM patients following blood-flow restricted resistance training. Neuromuscul Disord. 2022;32(6):493-502.
223. Barohn RJ, Herbelin L, Kissel JT, King W, McVey AL, Saperstein DS, et al. Pilot trial of etanercept in the treatment of inclusion-body myositis. Neurology. 2006;66(2 Suppl 1):S123-4.
224. Kosmidis ML, Alexopoulos H, Tzioufas AG, Dalakas MC. The effect of anakinra, an IL1 receptor antagonist, in patients with sporadic inclusion body myositis (sIBM): a small pilot study. J Neurol Sci. 2013;334(1-2):123-5.
225. Sfriso P, Bindoli S, Doria A, Feist E, Galozzi P. Canakinumab for the treatment of adult-onset Still's disease. Expert Rev Clin Immunol. 2020;16(2):129-38.

226. Kosmidis ML, Pikazis D, Vlachoyiannopoulos P, Tzioufas AG, Dalakas MC. Trial of canakinumab, an IL-1β receptor antagonist, in patients with inclusion body myositis. Neurol Neuroimmunol Neuroinflamm. 2019;6(4):e581.
227. Goel N, Needham M, Soler-Ferran D, Cotreau MM, Escobar J, Greenberg S. POS1342 DEPLETION OF KLRG1+ T CELLS IN A FIRST-IN-HUMAN CLINICAL TRIAL OF ABC008 IN INCLUSION BODY MYOSITIS (IBM). Annals of the Rheumatic Diseases. 2022;81(Suppl 1):1008.
228. Alfano LN, Focht Garand KL, Malandraki GA, Salam S, Machado PM, Dimachkie MM. Measuring change in inclusion body myositis: clinical assessments versus imaging. Clin Exp Rheumatol. 2022;40(2):404-13.
229. Laurent D, Riek J, Sinclair CDJ, Houston P, Roubenoff R, Papanicolaou DA, et al. Longitudinal Changes in MRI Muscle Morphometry and Composition in People With Inclusion Body Myositis. Neurology. 2022;99(9):e865-e76.
230. Cox FM, Reijnierse M, van Rijswijk CS, Wintzen AR, Verschuuren JJ, Badrising UA. Magnetic resonance imaging of skeletal muscles in sporadic inclusion body myositis. Rheumatology (Oxford). 2011;50(6):1153-61.
231. Ansari B, Salort-Campana E, Ogier A, Le Troter Ph DA, De Sainte Marie B, Guye M, et al. Quantitative muscle MRI study of patients with sporadic inclusion body myositis. Muscle Nerve. 2020;61(4):496-503.
232. Findlay AR, Goyal NA, Mozaffar T. An overview of polymyositis and dermatomyositis. Muscle & nerve. 2015;51(5):638-56.
233. Lundberg IE, Fujimoto M, Vencovsky J, Aggarwal R, Holmqvist M, Christopher-Stine L, et al. Idiopathic inflammatory myopathies. Nat Rev Dis Primers. 2021;7(1):86.
234. Oray M, Abu Samra K, Ebrahimiadib N, Meese H, Foster CS. Long-term side effects of glucocorticoids. Expert Opin Drug Saf. 2016;15(4):457-65.
235. Malik A, Hayat G, Kalia JS, Guzman MA. Idiopathic Inflammatory Myopathies: Clinical Approach and Management. Front Neurol. 2016;7:64.
236. Witt LJ, Curran JJ, Strek ME. The Diagnosis and Treatment of Antisynthetase Syndrome. Clin Pulm Med. 2016;23(5):218-26.
237. Yang SH, Chang C, Lian ZX. Polymyositis and dermatomyositis - challenges in diagnosis and management. J Transl Autoimmun. 2019;2:100018.
238. Mammen AL. Dermatomyositis and polymyositis: Clinical presentation, autoantibodies, and pathogenesis. Ann N Y Acad Sci. 2010;1184:134-53.
239. van der Meulen MF, Bronner IM, Hoogendijk JE, Burger H, van Venrooij WJ, Voskuyl AE, et al. Polymyositis: an overdiagnosed entity. Neurology. 2003;61(3):316-21.
240. Tanboon J, Uruha A, Stenzel W, Nishino I. Where are we moving in the classification of idiopathic inflammatory myopathies? Curr Opin Neurol. 2020;33(5):590-603.
241. Leclair V, Notarnicola A, Vencovsky J, Lundberg IE. Polymyositis: does it really exist as a distinct clinical subset? Curr Opin Rheumatol. 2021;33(6):537-43.
242. Temiz P, Weihl CC, Pestronk A. Inflammatory myopathies with mitochondrial pathology and protein aggregates. J Neurol Sci. 2009;278(1-2):25-9.
243. Kleefeld F, Uruha A, Schänzer A, Nishimura A, Roos A, Schneider U, et al. Morphological and Molecular Patterns of Polymyositis With Mitochondrial Pathology and Inclusion Body Myositis. Neurology. 2022.
244. Kronzer VL, Kimbrough BA, Crowson CS, Davis JM, 3rd, Holmqvist M, Ernste FC. Incidence, Prevalence, and Mortality of Dermatomyositis: A Population-Based Cohort Study. Arthritis Care Res (Hoboken). 2021.
245. Bendewald MJ, Wetter DA, Li X, Davis MD. Incidence of dermatomyositis and clinically amyopathic dermatomyositis: a population-based study in Olmsted County, Minnesota. Arch Dermatol. 2010;146(1):26-30.

246. Ashton C, Paramalingam S, Stevenson B, Brusch A, Needham M. Idiopathic inflammatory myopathies: a review. Intern Med J. 2021;51(6):845-52.
247. Bogdanov I, Kazandjieva J, Darlenski R, Tsankov N. Dermatomyositis: Current concepts. Clin Dermatol. 2018;36(4):450-8.
248. Greenberg SA, Pinkus JL, Pinkus GS, Burleson T, Sanoudou D, Tawil R, et al. Interferon-alpha/beta-mediated innate immune mechanisms in dermatomyositis. Ann Neurol. 2005;57(5):664-78.
249. Liang L, Zhang YM, Chen H, Ye LF, Li SS, Lu X, et al. Anti-Mi-2 antibodies characterize a distinct clinical subset of dermatomyositis with favourable prognosis. Eur J Dermatol. 2020.
250. Tanboon J, Inoue M, Hirakawa S, Tachimori H, Hayashi S, Noguchi S, et al. Pathologic Features of Anti-Mi-2 Dermatomyositis. Neurology. 2021;96(3):e448-e59.
251. Nguyen M, Do V, Yell PC, Jo C, Liu J, Burns DK, et al. Distinct tissue injury patterns in juvenile dermatomyositis auto-antibody subgroups. Acta Neuropathol Commun. 2020;8(1):125.
252. Allenbach Y, Benveniste O, Stenzel W, Boyer O. Immune-mediated necrotizing myopathy: clinical features and pathogenesis. Nat Rev Rheumatol. 2020;16(12):689-701.
253. Merlonghi G, Antonini G, Garibaldi M. Immune-mediated necrotizing myopathy (IMNM): A myopathological challenge. Autoimmun Rev. 2022;21(2):102993.
254. Opinc AH, Makowska JS. Antisynthetase syndrome - much more than just a myopathy. Semin Arthritis Rheum. 2021;51(1):72-83.
255. Wielosz E, Majdan M, Dryglewska M, Targońska-Stępniak B. Overlap syndromes in systemic sclerosis. Postepy Dermatol Alergol. 2018;35(3):246-50.
256. Larman HB, Salajegheh M, Nazareno R, Lam T, Sauld J, Steen H, et al. Cytosolic 5'-nucleotidase 1A autoimmunity in sporadic inclusion body myositis. Ann Neurol. 2013;73(3):408-18.
257. Paul P, Liewluck T, Ernste FC, Mandrekar J, Milone M. Anti-cN1A antibodies do not correlate with specific clinical, EMG or pathological findings in sporadic inclusion body myositis. Muscle & nerve. 2020.
258. Amlani A, Choi MY, Tarnopolsky M, Brady L, Clarke AE, Garcia-De La Torre I, et al. Anti-NT5c1A Autoantibodies as Biomarkers in Inclusion Body Myositis. Front Immunol. 2019;10:745.
259. Pluk H, van Hoeve BJ, van Dooren SH, Stammen-Vogelzangs J, van der Heijden A, Schelhaas HJ, et al. Autoantibodies to cytosolic 5'-nucleotidase 1A in inclusion body myositis. Ann Neurol. 2013;73(3):397-407.
260. Lilleker JB, Rietveld A, Pye SR, Mariampillai K, Benveniste O, Peeters MT, et al. Cytosolic 5'-nucleotidase 1A autoantibody profile and clinical characteristics in inclusion body myositis. Ann Rheum Dis. 2017;76(5):862-8.
261. Tawara N, Yamashita S, Zhang X, Korogi M, Zhang Z, Doki T, et al. Pathomechanisms of anti-cytosolic 5'-nucleotidase 1A autoantibodies in sporadic inclusion body myositis. Ann Neurol. 2017;81(4):512-25.
262. Kramp SL, Karayev D, Shen G, Metzger AL, Morris RI, Karayev E, et al. Development and evaluation of a standardized ELISA for the determination of autoantibodies against cN-1A (Mup44, NT5C1A) in sporadic inclusion body myositis. Auto Immun Highlights. 2016;7(1):16.
263. Goyal NA, Cash TM, Alam U, Enam S, Tierney P, Araujo N, et al. Seropositivity for NT5c1A antibody in sporadic inclusion body myositis predicts more severe motor, bulbar and respiratory involvement. J Neurol Neurosurg Psychiatry. 2016;87(4):373-8.
264. Katsumata Y, Ascherman DP. Animal models in myositis. Curr Opin Rheumatol. 2008;20(6):681-5.
265. Afzali AM, Ruck T, Wiendl H, Meuth SG. Animal models in idiopathic inflammatory myopathies: How to overcome a translational roadblock? Autoimmun Rev. 2017;16(5):478-94.

266. Yeo BK, Yu S-W. Valosin-containing protein (VCP): structure, functions, and implications in neurodegenerative diseases. Animal Cells and Systems. 2016;20(6):303-9.
267. Weihl CC, Pestronk A, Kimonis VE. Valosin-containing protein disease: inclusion body myopathy with Paget's disease of the bone and fronto-temporal dementia. Neuromuscul Disord. 2009;19(5):308-15.
268. Custer SK, Neumann M, Lu H, Wright AC, Taylor JP. Transgenic mice expressing mutant forms VCP/p97 recapitulate the full spectrum of IBMPFD including degeneration in muscle, brain and bone. Hum Mol Genet. 2010;19(9):1741-55.
269. Sugarman MC, Yamasaki TR, Oddo S, Echegoyen JC, Murphy MP, Golde TE, et al. Inclusion body myositis-like phenotype induced by transgenic overexpression of beta APP in skeletal muscle. Proc Natl Acad Sci U S A. 2002;99(9):6334-9.
270. Sugarman MC, Kitazawa M, Baker M, Caiozzo VJ, Querfurth HW, LaFerla FM. Pathogenic accumulation of APP in fast twitch muscle of IBM patients and a transgenic model. Neurobiol Aging. 2006;27(3):423-32.
271. Kelleher RJ, 3rd, Shen J. Presenilin-1 mutations and Alzheimer's disease. Proc Natl Acad Sci U S A. 2017;114(4):629-31.
272. Chen X, Petranovic D. Amyloid-β peptide-induced cytotoxicity and mitochondrial dysfunction in yeast. FEMS Yeast Res. 2015;15(6).
273. Kitazawa M, Green KN, Caccamo A, LaFerla FM. Genetically augmenting Abeta42 levels in skeletal muscle exacerbates inclusion body myositis-like pathology and motor deficits in transgenic mice. Am J Pathol. 2006;168(6):1986-97.
274. Luo YB, Johnsen RD, Griffiths L, Needham M, Fabian VA, Fletcher S, et al. Primary over-expression of AβPP in muscle does not lead to the development of inclusion body myositis in a new lineage of the MCK-AβPP transgenic mouse. Int J Exp Pathol. 2013;94(6):418-25.
275. Jeong JH, Yang DS, Koo JH, Hwang DJ, Cho JY, Kang EB. Effect of Resistance Exercise on Muscle Metabolism and Autophagy in sIBM. Med Sci Sports Exerc. 2017;49(8):1562-71.
276. Koo JH, Kang EB, Cho JY. Resistance Exercise Improves Mitochondrial Quality Control in a Rat Model of Sporadic Inclusion Body Myositis. Gerontology. 2019;65(3):240-52.
277. Chen X, Ghribi O, Geiger JD. Rabbits fed cholesterol-enriched diets exhibit pathological features of inclusion body myositis. Am J Physiol Regul Integr Comp Physiol. 2008;294(3):R829-35.
278. Blau HM, Pavlath GK, Hardeman EC, Chiu CP, Silberstein L, Webster SG, et al. Plasticity of the differentiated state. Science. 1985;230(4727):758-66.
279. Mierzejewski B, Archacka K, Grabowska I, Florkowska A, Ciemerych MA, Brzoska E. Human and mouse skeletal muscle stem and progenitor cells in health and disease. Semin Cell Dev Biol. 2020;104:93-104.
280. Francis TG, Jaka O, Ellison-Hughes GM, Lazarus NR, Harridge SDR. Human primary skeletal muscle-derived myoblasts and fibroblasts reveal different senescent phenotypes. JCSM Rapid Communications. 2022;5(2):226-38.
281. Alsharidah M, Lazarus NR, George TE, Agley CC, Velloso CP, Harridge SD. Primary human muscle precursor cells obtained from young and old donors produce similar proliferative, differentiation and senescent profiles in culture. Aging Cell. 2013;12(3):333-44.
282. Askanas V, McFerrin J, Alvarez RB, Baqué S, Engel WK. Beta APP gene transfer into cultured human muscle induces inclusion-body myositis aspects. Neuroreport. 1997;8(9-10):2155-8.
283. Fratta P, Engel WK, McFerrin J, Davies KJ, Lin SW, Askanas V. Proteasome inhibition and aggresome formation in sporadic inclusion-body myositis and in amyloid-beta precursor protein-overexpressing cultured human muscle fibers. The American journal of pathology. 2005;167(2):517-26.

284. Nogalska A, Wojcik S, Engel WK, McFerrin J, Askanas V. Endoplasmic reticulum stress induces myostatin precursor protein and NF-kappaB in cultured human muscle fibers: relevance to inclusion body myositis. Exp Neurol. 2007;204(2):610-8.
285. Nogalska A, D'Agostino C, Engel WK, Davies KJ, Askanas V. Decreased SIRT1 deacetylase activity in sporadic inclusion-body myositis muscle fibers. Neurobiol Aging. 2010;31(9):1637-48.
286. Wojcik S, Engel WK, McFerrin J, Paciello O, Askanas V. AbetaPP-overexpression and proteasome inhibition increase alphaB-crystallin in cultured human muscle: relevance to inclusion-body myositis. Neuromuscul Disord. 2006;16(12):839-44.
287. Muth IE, Barthel K, Bähr M, Dalakas MC, Schmidt J. Proinflammatory cell stress in sporadic inclusion body myositis muscle: overexpression of alphaB-crystallin is associated with amyloid precursor protein and accumulation of beta-amyloid. J Neurol Neurosurg Psychiatry. 2009;80(12):1344-9.
288. Banwell BL, Engel AG. AlphaB-crystallin immunolocalization yields new insights into inclusion body myositis. Neurology. 2000;54(5):1033-41.
289. Li K, Pu C, Huang X, Liu J, Mao Y, Lu X. Proteomic study of sporadic inclusion body myositis. Proteome Sci. 2014;12(1):45.
290. Muth IE, Zschüntzsch J, Kleinschnitz K, Wrede A, Gerhardt E, Balcarek P, et al. HMGB1 and RAGE in skeletal muscle inflammation: Implications for protein accumulation in inclusion body myositis. Exp Neurol. 2015;271:189-97.
291. Paudel YN, Shaikh MF, Chakraborti A, Kumari Y, Aledo-Serrano Á, Aleksovska K, et al. HMGB1: A Common Biomarker and Potential Target for TBI, Neuroinflammation, Epilepsy, and Cognitive Dysfunction. Front Neurosci. 2018;12:628.
292. Du Yan S, Zhu H, Fu J, Yan SF, Roher A, Tourtellotte WW, et al. Amyloid-beta peptide-receptor for advanced glycation endproduct interaction elicits neuronal expression of macrophage-colony stimulating factor: a proinflammatory pathway in Alzheimer disease. Proc Natl Acad Sci U S A. 1997;94(10):5296-301.
293. Haslbeck KM, Friess U, Schleicher ED, Bierhaus A, Nawroth PP, Kirchner A, et al. The RAGE pathway in inflammatory myopathies and limb girdle muscular dystrophy. Acta Neuropathol. 2005;110(3):247-54.
294. Ulfgren AK, Grundtman C, Borg K, Alexanderson H, Andersson U, Harris HE, et al. Down-regulation of the aberrant expression of the inflammation mediator high mobility group box chromosomal protein 1 in muscle tissue of patients with polymyositis and dermatomyositis treated with corticosteroids. Arthritis Rheum. 2004;50(5):1586-94.
295. Schmidt J, Barthel K, Zschüntzsch J, Muth IE, Swindle EJ, Hombach A, et al. Nitric oxide stress in sporadic inclusion body myositis muscle fibres: inhibition of inducible nitric oxide synthase prevents interleukin-1β-induced accumulation of β-amyloid and cell death. Brain. 2012;135(Pt 4):1102-14.
296. Bandookwala M, Sengupta P. 3-Nitrotyrosine: a versatile oxidative stress biomarker for major neurodegenerative diseases. Int J Neurosci. 2020;130(10):1047-62.
297. Yang CC, Alvarez RB, Engel WK, Askanas V. Increase of nitric oxide synthases and nitrotyrosine in inclusion-body myositis. Neuroreport. 1996;8(1):153-8.
298. Martyn JAJ, Kaneki M. Muscle Atrophy and the Sestrins. N Engl J Med. 2020;383(13):1279-82.
299. Ro SH, Fay J, Cyuzuzo CI, Jang Y, Lee N, Song HS, et al. SESTRINs: Emerging Dynamic Stress-Sensors in Metabolic and Environmental Health. Front Cell Dev Biol. 2020;8:603421.
300. Kumar A, Shaha C. SESN2 facilitates mitophagy by helping Parkin translocation through ULK1 mediated Beclin1 phosphorylation. Sci Rep. 2018;8(1):615.

301. Lee JH, Budanov AV, Park EJ, Birse R, Kim TE, Perkins GA, et al. Sestrin as a feedback inhibitor of TOR that prevents age-related pathologies. Science (New York, NY). 2010;327(5970):1223-8.
302. Chen Y, Huang T, Yu Z, Yu Q, Wang Y, Hu J, et al. The functions and roles of sestrins in regulating human diseases. Cell Mol Biol Lett. 27: © 2022. The Author(s). 2022. p. 2.
303. Zeng N, D'Souza RF, Figueiredo VC, Markworth JF, Roberts LA, Peake JM, et al. Acute resistance exercise induces Sestrin2 phosphorylation and p62 dephosphorylation in human skeletal muscle. Physiological reports. 2017;5(24):e13526.
304. Crisol BM, Lenhare L, Gaspar RS, Gaspar RC, Muñoz VR, da Silva ASR, et al. The role of physical exercise on Sestrin1 and 2 accumulations in the skeletal muscle of mice. Life Sci. 2018;194:98-103.
305. Kim M, Sujkowski A, Namkoong S, Gu B, Cobb T, Kim B, et al. Sestrins are evolutionarily conserved mediators of exercise benefits. Nat Commun. 2020;11(1):190.
306. Segalés J, Perdiguero E, Serrano AL, Sousa-Victor P, Ortet L, Jardí M, et al. Sestrin prevents atrophy of disused and aging muscles by integrating anabolic and catabolic signals. Nat Commun. 2020;11(1):189.
307. Yang BA, Castor-Macias J, Fraczek P, Cornett A, Brown LA, Kim M, et al. Sestrins regulate muscle stem cell metabolic homeostasis. Stem Cell Reports. 2021.
308. Zeng N, D'Souza RF, Mitchell CJ, Cameron-Smith D. Sestrins are differentially expressed with age in the skeletal muscle of men: A cross-sectional analysis. Exp Gerontol. 2018;110:23-34.
309. Rai N, Dey S. Protective response of Sestrin under stressful conditions in aging. Ageing Res Rev. 2020;64:101186.
310. Lanna A, Gomes DC, Muller-Durovic B, McDonnell T, Escors D, Gilroy DW, et al. A sestrin-dependent Erk-Jnk-p38 MAPK activation complex inhibits immunity during aging. Nat Immunol. 2017;18(3):354-63.
311. Pereira BI, De Maeyer RPH, Covre LP, Nehar-Belaid D, Lanna A, Ward S, et al. Sestrins induce natural killer function in senescent-like CD8(+) T cells. Nat Immunol. 2020;21(6):684-94.
312. Piochi LF, Machado IF, Palmeira CM, Rolo AP. Sestrin2 and mitochondrial quality control: Potential impact in myogenic differentiation. Ageing Res Rev. 2021;67:101309.
313. Jegal KH, Park SM, Cho SS, Byun SH, Ku SK, Kim SC, et al. Activating transcription factor 6-dependent sestrin 2 induction ameliorates ER stress-mediated liver injury. Biochim Biophys Acta Mol Cell Res. 2017;1864(7):1295-307.
314. Masschelein E, D'Hulst G, Zvick J, Hinte L, Soro-Arnaiz I, Gorski T, et al. Exercise promotes satellite cell contribution to myofibers in a load-dependent manner. Skelet Muscle. 2020;10(1):21.
315. Jang YN, Baik EJ. JAK-STAT pathway and myogenic differentiation. Jak-stat. 2013;2(2):e23282.
316. Olguín HC, Pisconti A. Marking the tempo for myogenesis: Pax7 and the regulation of muscle stem cell fate decisions. J Cell Mol Med. 2012;16(5):1013-25.
317. Yablonka-Reuveni Z. The skeletal muscle satellite cell: still young and fascinating at 50. J Histochem Cytochem. 2011;59(12):1041-59.
318. Asfour HA, Allouh MZ, Said RS. Myogenic regulatory factors: The orchestrators of myogenesis after 30 years of discovery. Exp Biol Med (Maywood). 2018;243(2):118-28.
319. Schmidt M, Schüler SC, Hüttner SS, von Eyss B, von Maltzahn J. Adult stem cells at work: regenerating skeletal muscle. Cell Mol Life Sci. 2019;76(13):2559-70.
320. Bentzinger CF, Wang YX, Rudnicki MA. Building muscle: molecular regulation of myogenesis. Cold Spring Harb Perspect Biol. 2012;4(2).

321. Agley CC, Lewis FC, Jaka O, Lazarus NR, Velloso C, Francis-West P, et al. Active GSK3β and an intact β-catenin TCF complex are essential for the differentiation of human myogenic progenitor cells. Sci Rep. 2017;7(1):13189.
322. Sampath SC, Millay DP. Myoblast fusion confusion: the resolution begins. Skelet Muscle. 2018;8(1):3.
323. Noë S, Corvelyn M, Willems S, Costamagna D, Aerts JM, Van Campenhout A, et al. The Myotube Analyzer: how to assess myogenic features in muscle stem cells. Skelet Muscle. 2022;12(1):12.
324. Hong J, Park JS, Lee H, Jeong J, Hyeon Yun H, Yun Kim H, et al. Myosin heavy chain is stabilized by BCL-2 interacting cell death suppressor (BIS) in skeletal muscle. Exp Mol Med. 2016;48(4):e225.
325. Kodaka M, Mao F, Arimoto-Matsuzaki K, Kitamura M, Xu X, Yang Z, et al. Characterization of a novel compound that promotes myogenesis via Akt and transcriptional co-activator with PDZ-binding motif (TAZ) in mouse C2C12 cells. PloS one. 2020;15(4):e0231265.
326. Thurner M, Asim F, Garczarczyk-Asim D, Janke K, Deutsch M, Margreiter E, et al. Development of an in vitro potency assay for human skeletal muscle derived cells. PloS one. 2018;13(3):e0194561-e.
327. Vogler TO, Wheeler JR, Nguyen ED, Hughes MP, Britson KA, Lester E, et al. TDP-43 and RNA form amyloid-like myo-granules in regenerating muscle. Nature. 2018;563(7732):508-13.
328. Strah N, Romano G, Introna C, Klima R, Marzullo M, Ciapponi L, et al. TDP-43 promotes the formation of neuromuscular synapses through the regulation of Disc-large expression in Drosophila skeletal muscles. BMC Biol. 2020;18(1):34.
329. Fortini P, Ferretti C, Iorio E, Cagnin M, Garribba L, Pietraforte D, et al. The fine tuning of metabolism, autophagy and differentiation during in vitro myogenesis. Cell Death Dis. 2016;7(3):e2168.
330. Brearley MC, Li C, Daniel Z, Loughna PT, Parr T, Brameld JM. Changes in expression of serine biosynthesis and integrated stress response genes during myogenic differentiation of C2C12 cells. Biochem Biophys Rep. 2019;20:100694.
331. Ellman GL, Courtney KD, Andres V, Jr., Feather-Stone RM. A new and rapid colorimetric determination of acetylcholinesterase activity. Biochem Pharmacol. 1961;7:88-95.
332. Davegårdh C, Broholm C, Perfilyev A, Henriksen T, García-Calzón S, Peijs L, et al. Abnormal epigenetic changes during differentiation of human skeletal muscle stem cells from obese subjects. BMC Med. 2017;15(1):39.
333. O'Leary MF, Wallace GR, Davis ET, Murphy DP, Nicholson T, Bennett AJ, et al. Obese subcutaneous adipose tissue impairs human myogenesis, particularly in old skeletal muscle, via resistin-mediated activation of NFκB. Sci Rep. 2018;8(1):15360.
334. Akhmedov D, Berdeaux R. The effects of obesity on skeletal muscle regeneration. Frontiers in physiology. 2013;4:371.
335. Sinha I, Sakthivel D, Varon DE. Systemic Regulators of Skeletal Muscle Regeneration in Obesity. Front Endocrinol (Lausanne). 2017;8:29.
336. Gajsek N, Jevsek M, Mars T, Mis K, Pirkmajer S, Brecelj J, et al. Synaptogenetic mechanisms controlling postsynaptic differentiation of the neuromuscular junction are nerve-dependent in human and nerve-independent in mouse C2C12 muscle cultures. Chem Biol Interact. 2008;175(1-3):50-7.
337. Guettier-Sigrist S, Coupin G, Warter JM, Poindron P. Cell types required to efficiently innervate human muscle cells in vitro. Exp Cell Res. 2000;259(1):204-12.
338. Olsson K, Cheng AJ, Alam S, Al-Ameri M, Rullman E, Westerblad H, et al. Intracellular Ca(2+)-handling differs markedly between intact human muscle fibers and myotubes. Skelet Muscle. 2015;5:26.

339. Guo X, Greene K, Akanda N, Smith A, Stancescu M, Lambert S, et al. In vitro Differentiation of Functional Human Skeletal Myotubes in a Defined System. Biomater Sci. 2014;2(1):131-8.
340. Brunetti J, Koenig S, Monnier A, Frieden M. Nanopattern surface improves cultured human myotube maturation. Skelet Muscle. 2021;11(1):12.
341. Yang Z, Nakagawa K, Sarkar A, Maruyama J, Iwasa H, Bao Y, et al. Screening with a novel cell-based assay for TAZ activators identifies a compound that enhances myogenesis in C2C12 cells and facilitates muscle repair in a muscle injury model. Molecular and cellular biology. 2014;34(9):1607-21.
342. Ami D, Natalello A, Lotti M, Doglia SM. Why and how protein aggregation has to be studied in vivo. Microb Cell Fact. 2013;12:17.
343. Kalovidouris AE, Plotkin Z. Synergistic cytotoxic effect of interferon-gamma and tumor necrosis factor-alpha on cultured human muscle cells. J Rheumatol. 1995;22(9):1698-703.
344. Kalovidouris AE, Plotkin Z, Graesser D. Interferon-gamma inhibits proliferation, differentiation, and creatine kinase activity of cultured human muscle cells. II. A possible role in myositis. J Rheumatol. 1993;20(10):1718-23.
345. Rajamohamedsait HB, Sigurdsson EM. Histological staining of amyloid and pre-amyloid peptides and proteins in mouse tissue. Methods in molecular biology (Clifton, NJ). 2012;849:411-24.
346. Highley JR, Kirby J, Jansweijer JA, Webb PS, Hewamadduma CA, Heath PR, et al. Loss of nuclear TDP-43 in amyotrophic lateral sclerosis (ALS) causes altered expression of splicing machinery and widespread dysregulation of RNA splicing in motor neurones. Neuropathol Appl Neurobiol. 2014;40(6):670-85.
347. Mitra J, Guerrero EN, Hegde PM, Liachko NF, Wang H, Vasquez V, et al. Motor neuron disease-associated loss of nuclear TDP-43 is linked to DNA double-strand break repair defects. Proc Natl Acad Sci U S A. 2019;116(10):4696-705.
348. Tsuji H, Nonaka T, Yamashita M, Masuda-Suzukake M, Kametani F, Akiyama H, et al. Epitope mapping of antibodies against TDP-43 and detection of protease-resistant fragments of pathological TDP-43 in amyotrophic lateral sclerosis and frontotemporal lobar degeneration. Biochem Biophys Res Commun. 2012;417(1):116-21.
349. Kumar-Singh S. Progranulin and TDP-43: mechanistic links and future directions. J Mol Neurosci. 2011;45(3):561-73.
350. Pinkus JL, Amato AA, Taylor JP, Greenberg SA. Abnormal distribution of heterogeneous nuclear ribonucleoproteins in sporadic inclusion body myositis. Neuromuscul Disord. 2014;24(7):611-6.
351. Li Y, Chen W, Ogawa K, Koide M, Takahashi T, Hagiwara Y, et al. Feeder-supported in vitro exercise model using human satellite cells from patients with sporadic inclusion body myositis. Sci Rep. 2022;12(1):1082.
352. Rai M, Curley M, Coleman Z, Nityanandam A, Jiao J, Graca FA, et al. Analysis of proteostasis during aging with western blot of detergent-soluble and insoluble protein fractions. STAR Protoc. 2021;2(3):100628.
353. Lee S, Kim S, Kang HY, Lim HR, Kwon Y, Jo M, et al. The overexpression of TDP-43 in astrocytes causes neurodegeneration via a PTP1B-mediated inflammatory response. J Neuroinflammation. 2020;17(1):299.
354. Leal-Lasarte MM, Franco JM, Labrador-Garrido A, Pozo D, Roodveldt C. Extracellular TDP-43 aggregates target MAPK/MAK/MRK overlapping kinase (MOK) and trigger caspase-3/IL-18 signaling in microglia. FASEB J. 31. United States: © Faseb.; 2017. p. 2797-816.
355. Zhao W, Beers DR, Bell S, Wang J, Wen S, Baloh RH, et al. TDP-43 activates microglia through NF-κB and NLRP3 inflammasome. Exp Neurol. 2015;273:24-35.

356. Yu CH, Davidson S, Harapas CR, Hilton JB, Mlodzianoski MJ, Laohamonthonkul P, et al. TDP-43 Triggers Mitochondrial DNA Release via mPTP to Activate cGAS/STING in ALS. Cell. 2020;183(3):636-49.e18.
357. Correia AS, Patel P, Dutta K, Julien JP. Inflammation Induces TDP-43 Mislocalization and Aggregation. PloS one. 2015;10(10):e0140248.
358. Bright F, Chan G, van Hummel A, Ittner LM, Ke YD. TDP-43 and Inflammation: Implications for Amyotrophic Lateral Sclerosis and Frontotemporal Dementia. Int J Mol Sci. 2021;22(15).
359. Rivera-Escalera F, Matousek SB, Ghosh S, Olschowka JA, O'Banion MK. Interleukin-1β mediated amyloid plaque clearance is independent of CCR2 signaling in the APP/PS1 mouse model of Alzheimer's disease. Neurobiol Dis. 2014;69:124-33.
360. Rivera-Escalera F, Pinney JJ, Owlett L, Ahmed H, Thakar J, Olschowka JA, et al. IL-1β-driven amyloid plaque clearance is associated with an expansion of transcriptionally reprogrammed microglia. J Neuroinflammation. 2019;16(1):261.
361. Chakrabarty P, Ceballos-Diaz C, Beccard A, Janus C, Dickson D, Golde TE, et al. IFN-gamma promotes complement expression and attenuates amyloid plaque deposition in amyloid beta precursor protein transgenic mice. J Immunol. 2010;184(9):5333-43.
362. Chakrabarty P, Herring A, Ceballos-Diaz C, Das P, Golde TE. Hippocampal expression of murine TNFα results in attenuation of amyloid deposition in vivo. Mol Neurodegener. 2011;6:16.
363. Chakrabarty P, Jansen-West K, Beccard A, Ceballos-Diaz C, Levites Y, Verbeeck C, et al. Massive gliosis induced by interleukin-6 suppresses Abeta deposition in vivo: evidence against inflammation as a driving force for amyloid deposition. Faseb j. 2010;24(2):548-59.
364. Tawara N, Yamashita S, Kawakami K, Kurashige T, Zhang Z, Tasaki M, et al. Muscle-dominant wild-type TDP-43 expression induces myopathological changes featuring tubular aggregates and TDP-43-positive inclusions. Exp Neurol. 2018;309:169-80.
365. Tanida I, Ueno T, Kominami E. LC3 and Autophagy. Methods in molecular biology (Clifton, NJ). 2008;445:77-88.
366. Mizushima N, Yoshimori T. How to interpret LC3 immunoblotting. Autophagy. 2007;3(6):542-5.
367. Gottlieb RA, Andres AM, Sin J, Taylor DP. Untangling autophagy measurements: all fluxed up. Circ Res. 2015;116(3):504-14.
368. Nogalska A, D'Agostino C, Terracciano C, Engel WK, Askanas V. Impaired autophagy in sporadic inclusion-body myositis and in endoplasmic reticulum stress-provoked cultured human muscle fibers. The American journal of pathology. 2010;177(3):1377-87.
369. Pugsley HR. Assessing Autophagic Flux by Measuring LC3, p62, and LAMP1 Co-localization Using Multispectral Imaging Flow Cytometry. Journal of visualized experiments : JoVE. 2017(125).
370. Sánchez-Martín P, Saito T, Komatsu M. p62/SQSTM1: 'Jack of all trades' in health and cancer. Febs j. 2019;286(1):8-23.
371. Chang MA, Patel V, Gwede M, Morgado M, Tomasevich K, Fong EL, et al. IL-1β induces p62/SQSTM1 and represses androgen receptor expression in prostate cancer cells. J Cell Biochem. 2014;115(12):2188-97.
372. Nawas AF, Kanchwala M, Thomas-Jardin SE, Dahl H, Daescu K, Bautista M, et al. IL-1-conferred gene expression pattern in ERα(+) BCa and AR(+) PCa cells is intrinsic to ERα(-) BCa and AR(-) PCa cells and promotes cell survival. BMC Cancer. 2020;20(1):46.
373. Shen J, Xu S, Zhou H, Liu H, Jiang W, Hao J, et al. IL-1β induces apoptosis and autophagy via mitochondria pathway in human degenerative nucleus pulposus cells. Sci Rep. 2017;7:41067.

374. Zhong Z, Umemura A, Sanchez-Lopez E, Liang S, Shalapour S, Wong J, et al. NF-κB Restricts Inflammasome Activation via Elimination of Damaged Mitochondria. Cell. 2016;164(5):896-910.
375. François A, Terro F, Janet T, Rioux Bilan A, Paccalin M, Page G. Involvement of interleukin-1β in the autophagic process of microglia: relevance to Alzheimer's disease. J Neuroinflammation. 2013;10:151.
376. Li P, Du Q, Cao Z, Guo Z, Evankovich J, Yan W, et al. Interferon-γ induces autophagy with growth inhibition and cell death in human hepatocellular carcinoma (HCC) cells through interferon-regulatory factor-1 (IRF-1). Cancer Lett. 2012;314(2):213-22.
377. Wang BF, Cao PP, Wang ZC, Li ZY, Wang ZZ, Ma J, et al. Interferon-γ-induced insufficient autophagy contributes to p62-dependent apoptosis of epithelial cells in chronic rhinosinusitis with nasal polyps. Allergy. 2017;72(9):1384-97.
378. Kim JY, Ozato K. The sequestosome 1/p62 attenuates cytokine gene expression in activated macrophages by inhibiting IFN regulatory factor 8 and TNF receptor-associated factor 6/NF-kappaB activity. J Immunol. 2009;182(4):2131-40.
379. Lee Y, Sasai M, Ma JS, Sakaguchi N, Ohshima J, Bando H, et al. p62 Plays a Specific Role in Interferon-γ-Induced Presentation of a Toxoplasma Vacuolar Antigen. Cell Rep. 2015;13(2):223-33.
380. Assani K, Tazi MF, Amer AO, Kopp BT. IFN-γ stimulates autophagy-mediated clearance of Burkholderia cenocepacia in human cystic fibrosis macrophages. PloS one. 2014;9(5):e96681.
381. Fang C, Weng T, Hu S, Yuan Z, Xiong H, Huang B, et al. IFN-γ-induced ER stress impairs autophagy and triggers apoptosis in lung cancer cells. Oncoimmunology. 2021;10(1):1962591.
382. Lee JH, Budanov AV, Talukdar S, Park EJ, Park HL, Park HW, et al. Maintenance of metabolic homeostasis by Sestrin2 and Sestrin3. Cell Metab. 2012;16(3):311-21.
383. Kimball SR, Gordon BS, Moyer JE, Dennis MD, Jefferson LS. Leucine induced dephosphorylation of Sestrin2 promotes mTORC1 activation. Cell Signal. 2016;28(8):896-906.
384. Hirayama D, Iida T, Nakase H. The Phagocytic Function of Macrophage-Enforcing Innate Immunity and Tissue Homeostasis. Int J Mol Sci. 2017;19(1).
385. Ross EA, Devitt A, Johnson JR. Macrophages: The Good, the Bad, and the Gluttony. Front Immunol. 2021;12:708186.
386. Barker RN, Erwig LP, Hill KS, Devine A, Pearce WP, Rees AJ. Antigen presentation by macrophages is enhanced by the uptake of necrotic, but not apoptotic, cells. Clin Exp Immunol. 2002;127(2):220-5.
387. Wu Y, Hirschi KK. Tissue-Resident Macrophage Development and Function. Front Cell Dev Biol. 2020;8:617879.
388. Lavin Y, Mortha A, Rahman A, Merad M. Regulation of macrophage development and function in peripheral tissues. Nat Rev Immunol. 15. England2015. p. 731-44.
389. Italiani P, Boraschi D. From Monocytes to M1/M2 Macrophages: Phenotypical vs. Functional Differentiation. Front Immunol. 2014;5:514.
390. Ruytinx P, Proost P, Van Damme J, Struyf S. Chemokine-Induced Macrophage Polarization in Inflammatory Conditions. Front Immunol. 2018;9:1930.
391. Vogel DY, Glim JE, Stavenuiter AW, Breur M, Heijnen P, Amor S, et al. Human macrophage polarization in vitro: maturation and activation methods compared. Immunobiology. 2014;219(9):695-703.
392. Atri C, Guerfali FZ, Laouini D. Role of Human Macrophage Polarization in Inflammation during Infectious Diseases. Int J Mol Sci. 2018;19(6).
393. Locati M, Curtale G, Mantovani A. Diversity, Mechanisms, and Significance of Macrophage Plasticity. Annu Rev Pathol. 2020;15:123-47.

394. Wang X, Zhou L. The Many Roles of Macrophages in Skeletal Muscle Injury and Repair. Front Cell Dev Biol. 2022;10:952249.
395. Martins L, Gallo CC, Honda TSB, Alves PT, Stilhano RS, Rosa DS, et al. Skeletal muscle healing by M1-like macrophages produced by transient expression of exogenous GM-CSF. Stem Cell Res Ther. 2020;11(1):473.
396. Rigamonti E, Zordan P, Sciorati C, Rovere-Querini P, Brunelli S. Macrophage plasticity in skeletal muscle repair. Biomed Res Int. 2014;2014:560629.
397. De Paepe B, Racz GZ, Schröder JM, De Bleecker JL. Expression and distribution of the nitric oxide synthases in idiopathic inflammatory myopathies. Acta Neuropathol. 2004;108(1):37-42.
398. Li P, Hao Z, Wu J, Ma C, Xu Y, Li J, et al. Comparative Proteomic Analysis of Polarized Human THP-1 and Mouse RAW264.7 Macrophages. Front Immunol. 2021;12:700009.
399. Genin M, Clement F, Fattaccioli A, Raes M, Michiels C. M1 and M2 macrophages derived from THP-1 cells differentially modulate the response of cancer cells to etoposide. BMC Cancer. 2015;15:577.
400. Chanput W, Mes JJ, Savelkoul HF, Wichers HJ. Characterization of polarized THP-1 macrophages and polarizing ability of LPS and food compounds. Food Funct. 2013;4(2):266-76.
401. Tedesco S, De Majo F, Kim J, Trenti A, Trevisi L, Fadini GP, et al. Convenience versus Biological Significance: Are PMA-Differentiated THP-1 Cells a Reliable Substitute for Blood-Derived Macrophages When Studying in Vitro Polarization? Front Pharmacol. 2018;9:71.
402. Larrick JW, Wright SC. Cytotoxic mechanism of tumor necrosis factor-alpha. Faseb j. 1990;4(14):3215-23.
403. Lee MK, Choi YH, Nam TJ. Pyropia yezoensis protein protects against TNF-α-induced myotube atrophy in C2C12 myotubes via the NF-κB signaling pathway. Mol Med Rep. 2021;24(1).
404. Langen RC, Schols AM, Kelders MC, Wouters EF, Janssen-Heininger YM. Inflammatory cytokines inhibit myogenic differentiation through activation of nuclear factor-kappaB. Faseb j. 2001;15(7):1169-80.
405. Yamaguchi A, Maeshige N, Langston PK, Noguchi H, Ma X, Ichikawa Y, et al., editors. Conditioned Media from Ultrasound-treated C2C12 Myotubes Regulate Macrophage Inflammatory Responses. The FASEB Journal; 2021 2021/05/01: John Wiley & Sons, Ltd.
406. Technical Resources N-2 Supplement (100X) liquid: ThermoFisher Scientific; [Available from: https://www.thermofisher.com/uk/en/home/technical-resources/media-formulation.166.html.
407. Technical Resources A10491 - RMPI 1640 (ATCC modification): ThermoFisher Scientific; 2022 [Available from: https://www.thermofisher.com/uk/en/home/technical-resources/media-formulation.244.html.
408. Technical Resources 11320 - DMEM/-F12: ThermoFisher Scientific; 2022 [Available from: https://www.thermofisher.com/uk/en/home/technical-resources/media-formulation.55.html.
409. Cohly H, Stephens J, Markhov A, Angel M, Campbell W, Ndebele K, et al. Cell culture conditions affect LPS inducibility of the inflammatory mediators in J774A.1 murine macrophages. Immunol Invest. 2001;30(1):1-15.
410. Menzies FM, Henriquez FL, Alexander J, Roberts CW. Selective inhibition and augmentation of alternative macrophage activation by progesterone. Immunology. 2011;134(3):281-91.
411. Latour YL, Gobert AP, Wilson KT. The role of polyamines in the regulation of macrophage polarization and function. Amino Acids. 2020;52(2):151-60.

412. Lian J, Liang Y, Zhang H, Lan M, Ye Z, Lin B, et al. The role of polyamine metabolism in remodeling immune responses and blocking therapy within the tumor immune microenvironment. Front Immunol. 2022;13:912279.
413. Fiedler SE, Spain RI, Kim E, Salinthone S. Lipoic acid modulates inflammatory responses of monocytes and monocyte-derived macrophages from healthy and relapsing-remitting multiple sclerosis patients. Immunol Cell Biol. 2021;99(1):107-15.
414. Pillon NJ, Bilan PJ, Fink LN, Klip A. Cross-talk between skeletal muscle and immune cells: muscle-derived mediators and metabolic implications. Am J Physiol Endocrinol Metab. 2013;304(5):E453-65.
415. Pillon NJ, Arane K, Bilan PJ, Chiu TT, Klip A. Muscle cells challenged with saturated fatty acids mount an autonomous inflammatory response that activates macrophages. Cell Commun Signal. 2012;10(1):30.
416. Zhang C, Li Y, Wu Y, Wang L, Wang X, Du J. Interleukin-6/signal transducer and activator of transcription 3 (STAT3) pathway is essential for macrophage infiltration and myoblast proliferation during muscle regeneration. J Biol Chem. 2013;288(3):1489-99.
417. Muñoz-Cánoves P, Scheele C, Pedersen BK, Serrano AL. Interleukin-6 myokine signaling in skeletal muscle: a double-edged sword? Febs j. 2013;280(17):4131-48.
418. Grodzki AC, Giulivi C, Lein PJ. Oxygen tension modulates differentiation and primary macrophage functions in the human monocytic THP-1 cell line. PLoS One. 2013;8(1):e54926.
419. Koo IC, Ohol YM, Wu P, Morisaki JH, Cox JS, Brown EJ. Role for lysosomal enzyme beta-hexosaminidase in the control of mycobacteria infection. Proc Natl Acad Sci U S A. 2008;105(2):710-5.
420. Chanput W, Mes JJ, Wichers HJ. THP-1 cell line: an in vitro cell model for immune modulation approach. International immunopharmacology. 2014;23(1):37-45.
421. Amemiya K, Granger RP, Dalakas MC. Clonal restriction of T-cell receptor expression by infiltrating lymphocytes in inclusion body myositis persists over time. Studies in repeated muscle biopsies. Brain. 2000;123 (Pt 10):2030-9.
422. Salajegheh M, Rakocevic G, Raju R, Shatunov A, Goldfarb LG, Dalakas MC. T cell receptor profiling in muscle and blood lymphocytes in sporadic inclusion body myositis. Neurology. 2007;69(17):1672-9.
423. Dimitri D, Benveniste O, Dubourg O, Maisonobe T, Eymard B, Amoura Z, et al. Shared blood and muscle CD8+ T-cell expansions in inclusion body myositis. Brain. 2006;129(Pt 4):986-95.
424. Paul S, Lal G. The Molecular Mechanism of Natural Killer Cells Function and Its Importance in Cancer Immunotherapy. Front Immunol. 2017;8:1124.
425. Prager I, Watzl C. Mechanisms of natural killer cell-mediated cellular cytotoxicity. J Leukoc Biol. 2019;105(6):1319-29.
426. Müller L, Aigner P, Stoiber D. Type I Interferons and Natural Killer Cell Regulation in Cancer. Front Immunol. 2017;8:304.
427. Lin AW, Gonzalez SA, Cunningham-Rundles S, Dorante G, Marshall S, Tignor A, et al. CD56(+dim) and CD56(+bright) cell activation and apoptosis in hepatitis C virus infection. Clin Exp Immunol. 2004;137(2):408-16.
428. Chiang SC, Theorell J, Entesarian M, Meeths M, Mastafa M, Al-Herz W, et al. Comparison of primary human cytotoxic T-cell and natural killer cell responses reveal similar molecular requirements for lytic granule exocytosis but differences in cytokine production. Blood. 2013;121(8):1345-56.
429. Goyal NA, Coulis G, Duarte J, Farahat PK, Mannaa AH, Cauchii J, et al. Immunophenotyping of Inclusion Body Myositis Blood T and NK Cells. Neurology. 2022;98(13):e1374-e83.

430. Yang H, Parkhouse RM, Wileman T. Monoclonal antibodies that identify the CD3 molecules expressed specifically at the surface of porcine gammadelta-T cells. Immunology. 2005;115(2):189-96.
431. Gomez GG, Read SB, Gerschenson LE, Santoli D, Zweifach A, Kruse CA. Interactions of the allogeneic effector leukemic T cell line, TALL-104, with human malignant brain tumors. Neuro Oncol. 2004;6(2):83-95.
432. Brando C, Mukhopadhyay S, Kovacs E, Medina R, Patel P, Catina TL, et al. Receptors and lytic mediators regulating anti-tumor activity by the leukemic killer T cell line TALL-104. J Leukoc Biol. 2005;78(2):359-71.
433. Cesano A, Santoli D. Two unique human leukemic T-cell lines endowed with a stable cytotoxic function and a different spectrum of target reactivity analysis and modulation of their lytic mechanisms. In Vitro Cell Dev Biol. 1992;28a(9-10):648-56.
434. Cesano A, Visonneau S, Clark SC, Santoli D. Cellular and molecular mechanisms of activation of MHC nonrestricted cytotoxic cells by IL-12. J Immunol. 1993;151(6):2943-57.
435. Kruse CA, Visonneau S, Kleinschmidt-DeMasters BK, Gup CJ, Gomez GG, Paul DB, et al. The human leukemic T-cell line, TALL-104, is cytotoxic to human malignant brain tumors and traffics through brain tissue: implications for local adoptive immunotherapy. Cancer research. 2000;60(20):5731-9.
436. Menasche BL, Davis EM, Wang S, Ouyang Y, Li S, Yu H, et al. PBRM1 and the glycosylphosphatidylinositol biosynthetic pathway promote tumor killing mediated by MHC-unrestricted cytotoxic lymphocytes. Sci Adv. 2020;6(48).
437. McKinney EF, Cuthbertson I, Harris KM, Smilek DE, Connor C, Manferrari G, et al. A CD8(+) NK cell transcriptomic signature associated with clinical outcome in relapsing remitting multiple sclerosis. Nat Commun. 2021;12(1):635.
438. Geng J, Raghavan M. CD8αα homodimers function as a coreceptor for KIR3DL1. Proc Natl Acad Sci U S A. 2019;116(36):17951-6.
439. Ahmad F, Hong HS, Jäckel M, Jablonka A, Lu IN, Bhatnagar N, et al. High frequencies of polyfunctional CD8+ NK cells in chronic HIV-1 infection are associated with slower disease progression. J Virol. 2014;88(21):12397-408.
440. Balato A, Unutmaz D, Gaspari AA. Natural killer T cells: an unconventional T-cell subset with diverse effector and regulatory functions. J Invest Dermatol. 2009;129(7):1628-42.
441. Krijgsman D, Hokland M, Kuppen PJK. The Role of Natural Killer T Cells in Cancer-A Phenotypical and Functional Approach. Front Immunol. 2018;9:367.
442. Singh AK, Tripathi P, Cardell SL. Type II NKT Cells: An Elusive Population With Immunoregulatory Properties. Front Immunol. 2018;9:1969.
443. Kawano T, Cui J, Koezuka Y, Toura I, Kaneko Y, Sato H, et al. Natural killer-like nonspecific tumor cell lysis mediated by specific ligand-activated Valpha14 NKT cells. Proc Natl Acad Sci U S A. 1998;95(10):5690-3.
444. Nieda M, Nicol A, Koezuka Y, Kikuchi A, Lapteva N, Tanaka Y, et al. TRAIL expression by activated human CD4(+)V alpha 24NKT cells induces in vitro and in vivo apoptosis of human acute myeloid leukemia cells. Blood. 2001;97(7):2067-74.
445. Wingender G, Krebs P, Beutler B, Kronenberg M. Antigen-specific cytotoxicity by invariant NKT cells in vivo is CD95/CD178-dependent and is correlated with antigenic potency. J Immunol. 2010;185(5):2721-9.
446. Wang C, Liu X, Li Z, Chai Y, Jiang Y, Wang Q, et al. CD8(+)NKT-like cells regulate the immune response by killing antigen-bearing DCs. Sci Rep. 2015;5:14124.
447. Boyman O, Sprent J. The role of interleukin-2 during homeostasis and activation of the immune system. Nat Rev Immunol. 2012;12(3):180-90.
448. Brinkmeier H, Kaspar A, Wiethölter H, Rüdel R. Interleukin-2 inhibits sodium currents in human muscle cells. Pflugers Arch. 1992;420(5-6):621-3.

449. Kaspar A, Brinkmeier H, Rüdel R. Local anaesthetic-like effect of interleukin-2 on muscular Na+ channels: no evidence for involvement of the IL-2 receptor. Pflugers Arch. 1994;426(1-2):61-7.
450. Romee R, Foley B, Lenvik T, Wang Y, Zhang B, Ankarlo D, et al. NK cell CD16 surface expression and function is regulated by a disintegrin and metalloprotease-17 (ADAM17). Blood. 2013;121(18):3599-608.
451. Yeap WH, Wong KL, Shimasaki N, Teo EC, Quek JK, Yong HX, et al. CD16 is indispensable for antibody-dependent cellular cytotoxicity by human monocytes. Sci Rep. 2016;6:34310.
452. Lu Y, Huang Y, Huang L, Xu Y, Wang Z, Li H, et al. CD16 expression on neutrophils predicts treatment efficacy of capecitabine in colorectal cancer patients. BMC Immunol. 2020;21(1):46.
453. Hohlfeld R, Engel AG. Lysis of myotubes by alloreactive cytotoxic T cells and natural killer cells. Relevance to myoblast transplantation. The Journal of clinical investigation. 1990;86(1):370-4.
454. Gossel LDH, Heim C, Pfeffermann LM, Moser LM, Bönig HB, Klingebiel TE, et al. Retargeting of NK-92 Cells against High-Risk Rhabdomyosarcomas by Means of an ERBB2 (HER2/Neu)-Specific Chimeric Antigen Receptor. Cancers (Basel). 2021;13(6).
455. Kamiya M, Mizoguchi F, Takamura A, Kimura N, Kawahata K, Kohsaka H. A new in vitro model of polymyositis reveals CD8+ T cell invasion into muscle cells and its cytotoxic role. Rheumatology (Oxford). 2020;59(1):224-32.
456. Hohlfeld R, Engel AG. Coculture with autologous myotubes of cytotoxic T cells isolated from muscle in inflammatory myopathies. Ann Neurol. 1991;29(5):498-507.
457. Pandya JM, Venalis P, Al-Khalili L, Shahadat Hossain M, Stache V, Lundberg IE, et al. CD4+ and CD8+ CD28(null) T Cells Are Cytotoxic to Autologous Muscle Cells in Patients With Polymyositis. Arthritis Rheumatol. 2016;68(8):2016-26.
458. Cesano A, Santoli D. Inducible expression of granulocyte-macrophage colony-stimulating factor, tumor necrosis factor-alpha, and interferon-gamma in two human cytotoxic leukemic T-cell lines. In Vitro Cell Dev Biol. 1992;28a(9-10):657-62.
459. O'Connor R, Cesano A, Lange B, Finan J, Nowell PC, Clark SC, et al. Growth factor requirements of childhood acute T-lymphoblastic leukemia: correlation between presence of chromosomal abnormalities and ability to grow permanently in vitro. Blood. 1991;77(7):1534-45.
460. Pores-Fernando AT, Bauer RA, Wurth GA, Zweifach A. Exocytic responses of single leukaemic human cytotoxic T lymphocytes stimulated by agents that bypass the T cell receptor. J Physiol. 2005;567(Pt 3):891-903.
461. Perdomo-Celis F, Velilla PA, Taborda NA, Rugeles MT. An altered cytotoxic program of CD8+ T-cells in HIV-infected patients despite HAART-induced viral suppression. PloS one. 2019;14(1):e0210540.
462. Chatila T, Silverman L, Miller R, Geha R. Mechanisms of T cell activation by the calcium ionophore ionomycin. J Immunol. 1989;143(4):1283-9.
463. Matthews SA, Cantrell DA. New insights into the regulation and function of serine/threonine kinases in T lymphocytes. Immunol Rev. 2009;228(1):241-52.
464. Mariño G, Niso-Santano M, Baehrecke EH, Kroemer G. Self-consumption: the interplay of autophagy and apoptosis. Nat Rev Mol Cell Biol. 2014;15(2):81-94.
465. Henry CM, Hollville E, Martin SJ. Measuring apoptosis by microscopy and flow cytometry. Methods. 2013;61(2):90-7.
466. Thomas MP, Liu X, Whangbo J, McCrossan G, Sanborn KB, Basar E, et al. Apoptosis Triggers Specific, Rapid, and Global mRNA Decay with 3' Uridylated Intermediates Degraded by DIS3L2. Cell Rep. 2015;11(7):1079-89.

467. Broer T, Khodabukus A, Bursac N. Can we mimic skeletal muscles for novel drug discovery? Expert Opin Drug Discov. 2020;15(6):643-5.
468. Dessauge F, Schleder C, Perruchot MH, Rouger K. 3D in vitro models of skeletal muscle: myopshere, myobundle and bioprinted muscle construct. Vet Res. 2021;52(1):72.
469. Khodabukus A. Tissue-Engineered Skeletal Muscle Models to Study Muscle Function, Plasticity, and Disease. Front Physiol. 2021;12:619710.
470. Jiang Y, Torun T, Maffioletti SM, Serio A, Tedesco FS. Bioengineering human skeletal muscle models: Recent advances, current challenges and future perspectives. Exp Cell Res. 2022;416(2):113133.
471. Volpi M, Paradiso A, Costantini M, Święszkowski W. Hydrogel-Based Fiber Biofabrication Techniques for Skeletal Muscle Tissue Engineering. ACS Biomater Sci Eng. 2022;8(2):379-405.
472. Urciuolo A, Serena E, Ghua R, Zatti S, Giomo M, Mattei N, et al. Engineering a 3D in vitro model of human skeletal muscle at the single fiber scale. PloS one. 2020;15(5):e0232081.
473. Takahashi H, Shimizu T, Okano T. Engineered Human Contractile Myofiber Sheets as a Platform for Studies of Skeletal Muscle Physiology. Sci Rep. 2018;8(1):13932.
474. Hosseini V, Ahadian S, Ostrovidov S, Camci-Unal G, Chen S, Kaji H, et al. Engineered contractile skeletal muscle tissue on a microgrooved methacrylated gelatin substrate. Tissue Eng Part A. 2012;18(23-24):2453-65.
475. Ostrovidov S, Ahadian S, Ramon-Azcon J, Hosseini V, Fujie T, Parthiban SP, et al. Three-dimensional co-culture of C2C12/PC12 cells improves skeletal muscle tissue formation and function. Journal of tissue engineering and regenerative medicine. 2017;11(2):582-95.
476. Flaibani M, Boldrin L, Cimetta E, Piccoli M, De Coppi P, Elvassore N. Muscle differentiation and myotubes alignment is influenced by micropatterned surfaces and exogenous electrical stimulation. Tissue Eng Part A. 2009;15(9):2447-57.
477. Kang MS, Lee SH, Park WJ, Lee JE, Kim B, Han DW. Advanced Techniques for Skeletal Muscle Tissue Engineering and Regeneration. Bioengineering (Basel). 2020;7(3).
478. Wang L, Wu Y, Guo B, Ma PX. Nanofiber Yarn/Hydrogel Core-Shell Scaffolds Mimicking Native Skeletal Muscle Tissue for Guiding 3D Myoblast Alignment, Elongation, and Differentiation. ACS Nano. 2015;9(9):9167-79.
479. Gilbert-Honick J, Iyer SR, Somers SM, Lovering RM, Wagner K, Mao HQ, et al. Engineering functional and histological regeneration of vascularized skeletal muscle. Biomaterials. 2018;164:70-9.
480. Yeo M, Kim GH. Anisotropically Aligned Cell-Laden Nanofibrous Bundle Fabricated via Cell Electrospinning to Regenerate Skeletal Muscle Tissue. Small. 2018;14(48):e1803491.
481. Kim JH, Seol YJ, Ko IK, Kang HW, Lee YK, Yoo JJ, et al. 3D Bioprinted Human Skeletal Muscle Constructs for Muscle Function Restoration. Sci Rep. 2018;8(1):12307.
482. Yeo M, Kim G. Three-Dimensional Microfibrous Bundle Structure Fabricated Using an Electric Field-Assisted/Cell Printing Process for Muscle Tissue Regeneration. ACS Biomater Sci Eng. 2018;4(2):728-38.
483. Afshar ME, Abraha HY, Bakooshli MA, Davoudi S, Thavandiran N, Tung K, et al. A 96-well culture platform enables longitudinal analyses of engineered human skeletal muscle microtissue strength. Sci Rep. 2020;10(1):6918.
484. Vandenburgh H, Shansky J, Benesch-Lee F, Barbata V, Reid J, Thorrez L, et al. Drug-screening platform based on the contractility of tissue-engineered muscle. Muscle & nerve. 2008;37(4):438-47.
485. Hansen A, Eder A, Bönstrup M, Flato M, Mewe M, Schaaf S, et al. Development of a drug screening platform based on engineered heart tissue. Circ Res. 2010;107(1):35-44.

486. Maffioletti SM, Sarcar S, Henderson ABH, Mannhardt I, Pinton L, Moyle LA, et al. Three-Dimensional Human iPSC-Derived Artificial Skeletal Muscles Model Muscular Dystrophies and Enable Multilineage Tissue Engineering. Cell Rep. 2018;23(3):899-908.
487. Osaki T, Uzel SGM, Kamm RD. Microphysiological 3D model of amyotrophic lateral sclerosis (ALS) from human iPS-derived muscle cells and optogenetic motor neurons. Sci Adv. 2018;4(10):eaat5847.
488. Gholobova D, Gerard M, Decroix L, Desender L, Callewaert N, Annaert P, et al. Human tissue-engineered skeletal muscle: a novel 3D in vitro model for drug disposition and toxicity after intramuscular injection. Sci Rep. 2018;8(1):12206.
489. Madden L, Juhas M, Kraus WE, Truskey GA, Bursac N. Bioengineered human myobundles mimic clinical responses of skeletal muscle to drugs. Elife. 2015;4:e04885.
490. Hinds S, Bian W, Dennis RG, Bursac N. The role of extracellular matrix composition in structure and function of bioengineered skeletal muscle. Biomaterials. 2011;32(14):3575-83.
491. Afshar Bakooshli M, Lippmann ES, Mulcahy B, Iyer N, Nguyen CT, Tung K, et al. A 3D culture model of innervated human skeletal muscle enables studies of the adult neuromuscular junction. Elife. 2019;8.
492. Khodabukus A, Kaza A, Wang J, Prabhu N, Goldstein R, Vaidya VS, et al. Tissue-Engineered Human Myobundle System as a Platform for Evaluation of Skeletal Muscle Injury Biomarkers. Toxicol Sci. 2020;176(1):124-36.
493. Davis BNJ, Santoso JW, Walker MJ, Oliver CE, Cunningham MM, Boehm CA, et al. Modeling the Effect of TNF-α upon Drug-Induced Toxicity in Human, Tissue-Engineered Myobundles. Ann Biomed Eng. 2019;47(7):1596-610.
494. Robertson D, Savage K, Reis-Filho JS, Isacke CM. Multiple immunofluorescence labelling of formalin-fixed paraffin-embedded (FFPE) tissue. BMC Cell Biol. 2008;9:13.
495. Gao QQ, McNally EM. The Dystrophin Complex: Structure, Function, and Implications for Therapy. Compr Physiol. 2015;5(3):1223-39.
496. Milush JM, Long BR, Snyder-Cappione JE, Cappione AJ, 3rd, York VA, Ndhlovu LC, et al. Functionally distinct subsets of human NK cells and monocyte/DC-like cells identified by coexpression of CD56, CD7, and CD4. Blood. 2009;114(23):4823-31.
497. Magleby KL, Pallotta BS. A study of desensitization of acetylcholine receptors using nerve-released transmitter in the frog. J Physiol. 1981;316:225-50.
498. Manthey AA. Kinetic evidence that desensitized nAChR may promote transitions of active nAChR to desensitized states during sustained exposure to agonists in skeletal muscle. Pflugers Arch. 2006;452(3):349-62.
499. Del Coso J, Hiam D, Houweling P, Pérez LM, Eynon N, Lucía A. More than a 'speed gene': ACTN3 R577X genotype, trainability, muscle damage, and the risk for injuries. Eur J Appl Physiol. 2019;119(1):49-60.
500. Mills M, Yang N, Weinberger R, Vander Woude DL, Beggs AH, Easteal S, et al. Differential expression of the actin-binding proteins, alpha-actinin-2 and -3, in different species: implications for the evolution of functional redundancy. Hum Mol Genet. 2001;10(13):1335-46.
501. Westerblad H, Lännergren J, Allen DG. Slowed relaxation in fatigued skeletal muscle fibers of Xenopus and Mouse. Contribution of [Ca2+]i and cross-bridges. J Gen Physiol. 1997;109(3):385-99.
502. Alway SE, Hughson RL, Green HJ, Patla AE. Human tibialis anterior contractile responses following fatiguing exercise with and without beta-adrenoceptor blockade. Clin Physiol. 1988;8(3):215-25.
503. Reggiani C, te Kronnie T. RyR isoforms and fibre type-specific expression of proteins controlling intracellular calcium concentration in skeletal muscles. J Muscle Res Cell Motil. 2006;27(5-7):327-35.

504. Hill C, Brunello E, Fusi L, Ovejero JG, Irving M. Myosin-based regulation of twitch and tetanic contractions in mammalian skeletal muscle. Elife. 2021;10.
505. Tribe RM, Moriarty P, Dalrymple A, Hassoni AA, Poston L. Interleukin-1beta induces calcium transients and enhances basal and store operated calcium entry in human myometrial smooth muscle. Biol Reprod. 2003;68(5):1842-9.
506. Smith MA, Moylan JS, Smith JD, Li W, Reid MB. IFN-gamma does not mimic the catabolic effects of TNF-alpha. American journal of physiology Cell physiology. 2007;293(6):C1947-52.
507. Li W, Moylan JS, Chambers MA, Smith J, Reid MB. Interleukin-1 stimulates catabolism in C2C12 myotubes. American journal of physiology Cell physiology. 2009;297(3):C706-14.
508. Corin G, Strutton PH, McGregor AH. Establishment of a protocol to test fatigue of the trunk muscles. Br J Sports Med. 2005;39(10):731-5.
509. Suzuki N, Mori-Yoshimura M, Yamashita S, Nakano S, Murata KY, Mori M, et al. The updated retrospective questionnaire study of sporadic inclusion body myositis in Japan. Orphanet J Rare Dis. 2019;14(1):155.
510. Alfano LN, Lowes LP, Dvorchik I, Yin H, Maus EG, Flanigan KM, et al. The 2-min walk test is sufficient for evaluating walking abilities in sporadic inclusion body myositis. Neuromuscul Disord. 2014;24(3):222-6.
511. Madhushri P, Dzhagaryan A, Jovanov E, Milenkovic A. An mHealth Tool Suite for Mobility Assessment. Information [Internet]. 2016; 7(3).
512. Stölting MN, Hefermehl LJ, Tremp M, Azzabi F, Sulser T, Eberli D. The role of donor age and gender in the success of human muscle precursor cell transplantation. Journal of tissue engineering and regenerative medicine. 2017;11(2):447-58.
513. Rosenblatt JD, Parry DJ, Partridge TA. Phenotype of adult mouse muscle myoblasts reflects their fiber type of origin. Differentiation. 1996;60(1):39-45.
514. Morosetti R, Broccolini A, Sancricca C, Gliubizzi C, Gidaro T, Tonali PA, et al. Increased aging in primary muscle cultures of sporadic inclusion-body myositis. Neurobiol Aging. 2008;31(7):1205-14.
515. Yoshihara I, Kondo Y, Okamoto K, Tanaka H. Sepsis-Associated Muscle Wasting: A Comprehensive Review from Bench to Bedside. Int J Mol Sci. 2023;24(5).
516. Wanschitz JV, Dubourg O, Lacene E, Fischer MB, Höftberger R, Budka H, et al. Expression of myogenic regulatory factors and myo-endothelial remodeling in sporadic inclusion body myositis. Neuromuscul Disord. 2013;23(1):75-83.
517. Londhe P, Davie JK. Interferon-γ resets muscle cell fate by stimulating the sequential recruitment of JARID2 and PRC2 to promoters to repress myogenesis. Sci Signal. 2013;6(305):ra107.
518. Yamada M, Iwata M, Warabi E, Oishi H, Lira VA, Okutsu M. p62/SQSTM1 and Nrf2 are essential for exercise-mediated enhancement of antioxidant protein expression in oxidative muscle. Faseb j. 2019;33(7):8022-32.
519. Thammisetty SS, Pedragosa J, Weng YC, Calon F, Planas A, Kriz J. Age-related deregulation of TDP-43 after stroke enhances NF-κB-mediated inflammation and neuronal damage. J Neuroinflammation. 2018;15(1):312.
520. Weihl CC, Pestronk A. Sporadic inclusion body myositis: possible pathogenesis inferred from biomarkers. Curr Opin Neurol. 2010;23(5):482-8.
521. Amici DR, Pinal-Fernandez I, Christopher-Stine L, Mammen AL, Mendillo ML. A network of core and subtype-specific gene expression programs in myositis. Acta Neuropathol. 2021.
522. Vencovský J, Klein M, Mann H, Kubínová K, Kryštůfková O, Šmucrová H, editors. Meeting Abstracts 4th Global Conference on Myositis (GCOM). 4th Global Conference on Myositis (GCOM); 2022; Prague, Czech Republic: Clinical and Experimental Rheumatology.

523. GCOM 2022 Global Conference on Myositis Program Handbook: Prague, Czech Republic; 2022 [Available from: https://www.congressprague.cz/en/kongresy/myositis2022/odborny-program.html.
524. Redmann M, Benavides GA, Wani WY, Berryhill TF, Ouyang X, Johnson MS, et al. Methods for assessing mitochondrial quality control mechanisms and cellular consequences in cell culture. Redox Biol. 2018;17:59-69.
525. Kovaleva IE, Tokarchuk AV, Zheltukhin AO, Dalina AA, Safronov GG, Evstafieva AG, et al. Mitochondrial localization of SESN2. PloS one. 2020;15(4):e0226862.

Appendix

Figure number	Donors used
Figure 3.3 Acetylcholinesterase expression was not different between myoblasts and myotubes.	HSMM 1, HSMM 3, HSKMDC 2, HSKMDC 3, HSKMDC 4, HSKMDC 6, HSKMDC 9 and 7 other Cook MyoSite and Lonza donors
Figure 3.4 Spontaneous contraction of myotubes in culture.	HSKMDC 9
Figure 3.5 Differentiation over time in myogenesis.	HSMM 17F, HSKMDC 2, HSKMDC 3, HSKMDC 3, HSKMDC 4, HSKMDC 9
Figure 3.6 Myosin heavy chain during myogenesis.	Western blot bands - HSKMDC 3 Graph - HSMM 1, HSKMDC 2, HSKMDC 3, HSKMDC 4, HSKMDC 6, HSKMDC 9
Figure 3.7 Examples of TDP-43 localisation classification.	HSMM 3
Figure 3.8 TDP-43 localisation and expression during myogenesis.	A: HSKMDC 6 B: HSMM 1, HSKMDC 2, HSKMDC 4, HSKMDC 6 C: bands – HSKMDC 6 graph - HSMM 1, HSKMDC 2, HSKMDC 3, HSKMDC 4, HSKMDC 6, HSKMDC 9
Figure 3.9 p62 during myogenesis.	A: HSMM 1 B: Western blot bands- HSKMDC 9 Graph - HSMM 1, HSKMDC 2, HSKMDC 3, HSKMDC 4, HSKMDC 6, HSKMDC 9
Figure 3.10 Sestrin-2 and sestrin-1 follow different expression patterns during myogenesis.	A: HSMM 1 B: Western blot bands – HSKMDC 6 Graph- HSMM 1, HSKMDC 2, HSKMDC 3, HSKMDC 4, HSKMDC 6, HSKMDC 9 C: Western blot bands – HSKMDC 6 Graph- HSMM 1, HSKMDC 2, HSKMDC 3, HSKMDC 4, HSKMDC 6, HSKMDC 9
Figure 4.1 Cytotoxicity of IL-1β and IFNγ alone or in combination on myotubes.	A: HSMM 1 B: HSMM 1, HSKMDC 2, HSKMDC 3, HSKMDC 4, HSKMDC 6, HSKMDC 9
Figure 4.2 TDP-43 and p62 staining with IL-1β and IFNγ.	HSMM 2
Figure 4.3 p62 puncta size was increased with IL-1β+IFNγ.	HSMM 1, HSMM 2, HSMM 3, HSKMDC 3, HSKMDC 4, HSKMDC 6
Figure 4.4 Examples of TDP-43 and p62 aggregates in myotubes.	HSMM 3

Figure 4.5 TDP-43 aggregate size or frequency was not affected by IL-1β+IFNγ.	HSMM 1, HSMM 2, HSMM 3, HSKMDC 3, HSKMDC 4, HSKMDC 6
Figure 4.6 IL-1β+IFNγ does not affect TDP-43 localisation.	Images: HSMM 1 Graph: HSMM 1, HSMM 2, HSMM 3, HSKMDC 3, HSKMDC 4
Figure 4.7 TDP-43 and p62 in IL-1β or IFNγ treated myotubes.	HSMM 1
Figure 4.8 p62 puncta frequency or size was not affected by IL-1β or IFNγ treatment.	HSMM 1, HSKMDC 2, HSKMDC 4, HSKMDC 6, HSKMDC 9
Figure 4.9 TDP-43 aggregate size or frequency was not affected by IL-1β or IFNγ.	HSMM 1, HSKMDC 2, HSKMDC 4, HSKMDC 6, HSKMDC 9
Figure 4.10 IL-1β or IFNγ does not affect TDP-43 localisation.	Images: HSMM 1 Graph: HSMM 1, HSKMDC 2, HSKMDC 4, HSKMDC 6, HSKMDC 9
Figure 4.11 p62 expression was increased with IL-1β and LC3II/LC3I ratio increased with IL-1β+IFNγ.	A: HSKMDC 2 B-E: HSMM1, HSKMDC 2, HSKMDC 3, HSKMDC 4, HSKMDC 6, HSKMDC 9
Figure 4.12 p62 nuclear puncta were not affected by IL-1β or IFNγ treatment.	A: HSMM 1 B: HSMM 1, HSKMDC 2, HSKMDC 4, HSKMDC 6, HSKMDC 9
Figure 4.13 Sestrin-2 and sestrin-1 expression with IL-1β and IFNγ treatment.	A: Western blot bands: HSMM 1 C: Western blot bands: HSKMDC 4 A-C graphs: HSMM 1, HSKMDC 2, HSKMDC 3, HSKMDC 4, HSKMDC 6, HSKMDC 9
Figure 5.3 Cytotoxicity of macrophage conditioned medium to myotubes.	HSMM 1, HSKMDC 2, HSKMDC 4, HSKMDC6, HSKMDC 9
Figure 5.4 Images of p62 and TDP-43 in macrophage conditioned medium-treated myotubes.	A: HSMM 1
Figure 5.5 p62 puncta analysis and protein expression was not affected by macrophage conditioned medium.	A, B, C (graph): HSMM1, HSKMDC 3, HSKMDC 4, HSKMDC 6 Western blot bands –HSMM 1
Figure 5.6 TDP-43 aggregation or protein expression was not affected by macrophage secreted factors.	A-E: HSMM1, HSKMDC 3, HSKMDC 4, HSKMDC 6 E: Western blot bands – HSMM 1
Figure 5.7 TDP-43 localisation with macrophage conditioned medium.	Images - HSKMDC 6 Graph - HSMM1, HSKMDC 3, HSKMDC 4, HSKMDC 6
Figure 5.8 Sestrin-2 or sestrin-1 protein expression was not altered by conditioned medium from M(PMA) or M(IFNγLPS) macrophages.	A, B (graphs): HSMM1, HSKMDC 3, HSKMDC 4, HSKMDC 6 A,B : Western blot bands – HSMM 1

Figure 5.9 Inflammatory primed myotubes caused macrophages to secrete more IL-6 than unprimed myotubes.	HSMM 1, HSKMDC 3, HSKMDC 4, HSKMDC 6, HSKMDC 9
Figure 6.1 Cytotoxicity of TALL-104 conditioned medium on myotubes.	HSMM 1, HSMM 2, HSKMDC 2, HSKMDC 3, HSKMDC 6, HSKMDC 9
Figure 6.2 Effect of inflammatory conditioned myotube medium on TALL-104 IFNγ secretion.	HSMM 1, HSKMDC 4, HSKMDC 6, HSKMDC 9
Figure 6.3 p62 and TDP-43 with TALL-104 conditioned medium.	A: HSMM 1
Figure 6.4 TALL-104 conditioned medium did not affect p62 puncta size or frequency.	HSMM 1, HSMM 2, HSKMDC 2, HSKMDC 3, HSKMDC 6, HSKMDC 9
Figure 6.5 TALL-104 conditioned medium did not affect TDP-43 aggregate frequency, size, or colocalisation with p62.	HSMM 1, HSMM 2, HSKMDC 2, HSKMDC 3, HSKMDC 6, HSKMDC 9
Figure 6.6 TDP-43 subcellular localisation was not affected by TALL-104 conditioned medium.	Image: HSMM 1 HSMM 1, HSKMDC 2, HSKMDC 3, HSKMDC 6, HSKMDC 9
Figure 6.7 TALL-104 coculture was cytotoxic to myotubes.	Image: HSKMDC 2 Graphs: HSMM 1, HSKMDC 2, HSKMDC 3, HSKMDC 6
Figure 6.8 IFNγ and TNFα secretion from TALL-104 cells co-cultured with myotubes.	HSMM 1, HSMM 2, HSKMDC 2, HSKMDC 3, HSKMDC 6, HSKMDC 9
Figure 6.9 Attachment and invasion of myotubes by TALL-104 cells.	A: HSMM 1 B: HSKMDC 6
Figure 6.10 p62 and TDP-43 in myotubes treated with IL-2 control or TALL-104 coculture.	A: HSMM 1
Figure 6.11 Coculture of TALL-104 cells with myotubes did not affect p62 particle size or frequency.	HSMM 1, HSKMDC 2, HSKMDC 3, HSKMDC 6, HSKMDC 9
Figure 6.12 TDP-43 aggregate frequency or size was not affected by TALL-104 coculture.	HSMM 1, HSKMDC 2, HSKMDC 3, HSKMDC 6, HSKMDC 9
Figure 6.13 TDP-43 subcellular localisation was affected by TALL-104 coculture.	HSMM 1, HSKMDC 2, HSKMDC 3, HSKMDC 6, HSKMDC 9
Figure 7.5 Force characteristics of myobundles.	HSMM 1
Figure 7.6 Myobundles respond to acetylcholine stimulation.	HSMM 1
Figure 7.7 Active twitch and tetanus force with IL-1β, IFNγ or combined.	HSMM 1, HSMM 2, HSKMDC 9
Figure 7.8 Tetanus kinetics with IL-1β, IFNγ or combined.	HSMM 1, HSMM 2, HSKMDC 9

Figure 7.9 Cross sectional area and myotube area of myobundles was not affected by cytokine treatment.	A, B: HSMM 1 Graphs: HSMM 1, HSMM 2, HSKMDC 9
Figure 7.10 Striated sarcomeric alpha actinin was lower with IFNγ and IL-1β+IFNγ treatment.	A-B: HSMM 1 C: HSMM 1, HSMM 2, HSKMDC 12
Figure 7.11 Active tetanus force with TALL-104 coculture with shaking.	HSMM 1, HSKMDC #9
Figure 7.12 Active twitch or tetanus force was not affected by TALL-104 coculture.	HSMM 1, HSMM 2, HSKMDC 9
Figure 7.13 Force kinetics were not affected by TALL-104 coculture.	HSMM 1, HSMM 2, HSKMDC 9
Figure 7.14 Fatigue with continuous tetanic stimulation was not affected by TALL-104 coculture.	A: HSMDC 9 Graphs: HSMM 1, HSMM 2, HSKMDC 9
Figure 7.15 TALL-104 coculture does not affect cross sectional area but may affect myotube area.	A: HSMM 1 Graphs: HSMM 1, HSMM 2, HSKMDC 9
Figure 7.16 Sarcomeric alpha actinin striations in myotubes were not affected by TALL-104 coculture.	A: HSMM 1 Graphs: HSMM 1, HSMM 2, HSKMDC 9

Appendix Table 0.1. Myogenic donors used by figure.

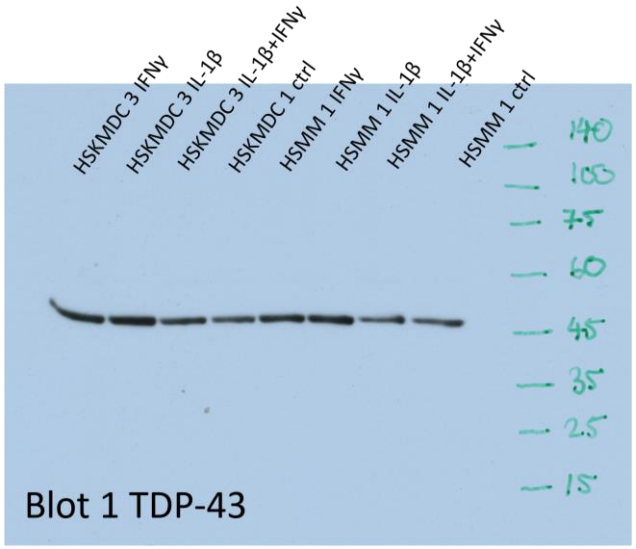
HSKMDC 3 IFNγ
HSKMDC 3 IL-1β
HSKMDC 3 IL-1β+IFNγ
HSKMDC 1 ctrl
HSMM 1 IFNγ
HSMM 1 IL-1β
HSMM 1 IL-1β+IFNγ
HSMM 1 ctrl
140
100
75
60
45
35
25
15
Blot 1 TDP-43

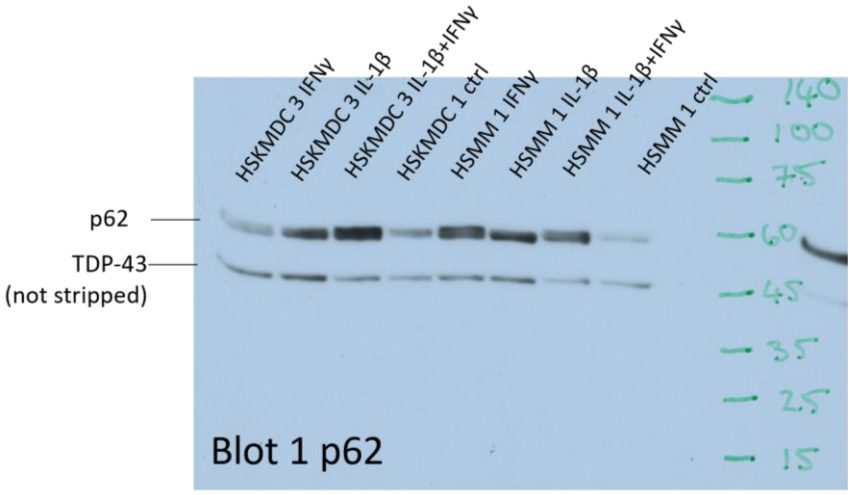
HSKMDC 3 IFNγ
HSKMDC 3 IL-1β
HSKMDC 3 IL-1β+IFNγ
HSKMDC 1 ctrl
HSMM 1 IFNγ
HSMM 1 IL-1β
HSMM 1 IL-1β+IFNγ
HSMM 1 ctrl
p62
TDP-43
(not stripped)
140
100
75
60
45
35
25
15
Blot 1 p62

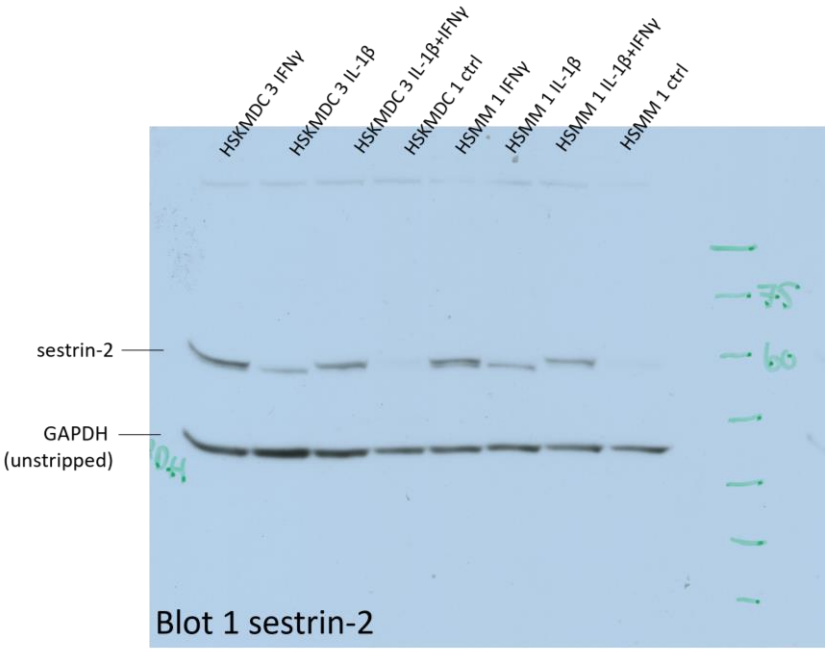
HSKMDC 3 IFNγ
HSKMDC 3 IL-1β
HSKMDC 3 IL-1β+IFNγ
HSKMDC 1 ctrl
HSMM 1 IFNγ
HSMM 1 IL-1β
HSMM 1 IL-1β+IFNγ
HSMM 1 ctrl
sestrin-2
GAPDH
(unstripped)
75
60
Blot 1 sestrin-2

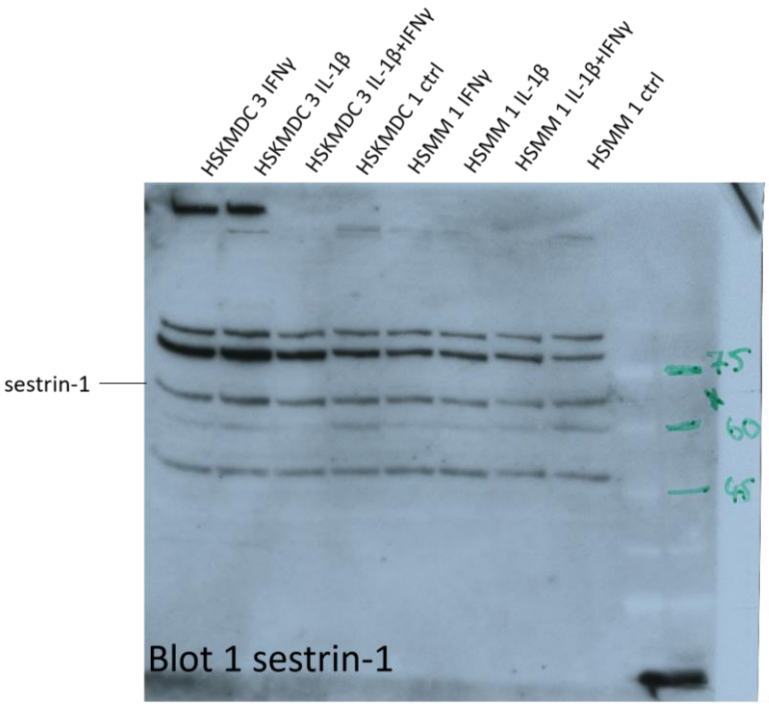
HSKMDC 3 IFNγ
HSKMDC 3 IL-1β
HSKMDC 3 IL-1β+IFNγ
HSKMDC 1 ctrl
HSMM 1 IFNγ
HSMM 1 IL-1β
HSMM 1 IL-1β+IFNγ
HSMM 1 ctrl
sestrin-1
75
60
45
Blot 1 sestrin-1

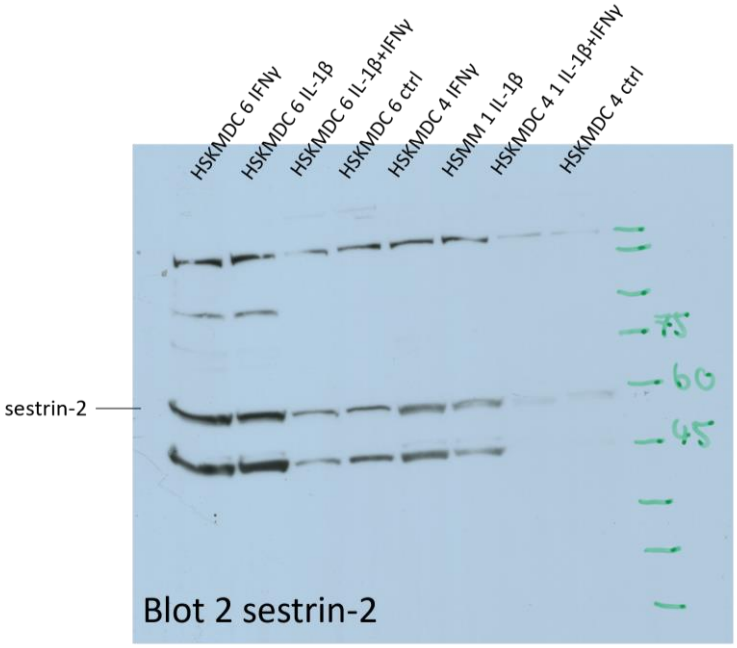
HSKMDC 6 IFNγ
HSKMDC 6 IL-1β
HSKMDC 6 IL-1β+IFNγ
HSKMDC 6 ctrl
HSKMDC 4 IFNγ
HSMM 1 IL-1β
HSKMDC 4 1 IL-1β+IFNγ
HSKMDC 4 ctrl
sestrin-2
75
60
45
Blot 2 sestrin-2

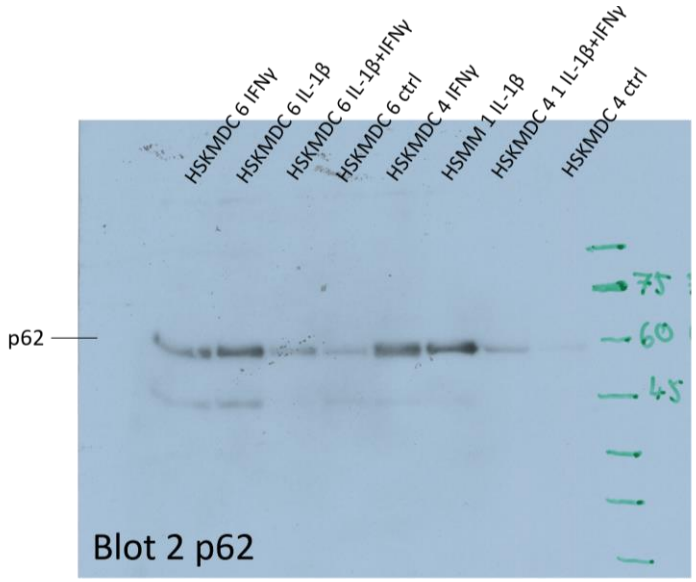
HSKMDC 6 IFNγ
HSKMDC 6 IL-1β
HSKMDC 6 IL-1β+IFNγ
HSKMDC 6 ctrl
HSKMDC 4 IFNγ
HSMM 1 IL-1β
HSKMDC 4 1 IL-1β+IFNγ
HSKMDC 4 ctrl
p62
75
60
45
Blot 2 p62

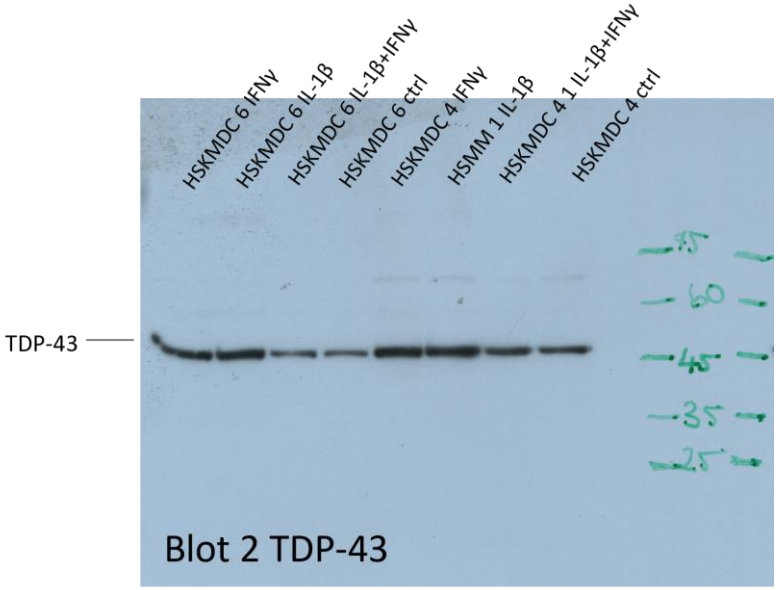
HSKMDC 6 IFNγ
HSKMDC 6 IL-1β
HSKMDC 6 IL-1β+IFNγ
HSKMDC 6 ctrl
HSKMDC 4 IFNγ
HSMM 1 IL-1β
HSKMDC 4 1 IL-1β+IFNγ
HSKMDC 4 ctrl
TDP-43
60
45
35
25
Blot 2 TDP-43

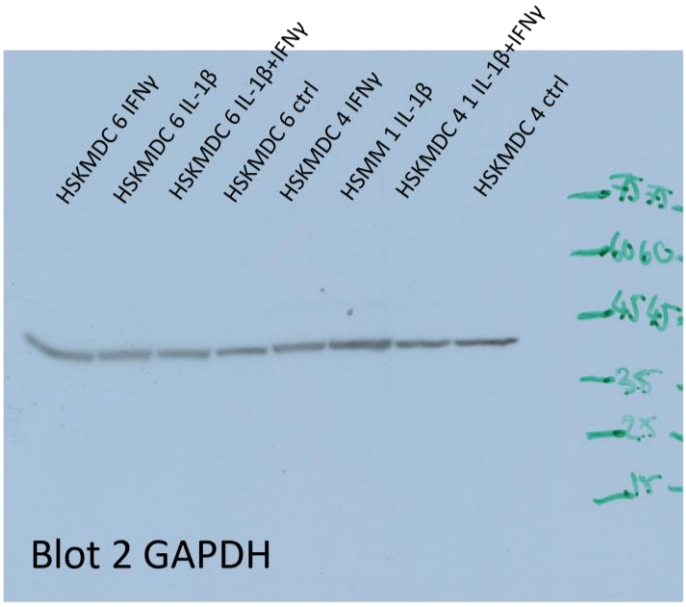
HSKMDC 6 IFNγ
HSKMDC 6 IL-1β
HSKMDC 6 IL-1β+IFNγ
HSKMDC 6 ctrl
HSKMDC 4 IFNγ
HSMM 1 IL-1β
HSKMDC 4 1 IL-1β+IFNγ
HSKMDC 4 ctrl
Blot 2 GAPDH

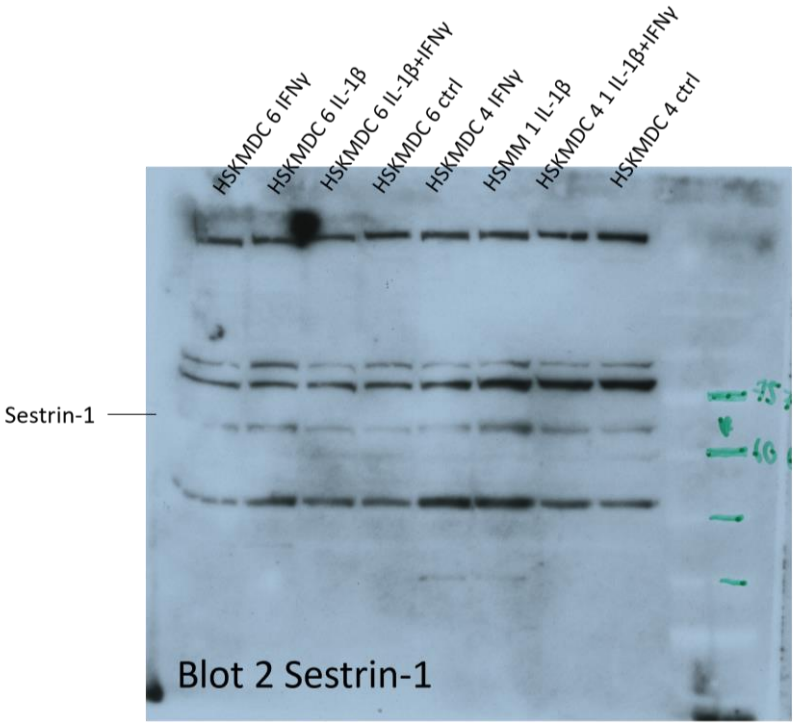
HSKMDC 6 IFNγ
HSKMDC 6 IL-1β
HSKMDC 6 IL-1β+IFNγ
HSKMDC 6 ctrl
HSKMDC 4 IFNγ
HSMM 1 IL-1β
HSKMDC 4 1 IL-1β+IFNγ
HSKMDC 4 ctrl
Sestrin-1
Blot 2 Sestrin-1

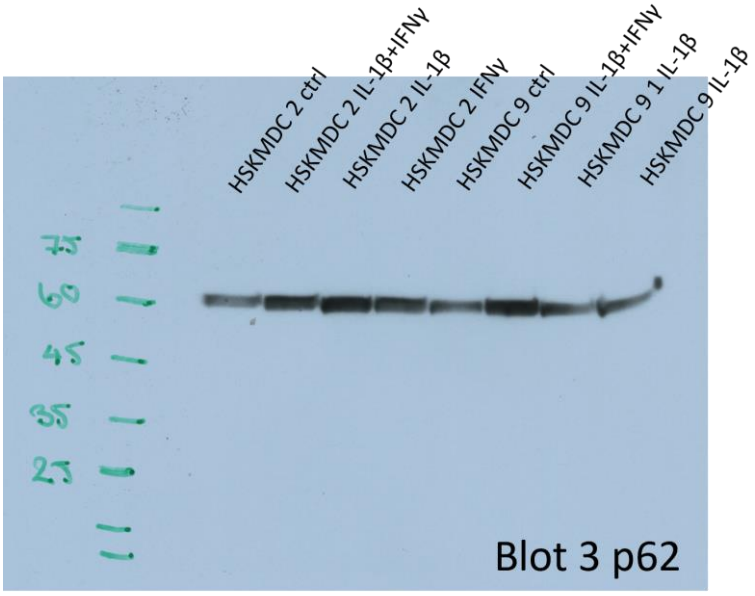
HSKMDC 2 ctrl
HSKMDC 2 IL-1β+IFNγ
HSKMDC 2 IL-1β
HSKMDC 2 IFNγ
HSKMDC 9 ctrl
HSKMDC 9 IL-1β+IFNγ
HSKMDC 9 1 IL-1β
HSKMDC 9 IL-1β
75
60
45
35
25
Blot 3 p62

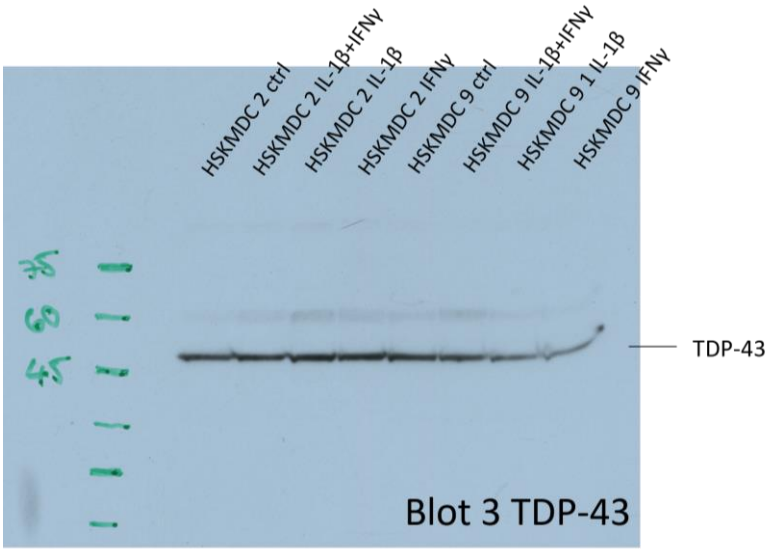
HSKMDC 2 ctrl
HSKMDC 2 IL-1β+IFNγ
HSKMDC 2 IL-1β
HSKMDC 2 IFNγ
HSKMDC 9 ctrl
HSKMDC 9 IL-1β+IFNγ
HSKMDC 9 1 IL-1β
HSKMDC 9 IFNγ
75
60
45
TDP-43
Blot 3 TDP-43

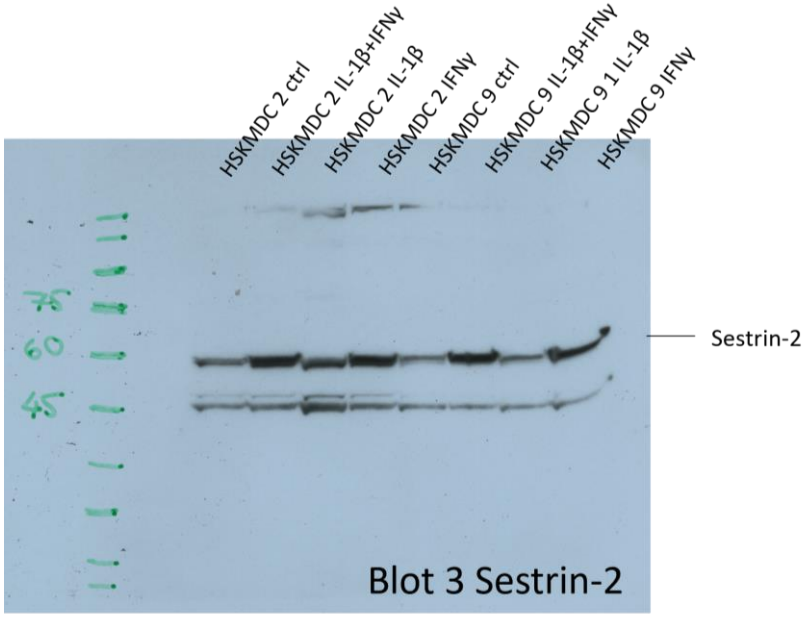
HSKMDC 2 ctrl
HSKMDC 2 IL-1β+IFNγ
HSKMDC 2 IL-1β
HSKMDC 2 IFNγ
HSKMDC 9 ctrl
HSKMDC 9 IL-1β+IFNγ
HSKMDC 9 1 IL-1β
HSKMDC 9 IFNγ
75
60
45
Sestrin-2
Blot 3 Sestrin-2

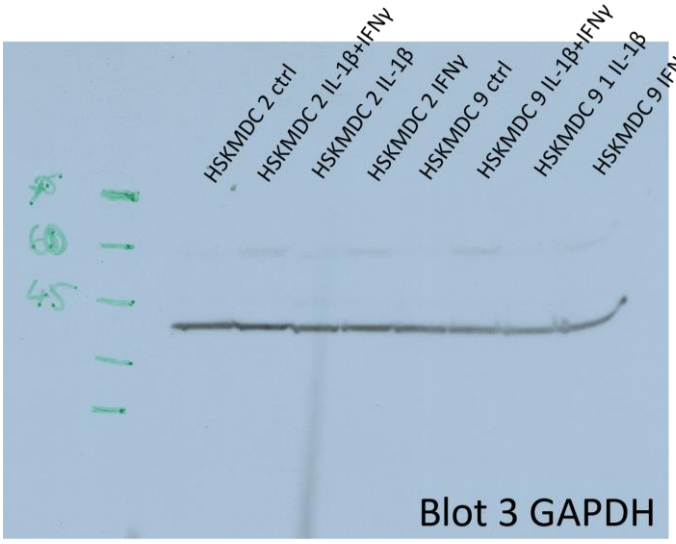
HSKMDC 2 ctrl
HSKMDC 2 IL-1β+IFNγ
HSKMDC 2 IL-1β
HSKMDC 2 IFNγ
HSKMDC 9 ctrl
HSKMDC 9 IL-1β+IFNγ
HSKMDC 9 1 IL-1β
HSKMDC 9 IFNγ
75
60
45
Blot 3 GAPDH

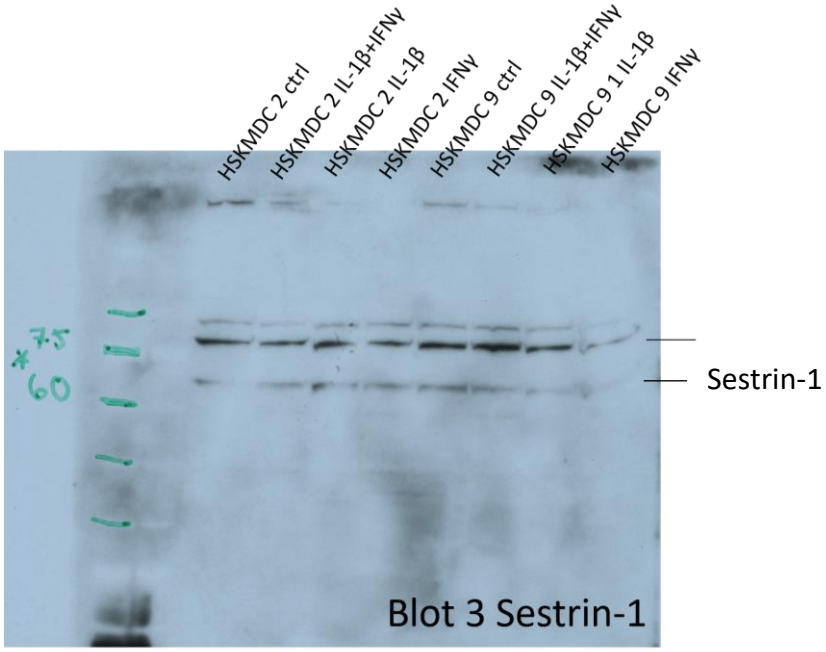
HSKMDC 2 ctrl
HSKMDC 2 IL-1β+IFNγ
HSKMDC 2 IL-1β
HSKMDC 2 IFNγ
HSKMDC 9 ctrl
HSKMDC 9 IL-1β+IFNγ
HSKMDC 9 1 IL-1β
HSKMDC 9 IFNγ
75
60
Sestrin-1
Blot 3 Sestrin-1

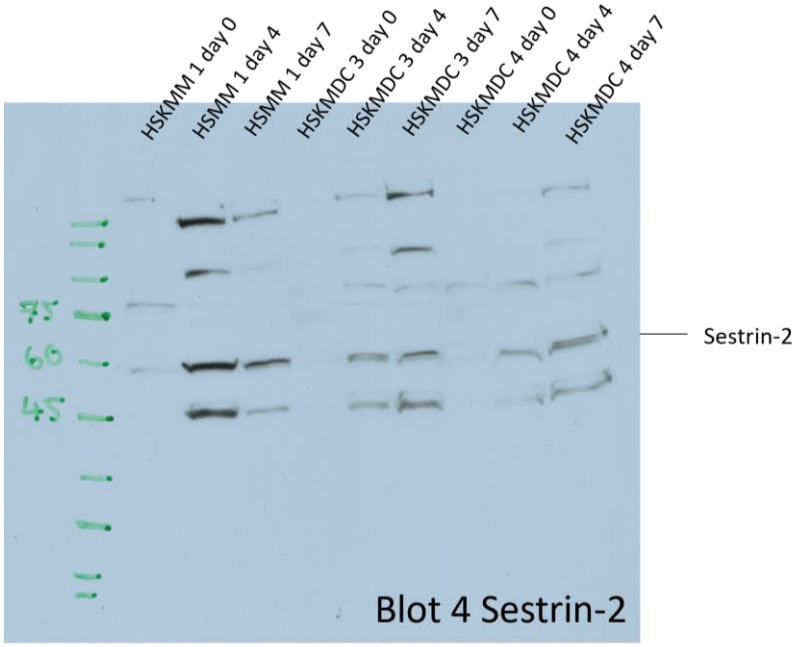
HSKMM 1 day 0
HSMM 1 day 4
HSMM 1 day 7
HSKMDC 3 day 0
HSKMDC 3 day 4
HSKMDC 3 day 7
HSKMDC 4 day 0
HSKMDC 4 day 4
HSKMDC 4 day 7
75
60
45
Sestrin-2
Blot 4 Sestrin-2

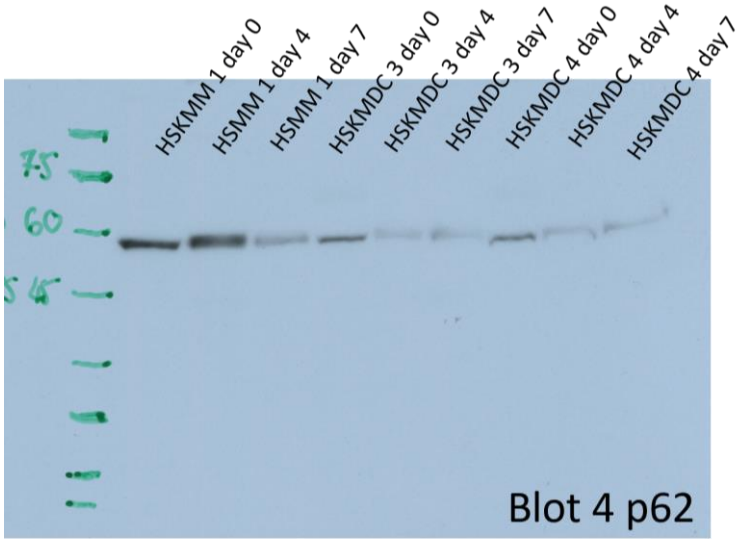
HSKMM 1 day 0
HSMM 1 day 4
HSMM 1 day 7
HSKMDC 3 day 0
HSKMDC 3 day 4
HSKMDC 3 day 7
HSKMDC 4 day 0
HSKMDC 4 day 4
HSKMDC 4 day 7
75
60
45
Blot 4 p62

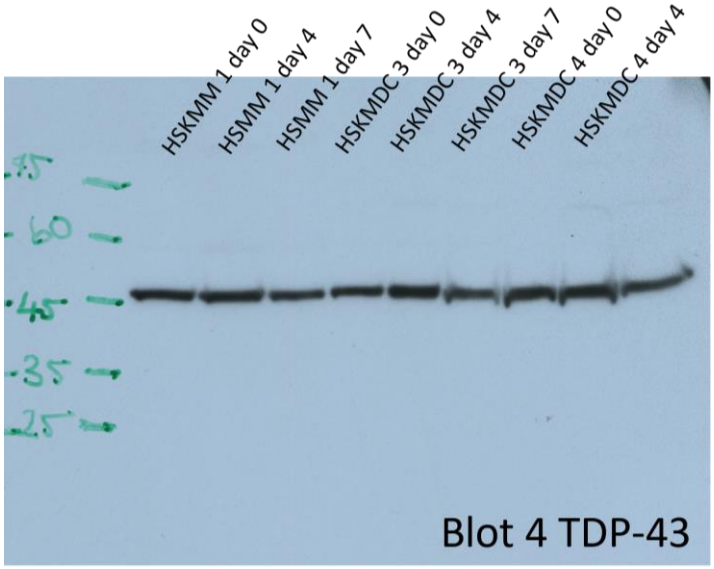
HSKMM 1 day 0
HSMM 1 day 4
HSMM 1 day 7
HSKMDC 3 day 0
HSKMDC 3 day 4
HSKMDC 3 day 7
HSKMDC 4 day 0
HSKMDC 4 day 4
60
45
35
Blot 4 TDP-43

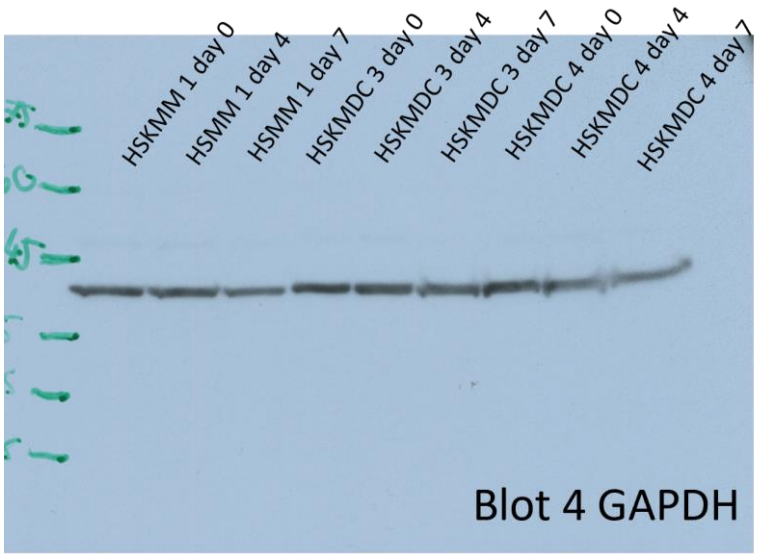
HSKMM 1 day 0
HSMM 1 day 4
HSMM 1 day 7
HSKMDC 3 day 0
HSKMDC 3 day 4
HSKMDC 3 day 7
HSKMDC 4 day 0
HSKMDC 4 day 4
HSKMDC 4 day 7
Blot 4 GAPDH

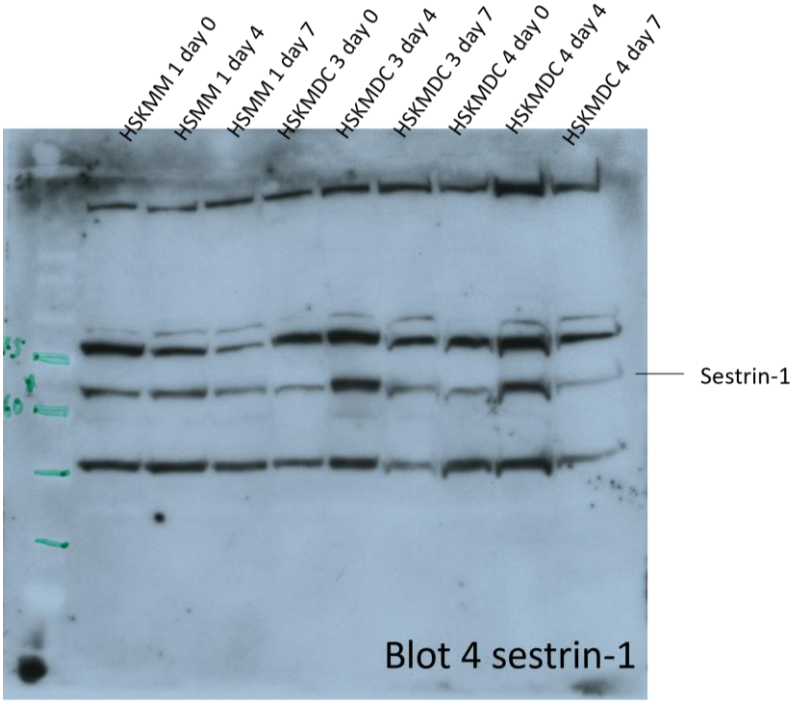
HSKMM 1 day 0
HSMM 1 day 4
HSMM 1 day 7
HSKMDC 3 day 0
HSKMDC 3 day 4
HSKMDC 3 day 7
HSKMDC 4 day 0
HSKMDC 4 day 4
HSKMDC 4 day 7
Sestrin-1
Blot 4 sestrin-1

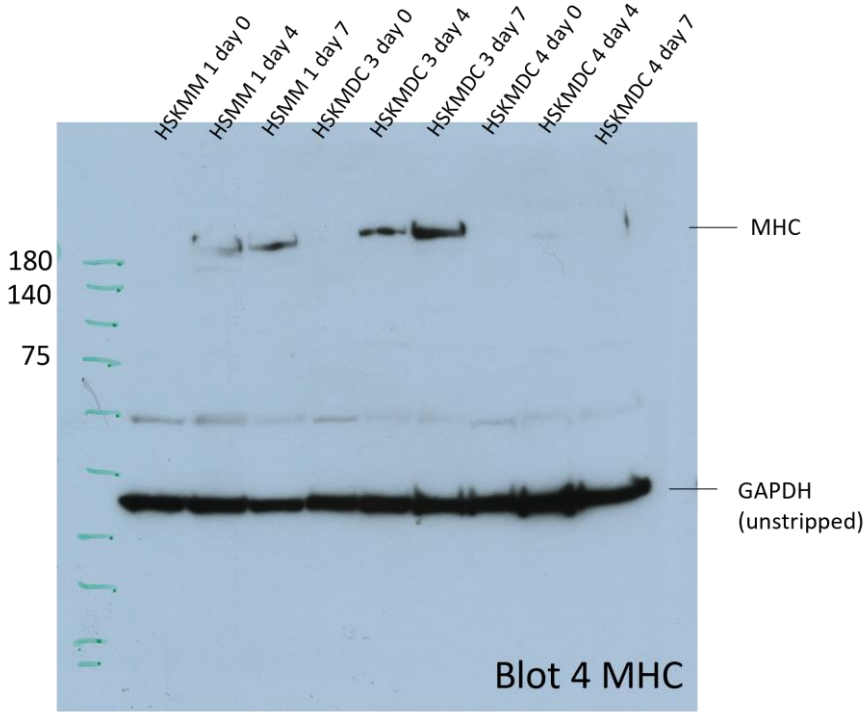
HSKMM 1 day 0
HSMM 1 day 4
HSMM 1 day 7
HSKMDC 3 day 0
HSKMDC 3 day 4
HSKMDC 3 day 7
HSKMDC 4 day 0
HSKMDC 4 day 4
HSKMDC 4 day 7
MHC
180
140
75
GAPDH
(unstripped)
Blot 4 MHC

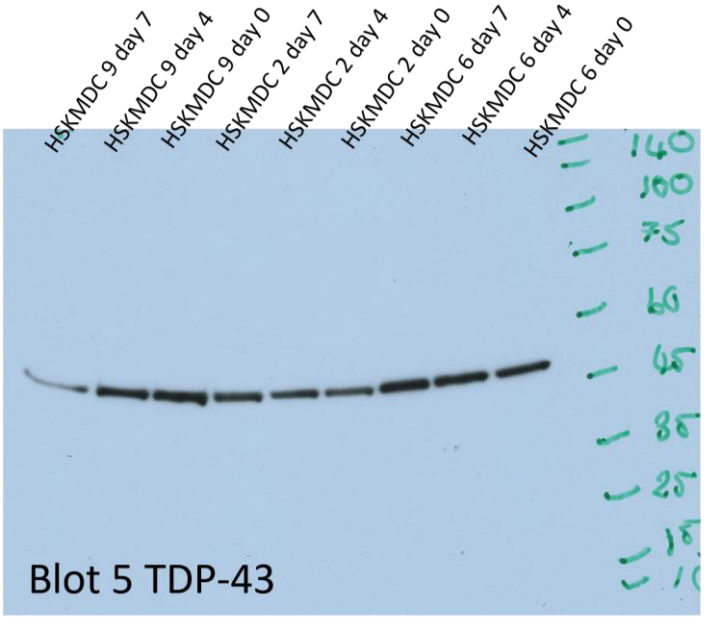
HSKMDC 9 day 7
HSKMDC 9 day 4
HSKMDC 9 day 0
HSKMDC 2 day 7
HSKMDC 2 day 4
HSKMDC 2 day 0
HSKMDC 6 day 7
HSKMDC 6 day 4
HSKMDC 6 day 0
140
100
75
60
45
35
25
15
Blot 5 TDP-43

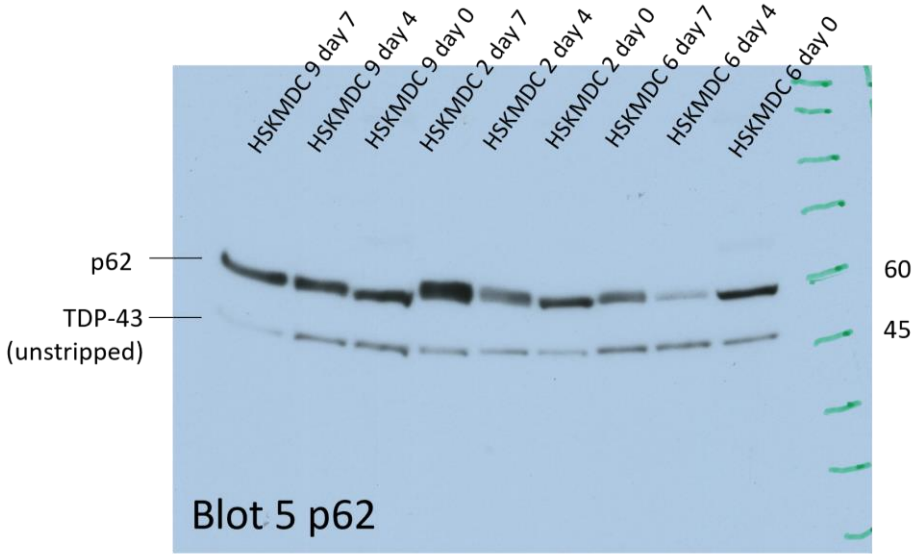
HSKMDC 9 day 7
HSKMDC 9 day 4
HSKMDC 9 day 0
HSKMDC 2 day 7
HSKMDC 2 day 4
HSKMDC 2 day 0
HSKMDC 6 day 7
HSKMDC 6 day 4
HSKMDC 6 day 0
p62
TDP-43
(unstripped)
60
45
Blot 5 p62

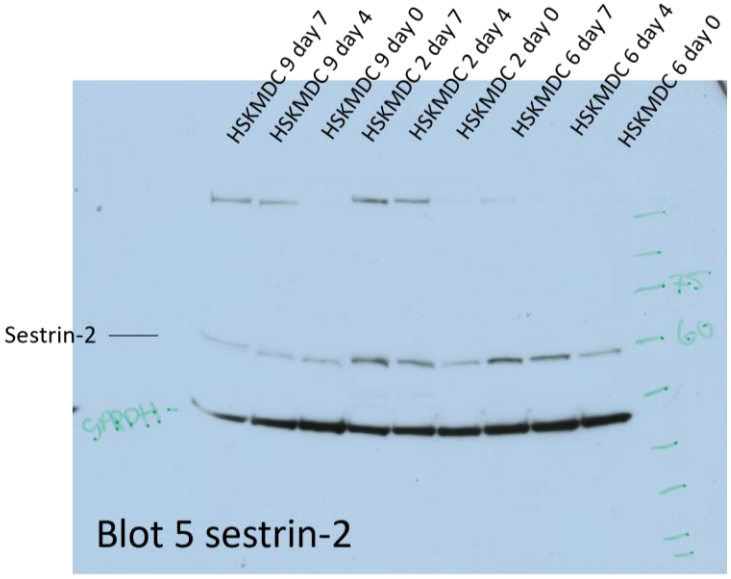
HSKMDC 9 day 7
HSKMDC 9 day 4
HSKMDC 9 day 0
HSKMDC 2 day 7
HSKMDC 2 day 4
HSKMDC 2 day 0
HSKMDC 6 day 7
HSKMDC 6 day 4
HSKMDC 6 day 0
Sestrin-2
75
60
Blot 5 sestrin-2

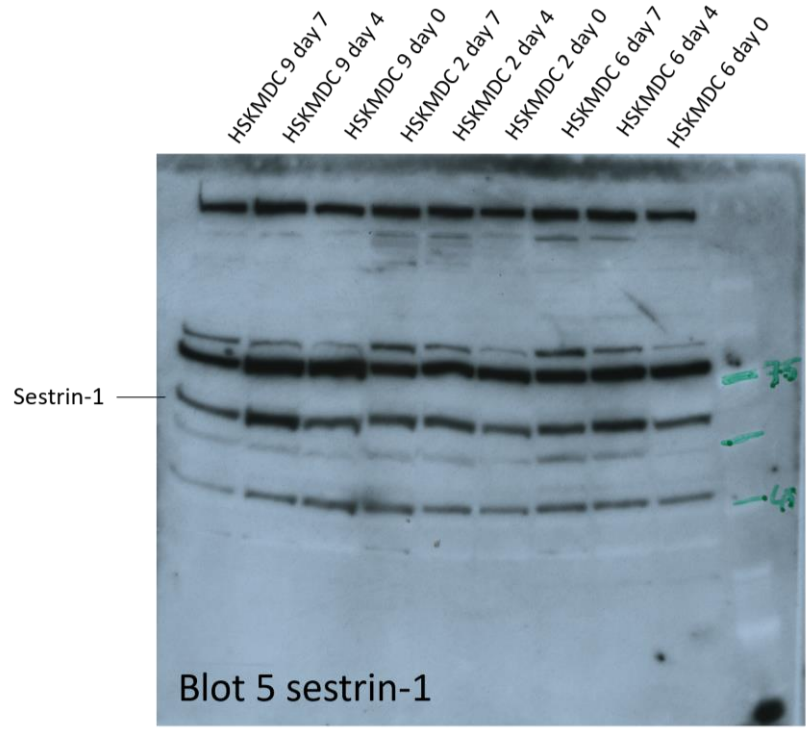
HSKMDC 9 day 7
HSKMDC 9 day 4
HSKMDC 9 day 0
HSKMDC 2 day 7
HSKMDC 2 day 4
HSKMDC 2 day 0
HSKMDC 6 day 7
HSKMDC 6 day 4
HSKMDC 6 day 0
Sestrin-1
Blot 5 sestrin-1

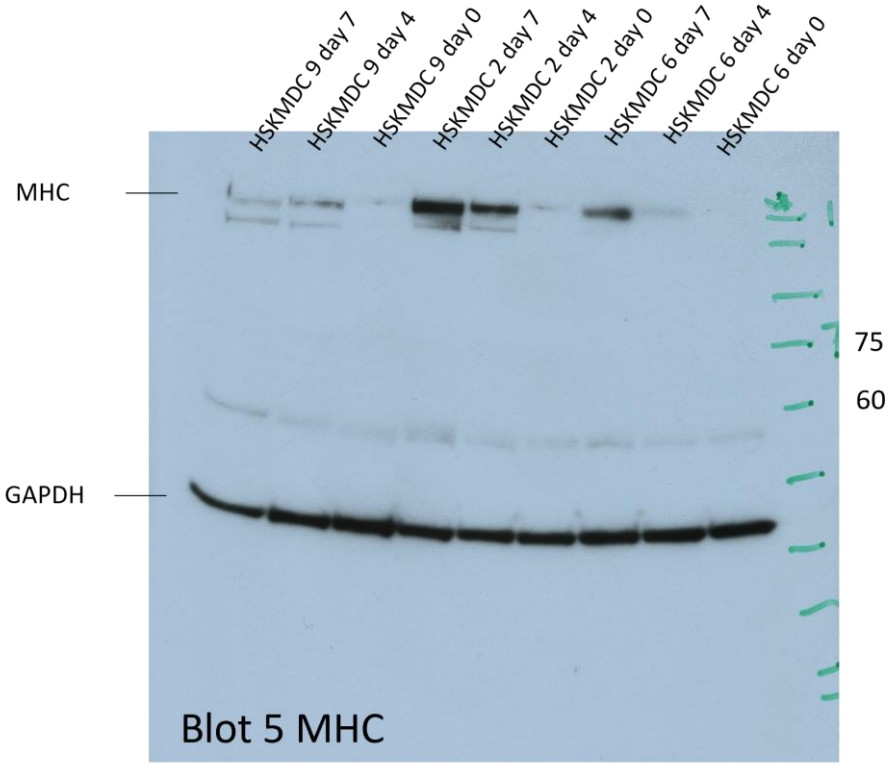
HSKMDC 9 day 7
HSKMDC 9 day 4
HSKMDC 9 day 0
HSKMDC 2 day 7
HSKMDC 2 day 4
HSKMDC 2 day 0
HSKMDC 6 day 7
HSKMDC 6 day 4
HSKMDC 6 day 0
MHC
GAPDH
75
60
Blot 5 MHC

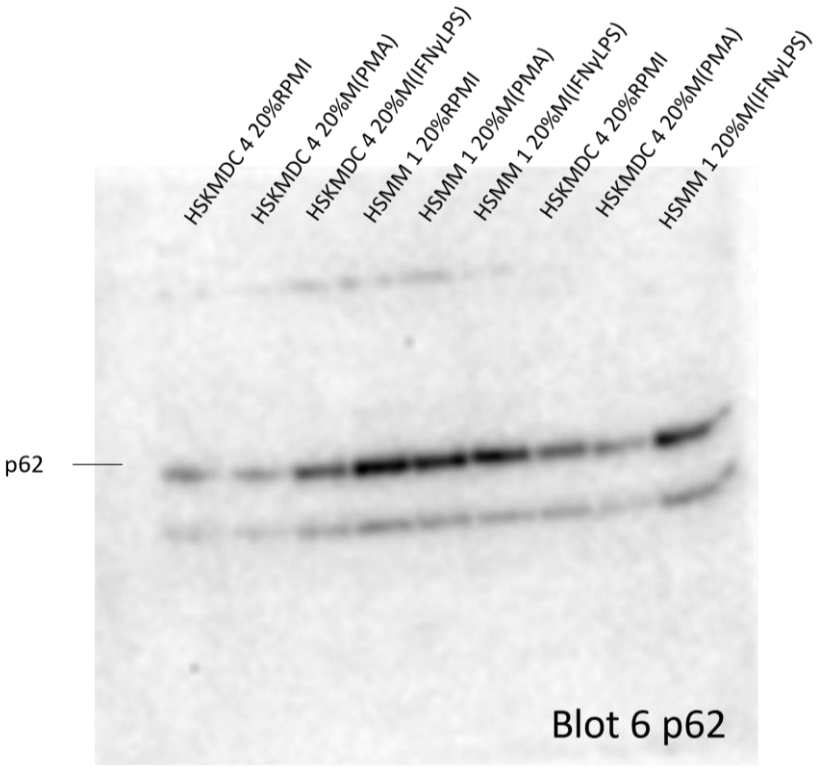
HSKMDC 4 20%RPMI
HSKMDC 4 20%M(PMA)
HSKMDC 4 20%M(IFNγLPS)
HSMM 1 20%RPMI
HSMM 1 20%M(PMA)
HSMM 1 20%M(IFNγLPS)
HSKMDC 4 20%RPMI
HSKMDC 4 20%M(PMA)
HSMM 1 20%M(IFNγLPS)
p62
Blot 6 p62

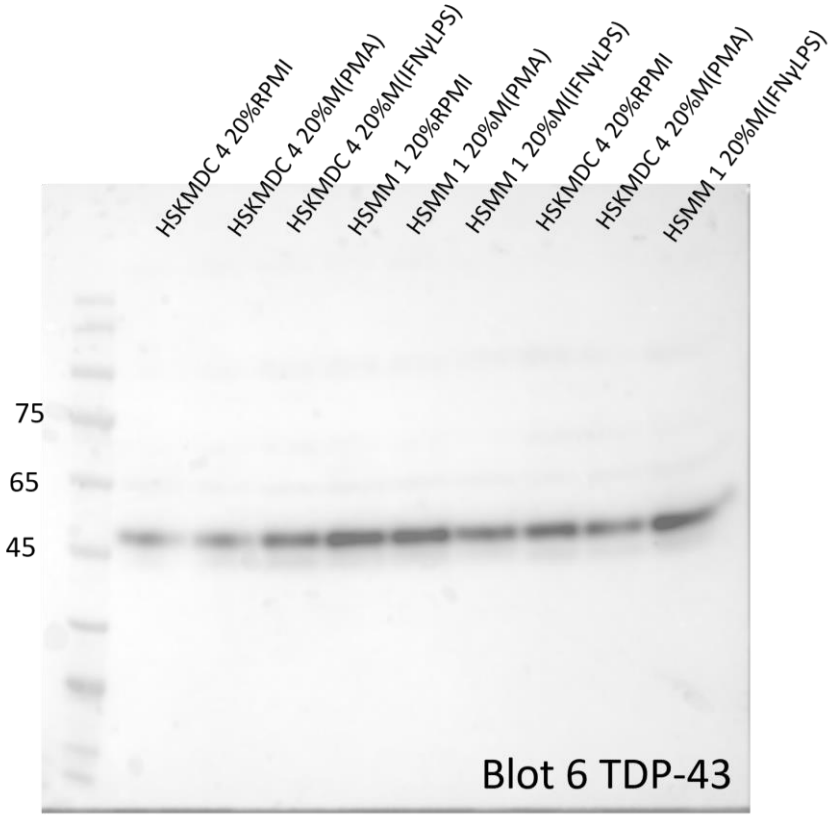
HSKMDC 4 20%RPMI
HSKMDC 4 20%M(PMA)
HSKMDC 4 20%M(IFNγLPS)
HSMM 1 20%RPMI
HSMM 1 20%M(PMA)
HSMM 1 20%M(IFNγLPS)
HSKMDC 4 20%RPMI
HSKMDC 4 20%M(PMA)
HSMM 1 20%M(IFNγLPS)
75
65
45
Blot 6 TDP-43

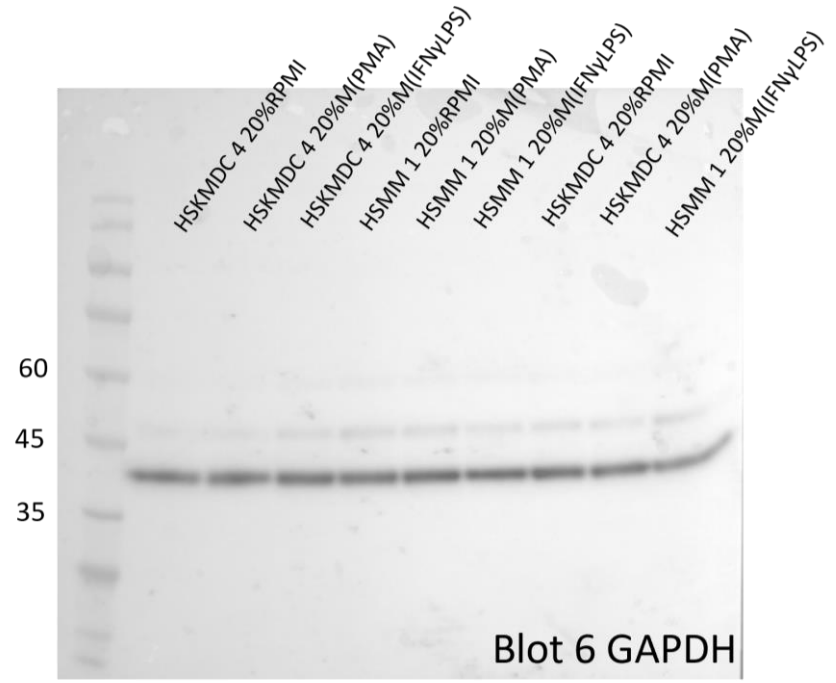
HSKMDC 4 20%RPMI
HSKMDC 4 20%M(PMA)
HSKMDC 4 20%M(IFNγLPS)
HSMM 1 20%RPMI
HSMM 1 20%M(PMA)
HSMM 1 20%M(IFNγLPS)
HSKMDC 4 20%RPMI
HSKMDC 4 20%M(PMA)
HSMM 1 20%M(IFNγLPS)
60
45
35
Blot 6 GAPDH

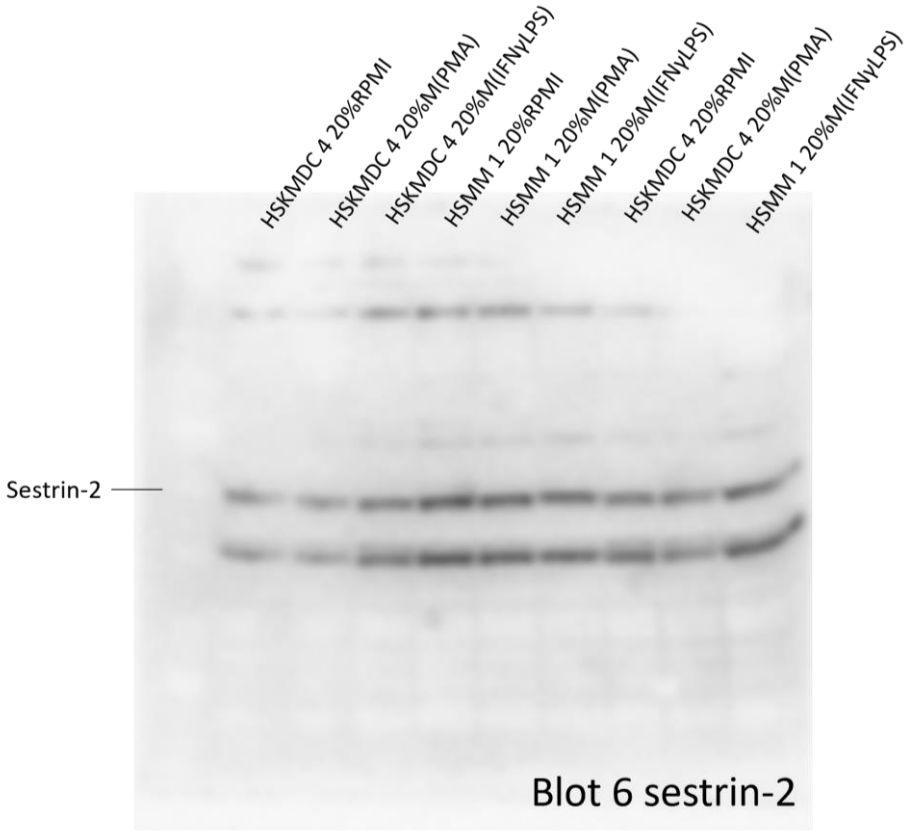
HSKMDC 4 20%RPMI
HSKMDC 4 20%M(PMA)
HSKMDC 4 20%M(IFNγLPS)
HSMM 1 20%RPMI
HSMM 1 20%M(PMA)
HSMM 1 20%M(IFNγLPS)
HSKMDC 4 20%RPMI
HSKMDC 4 20%M(PMA)
HSMM 1 20%M(IFNγLPS)
Sestrin-2
Blot 6 sestrin-2

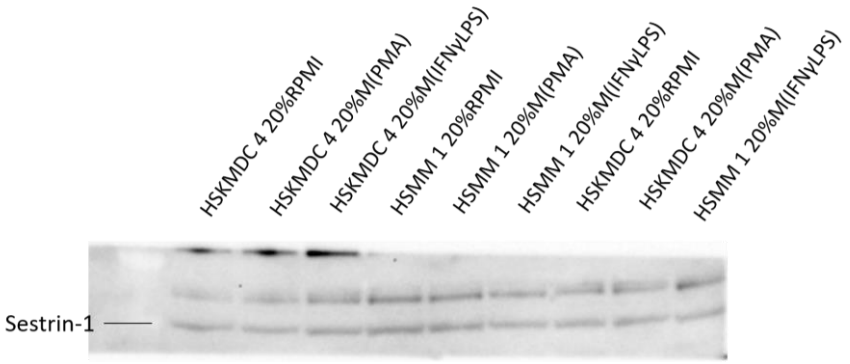

Blot 6 sestrin-1

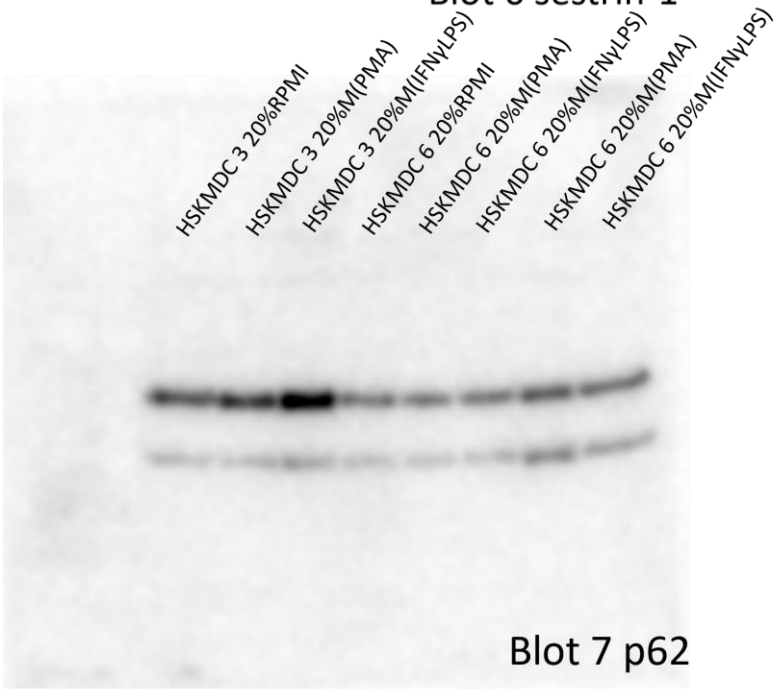

Blot 7 p62

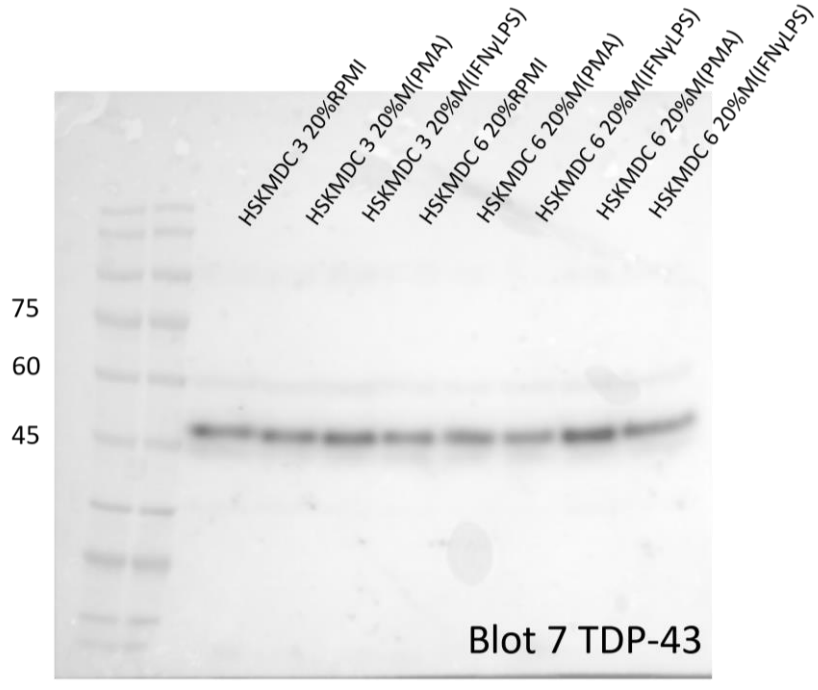

Blot 7 TDP-43

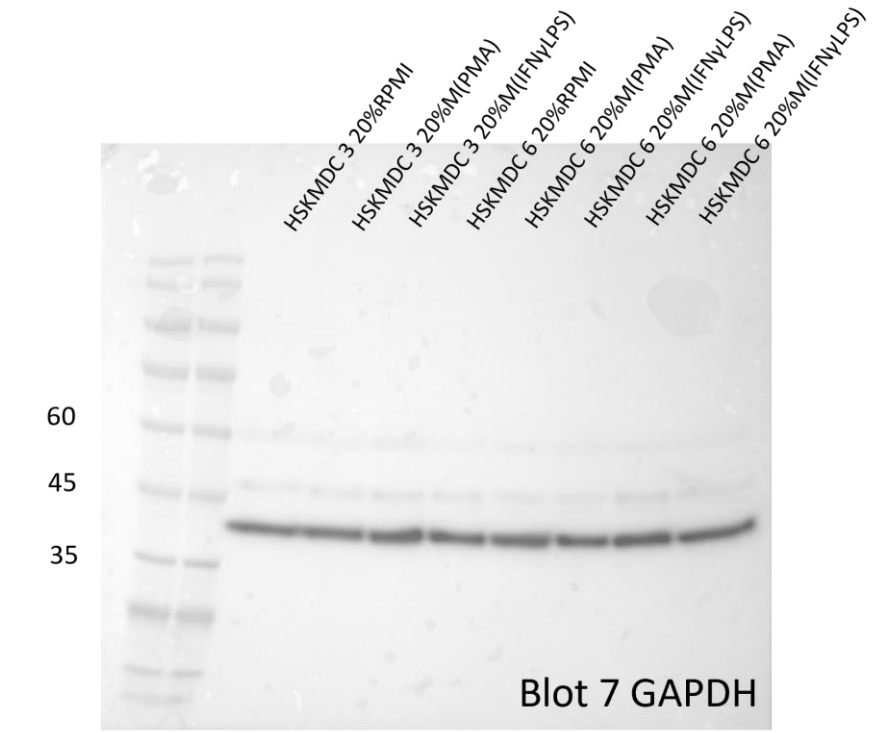
HSKMDC 3 20%RPMI
HSKMDC 3 20%M(PMA)
HSKMDC 3 20%M(IFNγLPS)
HSKMDC 6 20%RPMI
HSKMDC 6 20%M(PMA)
HSKMDC 6 20%M(IFNγLPS)
HSKMDC 6 20%M(PMA)
HSKMDC 6 20%M(IFNγLPS)
60
45
35
Blot 7 GAPDH

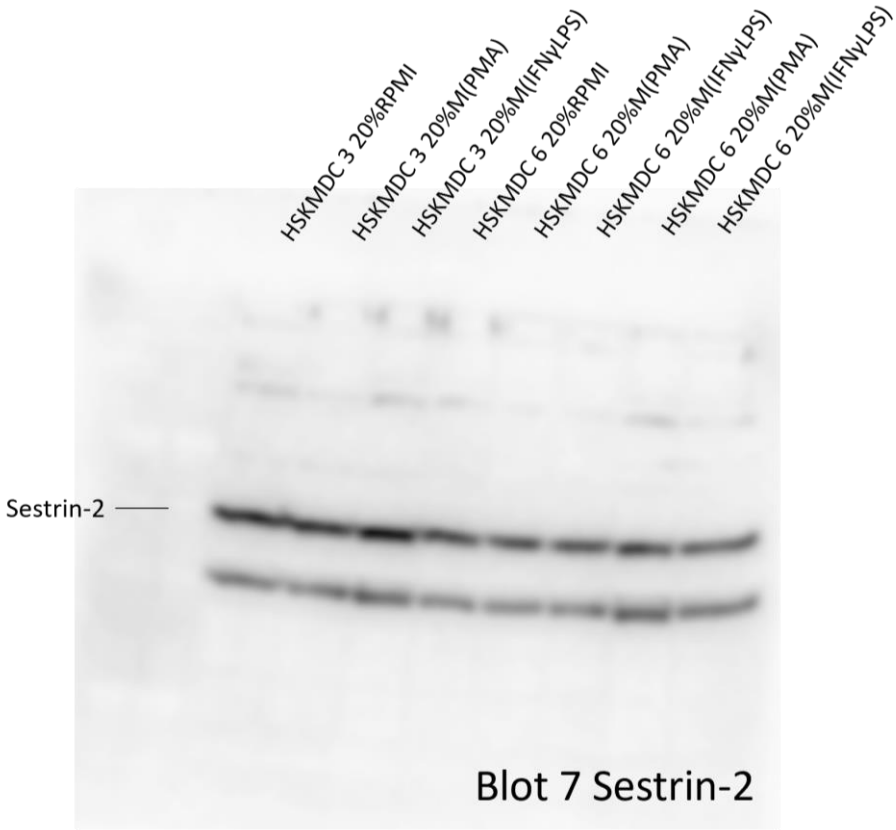
HSKMDC 3 20%RPMI
HSKMDC 3 20%M(PMA)
HSKMDC 3 20%M(IFNγLPS)
HSKMDC 6 20%RPMI
HSKMDC 6 20%M(PMA)
HSKMDC 6 20%M(IFNγLPS)
HSKMDC 6 20%M(PMA)
HSKMDC 6 20%M(IFNγLPS)
Sestrin-2
Blot 7 Sestrin-2

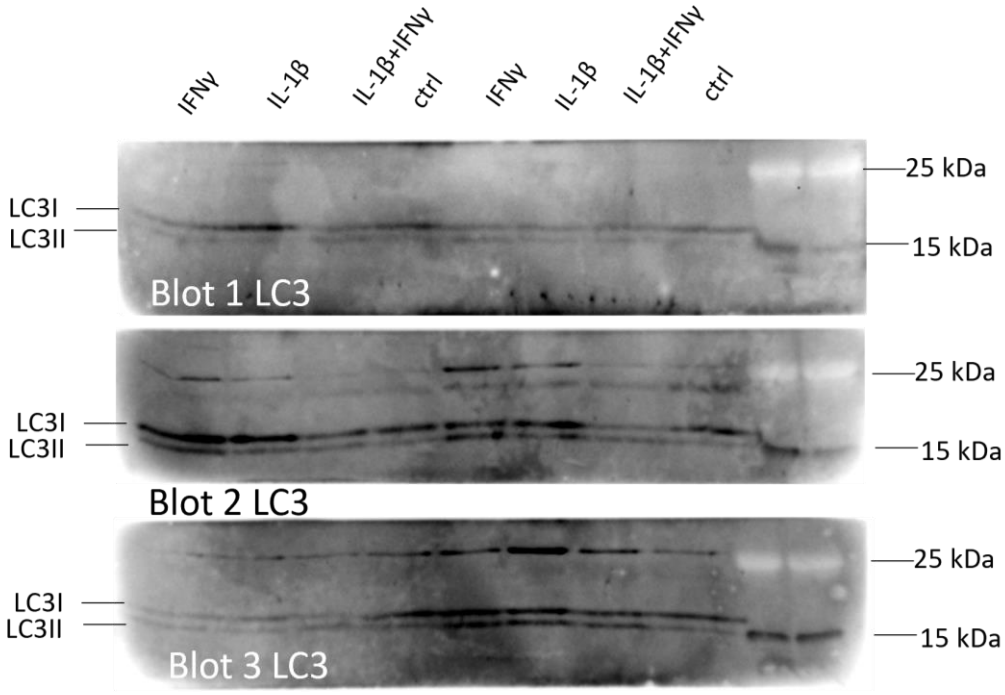

Appendix Figure 0.1 Uncropped blot images Scanned Western blot films or direct blot images. Display order represents staining order. All blots were conducted using the same prestained protein ladder, which is shown in green on film scans. Numbers to the side of blots correspond to molecular weight markers in kDa.

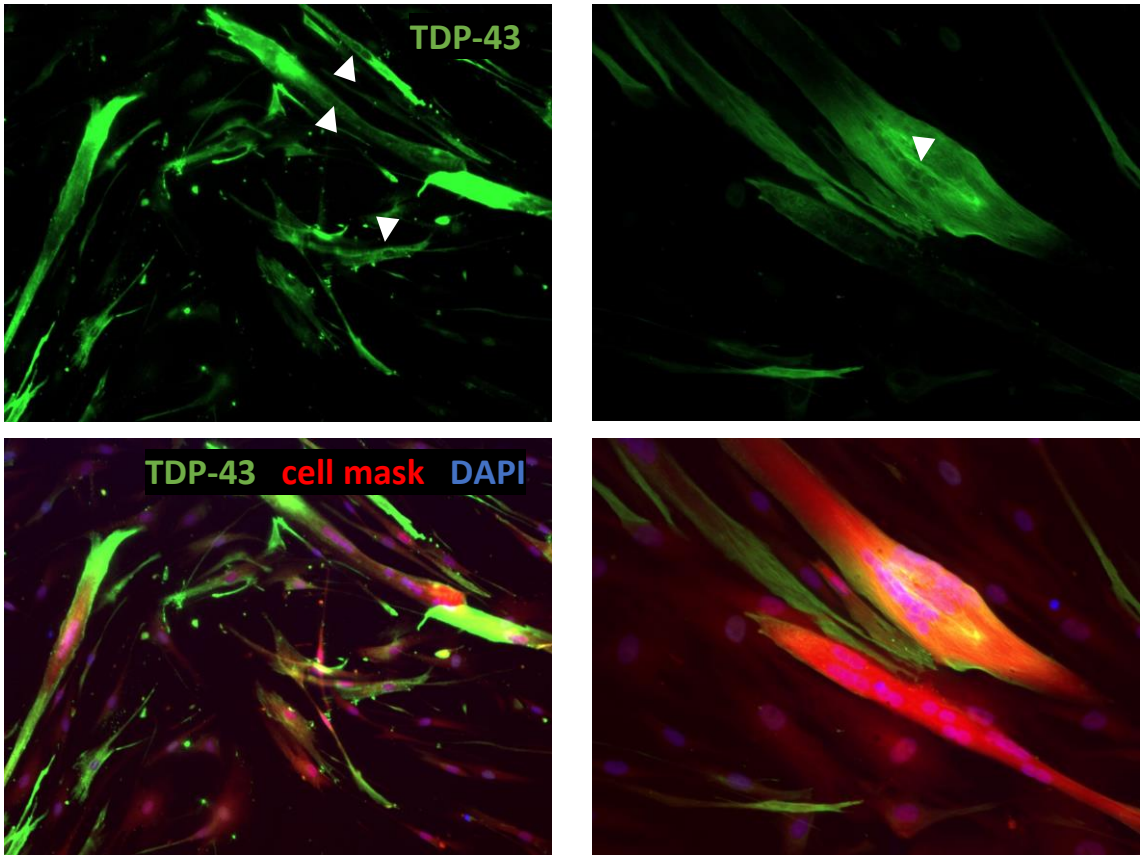

Appendix Figure 0.2 Lack of nuclear TDP-43 in early passage myotubes. Images from one donor (HSMM 1) showing no or little expression of TDP-43 in the nuclei of myotubes and some single nucleated cells. Both images from passage 3 cells. Images on left taken at 10 X and images on right taken at 20 X.